

**INVESTIGATIONS ON THE FORMULATION AND DRUG  
LOADING FEATURES OF SILICA NANOPARTICLES  
FROM AGRICULTURAL BIOMASS**

*Thesis submitted to  
University of Calicut in partial fulfillment of  
the requirement for the award of*

**DOCTOR OF PHILOSOPHY IN BIOCHEMISTRY**

*By*

**APARNA MENON A**



**DEPARTMENT OF BIOTECHNOLOGY  
UNIVERSITY OF CALICUT  
2024**



**DEPARTMENT OF BIOTECHNOLOGY  
UNIVERSITY OF CALICUT**



**CERTIFICATE**

This is to certify that the thesis entitled “**Investigations on the formulation and drug loading features of silica nanoparticles from agricultural biomass**” submitted to the University of Calicut, as a partial fulfillment of the Ph.D. programme for the award of the degree of **Doctor of Philosophy in Biochemistry** by **Aparna Menon A**, embodies the results of bonafide research work carried out by her under my supervision and guidance in the Department of Biotechnology, and the thesis has not previously formed the basis for the award of any degree, diploma, associateship, fellowship or other similar title or recognition.

Calicut University campus  
Date:

**Dr. Gopinathan C**  
Research supervisor



## **DECLARATION**

I hereby declare that the work presented in the thesis entitled **“Investigations on the formulation and drug loading features of silica nanoparticles from agricultural biomass”** is based on the original work done by me under the guidance of **Dr. Gopinathan C**, Department of Biotechnology, University of Calicut and had not been included in any other thesis submitted previously for the award of any degree. The contents of the thesis have undergone plagiarism check using **iThenticate** software at C.H.M.K Library, University of Calicut, and the similarity index was found to be within the permissible limit. I also declare that the thesis is free from AI-generated content.

Calicut University campus  
Date:

**Aparna Menon A**

*Signature of the Supervising teacher*



## **DECLARATION REGARDING CONFLICT OF INTERESTS**

We, **Dr. Gopinathan C** and **Ms. Aparna Menon A** declare that we are not interested in commercialization of the data presented in this thesis or any part thereof and also categorically state that we will not be using any of the technical data for the purpose of filing patents, copyright or for acquiring rights over intellectual property generated by Dr. G Radhakrishna Pillai. With this declaration, we also affirm that the ownership of all the data embodied in this thesis solely rests with Dr. G Radhakrishna Pillai, former Assistant Professor, Department of Life Sciences, University of Calicut and that there is no conflict of interests.

**Dr. Gopinathan C**  
Supervising teacher

**Ms. Aparna Menon A**  
Research scholar

Calicut University Campus  
Date:





## **ACKNOWLEDGEMENTS**

*Completion of this thesis would not have been possible without the earnest and untiring support from my Research supervisor Dr. Gopinathan C. No words can express my gratitude to my parents who are the ultimate pillars of my success and well-being, for being a beacon in the darkness, without whose well wishes no achievements would have been possible in my life and for teaching me patience, tolerance, positivity and aplenty of good things. I also am grateful to my forefathers who showed us ways in life and being a source of motivation, for the paths shown to trust in oneself and to be hopeful.*

*I am thankful to the teachers, friends and staff of my alma mater, School of Health Sciences, Department of Life Sciences, Department of Biotechnology, University of Calicut who rendered guidance and help all along.*

*I also acknowledge the help rendered by other departments of the University as well as from outside institutions, the Central Instrumentation Facility of the University of Calicut, and its staff for their help whenever requested. I thank Dr. Ananthakumar S, Chief Scientist and head at CSIR-National Institute for Interdisciplinary Science and Technology (NIIST), Thiruvananthapuram, Dr. Senoy Thomas and Dr. M Junaid Bushiri, Department of Physics, Cochin University of Science & Technology, Dr. John Bernet Johnson, Rajiv Gandhi Centre for Biotechnology and Dr. P Sreejith, Department of Zoology, University of Kerala, Dr. K Jayakumar, Department of*

*Statistics and Dr. M. Nasser, Department of Zoology, University of Calicut for their guidance and support.*

*I am also happy to have my friends who have been with me through thick and thin. I thank Navya Joseph, Tancia Rosalin, Faisal Moossa Athikkavil, Remya Johny, Surya, Dhaneesh Thengumtharayil, Shehna Sharaf, Niveditha Sandeep, Dijuraj M, Sivaprasad S, Manu Gopinathan, Sneha Francis, K C Shamjith, Edwin, Arya Damodharan, Keerthy, Hana, Meghna for their timely help and support.*

*I thank Dr. G Radhakrishna Pillai for inspiring, guiding, and supporting me. I am also thankful to Mr. Jamsheer N P, Mr. Iqbal (C.H.M.K library, University of Calicut), Mrs. Kalyanikkutty, Mrs. Shobhana Kumari K P, and Mrs. Mini Roshan Kunder (Airport Senior Secondary School, Karipur) for all the guidance and support they gave in person and in spirit. I also thank Mr. Rajesh and Mr. Shiju for helping me with the typesetting and printing of the thesis.*

*I also am grateful to the Almighty, time, energy and universe for teaching me lessons, for all the chances given, for making me stronger whenever I fell and for inspiring to rise and start all over again taking lessons from my failures.*

*- Aparna Menon A*

*Dedicated to*

---

***My Amma, Smt. Bindu P.  
My Achan, Sri. Govindaraj A.***

೧೯೯೯



## ABBREVIATIONS

|                   |   |  |
|-------------------|---|--|
| PEG               | - | poly ethylene glycol                                   |
| nm                | - | nanometer  |
| 3D                | - | three dimensional                                      |
| FeSi              | - | ferrosilicon   |
| SiCl <sub>4</sub> | - | silicon tetrachloride                                  |
| ADRs              | - | adverse drug reactions                                 |
| DDS               | - | drug delivery system                                   |
| API               | - | active pharmaceutical ingredient                       |
| MCM-41            | - | Mobil Composition of Matter No. 41                     |
| MCM-48            | - | Mobil Composition of Matter No. 48                     |
| SBA-15            | - | Santa Barbara Amorphous-15                             |
| Si-OH             | - | silanol  |
| FTIR              | - | Fourier Transform Infrared spectroscopy                |
| SEM               | - | Scanning Electron Microscopy                           |
| DLS               | - | Dynamic Light Scattering                               |
| XRD               | - | X-Ray diffraction                                      |
| HPLC              | - | High Performance Liquid Chromatography                 |
| UV                | - | Ultra Violet   |
| ζ-potential       | - | zeta potential   |
| RES               | - | reticuloendothelial system                             |
| μm                | - | micrometer   |
| RIP3/RIPK3        | - | Receptor-interacting serine/threonine-protein kinase 3 |
| RIP1/RIPK1        | - | Receptor-interacting serine/threonine-protein kinase 1 |
| IC <sub>50</sub>  | - | Half maximal inhibitory concentration                  |
| μg                | - | microgram  |
| mL                | - | millilitre   |

|                                |   |   |
|--------------------------------|---|---|
| h                              | - | hour  |
| FACS                           | - | fluorescence activated cell sorting   |
| >                              | - | greater than  |
| CPZ                            | - | chlorpromazine hydrochloride  |
| MBCD                           | - | methyl- $\beta$ -cyclodextrin   |
| PIa                            | - | polyinosinic acid   |
| DNA                            | - | deoxyribonucleic acid   |
| c-DNA                          | - | complementary deoxyribonucleic acid   |
| PEGylation                     | - | polyethylene glycolation  |
| DDA                            | - | degree of deacetylation   |
| pK <sub>a</sub>                | - | negative base -10 logarithm of the acid dissociation constant (K <sub>a</sub> ) of a solution |
| pH                             | - | negative log base 10 of the hydronium concentration   |
| NP                             | - | nanoparticle  |
| -OH                            | - | hydroxyl functional group   |
| -NH <sub>2</sub>               | - | amino functional group  |
| $\pi$ -bonds                   | - | pi-bond   |
| EPR                            | - | Enhanced permeability and retention effect  |
| MPS                            | - | mononuclear phagocyte system  |
| VEGF                           | - | vascular endothelial growth factor  |
| m-RNA                          | - | messenger ribonucleic acid  |
| H <sub>2</sub> O <sub>2</sub>  | - | hydrogen peroxide   |
| HCl                            | - | hydrochloric acid   |
| rpm                            | - | revolutions per minute  |
| psi                            | - | pounds per square inch  |
| °C                             | - | degree Celsius  |
| cm                             | - | centimeter  |
| H <sub>2</sub> SO <sub>4</sub> | - | sulfuric acid   |
| min                            | - | minute  |
| kV                             | - | kilovolt  |

|         |   |   |
|---------|---|---|
| mA      | - | milli ampere  |
| CHNS    | - | carbon, hydrogen, nitrogen, sulfur  |
| UV-Vis  | - | ultraviolet visible   |
| M       | - | molar   |
| NaOH    | - | sodium hydroxide  |
| xg      | - | relative centrifugal force (or g force)   |
| w/v     | - | weight by volume  |
| PBS     | - | phosphate buffer saline   |
| MWCO    | - | molecular weight cut off  |
| kDa     | - | kilo Dalton   |
| ELISA   | - | enzyme-linked immunosorbent assay   |
| DMEM    | - | Dulbecco's Modified Eagle's Medium  |
| DAPI    | - | 4',6-diamidino-2-phenylindole   |
| NC      | - | normal control  |
| BSN     | - | biogenic silica nanoparticle  |
| BSNP    | - | polyethylene glycolated biogenic silica nanoparticle                                      |
| BSNCH   | - | biogenic silica nanoparticle capped with chitosan   |
| BSNC    | - | biogenic silica nanoparticles loaded with curcumin  |
| BSNPC   | - | polyethylene glycolated biogenic silica nanoparticle loaded with curcumin                 |
| BSNCHC  | - | chitosan capped biogenic silica nanoparticle loaded with curcumin                         |
| BSNPCHC | - | chitosan capped polyethylene glycolated biogenic silica nanoparticle loaded with curcumin |
| BSNE    | - | biogenic silica nanoparticles loaded with epirubicin                                      |
| BSNPE   | - | polyethylene glycolated biogenic silica nanoparticle loaded with epirubicin               |
| BSNCHE  | - | chitosan capped biogenic silica nanoparticle loaded with epirubicin                       |
| BSNPCHE | - | chitosan capped polyethylene glycolated biogenic  |

|         |   |   |
|---------|---|---|
|         |   | silica nanoparticle loaded with epirubicin  |
| CSN     | - | chemically synthesized silica nanoparticle  |
| CSNP    | - | polyethylene glycolated chemically synthesized silica nanoparticle  |
| CSNC    | - | chemically synthesized silica nanoparticles loaded with curcumin  |
| CSNPC   | - | polyethylene glycolated chemically synthesized silica nanoparticle loaded with curcumin                   |
| CSNCHC  | - | chemically synthesized silica nanoparticle capped with chitosan and loaded with curcumin                  |
| CSNPCHC | - | chitosan capped polyethylene glycolated chemically synthesized silica nanoparticles loaded with curcumin  |
| CSNE    | - | chemically synthesized silica nanoparticles loaded with epirubicin  |
| CSNPE   | - | polyethylene glycolated chemically synthesized silica nanoparticle loaded with epirubicin                 |
| CSNCHE  | - | chitosan capped chemically synthesized silica nanoparticle loaded with epirubicin                         |
| CSNPCHE | - | chitosan capped polyethylene glycolated chemically synthesized silica nanoparticle loaded with epirubicin |



# CONTENTS

| <i>Sl. No.</i> | <i>Title</i>   | <i>Page No.</i> |
|----------------|--|-----------------|
| <b>1.</b>      | <b>Introduction</b>  | <b>1-14</b>     |
| 1.1.           | Nanoparticle-based drug carrier system                             | 1               |
| 1.2.           | Nanoparticles from biogenic sources                                | 7               |
| 1.3.           | Soaring incidence of cancer on global scale                        | 10              |
| 1.4.           | Objectives of the research work                                    | 14              |
| <b>2.</b>      | <b>Review of literature</b>  | <b>15-54</b>    |
| 2.1.           | Drug delivery system   | 15              |
| 2.1.1.         | Particulate drug delivery system                                   | 17              |
| 2.1.2.         | Inorganic nanocarrier system                                       | 19              |
| 2.1.3.         | Mesoporous nanocarrier systems                                     | 20              |
| 2.1.4.         | Mesoporous silica DDS  | 21              |
| 2.1.5.         | Biogenic silica-based DDS  | 22              |
| 2.2.           | Physical and chemical characterization of nanoparticles            | 23              |
| 2.2.1.         | Desirable characteristics of drug delivery vector                  | 29              |
| 2.3.           | Cellular interaction of drug carriers                              | 31              |
| 2.4.           | Surface modification for additional functionalities of nanocarrier | 39              |
| 2.4.1.         | Surface functionalization with polyethylene glycol (PEG)           | 40              |
| 2.4.2.         | Capping with chitosan  | 42              |
| 2.5.           | Encapsulation of drug into NP DDSs                                 | 43              |
| 2.5.1.         | Drug release from NP DDSs  | 43              |
| 2.6.           | Application of nano vectors in healthcare sector                   | 45              |
| 2.6.1.         | Conventional drug delivery versus nanoparticle-based drug delivery | 46              |
| 2.6.2.         | Nano formulations in cancer chemotherapy                           | 47              |

---

|   |              |
|---|--------------|
| 2.7. Curcumin   | 48           |
| 2.8. Epirubicin   | 49           |
| 2.9. Challenges and future prospects  | 51           |
| <b>3. Materials and methods</b>   | <b>55-88</b> |
| 3.1. Source identification of biogenic silica   | 55           |
| 3.2. Optimization of synthesis of biogenic silica nanoparticles                               | 55           |
| 3.2.1. Synthesis of silica nanoparticles from diatom frustules                                | 56           |
| 3.2.2. Synthesis of biogenic silica nanoparticles (BSN) from agricultural biomass             | 58           |
| 3.3. Physicochemical characterization   | 61           |
| 3.4. Surface modification   | 63           |
| 3.4.1. Polyethylene glycol modification and drug loading                                      | 64           |
| 3.4.2. Chitosan capping   | 65           |
| 3.5. Drug loading studies   | 65           |
| 3.5.1. Loading of curcumin  | 66           |
| 3.5.2. Loading of epirubicin  | 68           |
| 3.6. Drug release studies   | 68           |
| 3.7. Biocompatibility studies   | 70           |
| 3.7.1. In vitro degradation   | 70           |
| 3.7.2. Cell culture   | 71           |
| 3.7.3. Cell viability assay   | 71           |
| 3.7.4. Cytoprotective role of drug conjugated nano formulation against cypermethrin treatment | 73           |
| 3.7.5. Assay of glutathione peroxidase (EC 1.11.1.9)  | 73           |
| 3.7.6. Assay of superoxide dismutase (SOD, EC 1.15.1.1)                                       | 74           |
| 3.7.7. Assay of catalase (EC 1.11.1.6)  | 76           |
| 3.7.8. Assessment of lipid peroxidation inhibition activity                                   | 77           |

---

---

|   |               |
|---|---------------|
| 3.7.9. Cellular uptake studies  | 78            |
| 3.7.10. Nuclear morphology analysis using DAPI  | 78            |
| 3.7.11. Determination of intracellular ROS using DCFDA  | 81            |
| 3.7.12. Mitochondrial membrane potential ( $\Delta\Psi_m$ ) analysis using JC-10 dye  | 82            |
| 3.7.13. Gene expression studies (RT-PCR)  | 83            |
| 3.8. DPPH activity  | 88            |
| <b>4. Results</b>   | <b>89-142</b> |
| 4.1. Source identification, optimization of synthesis, and physicochemical analysis of biogenic silica nanoparticles                          | 89            |
| 4.1.1. Production of silica nanoparticles from diatomaceous earth using ball milling  | 89            |
| 4.1.2. Effect of ball-milling on other physical and chemical properties of silica nanoparticles   | 91            |
| 4.2. Production of silica nanoparticles from agricultural biomass   | 97            |
| 4.2.1. Optimization of biogenic silica nanoparticle synthesis in terms of acid pretreatment, incineration temperature, and time of combustion | 97            |
| 4.2.2. Physicochemical analysis of biogenic silica particles from agricultural biomass  | 101           |
| 4.3. Surface modification and drug loading studies using biogenic silica nanoparticles  | 115           |
| 4.3.1. Drug loading onto biogenic silica nanoparticles  | 115           |
| 4.4. Studies on drug release from different nano-formulations   | 120           |
| 4.4.1. Curcumin release from different nano-formulations  | 120           |
| 4.4.2. Epirubicin release from different nano-formulations  | 123           |

---

---

|           |  |                |
|-----------|--|----------------|
| 4.5.      | Assessment of nanoparticle toxicity and cytocompatibility using cell-lines             | 125            |
| 4.5.1.    | In vitro degradation behaviour of biogenic silica nanoparticles                        | 125            |
| 4.5.2.    | Assessment on cell viability   | 126            |
| 4.5.3.    | Dose response study  | 127            |
| 4.5.4.    | Cytoprotection against toxicity induced by cypermethrin                                | 129            |
| 4.5.5.    | Cellular uptake of curcumin  | 131            |
| 4.5.6.    | Effect of nano-formulation on the nuclear morphology                                   | 132            |
| 4.5.7.    | Estimation of intracellular ROS (DCFDA)  | 135            |
| 4.5.8.    | Mitochondrial membrane potential analysis  | 138            |
| 4.5.9.    | Gene expression studies  | 139            |
| 4.6.      | Study on anti-oxidant property of curcumin-loaded biogenic silica particle             | 142            |
| 4.6.1.    | 2,2-Diphenyl-1-picryl Hydrazine (DPPH) Scavenging activity                             | 142            |
| <b>5.</b> | <b>Discussion</b>  | <b>143-198</b> |
| 5.1.      | Optimization of synthesis of biogenic silica and physicochemical characterization      | 143            |
| 5.1.1.    | Diatoms as source of silica nano particles   | 147            |
| 5.1.2.    | Plant materials as source of silica nano particles                                     | 149            |
| 5.1.3.    | Source identification of biogenic silica   | 155            |
| 5.1.4.    | Effect of raw material pretreatment on physical and chemical properties of end-product | 156            |
| 5.2.      | Surface modification and drug loading studies  | 170            |
| 5.2.1.    | Modification with polyethylene glycol  | 173            |
| 5.2.2.    | Chitosan capping and pH responsive release of drug                                     | 174            |

---

---

|           |  |                |
|-----------|--|----------------|
| 5.3.      | Release pattern of drug from different nano-formulations                           | 178            |
| 5.4.      | Assessment of nanoparticle toxicity and cytocompatibility using cell lines         | 181            |
| 5.4.1.    | Degradation behaviour of biogenic silica particles                                 | 182            |
| 5.4.2.    | Cell viability assay   | 187            |
| 5.4.3.    | Assay of Glutathione Peroxidase (EC 1.11.1.9)                                      | 188            |
| 5.4.4.    | Assay of Superoxide Dismutase (SOD, EC 1.15.1.1)                                   | 189            |
| 5.4.5.    | Assay of Catalase (EC 1.11.1.6)  | 189            |
| 5.4.6.    | Lipid peroxidation inhibition activity   | 191            |
| 5.4.7.    | Cellular uptake of curcumin  | 191            |
| 5.4.8.    | Effect of nano-formulation on the nuclear morphology                               | 193            |
| 5.4.9.    | Estimation of intracellular ROS (DCFDA) and mitochondrial membrane potential (MMP) | 194            |
| 5.4.10.   | Gene expression study  | 196            |
| 5.5.      | Anti-oxidant property evaluation of nano formulations                              | 198            |
| 5.5.1.    | 2,2-Diphenyl-1-Picryl Hydrazine (DPPH) Scavenging activity                         | 198            |
| <b>6.</b> | <b>Summary and Conclusions</b>   | <b>199-201</b> |
| <b>7.</b> | <b>Recommendations</b>   | <b>203-209</b> |
| <b>8.</b> | <b>References</b>  | <b>211-238</b> |
|           | <b>Presentations</b>   |                |
|           | <b>Publications</b>  |                |
|           | <b>Appendix</b>  |                |

---



## LIST OF FIGURES

| <i>Figure No.</i> | <i>Title</i>  | <i>Page No.</i> |
|-------------------|---|-----------------|
| 2.4.1.            | Showing the structure of chitosan   | 42              |
| 2.7.1.            | Showing structure of enol form of curcumin  | 48              |
| 2.8.1.            | Showing structure of epirubicin   | 50              |
| 3.2.1.            | Methods employed for the synthesis of different silica nanoparticles  | 55              |
| 3.2.2.            | Finely ground food-grade diatomaceous earth sample  | 56              |
| 3.2.3.            | Raw materials used for the synthesis of biogenic silica nanoparticles   | 58              |
| 3.2.4.            | Flow diagram of synthesis of biogenic silica particles from agricultural biomass  | 59              |
| 3.2.5.            | Showing (A) Untreated rice husk, (B) Acid leached and washed rice husk, (C) Dried acid pretreated rice husk, (D) Incomplete combustion of rice husk samples at incineration temperature below 200 °C showing presence of carbon and (E) Rice husk-derived silica obtained after controlled incineration | 60              |
| 4.1.1.            | Particle size intensity distribution curves related to variation of size of silica nanoparticles with milling time (h) and speed (rpm)  | 90              |
| 4.1.2.            | XRD spectrum of ball-milled diatomaceous earth-derived silica particles   | 91              |
| 4.1.3.            | (A), (B), and (C) show FESEM images of diatom frustules before ball-milling, (D) to (J) show FESEM images of diatom frustules after ball-milling and (L) shows EDAX spectrum of the area marked in (K)  | 91              |
| 4.1.4.            | CHNS analysis result of ball-milled diatomaceous earth-derived silica particles   | 94              |

---

|         |   |     |
|---------|---|-----|
| 4.1.5.  | Variation of zeta potential values in ball-milled (A and B) and unmilled samples (C)  | 94  |
| 4.1.6.  | FTIR spectrum of silica particles from diatomaceous earth   | 96  |
| 4.2.1.  | XRD spectrum of samples heated at different temperatures at constant time of combustion   | 98  |
| 4.2.2.  | XRD Spectrum of rice husk-derived silica samples subjected to different incineration periods at constant temperatures of incineration             | 99  |
| 4.2.3.  | XRD diffractogram of the sample showing transition from amorphous to crystalline phase with an increase in incineration temperature               | 100 |
| 4.2.4.  | FESEM images of silica particles from Indian goose grass (A) at magnification of 75K X and (B) 200K X   | 101 |
| 4.2.5.  | FESEM images of silica particles from coffee husk   | 101 |
| 4.2.6.  | FESEM images of silica particles from corn husk   | 102 |
| 4.2.7.  | FESEM images of silica particles from rice husk   | 102 |
| 4.2.8.  | TEM analysis images of rice husk derived silica particles   | 103 |
| 4.2.9.  | EDAX analysis result of samples from (A) rice husk, (B) Indian goose grass, (C) sugarcane bagasse, (D) corn husk and (E) coffee husk respectively | 103 |
| 4.2.10. | CHNS analysis result of rice husk-derived silica particles  | 106 |
| 4.2.11. | Adsorption-desorption isotherm of silica nano particles from rice husk showing type IV pattern characteristic of mesoporous particles             | 107 |
| 4.2.12. | Showing correlation between particle size of end-product with incineration temperature and time   | 109 |

---



---

|         |  |     |
|---------|--|-----|
| 4.2.13. | FTIR spectrum of (A) rice husk-derived silica particles (B) chemically synthesized and biogenic silica particles and (C) silica particles derived from Indian goose grass, sugarcane bagasse, corn husk and coffee husk respectively | 110 |
| 4.2.14. | XRF spectrum of rice husk derived silica nanoparticles   | 111 |
| 4.2.15. | Zeta potential analysis report of (A) rice husk, (B) Indian goose grass, (C) corn husk, (D) sugarcane bagasse and (E) coffee husk respectively   | 113 |
| 4.3.1.  | FTIR spectrum of surface modified (A) and drug loaded silica nanoparticles (B) and (C)   | 115 |
| 4.3.2.  | Thermogravimetric analysis curve to assess drug loading into rice husk-derived silica nanoparticles  | 118 |
| 4.4.1.  | Showing release of curcumin from unmodified silica nanoparticles and control at pH 5.4 and 7.4   | 120 |
| 4.4.2.  | Showing release of curcumin from polyethylene glycolated silica nanoparticles and control at pH 5.4 and 7.4  | 121 |
| 4.4.3.  | Showing release of curcumin from polyethylene glycolated, chitosan capped silica nanoparticles and control at pH 5.4 and 7.4   | 121 |
| 4.4.4.  | Showing mechanism of pH-responsive drug release from chitosan capped nano-formulation  | 122 |
| 4.4.5.  | Showing release of epirubicin from unmodified silica nanoparticles and control at pH 5.4 and 7.4   | 123 |
| 4.4.6.  | Showing release of epirubicin from polyethylene glycolated silica nanoparticles and control at pH 5.4 and 7.4  | 123 |
| 4.4.7.  | Showing release of epirubicin from polyethylene glycolated, chitosan capped silica nanoparticles and control at pH 5.4 and 7.4   | 124 |

---

---

|         |  |     |
|---------|--|-----|
| 4.5.1.  | Images (A), (B), (C) and (D) showing degradation behaviour of biogenic silica as observed employing FESEM technique  | 125 |
| 4.5.2.  | Showing the viability of HEK 293 and HeLa cells treated with different doses of biogenic silica nano particles from rice husk  | 126 |
| 4.5.3.  | Images (A), (B) and (C) showing HeLa cells after 24, 48 and 72 h of incubation in PEG-Modified chitosan capped drug bound biogenic silica nano-formulation respectively  | 126 |
| 4.5.4.  | Images (A), (B) and (C) showing HEK293 cells after 24, 48 and 72 h of incubation in PEG-Modified chitosan capped drug bound biogenic silica nano-formulation respectively  | 127 |
| 4.5.5.  | Dose response study of curcumin  | 127 |
| 4.5.6.  | Dose response study of epirubicin  | 128 |
| 4.5.7.  | Assessment of Cytoprotection against cypermethrin induced toxicity   | 129 |
| 4.5.8.  | Assessment of glutathione peroxidase activity  | 129 |
| 4.5.9.  | Assessment of superoxide dismutase activity  | 130 |
| 4.5.10. | Assessment of catalase activity  | 130 |
| 4.5.11. | Assessment of lipid peroxidation inhibition activity   | 131 |
| 4.5.12. | Assessment of curcumin uptake by cells   | 131 |
| 4.5.13. | Showing HeLa cells stained with DAPI which were subjected to treatment to observe for any alterations in its nuclear morphology (A-Normal control, B-biogenic silica exposed at 200µg/mL concentration, C-treated with 200µg/mL PEG coated, chitosan capped biogenic silica, D-Biogenic silica bound with drug, E- PEG modified biogenic silica bound with drug and F-PEG modified chitosan capped drug bound biogenic silica) | 132 |

---

---

|         |  |     |
|---------|--|-----|
| 4.5.14. | Showing stages of apoptosis  | 133 |
| 4.5.15. | Showing stages of apoptosis where (A) shows normal cell, white arrows in (B) showing visible signs of chromatin condensation and nuclear membrane blebs while the white arrows in (C) showing signs of final stage apoptosis   | 134 |
| 4.5.16  | Evaluation of ROS generation using flow cytometry analysis. (A) Showing ROS production in HeLa cells subjected to treatment with different nano-formulations, (B1 and B2) Showing dot-plot and population distribution of samples treated with different nano-formulations | 135 |
| 4.5.17. | Analysis of mitochondrial membrane potential. (i) Fluorescence pattern obtained using flow cytometry analysis of HeLa cells subjected to treatment with different nano-formulations (ii) Red/green intensity ratio of samples A, B and C                                   | 138 |
| 4.5.18. | Expression of Bcl2 gene  | 139 |
| 4.5.19. | Expression of Bax gene   | 140 |
| 4.5.20. | Caspase 3 expression in cells (A) in set of studies using curcumin, (B) in set of studies using epirubicin drugs   | 140 |
| 4.6.1.  | 2,2-Diphenyl-1-Picryl Hydrazine (DPPH) Scavenging activity   | 142 |
| 5.4.1.  | Showing mechanism of Enhanced Permeation and Retention (EPR) effect for passive targeting of active pharmaceuticals in solid tumour cells  | 192 |
| 5.4.2.  | Showing predicted mechanism of induction of apoptosis in the cells treated with different nano-formulations  | 196 |

---



## LIST OF TABLES

| <i>Table No.</i> | <i>Title</i>  | <i>Page No.</i> |
|------------------|---|-----------------|
| 3.2.1.           | Ball milling parameters varied in the study for optimization of production  | 57              |
| 3.2.2.           | Optimization of silica nanoparticle synthesis in terms of acid pretreatment, incineration temperature and time    | 61              |
| 3.3.1.           | Characterization techniques used in the study   | 63              |
| 3.5.1.           | Showing the different concentrations of curcumin added onto fixed quantity of drug carrier-silica nano particles. | 67              |
| 3.7.1.           | Primer sequences used for gene expression studies   | 87              |
| 4.1.1.           | Variation of size of silica particles with milling time and speed   | 89              |
| 4.1.2.           | Nitrogen sorption analysis of surface area and pore parameters of silica particles from diatomaceous earth        | 95              |
| 4.1.3.           | Chemical interaction as seen from FTIR spectrum of diatomaceous earth derived silica sample                       | 96              |
| 4.1.4.           | XRF analysis of silica particles derived from diatomaceous earth  | 96              |
| 4.2.1.           | Yield of silica particles from different raw materials used   | 97              |
| 4.2.2.           | Nitrogen sorption evaluation of silica particles derived from different agricultural biomass                      | 107             |
| 4.2.3.           | Nitrogen sorption evaluation of rice husk-derived silica particles as a function of acid pretreatment             | 108             |

---

|        |  |     |
|--------|--|-----|
| 4.2.4. | Variation of particle size of rice husk-derived silica particles as a function of incineration temperature and incineration time   | 108 |
| 4.2.5. | Variation of particle size of rice husk-derived silica particles as a function of incineration temperature and acid pretreatment   | 108 |
| 4.2.6. | Chemical interaction as seen from FTIR spectrum of rice husk derived silica sample   | 111 |
| 4.2.7. | XRF analysis of silica particles derived from rice husk  | 112 |
| 4.2.8. | XRF analysis of silica particles derived from agricultural biomass   | 112 |
| 4.2.9. | Zeta potential values of silica samples from different raw materials used in the study   | 112 |
| 4.3.1. | Showing different interactions as observed in the FTIR spectra above   | 116 |
| 4.3.2. | Evaluation of curcumin loading using TGA   | 119 |
| 4.3.3. | Results of spectrophotometric analysis of drug loading   | 119 |
| 4.5.1. | Variation in IC <sub>50</sub> values of curcumin and epirubicin as a function of silica encapsulation for HeLa cells under incubation in test samples for a period of 48 h | 128 |

---

## ABSTRACT

---

Application of nanoparticles as drug carriers in chemotherapy has gained much importance over the past few years for its ability to carry the payload to the specific site of action, which will greatly reduce drug dosage and frequency of administration. It also reduces toxicity to healthy cells thereby increasing the overall efficiency of the therapy. This study attempted to manufacture amorphous silica nanoparticles from otherwise discarded, yet easily available agricultural waste products, employing facile methods utilizing least toxic reagents and requiring minimal processing steps. The efficiency of silica nanoparticles derived from biogenic sources like rice husk were tested for use as a drug carrier in curcumin and epirubicin based formulations for chemotherapy of cancer. Silica nanoparticles of size ~50 nm was synthesized by pressurized acid leaching and controlled incineration techniques. Physicochemical characterization of these particles was carried out. Drug loading and cytostatic effects of the drug loaded nano-formulation on cervical cancer (HeLa) cells were also studied. Biocompatibility tests indicated high compatibility of these particles to normal human embryonic cell lines (HEK293). Loading the drug on to silica nanoparticles enhanced its cytostatic effect as revealed from MTT assay, enhanced expression of the pro-apoptotic gene (Bax) and the suppression of anti-apoptotic gene (Bcl2). Caspase-3 mediated apoptotic pathways were also modulated. Cancer cells treated with drug loaded nano-formulations also resulted in alterations in its nuclear morphology coupled with generation of ROS and fluctuations in mitochondrial membrane potential. The results obtained from cellular uptake studies as well as antioxidant assays indicated enhancement of the therapeutic efficiency of the drug when loaded onto silica nanoparticles. Studies also showed that drug conjugated to the mesoporous silica nanoparticles derived from agricultural biomass like rice husk could still maintain its activity and that it could enhance drug bioavailability. This study resulted in facile

synthesis of amorphous, mesoporous silica nanoparticles from biogenic sources which would aid in value-addition of underexploited agricultural by-products. Considering its high biocompatibility, these biogenic nanoparticles could find other medical applications, as in tissue engineering, enzyme immobilization, dental and bone implants and fillers. Its unique physical and chemical properties like inertness and stability at higher temperatures makes them useful for non-medical applications as food additives and bulking agents, in cement industry, water purification systems etc. The high biocompatibility of these biogenic silica nanoparticles could make them a least toxic substitute to those synthesized by conventional methods. Further improvements to these biogenic nanoparticles could in future be helpful for substantial reduction in treatment costs for different ailments, especially cancer.

**Key words:** Agricultural biomass, rice husk, biogenic nanoparticles, amorphous silica, drug carrier, biocompatibility.



ഔഷധവാഹികൾ ഉപയോഗിച്ചുള്ള ചികിത്സാരീതിയിൽ കൃത്രിമ നാനോകണങ്ങൾക്കുപകരം നെല്ലിന്റെയും മറ്റും ഉമി, കരിമ്പിൻ തണ്ടിന്റെ അവശിഷ്ടങ്ങൾ തുടങ്ങിയ ചിലവുകുറഞ്ഞ ജൈവവിഭവങ്ങളിൽനിന്നും സുഗമമായ രീതിയിൽ വേർതിരിച്ചെടുക്കാവുന്ന ക്ഷീപ്രപരിപാലിത സിലിക്കയുടെ ഉപയോഗത്തെയാണ് ഇവിടെ പഠനവിധേയമാക്കിയിരിക്കുന്നത്. ഈ ചികിത്സാരീതിവഴി രോഗബാധിത ഭാഗങ്ങളിൽ പ്രത്യേകമായി ഔഷധത്തെ എത്തിയ്ക്കുന്നതിലൂടെ അളവിൽക്കൂടുതലുള്ള മരുന്നപയോഗത്തെ കുറച്ച് രോഗമില്ലാത്ത കോശങ്ങളുടെ നാശത്തെ തടയാനും കഴിയും. കൂടാതെ, കാർഷിക ജൈവ അവശിഷ്ടങ്ങളുടെ മൂല്യവർദ്ധനവിനും, അവയുടെ അശാസ്ത്രീയമായ കൈകാര്യം ചെയ്തൽ വഴി ഉണ്ടായേക്കാവുന്ന പരിസ്ഥിതി ദോഷത്തെ കുറയ്ക്കാനും സാധിക്കും. സമ്മർദ്ദതന്ത്രം ഉപയോഗിച്ചും, അമ്ലശോധന നടത്തിയും നിയന്ത്രിത ദഹനം വഴി നിർമ്മിച്ച ഈ സൂക്ഷ്മസൂക്ഷിര കണങ്ങളുടെ ഭൗതികവും രാസികവുമായ സ്വഭാവനിർണ്ണയം സൂചിപ്പിക്കുന്നത് ഇവയെ ഔഷധവാഹികളായി ഉപയോഗപ്പെടുത്താം എന്നതാണ്. ഔഷധധാരികളായ ഈ കണങ്ങൾക്ക് ഗർഭാശയമുഖ അർബുദ കോശങ്ങളെ നശിപ്പിക്കാനും, ആരോഗ്യമുള്ള ഭ്രൂണകോശങ്ങളെ നിലനിർത്താനും ശേഷിയുള്ളതായി ജൈവ അനുഗുണ പഠനങ്ങൾ തെളിയിക്കുന്നു. ഈ ജൈവസിലിക്കാകണങ്ങളിൽമരുന്നൾക്കൊള്ളിക്കുന്നതുവഴി ഔഷധത്തിന്റെ കാര്യക്ഷമത വർദ്ധിക്കുന്നതായി കോശജീവനസാമർത്ഥ്യപരിശോധന തെളിയിക്കുന്നു. കോശശിഥിലീകരണ അനുകൂല പാരമ്പര്യഏകകമായ Bax-ന്റെ വർദ്ധിത പ്രകടനവും, കോശശിഥിലീകരണ പ്രതികൂല പാരമ്പര്യ ഏകകമായ, Bcl2- ന്റെ അമർച്ചയും ഇതുതന്നെയാണ് വ്യക്തമാക്കുന്നത്. കൂടാതെ, ഇവ caspase-3 വഴിയുള്ള കോശശിഥിലീകരണ സഞ്ചാരപഥത്തെ ക്രമീകരിക്കുന്നതായും കാണപ്പെടുന്നു. മരുന്നൾക്കൊണ്ട ഈ കണങ്ങൾ പ്രയോഗിക്കപ്പെട്ട അർബുദകോശങ്ങളുടെ രൂപഘടനയിൽ വ്യത്യാസവും, സൂത്രകണികാകോശസ്റ്ററേഷിക്ക് വ്യതിയാനവും, പ്രതികരണക്ഷമമായ ഓക്സിജൻ ഗണം ഉൽപന്നമായതായും കണ്ടെത്താനായി. കോശ-ആഗീരണ പഠനങ്ങളും, ആന്റി-ഓക്സിഡന്റ് പരിശോധനയും ഔഷധധാരികൾ ആയ സിലിക്കാകണങ്ങൾക്ക് ഔഷധഗുണത്തെ നിലനിർത്താനും, അതിന്റെ വീര്യത്തെ വർദ്ധിപ്പിക്കാനും ശേഷി ഉണ്ടെന്നു സൂചന നൽകുന്നു. ഇവയുടെ ഉയർന്ന ജൈവ അനുയോജ്യത ഇവയെ സംയുക്തകോശയന്ത്രശാസ്ത്രം, ദീപനരസസ്തംഭനതന്ത്രം, ദന്ത ഇസ്സാൻറുകൾ, അസ്ഥികളിലെ സൂക്ഷിരങ്ങൾ അടയ്ക്കാനുള്ള വസ്തുക്കൾ എന്നിവയുടെ

നിർമ്മാണത്തിലേക്കും ഉപയോഗപ്രദമാക്കുന്നു. നിഷ്ഠിയത, ഉയർന്ന ഊഷ്മാവിലുള്ള സ്ഥിരത എന്നീ സ്വഭാവങ്ങൾ ഇവയെ ഭക്ഷ്യസംസ്കരണം, ജലശുദ്ധീകരണം, കൂട്ടുകുമാര്യ വ്യവസായം തുടങ്ങിയ മേഖലകളിലേക്കും ഉപയോഗപ്പെടുത്താം.

**താഴെക്കാൽ വാക്കുകൾ:** കാർഷിക ജൈവവസ്തുക്കൾ, നെല്ലിന്റെ ഉമി, ജൈവനാനോകണങ്ങൾ, ക്ഷീരപരിപാലിപ്പാത്ത സിലിക്ക, ഔഷധവാഹി, ജൈവ അനുഗ്രണം.

---

# INTRODUCTION

---

## **1.1. Nanoparticle-based drug carrier system**

Nanotechnology involves the manipulation, engineering and manufacturing of materials at the level of atoms and molecules. The size of nanoparticle structures range of 1-100 nm in at least one dimension and are produced using two common approaches- top-down or bottom-up techniques of engineering individual components.

Nanoparticles have received wide acceptance in different fields of science and technology, medicine and pharmaceutical industries primarily due to peculiarity in its physical and chemical properties as well as its responses in biological environment. Reduced size of nanoparticles as compared to the bulk material from which it is derived results in variations in the internal and surface energies. A decrease in particle size concertededly results in the reduction in number of internal atoms which is accompanied by a reduction in internal energy. A reduction in internal energy can be expected to compensate for an increment in surface energy during generation of nanoparticles. In cases where extension atoms are unavailable for compensating for energy variations, the surface energy of nanoparticles are higher and can result in special characteristics different from the parent material.

In pharmaceutical industry, nanotechnology is primarily utilized for applications involving its use as drug delivery vectors which aid in the improvement of pharmacokinetic and

pharmacodynamic properties of drugs, especially hydrophobic ones. It also finds use as for site-specific drug delivery. It could facilitate easier penetration across biological membranes and could also be employed as therapeutic agent combined with diagnostic tools (theragnostic) which can help in monitoring real-time effect of the treatment <sup>1</sup>. Drawbacks of drug toxicity, non-specific interactions, multiple dosage requirements, solubility issues, rapid clearance and low half-lives, generation of toxic metabolites and physicochemical instabilities of classical drug delivery systems have led researchers to look for better alternatives, and these investigations have resulted in employing particulate systems for various drug delivery applications. Use of micro- and nano- particles as drug delivery vectors have resulted in improvement in therapeutic outputs of pharmaceuticals. In addition to acting as vehicles for the transport and delivery of payload, particulate systems also provide protection against chemical, physical and biological degradation to the active pharmaceutical ingredient which aids in enhancement of its circulation half-life. Earlier, patients had to consume elevated levels of drugs for it to exert desired therapeutic effect considering its depreciating concentrations before reaching the target site. On the other hand, consumption of several drugs resulted in unprecedented side effects leading to additional complications which would demand the clinician to recommend alternative medication, ultimately prolonging the whole course of treatment. These effects may vary from person-to-person, ranging from sleep disturbances, fatigue, edema, diarrhea, delirium to anemia, fertility issues, alopecia to thrombocytopenia and many more. Low drug bioavailability is one of the major concerns faced by conventional chemotherapy. It is also

fraught with the problem of non-specificity, leading to unprecedented side effects <sup>2</sup>. This could be very demanding to patients, depending on multiple factors like overall health and pathophysiology, disease condition and its extent of spreading, recurrence, other infections and complications. Use of particulate drug delivery systems address problems related to solubility of drugs, off-targeted effects, premature drug release, circulation half-lives and in several cases combine the function of delivery vector as well as disease diagnostic tool which aids in real time monitoring of delivery system as well as disease regression.

Low bioavailability of drug demands the patient to consume higher doses of the therapeutic agent so as to address the dosage demand for the medication which may further lead to overdosing of the drug and complications that may arise from it <sup>3-6</sup>. All these situation calls for efforts to look for ways to solve these immediate problems, where the relevance of drug carriers lies. A drug carrier is essentially a substrate capable of incorporating a known amount of therapeutic agent, to act as a vehicle for its delivery to the site of interest.

Carrier mediated drug delivery aids in improving drug selectivity and bioavailability. This adds to the safety of drug administration thereby enhancing its effectiveness. The release kinetics of the medicament can be controlled as per the dosage demand adding to its advantages. The surface-tuning and modification of the drug carriers can be done to vary different properties thereby imparting peculiar traits to the carrier system. Accordingly, various pharmacodynamic properties of the drug can be altered for targeted

release, transversing membrane barriers, residence time in physiological circulation and interaction with different metabolic pathways. Additionally, drug carriers also provide protection to the drug against undesirable degradation. Over the past few decades nanotechnology has been gaining widespread attention in carrier-mediated chemotherapy due to its high surface area, stability, high cargo-loading capacity, surface tunability, which also allow them to be applied both as a therapeutic as well as diagnostic tool, which opens countless possibilities of designs efficient enough to override many handicaps of conventional chemotherapy and helps in the early detection of tumors, which is inevitable for enhancement of the success rates of cancer treatment <sup>7,8</sup>.

Increasing cancer cases worldwide demand for better and cheap treatment options. Particulate drug delivery systems exploit peculiar features of the tumour microenvironment for carrying out targeted delivery of therapeutics. Naturally derived compounds like curcumin, a polyphenolic compound have shown to exhibit antioxidant, immunomodulatory <sup>9</sup>, anti-hyperalgesic <sup>10</sup>, anti-inflammatory properties with significant activity against variety of cancer <sup>11</sup>. However, innate instability and hydrophobicity have resulted in looking for structural analogues with better characteristics and employing carrier system for improvement in pharmaceutical activity.

Amalgamation of properties of nanoparticulate drug delivery agents with diagnostic potential have resulted in generation of efficient ‘theragnostic’ devices. Advancement in the field of nanomedicine has provided us with a wide array of nanoparticles to choose from,

however there is also a subsequent rise in the concern over the use of several otherwise efficient nanoparticles *in vivo*. Researchers are still uncertain over the predictability of effects of these particles in the physiological milieu. This has made scientists delve into finding answers to problems concerning the use of synthetic nanoparticles and fate of the carriers in physiological system and its toxic responses. Many artificially engineered nanoparticles involve the use of harmful chemicals, if not one, may be several of it. In this regard, facile methods of synthesis involving nature-derived nanoparticles employing use of environmental-friendly reagents, which generates non-toxic products and by-products are of special interest to researchers. The synthesis methods come with minimal processing steps unlike that in the case of artificially engineered particles. The *in vivo* effects of such particles are an easy forecast and comes with the adjective of being a sustainable yet efficient alternative for artificial synthesis procedures. Of particular interest is biogenic mesoporous silica nanoparticles, the starting materials for its synthesis are easily available. The procedures for its synthesis are simple and the particles have shown to have excellent biocompatibility. These particles can also be subjected to surface modification which aids in its use for varied application. Studies have shown the particles to have high adsorption capacity and it escapes immunorecognition for prolonged periods of time. Upon direction, these particles are also capable of transversing across subcellular compartments. In nature, with the exception of certain rocks, silica mostly occur in amorphous opaline form, which is found to be less toxic than its crystalline counterpart<sup>12</sup>.

A fool-proof system for efficient drug delivery requires intensive studies to confirm its efficiency and safety of use which can be a costly affair which justifies the steepening cost of treatment. However, this increase in treatment costs can be amortized by the use of particles that are synthesized sustainably using nature- derived components, which can also greatly reduce the demand on harmful chemicals, sophisticated production strategies and technical know-how. Such an insight called for studies on application of particles derived from agricultural biomass for drug loading and delivery. This study focusses on the synthesis of silica nanoparticles from different biogenic sources, characterization of its different physical and chemical properties, investigating its efficiency in overriding major handicaps like drug non-selectivity. The study also examines the effect of nano-formulations on its impact on the bioavailability of the drug.

Efficiency of chemotherapy is ultimately determined by the achievement of desired level of drug at the specific site of action in the body and maintaining its level over the therapeutic window. The concept of nanoparticle-mediated drug delivery envisages the ability of transversing across biological membrane barriers, owing to the submicron size of the particles, longevity in circulation and possibility of surface functionalization as distinctive advantages in targeted delivery to cellular and sub-cellular locations and controlled release of drugs<sup>13</sup>. Surface modification with compounds like poly ethylene glycol (PEG) enhances the circulation properties of the drug carrier particles in the bloodstream by reducing its interaction with the immune system, opsonins, leukocytes and erythrocytes, which can also



help prevent hemolysis of cells<sup>14-16</sup>. Chitosan is a naturally occurring polysaccharide employed in the pH-responsive release of pharmaceuticals, wherein the compound undergoes structural disintegration in highly acidic conditions, resulting in the elution of the payload to the microenvironment. Targeted delivery of chemotherapeutics mainly utilizes the overexpression of several surface receptors in cancer cells or in certain cases, passive delivery of drugs owing to the enhanced uptake and retention of therapeutics in cancer cells occurring due to anomaly in its cellular biochemistry.

## **1.2. Nanoparticles from biogenic sources**

Agricultural activities are essential to feed the hunger of mankind upon which his very survival depends. By-products obtained from such activities are put to use for different purposes like use as fuel, fodder and feed. Although a proportion of the by-products are utilized for different purposes, a significant majority of it remain unexploited, the discarding of which if done unscientifically can pose severe threat to the environment as well as to other life forms. Proper integrated management of disposal of these by-products and its utilization as raw materials for large-scale production of different value-added products are some of the strategies open to work for effective exploitation of these materials. Several research have been done in this regard and have devised use of by-products for use in enzyme technology, finding application as adsorbents, in fermentation technology for the production of economically viable products like acetic acid, alcohol, enzymes, in medical field for use in tissue and bone engineering as well as in electrochemistry and material science.

Another novel branch of science that involves the utilization of these by-products is Nanotechnology, which involves the synthesis of different nanoparticles for use in application in different fields of life. One of the major advantages of using agricultural by-products in the generation and application of nanoparticles is its environmental-friendly strategy, as compared to bottom-up approaches, which mostly utilize hazardous chemicals, which would also result in toxic end-products.

Wheat, maize, rice, millets and pulses are the chief food crops grown in India. According to 4<sup>th</sup> Advance Estimates of the Directorate of Economics & Statistics, DA&FW, the year 2020-21 witnessed a yield of 2386 kg/hectare of food grains over a cultivation area of 129.34 million hectares, of which total rice production accounted for 2713 kg/hectare over the time period within an area of 45.07 million hectares coming next only to total wheat produced (3464 kg/hectare over 31.61 million hectares). Phytoliths are microscopic structures seen in different monocots, dicots, sphenophytes and conifers which accumulate silica in its hydrated form <sup>17</sup>. With rice being the staple food of Kerala, a large number of rice-milling centers are available, resulting in generation of large quantities of by-products chiefly rice husk, which is a rich source of silica. The silica is formed as a result of different polymerization reactions and is present in its amorphous form, which is found to be the least toxic form in comparison to its crystalline counterparts <sup>18</sup>. The major organic constituents of rice husk are ~38 % cellulose, 20 % hemicellulose, ~22 % lignin and 14-20 % inorganic constituents like silicon dioxide <sup>19</sup>. Silicon being an abundant

element on earth's crust and oldest natural bio-skeleton (as silicon dioxide) finds biomedical application in its oxide form. The ones with a long-range order of arrangement of atoms result in the generation of crystalline silica while those that have a short-range order forms amorphous silica, with porous structures of size less than 2 nm, between 2-50 nm and above 50 nm respectively called micro-, meso- and macro-porous particles. The mesoporous silica particles owing to its large pore volumes and surface area also have tunable pore-sizes finding them applicable as drug delivery agents. They are also known to be physically and chemically inert, rendering high stability. High biocompatibility further adds to its advantages for use in *in vivo* applications as theragnostic tools, dental fillers and implants. It is also known to provide health benefits for maintenance and functioning of hair, nails and bone and is also used as a dietary supplement to check trace mineral deficiency <sup>20</sup>. Biogenic polyphosphates and biogenic silica seen in several deep ocean sponges and diatoms are known to elicit cytokines and are known to play major role in hydroxyapatite formation involved in bone mineralization, which are harnessed for applications in biomimetic fabrication of bone, employing 3D printing techniques <sup>21</sup>.

Of the different methods of synthesis of biogenic silica nanoparticles like microwave hydrothermal process, fluidized bed and flame method, precipitation and non-isothermal methods, acid pretreatment under pressurized conditions followed by controlled incineration has been employed in this study. This method employs the use of least toxic, least polluting components, less complicated

processes involving minimal pretreatment of raw material, which also has high scalability. Development of nanoparticles from biogenic sources are an attractive perspective in the wake of complexity in understanding the fate of artificially engineered nanoparticle-based drug carrier and its polymeric constituents in the physiological milieu, together with the risk of toxicity associated with the residual organic solvents. Synthetic silica which finds major applications in pharmaceutical as well as agrochemical industries are chiefly synthesized by methods involving bottom-up approaches, which are complex and utilizes non-renewable precursors which can result in the subsequent production of several hazardous by-products like ferrosilicon (FeSi) and silicon tetrachloride (SiCl<sub>4</sub>) that also cause severe health hazards and air pollution<sup>22</sup>.

Liposomes, lipid nano-capsules, micelles and polymer nanoparticles are commonly used organic nano-carriers owing to its ability to easily solubilize and conjugate hydrophobic drug into hydrophobic cores but are bound to have physicochemical instability and proneness to unprecedented drug leakage<sup>23</sup>. However, inorganic nano-carriers employing mesoporous silica nanoparticles and carbon nanomaterials have exceptional physicochemical stability and tunable morphologies<sup>24-27</sup>.

### **1.3. Soaring incidence of cancer on global scale**

Recently, with the number of people diagnosed with cancer reporting a surge at an alarming level, inaccessibility to modern efficient cancer treatment knocks a heavy toll on mortality. Together

with patient variability, additional disease history complicates and further add hurdles to efficiency of treatment. Awareness and emphasis on diagnosis at earlier stages of disease and pocket-friendly treatment regimens are to be developed to reduce mortality rates. New age treatment options which are proven to be highly efficient like epigenetic drugs, precision medicine and chimeric antigen receptor base therapy are not a common man's piece of cake.

World Health Organization has categorized cancer as the second major cause of death globally, second only to cardiovascular diseases, and the cases are on rise. Cancer is the uncontrolled proliferation and growth of cells which could be caused due to composite reasons ranging from exposure to harmful radiations and toxins to use of tobacco, poor diet, lack of exercise, obesity and other life style disorders<sup>28</sup>. Talking in terms of gender, cancer of the breast is most prevalent among female population and that of prostate in males, in addition to lung and colon cancers which are common to both<sup>29</sup>. Global Cancer Incidence, Mortality And Prevalence (GLOBOCON) foresees an increment in cancer incidences from 18.1 million cases in 2018 to about 27.5 million (61.7 % rise) by the year 2040, with the death tolls likely to remain high mainly due to inaccessibility to early diagnosis and screening to efficient treatment<sup>28</sup>. There are a large variety of treatment methods to choose to suit with the type of cancer, and which are used either prescribed alone or in combination with other regimens. It may vary from surgical removal of tumorous tissues to radiation therapy, hormonal therapy to bone marrow transplantation to name a few. The increasing occurrence of cancer on a global-scale in

spite of the multitude treatment choices presses on the importance to turn our attention to check into the bottlenecks of the commonly employed treatment options and improvement of the same.

The physician decides on the type of treatment for a patient mainly considering factors like type, site, spread and occurrence, age and the health condition, with chemotherapy still being the most widely used, which is sometimes accompanied with other treatment forms for better results<sup>30</sup>. But most of the treatment options come with side effects. Though effects may vary from person-to-person, it may range from sleep disturbances, fatigue, edema, diarrhea, delirium to anemia, fertility issues, alopecia to thrombocytopenia as mentioned before. The problem of developing multiple-drug resistance is yet another complication that may arise from over-dosing<sup>3-6</sup>. All these situation calls for efforts to look for ways to solve these immediate problems and development of efficient drug delivery vectors is one of the many solutions. A drug carrier is vehicle that can act as a substrate to enable conjugation of a known amount of payload, capable of its delivery and if targeted can help release the drug at the site of interest.

Drug delivery system based on nanoparticles has been evolving as a major technological improvement attributed to the high particle stability, high cargo-loading capacity, ability to incorporate myriad varieties of drugs, hydrophobic and hydrophilic drugs, ability to cross membrane barriers and suitability to application through different routes of administration permitting controlled release of active pharmaceutical ingredient facilitating reduction in dosage and

frequency thereby reducing chances of drug overdosing and associated complications <sup>8</sup>.

This study also investigates the applicability of using silica nanoparticles obtained from natural sources as a drug carrier using curcumin as a model chemotherapeutic agent. Curcumin which is extracted from the rhizomes of *Curcuma longa* is a natural hydrophobic polyphenol possessing the ability to cross the blood brain barrier and has neuroprotective effect. It also exhibits anti-inflammatory activity. It is also reported to reduce and inhibit the proliferation of cancer cells. In spite of the benefits, the compound has poor aqueous solubility, hence low bioavailability and is rapidly cleared from circulation in addition to its low stability. All of these factors altogether reduce its therapeutic potential to a great extent. Several nanoparticle-based systems have been studied to improve its clinical application. Here, we used silica nanoparticles of biogenic origin to improve the qualities of curcumin to be used as a therapeutic agent against cancer. To the best of knowledge this is the first of its kind of work to report conjugation of surface modified, rice husk derived silica nanoparticle with natural potent anti-cancer agent, curcumin, impact on drug bioavailability, release pattern and evaluation of cellular effects. The studies were also replicated with a commonly employed hydrophilic synthetic drug, epirubicin for different comparative studies. The study can in the future be translated into developing new drug-carrier systems that can effectively conjugate drug, aid in targeted drug delivery and which can ultimately

reduce the cost of cancer treatment using highly biocompatible nanocarriers like biogenic silica.

#### **1.4. Objectives of the research work**

The ultimate aim of this study was to synthesize mesoporous silica nanoparticles from biogenic sources employing simple, economically viable, scalable process utilizing least toxic reagents and minimal pretreatment and processing steps from easily available raw materials and to check on its efficiency for biomedical applications.

Concisely, attempts were done to:

- ◆ Manufacture/isolate biogenic silica nanoparticles that could be harnessed for drug delivery applications.
- ◆ Evaluation of physicochemical properties of the synthesized biogenic silica nanoparticles to check for its possible use as drug delivery vectors.
- ◆ Surface modification of the biogenic silica nanoparticles for incorporating additional functionalities like pH-responsive payload release.
- ◆ Analyze the drug release pattern from the synthesized biogenic silica nano-formulations and assess possible impact on drug activity up on conjugation with biogenic silica nanoparticle.
- ◆ Check biocompatibility and cellular interactions of the biogenic silica nano-formulations *in vitro*.



# REVIEW OF LITERATURE

---

A substance that exhibits physiological response once inside a biological system through modification of the functionality of its target can be generally referred to as a drug. Well-developed drugs have improved the healthcare standards, but myriad problems are associated with the use of chemical drugs in therapy. Reducing side effects, drug targeting, reducing multidrug resistance, drug over dosage etc. still remain as challenges before us. With the complexity of therapeutics increasing, adverse drug reactions (ADRs) continue to be a challenge in modern healthcare. The difficulty in drug targeting necessitates the administration of larger concentration of drugs. Of all the major causes of acute poisoning studied, drug overdosing stands out as the most prominent one. Past few years have recorded the levels of drug overdose in United States of America single-handedly grossing 4-5 million cases. Hence, development of systems for reducing the incidences of drug overdosing and the associated toxic side effects by focusing on directed drug delivery systems for effective delivery of therapeutic payload is one of the important priorities of biomedical researchers.

## **2.1. Drug delivery system**

A formulation or a tool that instigates the introduction of therapeutic component to the physiological system thereby enhancing its safety and efficiency of performance is considered as a drug delivery system (DDS) with fine control on the rate, location and

moment of release of the active ingredient <sup>31</sup>. DDS results in the administration of drug to the living system, followed by its release. The transport of the pharmaceutical to the site of action often requires the active pharmaceutical ingredient to pass through various biochemical barriers which may be systemic, microenvironment-based or cellular and sub cellular <sup>32</sup> to finally exert the therapeutic effect. Many a times, the therapeutic formulation in itself may act as the DDS as in the case with gene therapy and other controlled release drug formulations, while in certain instances may include vectors or devices used to incorporate and deliver drug to the site of interest to exert the desired therapeutic effect <sup>31</sup>. DDS is particularly helpful in the cases where the handling and dose control of potent drug is difficult, like administration to body cavities. The DDS aids in preserving the active pharmaceutical ingredient (API) against degradation at the site of administration or against environmental factors thereby imparting chemical stability. This can also improve bioavailability as well as storage stability.

Based on the type of disease, nature of the drug formulation and the therapeutic effect desired, several different anatomical routes of administration may be undertaken. While the susceptibility to digestion under severe acidic environment of stomach, variable rates of absorption and serum concentrations are the disadvantages of oral drug delivery, immune reactions, nerve injury, hematoma, leading to thrombophlebitis are complications of parenteral mode of administration. These led to the development of drug formulations with variable drug release profile to comply with the requirement of the

disease treatment, which controls the amount of drug available over a certain period, as with the cases of immediate release, delayed release, sustained release system. Drug delivery systems are also classified based on the action of the drug, whether systemic or localized, whether targeted or non-targeted, those with stimuli-responsive drug release mechanism and others driven by receptor-ligand interactions<sup>31</sup>.

### **2.1.1. Particulate drug delivery system**

Improvement in the field of particle based drug delivery system from mere scientific curiosities to areas of active research has led to their important applications in clinical medicine and pharmaceuticals<sup>33</sup>. They also favour ease of administration of the drug through different anatomical routes to suit its systemic or localized action<sup>33</sup>. Particulate drug delivery system chiefly includes micro- and nano- particles each of which possess distinctive physiological, anatomical and physicochemical properties<sup>33</sup>. An important aspect of particulate drug delivery agents is the surface area-to-volume ratio. Considering the particles to exist as spheres in a suspension, the surface area-to-volume ratio will be inversely proportional to radius of the particle, which means that compared to the bulk sample of similar volume the microparticles have higher surface area-to-volume ratio but only lesser than nanoparticles. As the particle radius decreases further, the ratio increases proportionately resulting in variable properties like increased chemical reactivity as compared to the bulk<sup>33</sup>. Some literature reported that nanoparticles are considered to be too small to cause vascular embolism which permits it to freely circulate in the system and its surface modification can further improve its safety as well as aid in

prolonging its residence time as per requirement <sup>33</sup>. Particulate DDS employs particles for the purpose of delivery of drug molecules to a particular target in the body and were devised initially for its use in diagnostic applications involving radioactive particles. Since the size of particles used are often less than 300  $\mu\text{m}$ , it is capable of being administered directly into the systemic circulation or to a particular target site in the body. Since in this system a close association of the drug and the carrier molecules occur, the release of the drug is dependent on several factors like the physicochemical properties of the drug in itself as well as its interaction with the carrier molecule, like its location in the delivery vector whether encapsulated or tagged onto its surface, the nature of the particle employed for drug conjugation, its size, density, the physical environmental factors like temperature, light, presence of enzymes, pH, presence of receptors, to name a few <sup>31</sup>.

Size also decides on the ability of the particles to cross various biological barriers permitting easy transit of nanoparticles as compared to microparticles <sup>33</sup>. The theory applies to cellular penetration, wherein particles of size up to 10  $\mu\text{m}$  are up taken by specialized cells called phagocytes by a process known as ‘phagocytosis’ <sup>34</sup>. ‘Pinocytosis’ is another cellular uptake mechanism which is exhibited by most cells and sub-micron sized particles find access into cells through this process which suggests that microparticles can only be delivered into phagocytic cells while nanoparticles can gain access to any type of cell <sup>33</sup>. The author also discusses that when sufficient local assemblage of particles occur, it could evoke acute inflammatory responses involving macrophages and neutrophils and after around 7-14 days chronic

inflammation is impacted involving lymphocytes and macrophages<sup>33</sup>, so evaluation of the biological responses to the particles before administering *in vivo* is essential. Based on the nature of nanocarrier and the type of cell other major endocytic internalization pathways like endocytosis is mediated by clathrin and caveolae as well as through the lipid-raft<sup>35</sup>. Particle heterogeneity, larger size and possibility of interference with various cellular pathways limits the use of microparticles from different biomedical applications,<sup>36</sup> while nanoparticle-based drug delivery systems, owing to its unique physical properties and chemical set up aids in better cellular uptake bypassing the drug efflux pumps have gained much importance over the past decades<sup>37,38</sup>.

### **2.1.2. Inorganic nanocarrier system**

Inorganic DDS are an important class of particulate DDS owing to its properties like high bio-tolerability, capacity to load drugs with different properties, high ion exchange capacity, high physiological stability, ease of availability for modifications to improve upon properties like drug payload, targeting<sup>39</sup> etc. Broadly classified into two categories- metallic nanoparticles like platinum, gold, silver and ceramic nanoparticles like silica, alumina based nanoparticles, quantum-dots etc. which have the ability to remain inert in the physiological system adds to its benefit as nanocarrier<sup>40</sup>. Metallic inorganic nanocarriers find special application for its ability of local heating owing to its metallic core, finding application in photodynamic therapy for healing various types of cancer<sup>41</sup>. Ceramic inorganic nanocarriers on the other hand may have a solid core as in

the case with several iron oxide based carriers, or may have a porous core as in the case with silica nanocarriers<sup>40</sup>. Innate non-toxic nature, high biocompatibility, tunability of particle and pore sizes, ordered hierarchical arrangement and pattern of molecules, selective functionalization of internal as well as external surfaces, ability for controlled release of drug, large surface area-to-volume ratio, which promotes efficient drug loading, thermal, mechanical, chemical and biological stability make mesoporous silica nanoparticle stand out from other polymer-based drug carriers<sup>42-48</sup>. Structural integrity of ceramic nanocarriers make them effective drug delivery vehicles as they resist particle swelling, which can prevent initial burst release of drug payloads in aqueous conditions, which is otherwise a common problem associated with polymer-based nanoparticle system<sup>49,50</sup>. Since the nanoparticles take longer times for degradation under the biological milieu it is often used for applications requiring prolonged controlled release of drugs,<sup>49,51</sup> as well as for bone-regenerative applications<sup>52</sup>. Hydrophilicity and low toxicity profile, resistance to microbial growth, degradation and better stability are other added advantages of inorganic nanoparticles<sup>47,53</sup>.

### **2.1.3. Mesoporous nanocarrier systems**

Mesoporous systems contain particles with a uniform array of various nano-channels<sup>54,55</sup> and pore-diameters in the range of 2-50 nm<sup>56</sup>. MCM-41, MCM-48 and SBA-15 have attracted much attention in this area as mesoporous particles possessing higher surface area and definitely ordered large pore-system<sup>57</sup>. The pore-size distribution,

large surface area and pore volumes find their applications in catalysis, particle separation and adsorption purposes<sup>54</sup>.

Mesoporous carrier systems are particularly useful for the controlled dissolution of pharmaceutical ingredient<sup>58</sup> and are accordingly categorized into drug-carrier system that aids in prolonged release<sup>59</sup>, release profile based on zero-order kinetics<sup>60</sup>, systems responsive to various stimuli like pH<sup>61</sup>, temperature<sup>62</sup>, light<sup>63</sup>, enzymes<sup>64</sup> and other biological stimuli<sup>65</sup> and it helps in the targeted delivery of poorly water soluble drugs<sup>66,67</sup>. The textural parameters of mesoporous materials prevents premature release of the drug and protects it from getting degraded before reaching the target site for action<sup>68,69</sup>.

#### **2.1.4. Mesoporous silica DDS**

Nano-silica finds application in a variety of fields like electronics, health and allied sectors, for use in chromatography, catalysis, in food industries as emulsifiers and stabilizers<sup>70-74</sup>. Mesoporous silica finds widespread applications in various walks of life owing to its unique physicochemical characteristics like higher surface area and pore-volume, tunable surface chemistry, biocompatibility, acceptable degradation profile inside living system, where it is more efficiently converted to absorbable monosilicic acid and due to its high drug loading capacity with ability to encapsulate a variety of payload from biologics to pesticides<sup>75,76</sup>. Considering the surface chemistry of mesoporous silica particles, the silanol (Si-OH) groups are responsible for imparting hydrophilic character to the

particle, the presence of which can be evaluated using Fourier Transform Infrared (FTIR) spectroscopic technique<sup>75,77</sup>. To meet up with its demand, large-scale production strategies were undertaken to produce nano-sized silica particles of varied sizes and shapes using different manufacturing methods utilizing vapour-phase reactions, sol-gel methods and processes involving thermal decomposition<sup>44,77,78</sup>. Even though chemical synthesis processes can yield silica particles of desired morphological traits, demand for large quantities of initial precursor, delayed reaction time, difficulty in completely removing solvents and high cost of production together with negative impact on ecosystem due to toxic end-products calls for the need to develop other sustainable methods of manufacture<sup>79</sup>.

#### **2.1.5. Biogenic silica-based DDS**

Conventional methods of synthesis of silica nanoparticles with reasonable levels of purity is a costly affair and attention has been directed to look into facile manufacturing methods which are reproducible, viable and produces high purity end products to put into different applications as in healthcare and semiconductor sectors<sup>79</sup>. Accordingly, studies were conducted on plausibility of deriving high-purity silica particles by value addition of agricultural by-products like rice and wheat husks, sugarcane bagasse which could otherwise pose a burden to farmers concerning its disposal and associated environmental hazards<sup>79</sup>. Milling industry by-products like rice husk is a rich source of silica in its amorphous form, which can be easily isolated by simple acid-leaching processes which also remove other metallic impurities, finally resulting in silica particles of high purity<sup>80,81</sup>. Of all the



agricultural biomass, rice husk is reported to contain levels higher than 95 % of silica and several production methods resulting in minimal impact on environmental health have been devised and used for sustainable production of silica particles <sup>79</sup>.

## **2.2. Physical and chemical characterization of nanoparticles**

In order to analyze the safety and efficiency of application of any nano-carrier, it is quintessential to characterize the particles before putting it to test under physiological conditions <sup>40</sup>. The interaction of nanocarriers with the biological system are greatly dependent on properties like particle morphology, size, shape, porosity, surface topography and associated zeta potential, interaction with the drug cargo, payload capacity, availability for surface modifications which is otherwise chiefly determined by the chemical set up of the particles and finally the cargo release profile from the carrier <sup>82</sup>. The sub-micron sized particle nature of nanoparticles require it to be characterized using sensitive equipment capable of detecting such small-sized particles <sup>82</sup>. The most common techniques used for nanoparticle characterization include Scanning Electron Microscopy (SEM), Dynamic Light Scattering (DLS), X-Ray diffraction (XRD), Fourier Transform Infrared Radiation spectroscopy (FTIR), zeta potential analyzer, liquid nitrogen porosimetry which aid in the analyses of particle morphology, particle aggregation, particle phase, chemical nature, surface charge, pore-size and pore-volume respectively <sup>40,83-87</sup>.

The physical and chemical characterization of the nanocarriers help determine the loading efficiency and interaction with the drug

cargo which can help in deriving methods to enhance the overall performance of the carriers. The usability of a nanocarrier depends to a great extent on the amount of drug that can be loaded. The quantity of drug payload in the carrier formulation can simply be evaluated by calculating the difference in the levels of drug added to the system and the levels of remnant pristine drug in the solution after incorporation into the carriers<sup>88</sup>. Drug release pattern is usually determined by first incubating the drug-loaded nanocarriers in a release medium with specific pH, maintained at specific temperature over a period of time and then analyzing the aliquots collected at predetermined time intervals using techniques like High Performance Liquid Chromatography (HPLC) or Ultra Violet (UV) spectroscopy and plotting the cumulative drug release curves over the period of time<sup>89</sup>. All these analyses help predict the interaction, metabolism, therapeutic efficiency, targeting and finally elimination of nanocarriers in biological settings<sup>40</sup>.

Pharmacokinetics is another important parameter that determines the *in vivo* fate of the drug-loaded nanocarrier. The term ‘pharmacokinetics’ refers to the effect that the body exerts on the drug system and so it is important to first have an idea of the pharmacokinetics of the carrier as well as the drug, ranging from the mode of administration, absorption into the blood-stream, distribution of the drug-carrier complex in the body, its metabolism, finally its elimination and clearance from the physiological system<sup>40</sup>. The drug first needs to be carried to the site of action and then is released in the microenvironment depending on several factors like pH, nature of

biological membrane, temperature, presence of ligand receptors, magnetic field and other chemical and physical interactions and the released drug is absorbed by the target tissue to exert its therapeutic effect. The drug absorption is greatly determined by its 'bioavailability', which is the extent to which the active pharmaceutical ingredient is available in unaltered form<sup>90</sup> at the target, to exerts its pharmacological effect based on the dosage form and properties of the drug-carrier system. Incorporation of drug to the carrier in a bioavailable form results in rapid absorption by the system, unlike in the case with pro-drugs which require it first to be converted into an active form<sup>40,91</sup>. It can be understood that if the bioavailability of drug is poor, the patient needs to be administered with larger quantities of the drug, which can on the other hand increase the chances of drug toxicity. Similar is the case with excretion of drug, with higher the elimination rates, lesser the drug half-life and hence higher the dosage frequency, which again raises the chances of drug toxicity and associated complications. The absorption rate of drug is determined by its level of release from the carrier assembly, the site of release, whether in extracellular compartment, within the cell or the tissue and the stability of the form after release<sup>40</sup>. The stability of the drug is also affected the method of loading into the carrier particles<sup>40</sup>.

The nanoparticle size and surface charge greatly influence the biodistribution of the drug-nanocarrier system, wherein polar nanocarriers as in the case with certain polyamide dendrimers with cationic properties are generally accumulated in kidneys<sup>92</sup>, while smaller sized nanoparticles with hydrophobic groups as in the case

with carbon nanotubes are directed to the brain <sup>93</sup>. Yet another important parameter is the particle surface charge which help predict the nanoparticle dispersibility and storage stability, wherein a higher zeta ( $\zeta$ ) potential calls for increase in electrostatic repulsive forces between particles which help reduce particle agglomeration, which in turn increases suspension stability of the particles <sup>94</sup>. Since  $\zeta$ -potential is altered by variations in pH, ionic strength and the ionic composition of the dispersion medium, the relevant measurements are carried out in simulated body fluids <sup>94</sup> to predict the interaction of the particles in the biological milieu and higher  $\zeta$ -potential values greater than  $\pm 30$  mV are proven to stabilize the nanocarrier dispersion <sup>95</sup>. A different study has reported the toxicity of cationic nanoparticles owing to their affinity to anionic cellular components <sup>96</sup>. In terms of macrophage uptake on the basis of nanoparticle surface charge, it was seen that cationic nanoparticles were the first ones to be recognized by the immune system, followed by anionic and finally neutral nanoparticles <sup>97</sup>. Based on the studies conducted by Hillyer and Albrecht in 2001 on the gastro-intestinal absorption of citrate-stabilized gold nanoparticles in mice as a function of size, it was found that smaller sized particles (ranging from 4-58 nm) could rapidly cross the intestinal barrier than larger ones <sup>98</sup>.

Drugs like doxorubicin are checked for cardiotoxicity due to its susceptibility to be accumulated in the heart <sup>99</sup>. Techniques like HPLC, gamma counting are employed for studying accumulation at different sites like heart, lungs, spleen, tumour tissue by analyzing the levels of nanocarrier or drug <sup>40</sup>. Another hurdle before the nanocarrier system is

the type and degree to which the drug-carrier complex is susceptible to metabolism, which also plays essential role in effectively removing the particles or its metabolites from the body, which if otherwise remain in the system can lead to unprecedented side effects causing toxicity<sup>100</sup>. Any metabolism may occur through processes involving hydrolysis and enzymatic action triggered by immune response. Depending upon the type of metabolites formed and the mode of action required, in certain cases metabolic inhibitors are attached to the cargo-carrier complex so as to escape metabolism and it can also block uptake by endocytosis and to non-target sites which help alleviating associated toxicity and drug performance<sup>40,101</sup>. Since organic particles are likely to be eliminated by enzymatic degradation and self-disassembly upon dilution in circulation, nanoparticles comprising of self-assembled polymers size reduced to about 5-6 nm are filtered by renal glomerulus<sup>100</sup>.

After the designated roles are played by the nanocarrier-drug system, it is necessary for it to be effectively excreted out of the living system so as to eliminate any accumulation, which can otherwise call for infelicitous side effects to crucial organs like kidney, brain, liver, inflicting oxidative stress on cells, inflammation, generation of free radicals, apoptosis etc.<sup>102</sup>. The excretion process chiefly depends upon the mode of administration, which can either be systemic or local<sup>40</sup>. Particles in systemic circulation are cleared by extravasating into tissues, while locally administered ones as in the case of dermal patches or local injections to tumors are mostly filtered through liver and kidney<sup>100</sup>. Renal clearance is particularly exclusive for polar

particles and particles of size larger than 250 nm are twice more likely to be cleared than those of sizes less than 100 nm resulting in better circulation time of nanoparticles compared to microparticles thereby enhancing nanoparticle accumulation in tumour sites <sup>103</sup>. Hepatic clearance often results in the metabolism of nanocarriers and/or drug and involves the activity of hepatic B-cells and Kupffer cells in addition to liver sinusoidal endothelial cells, and are subsequently removed through fecal excretion of the metabolites <sup>40,104</sup>. Biliary route and pulmonary routes are other modes of excretion of different nanocarriers based on their physical properties <sup>40</sup>. The design of the nanocarrier hence should be carefully done considering all these factors. Accumulation is important in targeted drug delivery and requires larger quantities of the nanocarrier-drug system in the target site than non-specific site. In such cases the physical and chemical properties of the carrier system are modified to enhance the build-up. Some parameters to be considered to increase the circulation time include decreasing particle size and polydispersity, altering surface charge which reduces clearance by the reticuloendothelial system (RES) <sup>82</sup>. Target-site accumulation is also favored by attaching ligands like antibodies, proteins, aptamers to the particle surface or stimuli-sensitive molecules for controlled release of therapeutic compound <sup>41,84,86,105</sup>.

In general nanoparticles to be put to use as efficient drug delivery vectors is expected to satisfy certain criterion to exhibit optimal performance intended. The particles shall remain in circulation for sufficient periods of time <sup>106</sup> so as to facilitate efficient delivery of the

payload to the site of action, which also help in preserving the necessary bioactivity of the active pharmaceutical ingredient. It shall also improve the bioavailability of different hydrophobic drug formulations, permit for manipulations and refinement of properties so as to incorporate additional applications of disease diagnosis, targeting or stimuli-responsive drug release <sup>107</sup>. The nanocarrier formulation should be stable so that it does not get disintegrated nor agglomerate so as not to elicit immune responses. It should have efficient drug loading ability to diminish drug dosage levels and prevent overdosing, controlled drug release profile to sustain the therapeutic dosage over required periods of time <sup>108</sup>, high biocompatibility, efficient bioelimination to prevent particle accumulation and subsequent toxic reactions <sup>109</sup>.

### **2.2.1. Desirable characteristics of drug delivery vector**

Drug delivery agents come under major categories like implants, which are surgically installed and designed for controlled release of various pharmaceutical components as in pumps and conduits for intravenous infusion or as microchips, microfluidic devices and vascular stents. Another important class of delivery system is particulate delivery system, including microsphere with diameters typically in the range of 1-100  $\mu\text{m}$ , nanoparticles with diameter range from 10-1000 nm, liposomes, collagen, cellular components like erythrocytes, platelets and several inorganic particles <sup>31,110</sup>.

In order for the therapeutic agent to reach a desired location before releasing the active pharmaceutical ingredient without

disintegrating prematurely, it is advantageous to encapsulate it within the shell of an efficient drug delivery vector so that the structure and activity of the molecule be preserved <sup>111</sup>. So, it becomes a necessity that the delivery vector provides the necessary control of the drug in terms of its structure, shape and size. The drug-vector should be stable and enhance the bioavailability of drug so that it calls for minimum requirement of drug to achieve particular therapeutic effect, which can in turn reduce the chances of drug overdosing and associated toxicity in patients. Studies are particularly concentrated on identifying any individual effect of the delivery vector in the biological system so as to be assured of its biocompatibility as it is very important for the drug delivery agent to be non-toxic and eliminated efficiently from the physiological system.

In terms of the bonding between the drug and the vector, it should be such that it holds the molecules efficient enough for it not be released in transit before reaching the target site, while at the same time not strong enough not to let it release at the intended site. Experts claim the bonding not be as strong as covalent bond, but may facilitate bonding involving less strong H-bonds and other electrostatic interactions.

It must have efficient loading capacity, not trigger any immune responses and must be available for any surface modifications so as to incorporate any additional advantages to the drug-vector complex, proper cell adhesion, cellular internalization and internal trafficking of the active molecule to the nucleus or cytoplasm, controllable release of the pharmaceutical ingredient and avoid any non-specific interactions



in the biological milieu. Facile synthesis method which is also easily reproducible, consistent and has minimum repercussions on the environment and living beings are preferred. It should be capable of improving the safety of drugs and hence patient compliance. It shall extend the life of various of pharmaceutical agents, reduce the cost of development of drugs and improve the quality of life of patients <sup>31</sup>.

### **2.3. Cellular interaction of drug carriers**

Physicochemical properties of drug carriers play a major role in its interaction with cellular components, which determines particle biodistribution and pharmacokinetics <sup>112</sup>. It was seen that particles with size less than 30 nm were mainly excreted through kidney <sup>106</sup> while that falling in the range 30-150 nm were sequestered in bone marrow <sup>113</sup>. Particles larger than 200 nm were identified by the macrophages and targeted to RES <sup>114</sup>. Studies have also established the influence of particle shape on cellular uptake mechanism and kinetics as well particle toxicity <sup>115</sup>. In a study conducted by Mathaes *et al* using J774-A1 murine macrophage cell line, it was noted that particles with an elongated shape and falling in micrometer scale diameter showed minimal uptake as compared to spherical shaped nanoscale particles <sup>116</sup>. Shape of the particle as well as the point of interaction of the particles with the cell surface also determined the fate of particles <sup>116</sup>. Aspect ratio is yet another parameter in the case of non-spherical particles that determines its cytotoxicity, adhesion, migration, induction of oxidative stress and inflammatory responses <sup>115</sup>. Aspect ratio in case of cylindrical particles, is the ratio of length to its diameter <sup>117</sup> and reports suggest a decrease in aspect ratio to an increase in

apoptosis induction and cytotoxicity, possibly be due to variations in surface area <sup>118</sup>. Previous reports suggest the uptake of particles according to its shape, with maximal uptake of spherical particles followed by particles with cuboid symmetry and least absorption observed for rod-shaped and discoid particles. This trend is attributed to the ease of twisting cell membrane to cover the particle of particular shape <sup>119</sup>. Considering the impact of particle shape on cell membrane integrity, it was seen that needle-shaped particle resulted in significant disruption of membrane, while spherical and elliptical, disc-shaped particles did not cause any disruption <sup>120</sup>. Zhao and co-workers opined that cytotoxicity was not only the function of particle shape but also dependent on the type of cell lines used for the study <sup>121</sup>. While the cellular uptake mechanism of spherical particles is simple, that of non-spherical particles are dependent on multiple factors. These include particle adhesion energy, time taken for the nanoparticles to be wrapped by the plasma membrane forming invaginations, the extent of surface contact area between particles and cells <sup>115</sup>. Full wrapping of the nanoparticles by the cell membrane is feasible only when the adhesive forces between them is significantly strong enough to counteract for the energy expenditure during membrane bending, aiding in efficient cellular internalization of the nanoparticles <sup>122</sup>. Biodistribution of particles are also dependent to large extent on particle shape, with the discoid shaped particles having more affinity to drifting towards vessel wall. These escape the recognition by the RES and are minimally distributed in liver as compared to quasi-hemispherical, cylindrical and spherical shaped particles studied, with maximal liver disposition of cylindrical particles and maximal

macrophage uptake by spherical ones<sup>123</sup>. In another study conducted by Sun *et al*, it was seen that though the liver and spleen accumulation were similar for rod-shaped, cuboid and spherical particles, spherical ones showed minimum cytotoxicity while rods exhibited maximum toxicity<sup>124</sup>. *In vivo* performance of mesoporous silica was compared based on particle aspect-ratio as well as mode of administration and it was found that orally administered spherical particles accumulated more in the spleen, while the liver and lung accumulation of rod-shaped ones were significantly higher. It was also seen that when the aspect ratio was increased from 1 to 5, liver accumulation and urinary excretion decreased, which suggested that the biodistribution, renal toxicity and excretion of mesoporous silica were dependent on particle shape and these showed different biodistribution profiles when administered intravenously. Nanoparticles with short-rod shape were chiefly found to accumulate in liver while those with long-rod shape were distributed in spleen<sup>125</sup>. Short rods were excreted faster than long rods. It was also found that surface modification of these particles with polyethylene glycol (PEG) resulted in enhancement in lung deposition<sup>126</sup>. Particle shape and porosity also determine particle aggregation as well as biodegradation behaviour, with spherical shaped mesoporous particles degrading faster than rod shaped and amorphous counterparts<sup>127</sup>. In general, cellular uptake of different nanoparticles can be attributed to factors like aspect ratio, type of cell as well differences in number and type of cellular receptors available for interaction with different functional groups<sup>127</sup>. Studies were conducted to check upon the influence of particle size on eliciting immune responses, and was identified that variations in immune responses be possibly due to

variations in interactions with immune cells and antigen presentation <sup>128</sup>.

A study conducted by Kim et al (2019) tested the effect of various parameters like time, size, presence of serum proteins on cellular internalization of nanoparticles. Nanoparticles of varying sizes (20, 30, 40, 50 nm) with poly dispersity indices ranging from 0.04 to 0.15 and zeta potential values from  $-62\pm 6$  to  $+38\pm 6$  mV were tested. In order to nullify the effect of cytotoxicity that may arise due to protein-corona formation, a low serum levels (0.5 %) were maintained in the growth medium. It was observed that the particle sizes less than 30 nm (at 50  $\mu\text{g/mL}$  concentration) proved lethal to cells, whereas those above 40 nm showed reduced cytotoxicity. Flow cytometric analysis of the cells revealed that both apoptosis and necrosis were simultaneously induced in the cells exposed to varying particle diameters. An increment in the cleavage pro-caspase 3 supported induction of apoptosis. While enhancement in the interaction between RIP1 (RIPK1) and kinase RIP3 (RIPK3) resulted in the induction of necrosis. In a separate study where HepG2 cells treated with 20- and 50-nm sized particles at the  $\text{IC}_{50}$  values of 75.2  $\mu\text{g/mL}$  and 175.2  $\mu\text{g/mL}$  respectively, a linear reduction in the cell survival was observed in the cells treated with 50 nm particles, whereas a rapid reduction was observed within the first 3 h of treatment as confirmed by fluorescence activated cell sorting (FACS) technique. The results showed that necrosis induction to be the dominant mechanism observed. The ratio of apoptosis induction was relatively higher in those treated with 50 nm particles. When cellular uptake based on

particle was examined, it was observed that a considerable amount of 20 nm size particles was taken up by the cells during the initial 3 h of incubation and showed no significant differences even at 24 h. On the other hand, 50 nm-sized particle was taken up by the cells gradually over time. It is reported that endocytosis was the mechanism of particle uptake. It was also observed that most of the 20 nm sized particles entered the cells by directly permeating the cell membrane as the presence of endocytosis inhibitors did not significantly affect its uptake. In contrast, the inhibitors led to a reduction in intracellular uptake of the 50nm silica nanoparticles<sup>129</sup>. Serum stability of silica nanoparticle was yet another parameter that was put to test. 1, 5, 10 % foetal bovine serum (FBS) concentrations were chosen. A reduction in silica particle stability was observed with an increase in the serum protein concentration which was particularly dominant in particles of 50 nm, owing to particle agglomeration<sup>129</sup>. The 50 nm particles increased its size to >200 nm and showed excessive polydispersity in the presence of serum. When the level of serum concentration was increased to 1 % and higher, the uptake of 50 nm particles by the cells were minimal owing to aggregation of particle with serum protein. However, cell survival was not reported to be affected even after 24 h exposure. The uptake of 20 nm particle occurred in a time-dependent manner and mono-dispersity maintained even at 5 % serum concentration. However, in terms of cytotoxicity based on particle size, 50 nm particles exhibited least toxicity compared to 20 nm particles when tested in serum-free conditions<sup>129</sup>.

Since it was postulated that particle uptake was chiefly based on endocytosis mechanism, studies employing various endocytic inhibitors were carried out to determine the pathway of cellular uptake. For this, Saikia et al (2016) used chlorpromazine hydrochloride (CPZ) to inhibit clathrin-driven pathway, methyl- $\beta$ -cyclodextrin (MBCD) to inhibit caveolin-based and polyinosinic acid (PI) to inhibit scavenger-mediated pathways. The mesoporous silica nanoparticles of 50 nm diameter followed multiple endocytosis pathways. Larger sized particles followed caveolin-mediated and scavenger-mediated endocytosis pathway, while particles of size greater than 500 nm chiefly followed scavenger-receptor mediated endocytosis. 500 nm sized or slightly higher sized particles underwent macrophage uptake by phagocytosis <sup>130</sup>.

Another criteria that determines the efficacy of nano-drug carrier formulations are its interaction with physiological and physicochemical barriers *in vivo* and elaborate studies on these interactions are quintessential for predicting stability and distribution patterns inside living system and to help look for alternatives to improve upon various properties <sup>90</sup>. Once administered, the nano formulations encounter shear forces or be coated by plasma proteins (corona formation) and chances are that it might elicit immune responses which may result in its clearance from circulation <sup>32</sup>. Clearance of nano vectors from circulation depends on the physical and chemical properties of the particle and involves interaction with the reticuloendothelial system comprising of phagocytes, monocytes and dendritic cells responsible for the uptake of particles from

circulation and deposition in liver and spleen <sup>131</sup>. Previous studies report faster elimination of cationic nanoparticles while those with neutral or slightly negative charge exhibiting longest half-lives <sup>132</sup>. Intravenous delivery to the central nervous system requires the nano formulation to cross the endothelial and epithelial tight junctions (blood brain barrier) while it is gastrointestinal tract when it comes to oral delivery, congestion and mucus in the case of intranasal delivery applications respectively <sup>32</sup>. Biological membranes are chiefly made up of carbohydrates, proteins and several lipid units which carefully manage the entry of necessary chemicals into the cell to carry out necessary biological functions while selectively restricting the entry of other extraneous components. The membrane permeation of substances may either be through passive diffusion or mediated by specific transporters (active transport). While size and polarity are major factors determining passive diffusion across membrane which restricts the entry of large, hydrophilic charged molecules, specialized pumps are available for active transport of charged molecules essential for cellular functions <sup>133</sup>. Cellular uptake mechanisms are to be thoroughly understood to design nanocarriers with particular characteristics that specialize payload internalization through a particular uptake mechanism <sup>134</sup>. Generally, endocytosis is broadly classified into two major pathways-pinocytosis and phagocytosis. Pinocytosis includes pathways that are clathrin-dependent and clathrin-independent, with clathrin-independent pathways involving caveolae-mediated endocytosis and macropinocytosis <sup>135</sup>. While negatively charged particles may undergo clathrin or caveolin based endocytosis <sup>136</sup>, rod shaped particles of size less than 60 nm undergo internalization

through caveolin dependent pathways utilizing lipid raft <sup>137</sup>. Uptake of nanospheres commonly occur through clathrin-mediated pathways involving hydrophobic and electrostatic interactions between nanoparticles and clathrin expressed areas on cell membrane <sup>138</sup>. Nanoparticles of size ~50 nm are reported to exhibit maximal uptake and intracellular delivery <sup>139-143</sup>. Surface charge of particles plays a major part in determining the susceptibility of the particle aggregation and interaction with similar and oppositely charged cellular components with studies suggesting improved cellular internalization of cationic and neutral nanoparticles owing to the long range electrostatic forces, which increase propensity to be attracted to the negatively charged cell membrane surface <sup>144-147</sup>.

It can be generalised that unmodified nanoparticles possessing positive charge undergo rapid clearance by macrophages and neutral charged rod-shaped surface modified nanoparticles readily penetrate tumorous cells, while particles with positive charge which are smaller and surface coated, transverse across mucosal barriers better <sup>32</sup>. Once particles are up taken by the cell through specific internalization pathway based on particle properties mainly size, surface composition, charge, shape and based on the nature of the cell membrane, particles remain enfolded inside vesicles which are otherwise referred to as endosomes. However as time proceeds, these endosomes are acidified, and for effective functional intracellular delivery to occur it is inevitable for the particles to escape from endosomes before they are lysed and acted upon by proteolytic enzymes <sup>32</sup>.



#### **2.4. Surface modification for additional functionalities of nanocarrier**

Functionalization of nanoparticles are chiefly utilized for site-specific targeting of the active pharmaceutical ingredient loaded onto the carrier molecules<sup>148</sup>. Combining different groups to the nanocarriers adds to the enhancement of several properties enabling varied applications<sup>149</sup>. Surface modification for the control of drug release mostly involves chemical or structural manipulation of the drug carrier<sup>150</sup>. Nanocarriers can be conjugated with different ligands varying from low molecular weight ones like thiamine, folic acid to antibodies, lectins, polysaccharides like chitosan, dextran, phospholipids, deoxyribonucleic acid (DNA) and so forth, which confer the nanocarrier with properties like enhancement in ability to cross various biological membranes, selectivity towards particular site or tissue, stealth properties which reduces its immunogenicity and hence recognition by the reticuloendothelial system (RES) mostly upon the formation of a coating that prevents adhesion of plasma proteins thereby improving circulation time *in vivo*<sup>149,151</sup>. Nano formulations directed to pulmonary tissues with particular mucus penetrating properties aid in efficient delivery of therapeutics for treatment of cystic fibrosis where penetration across thicker layer of mucus is considered as a major hurdle that reduces therapeutic efficiency of treatments for the disease<sup>32</sup>. This could be achieved by modifying the nanoparticles with hydrophilic groups like PEG, polyethylene oxide<sup>152</sup> or using complexes capable of disintegrating mucus layer<sup>153</sup>, hyaluronic acid with thiolated side chains<sup>154</sup> and N-acetylcysteine<sup>155</sup>.

#### **2.4.1. Surface functionalization with polyethylene glycol (PEG)**

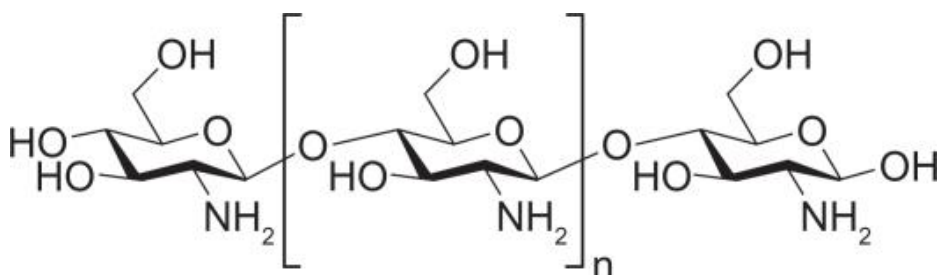
In many instances a sustained delivery of the pharmaceutical ingredient is demanded to achieve the expected therapeutic effect and for the carrier-drug complex to reside in the bloodstream, it is essential to preserve it from being evaded by the immune cells which would clear any exogenous particle from circulation thereby weakening the targeting potential of the carrier system. PEG is a commonly employed synthetic polymer that is biocompatible, which possesses low immunogenicity and acceptable excretion kinetics, capable of endowing ‘stealth’ properties to the carrier system<sup>156</sup>. Incorporation of molecules like phosphonates and PEG were shown to reduce particle agglomeration resulting in stable suspensions owing to generation of repulsive forces between particles<sup>157,158</sup>. PEG modification protects the carrier from recognition by RES which enhances residence time in the plasma<sup>159,160</sup>. Addition of PEG units aids in improving the hydrophilic properties of the drug-carrier complex<sup>151</sup> and these hydrophilic moieties form a hydrated overcoat which refrains nanoparticles interaction with blood components and other nanoparticles, thereby shielding the PEG-conjugated particles from recognition by the mononuclear phagocyte system (MPS). Otherwise mentioned as reticuloendothelial system (RES) in literature, MPS chiefly consists of dendritic cells, monocytes and blood granulocytes<sup>161</sup>. PEG modification reduces interaction between the nanocarrier and other blood components like serum proteins which would otherwise gather around the nanoparticles leading to particle agglomeration<sup>162</sup>. However, studies have shown that the surface shielding property of

PEG depends upon its molecular weight, of which 2 kDa or higher is considered necessary to impart sufficient hydrophilicity<sup>163</sup>. Interaction of the nanocarrier not only depends on the density of PEG surface coating, but also varies with particle size, curvature and the physicochemical properties of the core material, with the chances of interaction of larger spherical PEGylated particles with MPS being higher than that of smaller and longer ones<sup>164–166</sup>. Though PEGylation can help reduce interaction with blood components to an extent, a formulation with complete resistance to the interaction is not yet reported<sup>164,165</sup>. In addition to reduction in particle aggregation, PEGylation can help reduce unacceptable interactions of the nanoparticles with blood constituents like erythrocytes and hemoglobin which could lead to its aggregation and/or hemolysis, resulting in systemic toxicity<sup>167</sup>. Hemolysis products released into circulation may bind to the nanocarrier system facilitating recognition by macrophages and subsequent phagocytosis<sup>167</sup>. This is yet another mechanism that could help improve circulation time of the nanocarriers. PEG modification has also been devised to improve translocation of nanocarriers in various non-systemic applications requiring site-specific delivery of therapeutics to organs like brain by overcoming various extracellular barriers<sup>168</sup>. Circulation half-life of PEGylated nanoparticles depends on the surface density of PEG coating with circulation half-life highest in the case of nanospheres, followed by nano discs, nanocages and finally nanorods<sup>169</sup>.

### 2.4.2. Capping with chitosan

Chitosan capping is primarily done to mediate the release of the therapeutic in response to changes in hydrogen ion concentration, as chitosan is sensitive to fluctuations in pH. It is a naturally occurring polysaccharide formed by the deacetylation of chitin<sup>170</sup>, a major ingredient of crustacean exoskeletons, with acceptable safety profile, high charge density (cationic), mucoadhesive, hydrophilic and wound-healing properties. It are also used as vehicle to enhance the delivery performance of several drugs<sup>171</sup>.

**Figure 2.4.1.** Showing structure of chitosan



(Source: <https://www.ncbi.nlm.nih.gov/pmc/articles/PMC3090273/figure/f1-ijn-6-765/>; accessed on 29-December -2021)

Chitosan is reported to penetrate through intercellular tight junctions thereby traversing across epithelium<sup>172</sup>. The number of amino groups, the cationic charge density and hence physiological activities of the polymer are reported to be based on its degree of deacetylation (DDA)<sup>173,174</sup>. Another important parameter of the cationic polymer is its  $pK_a$  value with values above its  $pK_a$  resulting in polymer deionization and ionization below  $pK_a$  values, unlike the case with anionic polymer. This property is harnessed in the release of

payload upon variations in pH<sup>175</sup>. It is also known to exhibit low immunogenic potential<sup>176,177</sup>. Chitosan consists of free amino groups at neutral and alkaline pH, making it insoluble, however a drop in pH results in the amino groups getting protonated thereby making chitosan soluble in water<sup>178</sup>. Chitosan-based drug delivery systems make use of this property to fabricate drug delivery vectors to react to internal stimuli like pH and external ones like electromagnetic fields. These properties find intensive applications in tumour-targeting where the pH around tumour tissues is slightly lower than the normal pH, resulting in enhanced selectivity and release of drug near targeted tumour tissues<sup>179</sup>. Antibacterial activity and metal chelating property are other added advantages of chitosan biopolymer<sup>180</sup>.

## **2.5. Encapsulation of drug into NP DDSs**

Hydroxyl (-OH) and amino (-NH<sub>2</sub>) functional groups in epirubicin are responsible for covalent as well non-covalent interactions with the drug carrier particle. Non-covalent interactions expected include weaker interactions like hydrogen bonds, interactions owing to polarity and particle charge differences (electrostatic interactions) as well as  $\pi$ - $\pi$  bonds<sup>181</sup>. Amino groups aid in pH-responsive release of the drug<sup>182</sup>. Electrostatic interaction between positively charged epirubicin and negatively charged silanol groups on the surface of silica nanoparticles makes drug loading possible<sup>150</sup>.

### **2.5.1. Drug release from NP DDSs**

Drug carriers permitting targeted, pH-sensitive release ensure protection of the active pharmaceutical ingredient against premature

release before reaching the target, especially in delivery requirements to tumour tissues, thereby ensuring minimal side effects<sup>183-186</sup>. Conjugation of drug molecules to carrier particles sensitive to stimuli like redox potential and pH results in alterations in the pharmacokinetic and *in vivo* distribution properties of the drug<sup>187</sup>. Enhanced permeability and retention effect (EPR) of solid tumors is one of its pathophysiological characteristics exploited for site specific, passive targeting of several chemotherapeutic agents. Nanoparticles employed for passive targeting of chemotherapeutics harnessing the EPR effect are supposed to have longer residence time under biological circulation. Such particles are expected to have diameters that exempts it from renal clearance. To meet the enhanced demand for oxygen and nutrient, exceptionally high vascularization in tumors result in formation of structurally aberrant and functionally abnormal structures. Disorganized membrane structure with fenestrations is also observed in such tissues. Dysfunctional vasculature also results in inefficient drainage of lymphatic system. This anomaly is harnessed for accumulation and retention of the extravasated drug-loaded nanocarriers within the tumour tissue where the drug is released.

The drug release from a nano-formulation may occur as a result of detachment of drug molecules adsorbed onto the nanoparticles. Another mechanism is by simple diffusion of drug from the formulation. In certain cases, the microenvironment may favour the degradation of the polymer matrix which releases the conjugated drug payload. The interactions between the drug molecule and the nanoparticles, the chemical bonding and the microenvironment are

major factors that result in particular mechanism of drug release. Drug release study helps in predicting drug stability and the formulation can be altered according to the intended results expected.

## **2.6. Application of nano vectors in healthcare sector**

Nanotechnology exerts a predominant role in healthcare sector owing to its unique properties, that simplifies disease diagnosis to improve treatment specificity<sup>32</sup>. Nanoparticle-mediated cancer chemotherapy makes use of the enhanced permeation and retention (EPR) effect of the affected cells. The targeting efficiency of the carrier system is determined to a greater extent by the ability of the nanocarriers to escape from clearance by the mononuclear phagocyte system (MPS) which influences its tissue distribution, as well as the pharmacodynamic and pharmacokinetic properties of the therapeutic<sup>188-190</sup>. Development of nano vectors with structural architecture permitting bio-responsive release of drugs have simplified combination therapy, patient and treatment specificity with reduction in prevalence of drug resistance<sup>32</sup>. Though viral vectors were tested for delivery of gene editing contents through utero routes in mouse models, it was found to be toxic in comparison to delivery using nanoparticle formulations<sup>191</sup>. Nanoparticles are currently employed in areas of healthcare involving detection and molecular sensing, imaging, delivery applications etc.<sup>192</sup>. Gold and silver nanoparticles owing to their unique optical absorption and scattering properties are employed in disease diagnosis and photothermal therapy<sup>193</sup>. Nanoparticles responsive to magnetic fields are utilized for magnetic resonance imaging and targeted delivery, while mesoporous silica particles are

used for controlled drug release systems<sup>192</sup>. Inorganic particles like silica nanoparticles when metabolized, result in generation of non-toxic end products like silicic acid, making it biocompatible and be used for loading a variety of cargoes ranging from hydrophobic drugs to proteins. These were tested in human trials for transporting antibodies and were found to facilitate chronic tissue wound healing by preserving the activity of the antibody over the therapeutic window<sup>194</sup>. Silica particles loaded with curcumin were also reported to improve wound healing in mouse models infected with methicillin-resistant *Staphylococcus aureus* (MRSA) by reducing the bacterial load<sup>195</sup>.

### **2.6.1. Conventional drug delivery versus nanoparticle-based drug delivery**

When conventional drug delivery system was struggling with problems concerning efficient biodistribution and intracellular transport of pharmaceutical ingredients, nanoparticle-mediated delivery systems could overcome these limitations by adopting tissue and cell specific targeting strategies and by surface functionalization that aid in translocation across biological barriers<sup>32</sup>. Conventional drug delivery system resulted in administration of elevated doses of pharmaceuticals which had low solubility and stability *in vivo*, while careful selection, manipulation and optimization of nanoparticle-mediated drug delivery could improve the drug solubility and stability that could potentially reduce side effects and toxicity associated with administration of higher doses of potent pharmaceutical ingredients. Chemotherapy which is a common treatment regimen involving the use of pharmaceutically active ingredient to treat diseases like cancer.



Standard chemotherapeutic agents are known to be cytotoxic, but the levels to which it is specific to the tumour cells decide whether the adjacent normal cells be affected, with increased chances of its DNA and protein expression being disrupted. In most cases chemotherapy results in harm to normal healthy cells with the administered dose being insufficient to exert the necessary therapeutic effect. This demands for higher doses of drug, resulting in associated side effects, which may be acute or prolonged and the metabolic end-products may even be harmful to organs like liver and kidney <sup>196</sup>. Yet another factor that hampers the action of chemotherapeutic agents is its poor solubility, which can affect its absorption. Other side effects include suppression of immune system leading to increased susceptibility to infections, nausea, sterility, myelosuppression, diarrhea, fatigue, alopecia, chances of developing resistance to chemotherapy owing prior drug exposure, variation in drug sensitivity as a factor of tumour heterogeneity and activation of drug efflux pathways <sup>197</sup>.

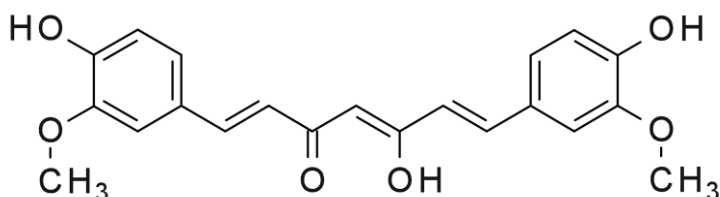
### **2.6.2. Nano formulations in cancer chemotherapy**

Apart from disease diagnosis and gene transfer applications, nanoparticles are also found to be effective in drug delivery to tumor cells, wherein they are taken up by enhanced permeation and retention effect (EPR) <sup>198</sup>. EPR is due to the combined effects of dysregulated angiogenesis, which results in development of defective epithelium with larger fenestrations (often larger than 300 nm), anomalous lymphatic drainage together with upregulation of factors that enhance vascular permeability (like vascular endothelial growth factor, VEGF) resulting in leaky blood vessels of tumour tissue. However, shrinking

of the blood vessels has the advantage of enhancing particle accumulation at the target site<sup>199,200</sup>. Variations in pH and presence of specific biomarkers are major criteria used for tumour targeting. Combined with diagnostic properties, nano formulations would be capable of monitoring particle distribution and disease condition to facilitate optimization of treatment strategies<sup>200</sup>.

## 2.7. Curcumin

**Figure 2.7.1.** Showing structure of enol form of curcumin



(Source: <https://en.wikipedia.org/wiki/Curcumin#/media/File:Curcumin.svg>; accessed on 23 February-2024)

Curcumin is a polyphenol with molecular weight of 368.38  $\text{gmol}^{-1}$ , the chemistry of which is responsible for several biological activities like protection of biological membranes from damages caused due to peroxidation of moieties like lipids, which could otherwise result in damage to cell membrane. The free radical scavenging property of curcumin targeting groups like oxygen ( $\text{O}_2^-$ ) and hydroxyl ( $\text{OH}^-$ ) moieties is attributed to the phenol ring in the structure, that prevents lipids being peroxidized, and this property is enhanced by the presence of methoxy group in its structure which also help prevent oxidative damage to DNA and associated protein groups<sup>201–203</sup>. The property of induction of apoptosis in cancerous cells makes

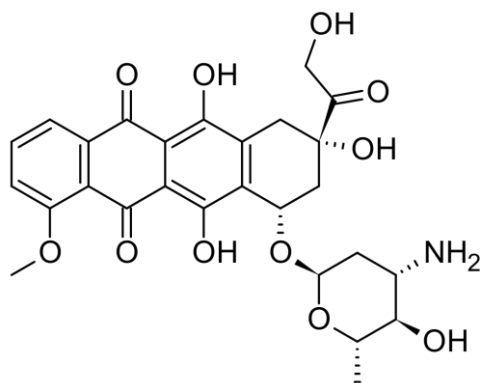
curcumin a potent agent used as against cancer cells <sup>204</sup>. It has been established that curcumin exhibits suppression of proliferation of cancer cells by BCl2-mediated pathways <sup>205</sup>. However low aqueous solubility and bioavailability of curcumin hampers translation of these benefits into clinical applications. Curcumin once enters the circulation rapidly undergoes metabolism which reduces the availability of free curcumin in plasma thereby limiting its application <sup>206</sup>. Studies were conducted to improve the stability and bioavailability of curcumin by developing curcumin analogues and by carrying out chemical modifications <sup>207</sup>, while other studies focused on developing novel drug delivery system that can improve pharmacokinetic behaviour of curcumin <sup>208</sup>. On this note, curcumin nano-formulations like, Lipocurc™ (liposomal curcumin for infusion) and Meriva® are proven to have enhanced bioavailability and improved treatment outcomes on studies conducted on human subjects suffering from pancreatic and lymphocytic leukemia <sup>209–211</sup>.

## **2.8. Epirubicin**

Anthracyclines are lauded for its effectiveness against cancer cells, with doxorubicin hydrochloride and epirubicin hydrochloride being its commonly available commercial forms <sup>212,213</sup>. Epirubicin drug is useful for treating broad spectrum of cancer associated with lungs, cervix, breast, ovary, colon, bladder and malignant lymphoma <sup>214,215</sup>. Epirubicin is also an epimer of doxorubicin formed by the reorientation of OH-group in its 4'-position in the daunosamine ring (amino-sugar moiety) <sup>216</sup> and this difference in structure results in differences in activity as well as pharmacokinetics <sup>217</sup>, making epirubicin a safer

alternative to doxorubicin in terms of cardiotoxicity and myelosuppression<sup>218,219</sup>.

**Figure 2.8.1.** Showing structure of epirubicin



(Source: <https://en.wikipedia.org/wiki/Epirubicin#/media/File:Epirubicin2DACS.svg>; accessed on 23-Feb-2024)

Different studies have been conducted to investigate the mode of action of epirubicin on cancerous cells and in one such study on human bladder cells, it was observed that epirubicin on combined action with Bacillus Calmette Guerin (BCG) could induce apoptosis by the upregulation of caspase-3, p53 and Bax pro-apoptotic factors. Downregulation of Bcl-2 antiapoptotic factor was also observed along with cell cycle arrest at the G0/G1 phase<sup>220</sup>. Others have reported that epirubicin works by intercalating into the DNA base pairs, interfering with transcription process, preventing mRNA formation. It is also involved in the inhibition of topoisomerase-II enzyme, but is said to be cell cycle non-specific<sup>220,221</sup>. Epirubicin is chiefly metabolized in the liver resulting in end-products like epirubicinol and epirubicin glucuronide<sup>222</sup>. The effectiveness of the drug is however restricted due

to allergic reactions, cardiotoxicity, hepatotoxicity, the metabolism of which generates free radicals<sup>223–226</sup>.

Previous studies have reported substantial tissue distribution of epirubicin with elimination primarily through, but not restricted to biliary routes. Epirubicin metabolism also occurs in other organs and red blood cells. The metabolism of epirubicin involving its biotransformation into glucuronides and epirubicinol explains its better tolerance than its 4' epimer, doxorubicin especially in terms of induction of cardiotoxicity<sup>227</sup>.

Hydroxyl and amino groups of epirubicin are available for linkages involving covalent and non-covalent interactions like hydrogen bonding and electrostatic interactions. The amino moiety is responsible for conferring pH sensitivity owing to the natural tendency of the amino group to get protonated<sup>150</sup>.

## **2.9. Challenges and future prospects**

Translation of clinical trials to nanomedicine requires to surpass hurdles ranging from cost efficiency, sustainability, scalability and regulatory approval of nano formulations to in depth assessment of behaviour and responses of these formulations under physiological environment in terms of stability, pharmacokinetics, tissue deposition, payload release criteria, cellular interactions, need of incorporation of multi-functionalities like simultaneous detection, targeted and controlled release of pharmaceuticals with provisions for real time monitoring<sup>109</sup>. Liposome nanocarriers were widely used for drug delivery applications due to its structure contributing to amphiphilicity,

with biocompatible lipid bilayer capable of attaching hydrophobic drugs and an internal layer that can accommodate hydrophilic ones <sup>228</sup>. Despite these benefits, liposomes were rapidly removed from circulation by the RES leading to accumulation in liver and spleen. Additionally, liposomes were also shown to trigger acute hypersensitivity reactions. <sup>228</sup>. These led scientists to look for natural alternatives for similar purposes <sup>229</sup>. Development of more effective nano formulations with properties enabling them to surpass immune system, but with acceptable safety profile and metabolism, calls for more studies concerning surface modification, clinical trials and to search for newer, better and sustainable sources and production processes <sup>148</sup>. Even though large number of animal studies have been conducted to test the effect of nanoparticles, the differences in physiology and pathology, heterogeneity in behaviour across species and in human beings have led to widening gap between development of new nano-formulation and its translation to clinical application <sup>32</sup>. Nano-formulations are to surpass various biological and physical barriers to reach the disease destination, which may vary from one disease to the other or from patient-to-patient, that personalized optimization of particles is to be done. This calls for more specialized research on these formulations on a case-to-case basis. Though attachment of different targeting moieties have increased the specificity in distribution of therapeutic across target site, for effective interaction to occur between the ligand and the receptor, or between antigen and antibody, or that between a particular enzyme and substrate requires careful analyses of the proportion of ligand-to-receptors and incorporation of targeting groups in sufficient levels that

may also vary between diseases <sup>32</sup>. Thorough evaluation of the response of nano formulations to the microenvironment, cellular and sub-cellular compartments like pH, presence of degrading enzymes, temperature variations, interstitial fluid pressure, variations in the type and number of cell surface receptors and transporters, time of contact, redox potential etc. are to be carried out for realistic application in targeted delivery applications <sup>32</sup>.

Administration of surface modified particles can trigger release of antibodies, which when exceeds the threshold levels can result in rapid clearance of the modified formulation, severely hampering success of the therapy. These could also be patient specific and are to be closely watched, which adds to efforts in formulating better performing nano drug carriers <sup>230</sup>. Lipid nano formulations loaded with messenger ribonucleic acid (m-RNA) showed allergic responses in exceptional cases raising public concern regarding safety of use of such formulations <sup>231</sup>. Also, chances exist that in transit during circulation the hemodynamics of systemically administered nano-formulation may change subject to varying levels of flow rates and shear stress exerted, leading to excoriation of surface ligands resulting in loss of functionality <sup>232</sup>. Addition of surface coatings may encourage non-specific attachment of lipids and serum proteins resulting in corona formation, which can alter the stability and biodistribution of the drug-carrier complex <sup>233</sup>. Interaction of nano vectors with reticuloendothelial system may not only result in particle clearance but can also evoke immune responses resulting in inflammation, necrosis as well as tissue damage <sup>234</sup>. It is seen that the performance of nano

formulations is only a tentative indication of its behaviour under the studied conditions. Studies are to be repeated on context basis before making generalized conclusions, because it is seen that a minute variation in the physicochemical properties of the particles in *in vivo* models could result in significant variations in the results. Often the cost of clinical trials in developing nano-formulations with desired features outweighs the probability of successful screening of these products for clinical applications, thereby increasing the financial risk associated with research<sup>32</sup>. However, personalized, disease-specific treatment regimen employing novel nanoparticle formulation can definitely improve patient compliance, standard of life, survival rates as well as dosing efficiency, calling for growth of niche market. Simultaneous use of nano-formulations for disease detection as well as targeted drug delivery applications result in earlier detection of various disease and its stage, thereby aiding in better understanding of pathology for developing customized treatment plan to improve disease conditions<sup>200</sup>. Conflicting demands like need for longer circulation times with decreased volume of distribution for nanotherapeutics, while lesser residence time for nano diagnostics demand for the fine tuning of particle properties for the development of a multifunctional theragnostic<sup>200</sup>. Development of a well-controlled, scalable and reproducible synthesis process generating monodisperse nanoparticles results in the particle displaying uniform properties like biodistribution, half-lives and target affinity that eases predicting particle response *in vivo*<sup>200</sup>.



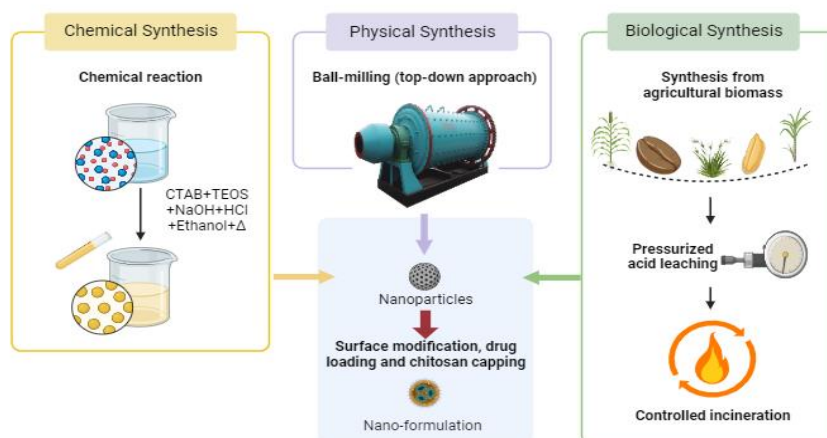
# MATERIALS AND METHODS

## 3.1. Source identification of biogenic silica

Diatom is known to be a rich and abundant source of naturally occurring silica and is also used as a dietary supplement for silica required for the body. Hence the samples were used for the study for generation of biogenic silica-based nanocarrier system. Also, currently available data on the results of compositional analysis of different plants over the past years have appeased the efforts required to identify sources rich in silica content. Accordingly, coffee husk, corn husk, Indian goose grass, sugarcane bagasse and rice husk which were locally resourced were also used for the isolation of biogenic silica particles.

## 3.2. Optimization of synthesis of biogenic silica nanoparticles

**Figure 3.2.1.** Different methods employed for the synthesis of silica nanoparticles



*Note:* Illustration created with [BioRender.com](https://www.biorender.com).

### **3.2.1. Synthesis of silica nanoparticles from diatom frustules**



**Figure 3.2.2.** Finely ground food-grade diatomaceous earth sample

#### **Procedure:**

Fresh water diatomaceous powder was procured from urban platter<sup>TM</sup>. The cleaning of diatom frustules was carried out as per <sup>235</sup> and subjected to size-reduction techniques for generation of biogenic silica nanoparticles as mentioned below.

1. The diatom frustules were cleaned using 10 % H<sub>2</sub>O<sub>2</sub> and maintained in water bath at a temperature of 100 °C for 15 min.
2. 10 % aqueous HCl was added to the mixture and centrifuged at 2000 rpm for 10 min.
3. The supernatant was pipetted out and the washing steps were carried out thrice using double distilled water.

4. The cleaned frustules were preserved in ethanol and another set of samples were oven-dried to carry out further size reduction procedures.
5. The dried samples were subjected to pulverization in dry mills<sup>236</sup> as diatom frustules were difficult to filter (table 3.2.1).
6. The milled samples were subjected to degassing at  $10^{-3}$  Torr vacuum condition for a period of 2 h to eliminate entrapped gases and other impurities<sup>237</sup>.
7. The samples were further subjected to screening for physicochemical characterization.

**Table 3.2.1.** Ball milling parameters varied in the study for optimization of production

---

| <b>Ball-to-powder ratio</b> | <b>Milling speed (rpm)</b> | <b>Milling time (h)</b> |
|-----------------------------|----------------------------|-------------------------|
| <b>1:1</b>                  | 100                        | 1                       |
| <b>2:1</b>                  | 200                        | 2                       |
| <b>4:1</b>                  | 400                        | 3                       |
| <b>8:1</b>                  | 600                        | 4                       |
| <b>10:1</b>                 | 800                        | 5                       |
| <b>20:1</b>                 | 1000                       | 6                       |

---

### 3.2.2. Synthesis of biogenic silica nanoparticles (BSN) from agricultural biomass

The procedure followed was as done by Athinarayanan *et al* (2017)<sup>238</sup> with some slight modifications.

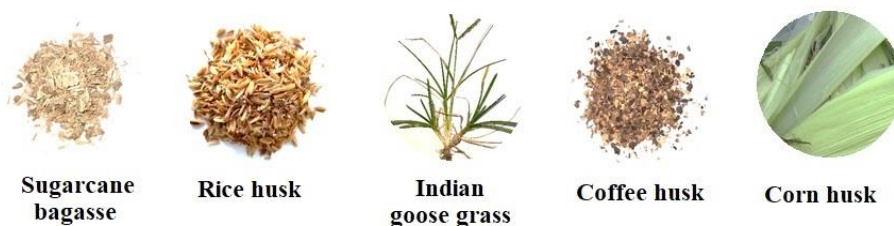


**Figure 3.2.3.** Raw materials used for the synthesis of biogenic silica nanoparticles

#### Procedure:

1. Raw materials obtained were washed thoroughly to remove extraneous particles and dirt and cut to a size range of 0.5-1 cm for easier processing in further steps to follow.
2. Prior to incineration, the raw materials were acid leached to remove metal ions and associated impurities. For the pretreatment, 90 g of weighed raw material was mixed with 600 mL acid and pressurized in an autoclave at 121 °C, 15 psi pressure for a period of 2 h.
3. Excess acid was removed by multiple washes to ensure near neutral pH of sample.
4. The washed samples were dried at 85 °C in a hot air oven.

5. The dried samples were incinerated at temperature ranging from 500-1000 °C for varied period from 1-4 h to facilitate removal of any remaining hydrocarbon groups in the sample.
6. White colored residue was obtained after combustion and labelled as biogenic silica and subjected to physicochemical characterization.

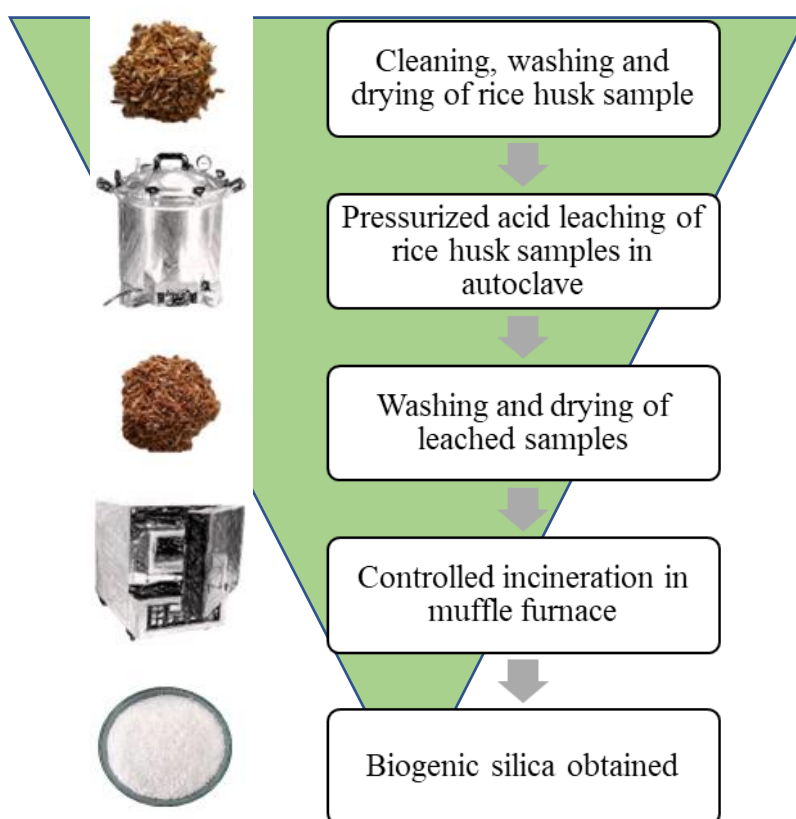


**Figure 3.2.4.** Flow diagram of synthesis of biogenic silica particles from agricultural biomass



**Figure 3.2.5.** Showing (A) Untreated rice husk, (B) Acid leached and washed rice husk, (C) Dried acid pretreated rice husk, (D) Incomplete combustion of rice husk samples at incineration temperature below 200 °C showing presence of carbon and (E) Rice husk-derived silica obtained after controlled incineration

The percentage yield of silica particles were calculated using the following equation <sup>239</sup>.

$$\text{Yield of silica ash (\%)} = \left[ \frac{\text{Mass of rice husk ash formed}}{\text{Mass of rice husk}} \right] * 100$$

**Table 3.2.2.** Optimization of silica nanoparticle synthesis in terms of acid pretreatment, incineration temperature and time

| Acid used                         | Incineration temperature employed (°C) | Time of combustion (min) |
|-----------------------------------|--|--------------------------|
| 1N HCl                            | 500                                    | 60                       |
|                                   | 600                                    | 80                       |
|                                   | 700                                    | 90                       |
|                                   | 800                                    | 100                      |
|                                   | 900                                    | 240                      |
|                                   | 1000                                   |                          |
| 5% H <sub>2</sub> SO <sub>4</sub> | 500                                    | 60                       |
|                                   | 600                                    | 80                       |
|                                   | 700                                    | 90                       |
|                                   | 800                                    | 100                      |
|                                   | 900                                    | 240                      |
|                                   | 1000                                   |                          |

Reference: <sup>238</sup>

### 3.3. Physicochemical characterization

The phase identification of the samples was carried out using Malvern Panalytical X'pert3 Powder diffractometer (Malvern Instruments Ltd., Netherlands) with copper anode, operated at 45 kV, 30 mA tube current, scan range of 10-90° and scan step size of 0.02. The chemical properties and molecular interactions of the samples were analyzed using Cary 620 FTIR Imaging system coupled with

Cary 660 FTIR Spectrometer (Agilent Technologies, Malaysia) with a spectral range of 5500- 850  $\text{cm}^{-1}$ .

Morphology of the silica particles were observed using GeminiSEM 300 field emission scanning electron microscope (Zeiss, Germany) coupled with Octane Plus EDAX system, transmission electron microscope (JEOL 1011,100 kV) (JEOL, USA). Surface area and pore characteristics were studied using BELSORP-max (MicrotracBEL, Japan) with BELMaster<sup>TM</sup> analysis program.

Elemental composition was studied employing X-ray fluorescence principle (SPECTRO XEPOS spectrometer with SPECTRO XRF Analyzer Pro operating software interface) and a CHNS-analyzer (Thermo Scientific FLASH 2000 HT analyzer, Thermo Fisher Scientific, USA).

The hydrodynamic diameter, poly dispersity index and zeta potential were analyzed using dynamic light scattering technique (Malvern Nano-S90 Zetasizer, Malvern Panalytical, USA), with Zetasizer software 7.11) (table 3.3.1).



**Table 3.3.1.** Characterization techniques used in the study

| <b>Parameter</b>  | <b>Tool</b>  | <b>Significance</b>              |
|---|--|----------------------------------|
| <b>Particle size, surface morphology</b>                | Field-emission scanning electron microscope / Transmission electron microscopy, Dynamic light scattering | Drug loading, drug release       |
| <b>Surface area, pore volume, average pore diameter</b> | Nitrogen adsorption/desorption method  | Drug loading, drug release       |
| <b>Zeta Potential</b>                                   | Zeta Potential analyzer  | Membrane interaction, stability  |
| <b>Functional groups</b>                                | Fourier transform infrared spectroscopy (FTIR)   | Chemical set up of nanoparticles |
| <b>Phase analysis</b>                                   | X-ray diffraction (XRD)  | Orientation of particles/ order  |
| <b>CHNS Analysis</b>                                    | CHNS Analyzer  | Presence of impurities           |
| <b>Drug loading</b>                                     | Spectrophotometric analysis  | Drug loading efficiency          |

References: <sup>238</sup>, <sup>237</sup>, <sup>240</sup>, <sup>241</sup>, <sup>242</sup>.

### 3.4. Surface modification

#### Reagents:

- i. Poly ethylene glycol (PEG-200) (Sigma-Aldrich, St. Louis, MO, USA)
- ii. Chitosan oligosaccharide (min. 90% deacetylation) (Sisco Research Laboratories Private Limited, SRL, Mumbai, India)
- iii. Acetic acid (Sisco Research Laboratories Private Limited, SRL, Mumbai, India)

- iv. Sodium hydroxide (Sisco Research Laboratories Private Limited, SRL, Mumbai, India)

### **3.4.1. Polyethylene glycol modification and drug loading**

PEG modification and subsequent drug loading was carried out following the method reported by Ghazaeian *et al* (2021) with slight modification<sup>S<sup>240</sup></sup>.

#### **Procedure:**

1. 200 mg of BSN and required quantity of curcumin were dissolved in PEG-200 (2 %) in distilled water and stirred for 24 h.
2. The solution was then centrifuged at 12,000 rpm for 10 min to remove unbound PEG-200. The drug formulation was washed twice with Milli Q<sup>®</sup> water and dried overnight to obtain PEGylated-BSN-curcumin complex (BSNPC).
3. UV-Vis spectrophotometric analysis was carried out to study the amount of unbound curcumin in the supernatant and wash solutions, thereby determining the drug loading and encapsulation efficiency of the modified particles.

### 3.4.2. Chitosan capping

#### Procedure:

1. 0.6 % (w/v) solution of chitosan was prepared in 10 % (v/v) aqueous acetic acid.
2. The pH was adjusted to 6.0 using 1M NaOH solution.
3. To 20 mL chitosan solution, 100 mg of silica particles were added (0.5 % w/v).
4. The suspension was stirred in a magnetic stirrer at room temperature for 48 h.
5. The chitosan coated particles were recovered by centrifuging at 6842 xg for 15 min.
6. The particles were washed using Milli Q<sup>®</sup> water and recovered by centrifugation as above.
7. The particles were suspended in Milli Q<sup>®</sup> water, lyophilized and subsequent analyses done<sup>241</sup>.

### 3.5. Drug loading studies

Drug loading procedure was carried out by the method of Yan *et al* (2020)<sup>243</sup> and Hanafi-Bojd *et al* (2015)<sup>242</sup> with slight modification.

#### Reagents:

- i. Curcumin (Sigma-Aldrich, St. Louis, MO, USA)

- ii. Epirubicin hydrochloride (Sisco Research Laboratories Private Limited, SRL, Mumbai, India)
- iii. Ethanol (MP Biomedicals, Mumbai, India)

### **Sample pretreatment:**

Prior to carrying out drug loading, the biogenic silica nanoparticles were suspended in absolute ethanol and subjected to sonication for an hour at 20 Hz, 30 % amplitude in ice bath so as to break down any clumps of the particles to facilitate better loading of drug. This also ensured sterility of the nanoparticles.

### **3.5.1. Loading of curcumin**

#### **Procedure:**

1. To prepare stock solution of the therapeutic agent, 36.8 mg of curcumin was dissolved in 10 mL of 99.5 % ethanol (10 mM curcumin).
2. 200 mg of biogenic silica formulations was suspended in 9.5 mL of absolute ethanol. Different volume of curcumin solution (10 mM curcumin) as shown in table 3.5.1 were used to obtain curcumin concentration varying between 100 to 800  $\mu$ M and stirred at room temperature for 24 h in dark.
3. Afterward, curcumin-loaded biogenic silica nanoparticles were collected by centrifuging at 14,000 rpm for 30 min and washed twice using Milli Q<sup>®</sup> water to remove the loosely attached curcumin.

4. The supernatant was collected, and the amount of unloaded curcumin was quantitatively assayed using a multi-well plate reader (Synergy™ HT with Gen5 2.05 software) by measuring the fluorescence intensity of curcumin at 420 nm (excitation) and 520 nm (emission).
5. The curcumin loading efficiency (%) and loading amount (μg of curcumin/mg of NPs) were calculated according to the following formulation:

$$\text{Loading Efficiency (\%)} = \left[ \frac{\text{Weight of curcumin in BSNP} - \text{Curcumin complex}}{\text{Weight of total curcumin used}} \right] \times 100$$

$$\begin{aligned} \text{Loading amount (\mu g/mg)} \\ = \left[ \frac{\text{Weight of curcumin in BSNP} - \text{Curcumin complex}}{\text{Weight of BSNP}} \right] \times 100 \end{aligned}$$

**Table 3.5.1.** Showing the different concentrations of curcumin added onto fixed quantity of drug carrier-silica nano particles

| <b>Volume of curcumin taken from stock solution (μL)</b> | <b>Volume of diluent used (Absolute ethanol) (mL)</b> | <b>Final concentration of solution (μM)</b> | <b>Quantity of BSNP used (mg)</b> |
|--|---|---|-----------------------------------|
| 0.1  | 9.9   | 100   | 200                               |
| 0.2  | 9.8   | 200   | 200                               |
| 0.3  | 9.7   | 300   | 200                               |
| 0.4  | 9.6   | 400   | 200                               |
| 0.5  | 9.5   | 500   | 200                               |
| 0.6  | 9.4   | 600   | 200                               |
| 0.7  | 9.3   | 700   | 200                               |
| 0.8  | 9.2   | 800   | 200                               |
| 0.9  | 9.1   | 900   | 200                               |
| 1  | 9   | 1000  | 200                               |

### **3.5.2. Loading of epirubicin**

#### **Procedure:**

1. 100 mg of different nanoparticle formulations were suspended in 50 mL of 2 mg/mL aqueous solution of epirubicin separately.
2. The suspension was stirred at room temperature for 24 h in dark.
3. Drug-loaded particles were separated by centrifugation at 14,000 rpm for 30 min and the unbound drug was removed by washing with Milli Q<sup>®</sup> water.
4. The supernatant and wash solutions were collected and subjected to quantitative estimation of unbound drug using a multi-well plate reader (Synergy<sup>TM</sup> HT and the data analyzed with Gen5 2.05 software) by measuring the fluorescence intensity of epirubicin at 488 nm (excitation wavelength) and 555 nm (emission wavelength).
5. The loading efficiency was calculated using the same equations as in the case with curcumin loading<sup>242</sup>.

The results obtained using spectrophotometric technique were confirmed using thermo-gravimetric analysis (TGA).

### **3.6. Drug release studies**

#### **Pretreatment of dialysis tubing:**

1. The dialysis membrane was kept in running tap water for 3-4 h.

2. After removing from water, the membrane was rinsed with 0.3 % (w/v) sodium sulfide at a temperature of 80 °C for a minute.
3. It was then washed with hot water (60 °C) 2 min.
4. The membrane was subjected to acidification under 0.2 % v/v of H<sub>2</sub>SO<sub>4</sub> for a minute followed by rinsing with hot water (60 °C) for 2 min and stored in sterile distilled water at 4 °C.

**Procedure:**

1. A total of 100 mg of drug-bound biogenic silica nanoparticle suspended in 1 mL PBS (pH 5.0 and 7.4) (simulated body fluids representing tumour microenvironment and normal physiological pH) was added into regenerated cellulose dialysis tubing (molecular weight cut off, MWCO 12–14 kDa for curcumin-bound particles and MWCO 10 kDa for epirubicin-bound particles).
2. The dialysis bag was dialyzed against 50 mL of PBS under gentle stirring (100-200 rpm) at 37 °C for 100 h.
3. At predetermined time intervals, 1 mL of the dialysate was removed, and the same volume of fresh PBS was added to maintain a constant volume.
4. The removed samples were then assayed for curcumin and epirubicin using an ELISA reader respectively at 420 nm and 488 nm to check for drug release as a function of time<sup>242</sup>.

### 3.7. Biocompatibility studies

#### Reagents:

DMEM (Himedia, Mumbai, India), Dulbecco's PBS (MPBio, Mumbai, India), antibiotic-antimycotic solution (Sigma-Aldrich, St. Louis, MO, USA), trypsin-EDTA (Sigma-Aldrich, St. Louis, MO, USA), L-glutamine (Sigma-Aldrich, St. Louis, MO, USA), (3-(4,5-Dimethylthiazol-2-yl)-2,5-Diphenyltetrazolium Bromide) (MTT) (Himedia, Mumbai, India), propidium iodide (Sisco Research Laboratories Private Limited, SRL, Mumbai, India), Prolong™ Gold Antifade reagent with DAPI (Invitrogen, USA), sodium bicarbonate (Himedia, Mumbai, India), 2',7'-Dichlorofluorescein diacetate (DCF-DA) (Sigma-Aldrich, St. Louis, MO, USA), dimethyl sulfoxide (Sisco Research Laboratories Private Limited, SRL, Mumbai, India), caspase-3 assay kit (Sigma Aldrich, St. Louis, MO, USA), fetal bovine serum (FBS) (MP Biomedicals, Mumbai, India), mitochondrial membrane potential kit (Sigma Aldrich, St. Louis, MO, USA) were used as received.

#### 3.7.1. *In vitro* degradation

##### Procedure:

1. 0.5 g of biogenic silica nanoparticle was suspended in 200 mL PBS (pH 7.4) (simulated body fluid representing normal physiological pH).
2. The suspension was maintained at 37 °C under stirring conditions (300 rpm)<sup>244</sup>.



3. 1 mL aliquots were drawn at regular intervals (1 to 14 days) and centrifuged.
4. The particle morphology was observed employing FESEM technique and results compared.

### **3.7.2. Cell culture**

Human embryonic kidney (HEK293) and Henrietta Lacks (HeLa) cells were obtained from National Centre for Cell Science (NCCS), Pune. The cells were cultured in Dulbecco's Modified Eagle medium (DMEM) with 4.5 g/L glucose, 10 % fetal bovine serum (FBS), 200 mM L-glutamine 100 IU/mL penicillin, and 100 µg/mL streptomycin in different cell culture containers (25 cm<sup>2</sup>, 75 cm<sup>2</sup> flasks and 6, 12, 24 and 96 well culture plates) at 37 °C in a humidified atmosphere containing 5 % CO<sub>2</sub> to carry out different estimations.

### **3.7.3. Cell viability assay**

The biocompatibility of the prepared biogenic silica nanoparticles were analyzed by MTT assay<sup>245</sup>.

1. Cells were seeded at a density of  $1 \times 10^3$  cells per well of a 96 well plate in 100 µL of fresh culture medium.
2. Media was removed after an overnight incubation and the cells were treated with different concentrations of BSNP (at concentrations of 0, 25, 50, 100, 200, 300 and 400 µM) prepared in cell culture medium and incubated for a period of 48 h.

3. Another set of cells were treated with BSN, BSNP, BSNCH, pristine drug, BSNP-drug, BSNP-chitosan-drug, BSNP-PEG-chitosan-drug prepared in cell culture medium and cells were incubated for 24, 48 and 72 h.
4. After the incubation period, the media with different test materials were removed by aspiration and 10  $\mu\text{L}$  of MTT solution (5 mg/ mL in phosphate-buffered saline) was added to each well.
5. The plates were wrapped with aluminum foil to avoid exposure to light and incubated for 4 h at 37  $^{\circ}\text{C}$ .
6. After incubation, the purple formazan product was dissolved by the addition of 100  $\mu\text{L}$  of dimethyl sulfoxide to each well.
7. The absorbance was monitored at a wavelength of 570 nm with background subtraction at 630 nm using a 96-well plate reader 204 .
8. Data were collected in triplicate for each concentration the mean was calculated.
9. The percentage of cell viability was calculated from these data by the following formula:

$$\text{Cell viability} = \left[ \frac{\text{Mean optical density of control (Untreated cells)} - \text{Mean optical density of test (Treated cells)}}{\text{Mean optical density of control (Untreated cells)}} \right] * 100$$

### **3.7.4. Cytoprotective role of drug conjugated nano formulation against cypermethrin treatment**

#### **Procedure:**

1. HEK 293 cells were pretreated with 200 µg/mL of different nanoparticle preparations for 2 h.
2. Following incubation period, cellular toxicity was induced by the addition of 200 µM cypermethrin (Cyp)<sup>246</sup> to check for possible cytoprotective effect of the drug loaded nano-formulation.
3. Cells treated with dimethyl sulphone (DMSO) served as normal control.
4. After 24 h of incubation, the cell viability was assessed employing MTT assay (following steps 1-8 described above) and cell viability calculated (step 9 above).

### **3.7.5. Assay of glutathione peroxidase (EC 1.11.1.9)**

This assay was carried out using protocol described by Lawrence and Burk, and modified by Agergaard and Jensen<sup>247</sup>.

#### **Procedure:**

1. Cells were lysed by hypotonic treatment as described above, followed by the addition of 1 mL of 100 mM phosphate buffer (pH 7.0) to it.

2. The reaction mixture contained 2 mL of 50 mM phosphate buffer (pH 7.0), 0.3 mL of 1 mM sodium azide, 0.2 mL of 1.5 mM EDTA, 0.1 mL of 1 mM reduced glutathione, and 0.1 mL of 0.2 mM NADPH and 0.3 mL of water.
3. To this 0.2 mL of enzyme solution (supernatant of cell lysate) was added and the mixture was incubated at room temperature for 5 minutes before the initiation of the reaction by the addition of 0.05 mL of 0.25 mM H<sub>2</sub>O<sub>2</sub> solution.
4. The absorbance was read at 340 nm at 15 seconds intervals<sup>247</sup>.
5. Readings of blank reaction in which enzyme solution was replaced by distilled water was subtracted from each assay<sup>246</sup>.

### **3.7.6. Assay of superoxide dismutase (SOD, EC 1.15.1.1)**

#### **Procedure:**

1. After cell treatment with nano formulations, the cells were subjected to hypotonic lysis as described earlier.
2. To the above mixture, 0.5 mL of 0.5 M sucrose buffer (pH 7.0) was added.
3. The above mixture was subjected to centrifugation at 5000 xg for 10 min at 4 °C and the supernatant obtained was used as the source of enzyme.
4. The assay mixture contained 1.2 mL sodium pyrophosphate buffer (0.052 M, pH 8.3), 0.1 mL of 186 μM phenazine

methosulphate (PMS), 0.3 mL of 300  $\mu$ M nitro blue tetrazolium (NBT), 0.2 mL of the enzyme preparation (cell extract) and water into a total volume of 3 mL.

5. The reaction was started by the addition of 0.2 mL of NADH.
6. After incubation at 30 °C for 90 seconds the reaction was stopped by the addition of 1 mL glacial acetic acid.
7. The reaction mixture was stirred vigorously and shaken with 4 mL of n-butanol.
8. The mixture was allowed to stand for 10 minutes, centrifuged and butanol layer was taken.
9. Colour intensity of the butanol layer was measured at 560 nm against a butanol blank. A system devoid of enzyme served as control.
10. One unit of enzyme activity is defined as the enzyme concentration required to inhibit the optical density of the chromogen production by 50 % in one minute under the assay condition and expressed as specific activity in units/mg protein. The assay was done for 90 seconds and hence a factor 2/3 was applied for calculating the unit<sup>248</sup>.

### **3.7.7. Assay of catalase (EC 1.11.1.6)**

#### **Procedure:**

1. Phosphate buffer containing hydrogen peroxide ( $\text{H}_2\text{O}_2$ ) was prepared by mixing 0.16 mL of 30 %  $\text{H}_2\text{O}_2$  and made up to 100 mL using phosphate buffer solution.
2. After treating cells with different nano formulations, the cells were trypsinized and washed with 0.01 M phosphate buffer and pelletized.
3. For lysis of cells under hypotonic condition, 0.5 mL distilled water was added to the pellet and pipetted up and down.
4. To this mixture, 0.5 mL of 0.02 M phosphate buffer (pH 7.0) was added and centrifuged at 5000 xg for 10 min at 4 °C and the supernatant was used as enzyme source.
5. To 3 mL of phosphate buffer containing  $\text{H}_2\text{O}_2$  (prepared in step 1 above) 10  $\mu\text{L}$  of enzyme solution was added and mixed well by tilting the cuvette upside down.
6. Readings were taken after 10 s for 2 min against a control cuvette containing enzyme solution and  $\text{H}_2\text{O}_2$ -free phosphate buffer.
7. The absorbance was read at 230 nm using a spectrophotometer

249

### **3.7.8. Assessment of lipid peroxidation inhibition activity**

#### **Principle:**

N-methyl-2-phenyl indole reacts with malondialdehyde or hydroxyalkenals formed in the cells at an incubation temperature of 45 °C to form a colored complex, the intensity of which is measured at 586 nm using spectrophotometer <sup>250</sup>.

#### **Procedure:**

1. Cells in the culture medium were thoroughly washed to remove any traces of serum and were homogenized in the presence of 0.5 M butylated hydroxy toluene (BHT) solution made in acetonitrile and treated at the levels of 10 µL per mL of cell lysate under aseptic conditions.
2. Cells were then centrifuged at 3000 xg in a cooling centrifuge maintained at temperature of 4 °C for 10 min.
3. Added 455 µL of freshly prepared N-methyl-2-phenylindole in acetonitrile (3:1 ratio) to 140 µL of homogenate from the above step taken in microcentrifuge tube and vortexed.
4. To assess the presence of malondialdehyde, 105 µL of 12 N (37 %) hydrochloric acid were added to the samples in step 3 above, thoroughly mixed and left to incubate for 60 min at a temperature of 45 °C.
5. The samples were then centrifuged at 15,000 xg for 10 min and absorbance read at 586 nm.

Calculation:

$$\text{Inhibition of lipid peroxidation} = 100 - \left\{ \left[ \frac{\text{Absorbance of sample}}{\text{Absorbance of control}} \right] * 100 \right\}$$

250

### 3.7.9. Cellular uptake studies

**Procedure:**

1. Cells were cultured in six well plates and treated with the nano formulations loaded with drug for different durations.
2. After the incubation, the culture medium with the particles was removed and fresh media was added.
3. After the specific time interval, the cells were washed twice with PBS and lysed using lysis buffer [Tris-HCl buffer (2  $\mu$ M, pH 8.0) containing 1  $\mu$ M EDTA, and 0.10 % SDS].
4. The lysate was centrifuged at 10000 xg for 10 minutes.

The amount of drug present in the supernatant was measured using a fluorescent spectrophotometer as described above and treated as taken up by the cells<sup>251</sup>.

### 3.7.10. Nuclear morphology analysis using DAPI

**Reagent preparation:**

Preparation of PBS<sup>+</sup> (PBS containing Ca<sup>2+</sup> and Mg<sup>2+</sup>)- First NaH<sub>2</sub>PO<sub>4</sub>, K<sub>2</sub>HPO<sub>4</sub>, and NaCl solutions were prepared without adjusting the pH, with a volume 10 % lower than the final volume of



the solution. Since the pH of this solution needs to be acidic use of  $\text{Na}_2\text{HPO}_4$  was avoided to maintain the acidity.

Then, 95 mg  $\text{MgCl}_2$  in 5 mL sterile water and 110 mg  $\text{CaCl}_2$  in 5 mL sterile water (for 1 L PBS) were added in drop-wise manner with constant stirring to avoid precipitation of the phosphate salts of Ca and Mg. 50  $\mu\text{L}$  each of the above prepared  $\text{MgCl}_2$  and  $\text{CaCl}_2$  solutions were then added to 5 mL PBS solution.

The pH of the solution was carefully adjusted to 7.5 using 0.1 M NaOH and made up to the volume of the solution. Precaution was taken for the pH not to exceed of 7.5 at any time.

**Procedure:**

1. To facilitate the attachment of cells onto cover slips, it was pretreated with sterile gelatin (2 % in Milli Q<sup>®</sup> water) under aseptic conditions, and placed carefully into the wells of 6-well plates.
2. HeLa cells were seeded at a density of  $0.3 \times 10^6$  per well in 6-well plates.
3. After overnight incubation at 37 °C and 5 %  $\text{CO}_2$ , the cells were subjected to treatment with test samples for required incubation period.
4. Following incubation, the cells were washed twice with cold 1x  $\text{PBS}^+$ .

5. The cover-slips placed in the well plates were removed and placed on clean glass slides.
6. Cells on the cover slips were fixed with a 1:1 solution of acetone and methanol for 5 min.
7. The fixative was aspirated and the cells were rinsed three times, 5 min each, in 1x PBS<sup>+</sup>.
8. The cells were permeabilized using 0.2 % Triton X-100 (in 1x PBS) for 5 min.
9. The Triton solution was aspirated and the cells were rinsed three times, 5 min each in 1x PBS<sup>+</sup>.
10. Any excess liquid was removed from the specimen by gently tapping the edges onto clean laboratory wipe.
11. A drop of Prolong™ Gold Antifade reagent with DAPI was applied on top of a clean glass slide and the specimen fixed cover slip was carefully placed over it with cells touching the reagent, carefully avoiding trapping of air bubbles.
12. The preparation was allowed to cure on flat surface for 30 min in dark and visualized using fluorescent microscope.
13. The samples were subjected to visualization again after 24 h of incubation<sup>252,253</sup>.

### **3.7.11. Determination of intracellular ROS using DCFDA**

#### **Procedure:**

1. Cells were seeded at a density 50,000-1,00,000 cells/well to 6-well plate.
2. Cells were let for overnight incubation in a CO<sub>2</sub> incubator at 37 °C to facilitate attachment onto wells.
3. After treatment with test samples for designated period of time, the cells were harvested using trypsin-EDTA (1 mL/well).
4. The cells were washed and suspended in 1x PBS to remove any traces of esterase likely to be present in the serum-containing medium, the presence of which may lead to hydrolysis of DCFDA (2',7' -dichlorofluorescein diacetate), which could lead to erroneous results.
5. A 50 µM stock solution of DCFDA was prepared in absolute ethanol and kept away from light to prevent photobleaching.
6. The cells were then suspended in loading buffer containing the dye (DCFDA) to a final volume of 10 µM and kept at 37 °C for 45 minutes in dark.
7. Untreated set of cells were taken as negative control and another set treated with hydrogen peroxide at 50 µM final concentration was taken as the positive control.

8. Finally, the fluorescence intensity was measured at excitation/emission wavelengths: 485/535 nm.
9. The increase in fluorescence at the emission wavelength determines the amount of DCF (2',7'-dichlorofluorescein) (oxidized form of DCFDA) accumulation in the cells when compared to the negative control which is expected to exhibit minimal fluorescence due to the elimination of oxygen radicals by the enzymes and/or antioxidants naturally present in healthy cells<sup>254</sup>.

#### **3.7.12. Mitochondrial membrane potential ( $\Delta\Psi_m$ ) analysis using JC-10 dye**

##### **Procedure:**

1. Cells were seeded at a density 50,000-1,00,000 cells/well to 6-well plate.
2. Cells were left for overnight incubation to facilitate attachment onto wells.
3. After incubation period, the spent medium was replaced with medium containing 2 % FBS with test samples and let to incubate for required period of time.
4. Positive controls were treated with carbonyl cyanide 3-chlorophenylhydrazone (CCCP) and untreated cells were maintained as negative controls.

5. The cells were harvested and treated with JC-10 dye loading solution for 30-60 min at 37 °C.
6. The cells were then washed with 1x PBS and resuspended in culture medium for flow cytometry analysis<sup>255,256</sup>.

### **3.7.13. Gene expression studies (RT-PCR)**

Real time polymerase chain reaction (RT-PCR) was used for the quantification of messenger RNA (m-RNA) levels using SYBR<sup>®</sup> green as the DNA intercalating dye. Beta-actin was used as the housekeeping gene for standardization of internal control for normalizing gene expression levels<sup>257</sup>.

#### **Procedure:**

##### **3.7.13.1. Pretreatment for RNA isolation:**

1. After incubation of cells with different nano formulations, the culture media was fully removed from the culture dish.
2. TRIzol<sup>®</sup> reagent was added directly to the cells in the culture dish (1 mL of TRIzol<sup>®</sup> reagent per 10 cm<sup>2</sup> of culture dish surface area).
3. Cells were lysed in the culture dish by pipetting the cells up and down several times<sup>244</sup>.
4. The cells were mixed until the fluid loses its colloidal nature and were transferred into a 1.5 mL sterile RNase free Eppendorf tubes.

### **3.7.13.2. Separating different phases:**

1. The homogenized samples from the above steps were incubated for 5 minutes at room temperature to facilitate complete dissociation of the nucleoprotein complex.
2. Chloroform was added to the samples in the proportion of 0.2 mL for every 1 mL TRIzol<sup>®</sup> reagent used for homogenization.
3. The tubes were shaken vigorously by hand for 15 seconds and incubated for 2-3 minutes at room temperature.
4. Following centrifugation of samples at 12,000 xg for 15 minutes at 4 °C, the mixture was seen to be separated into a lower red phenol chloroform phase, an interphase and a colorless upper aqueous phase.
5. The aqueous phase which contributed to ~50 % of the total volume of the mixture was removed by angling the tube at 45° and pipetting out the solution into another RNase free Eppendorf tube. Care was taken to avoid drawing of any of the interphase or organic layer into the pipette when removing the aqueous phase.

### **3.7.13.3. Precipitation of RNA:**

1. 0.5 mL of 100 % isopropanol was added to the aqueous phase for every 1mL TRIzol<sup>®</sup> reagent used for homogenization.
2. Mixed well and incubated the sample at room temperature for 10 min.

3. Centrifuged the cell suspension at 12,000 xg for 10 minutes at 4 °C.
4. Decanted the isopropanol taking care not to disturb the RNA pellet.
5. RNA washing and resuspension-
  - i. The pellet obtained in the above steps was washed with 1 mL of 75 % ethanol per 1 mL of TRIzol<sup>®</sup> reagent used in the initial homogenization procedure.
  - ii. The sample was briefly vortexed and then centrifuged at 7500 xg for 5 minutes at 4 °C. The wash solution was discarded.
  - iii. The RNA pellet was air dried for 5-10 minutes (vacuum drying was avoided to prevent extreme drying out of the pellet which can affect its solubility).
  - iv. The RNA pellet was re-suspended in RNase- free water (20-50 µL) by passing the solution up and down several times through the pipette tip.
  - v. It was then incubated on a heat block set at 55-60 °C for 10-15 minutes.

#### **3.7.13.4. Analysis of RNA yield and purity:**

1. A 100x dilution of the sample from the above RNA solution was prepared in RNase free water and measured its absorbance at 260 nm and 280 nm.
2. Used the formula:  $A_{260} \times \text{dilution} \times 40 = \mu\text{g RNA/mL}$  to determine the concentration.
3. A 260/280 ratio above 1.8 shows pure and high-quality RNA.

#### **3.7.13.5. Synthesis of c-DNA:**

1. Placed 1  $\mu\text{g}$  of total RNA in a micro centrifuge tube and incubated at 65 °C for 5 minutes, and then immediately placed on ice. Complementary DNA (c-DNA) synthesis was done using Thermo Scientific Verso cDNA synthesis Kit.
2. 10  $\mu\text{L}$  2x Reverse transcription mix which contained. i. 4  $\mu\text{L}$  Reverse Transcription 5x buffer ii. 1  $\mu\text{L}$  dNTP Mixture, 10 mM iii. 1  $\mu\text{L}$  Random Primers iv. 1  $\mu\text{L}$  RT Enhancer v. 1  $\mu\text{L}$  Verso Enzyme Mix, 15 units vi. 1  $\mu\text{g}$  Template RNA and vii. Nuclease- free water, made up to a final volume of 20  $\mu\text{L}$ , mixed well and spun down in a micro centrifuge.
3. Heated the reaction mix at 42 °C for 60 minutes.
4. Heated the sample at 95 °C for 2 minutes, and then incubated at 0-5 °C for 5 minutes. This will inactivate the reverse transcriptase and prevent it from binding to the c-DNA<sup>244</sup>.



**3.7.13.6. Gene expression studies:**

RNA was isolated from cell lines treated with different nano formulations over a period of time. Effect of these formulations on the expression of different genes were analyzed using real time PCR (RT-PCR) technique employing the c-DNA synthesized from the isolated RNA. The details of the genes studied and the sequences of the primers used are depicted in table 3.7.1.

**Table 3.7.1.** Primer sequences used for gene expression studies

| Sl. No. | Gene       | Sequence (5' to 3')                                | Annealing temp(°C) | Accession number   |
|---------|------------|--|--------------------|--------------------|
| 1.      | Beta actin | F- CTGTCTGGCGGCACCACCAT<br>R- GCAACTAAGTCATAGTCCGC | 59                 | X00351             |
| 2.      | Bcl2       | F- TCCTGCATCTCATGCCAAGG<br>R- TCCCAGAGGAAAAGCAACGG | 59                 | NM_00065 7.2       |
| 3.      | Bax        | F- TGACGGCAACTTCAACTGGG<br>R- AGTCGCTTCAGTGACTCGG  | 59                 | NM_00129<br>1428.1 |
| 4.      | Caspase-3  | F- TCTGGAATATCCCTGGACAA<br>R- ACGCATCAATTCACAATTT  | 58                 | NM_00135<br>4784.1 |

Gene specific primers mentioned in Table 3.7.1. were designed using Primer-3 software (<http://www.bioinformatics.nl/cgi-bin/primer3plus/primer3plus.cgi>) using the mRNA sequence of the gene from NCBI nucleotide database and custom synthesized by RFCL Science solutions, Bhopal, India.

### **3.8. DPPH activity**

#### **Procedure:**

1. DPPH solution was prepared by dissolving 1 mL of 0.1 mM DPPH stock solution and made up to 4 mL using 95 % ethanol.
2. The solution was mixed well and kept in dark condition.
3. The different nano formulations were mixed with DPPH solution and kept in dark for 30 min followed by analysis of decrease in the intensity of purple color of the original solution using a spectrophotometer at a wavelength of 517 nm against ethanol as blank.
4. A standard curve was plotted against values of ascorbic acid solutions with concentrations of 0, 0.25, 0.5, 2, 4, 6, 8, 10, 12 and 16 µg/mL obtained from stock culture prepared by dissolving 10 mg of ascorbic acid in 100 mL ethanol (100 µg/mL concentration).
5. The ability of the samples to reduce DPPH was expressed as percentage inhibition and determined using the following equation <sup>258</sup>:

$$\% \text{ Inhibition} = \frac{(\text{Absorbance of control} - \text{Absorbance of test sample})}{\text{Absorbance of control}} * 100$$

## RESULTS

### 4.1. Source identification, optimization of synthesis, and physicochemical analysis of biogenic silica nanoparticles

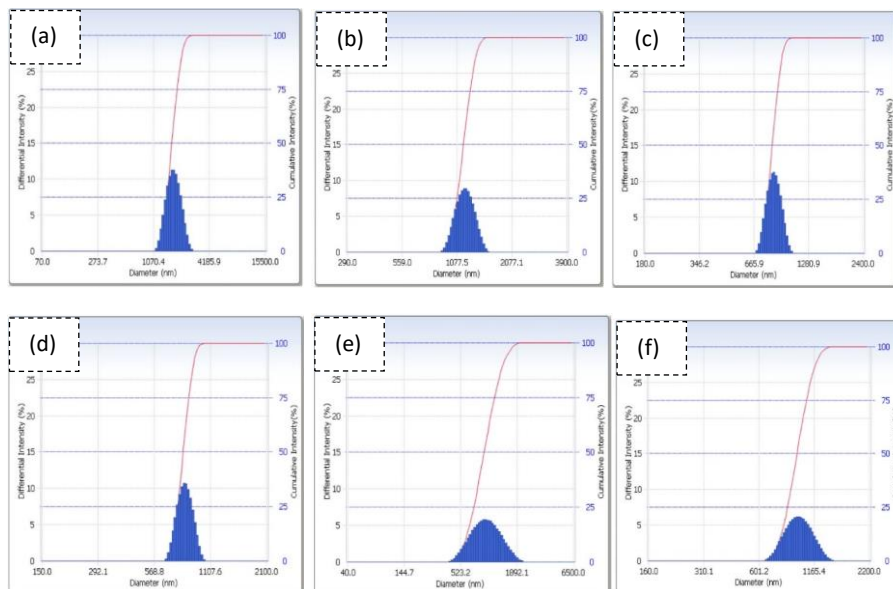
#### 4.1.1. Production of silica nanoparticles from diatomaceous earth using ball milling

**Table 4.1.1.** Variation of size of silica particles with milling time and speed

| Ball-to-powder ratio | Optimum parameters             |                  | Particle size of end-product (nm) |
|----------------------|--------------------------------|------------------|-----------------------------------|
|                      | Rotational speed of mill (rpm) | Milling time (h) |                                   |
| 1:1                  | 400                            | 5                | 1748.9±1.09 (a)                   |
| 2:1                  | 600                            | 4                | 1184.8±2.3 (b)                    |
| 4:1                  | 800                            | 6                | 842.1±1.89 (c)                    |
| 8:1                  | 1000                           | 6                | 814.8±1.03 (d)                    |
| 10:1                 | 1000                           | 6                | 966.8±3.29 (e)                    |
| 20:1                 | 1000                           | 6                | 972.1±2.4 (f)                     |

From the table above, it can be observed that the smallest particle size was obtained for the samples subjected to ball-milling at ball-to-powder of 8:1 and rotational speed of 1000 rpm for 6 h. However, a further increase in ball-to-powder ratio did not reduce the size of the particles. The final size of the particles did not fall into the range (>100 nm) expected for it to be used as drug carriers.

**Figure 4.1.1.** Particle size intensity distribution curves related to variation of size of silica particles with milling time (h) and speed (rpm)



*Note:* (a)-(f) are particles mentioned in table 4.1.1.

Figure 4.1.1 shows the particle size intensity distribution curves of the ball-milled samples. The narrower peaks indicate the distribution of particles within the sample to lie within a narrow range of size range, while the broader peaks are indicative of heterogeneity in the sample size distribution. Samples labelled a, b, c and d had more uniformly sized particles as compared to samples e and f. Increase in ball-to-powder ratio beyond 8:1 was not found to be effective to produce particles within uniformity in particle size.

### 4.1.2. Effect of ball-milling on other physical and chemical properties of silica nanoparticles

**Figure 4.1.2.** XRD spectrum of ball-milled diatomaceous earth-derived silica particles

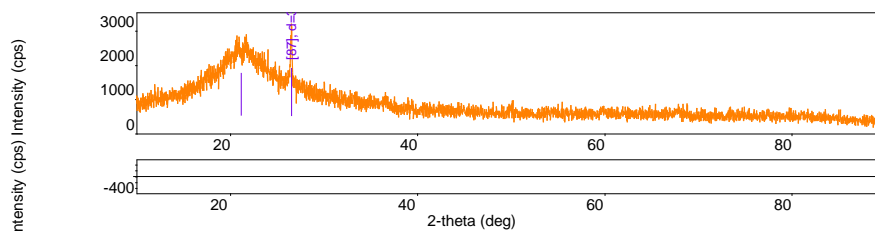
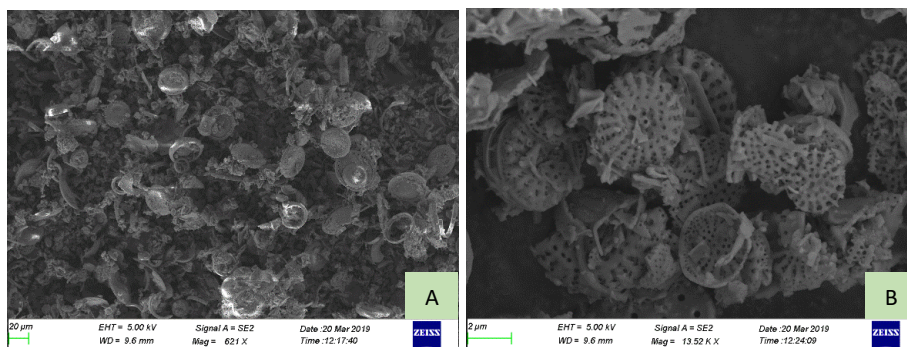
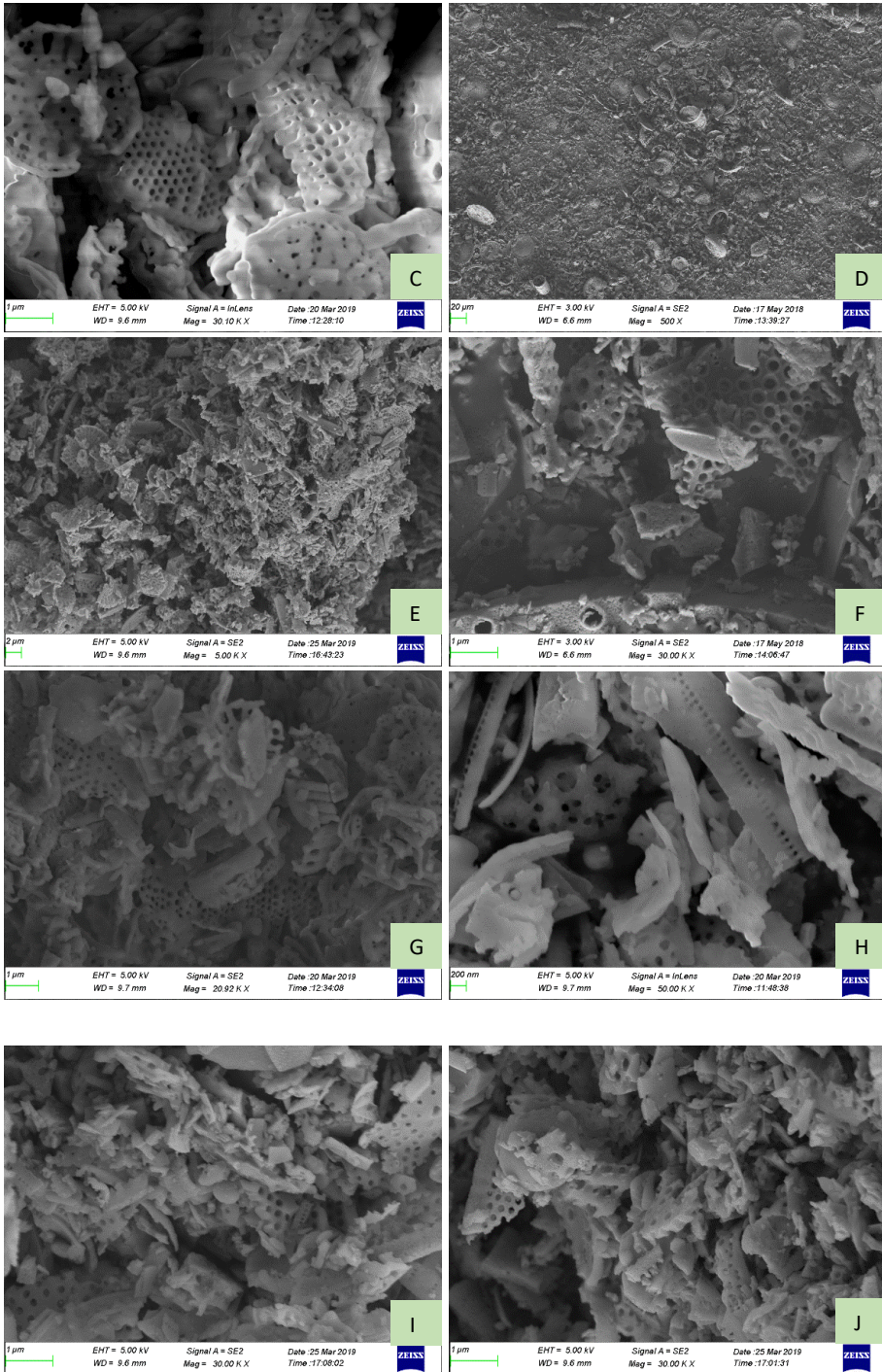
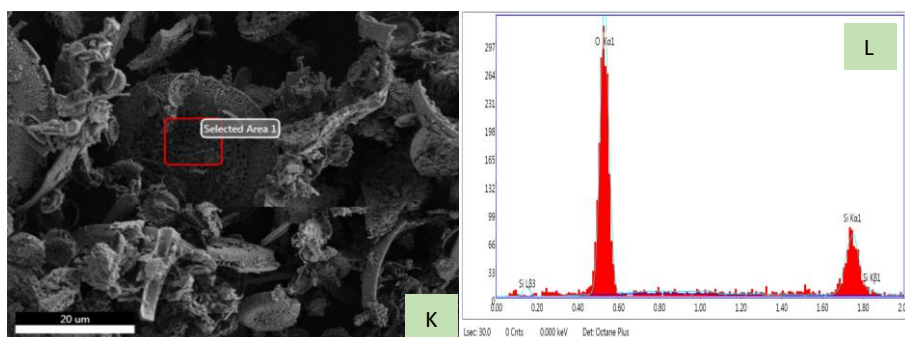


Figure 4.1.2 showing broader peak at  $2\theta$  angle of  $\sim 22^\circ$  is indicative of the presence of silica in its amorphous form. Crystalline phase of samples is normally seen as sharper peaks in the XRD spectrum, which is absent in this sample. Presence of peaks of only silica is an indicator of the purity of the sample.

**Figure 4.1.3.** (A), (B), and (C) show FESEM images of diatom frustules before ball-milling, (D) to (J) show FESEM images of diatom frustules after ball-milling and (L) shows EDAX spectrum of the area marked in (K)





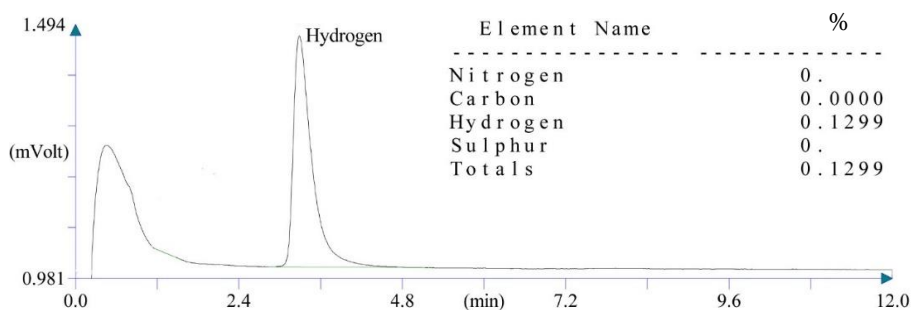


### eZAF Smart Quant Results

| Element | Weight % | Atomic % | Net Int. | Error % | K-ratio | Z      | A      | F      |
|---------|----------|----------|----------|---------|---------|--------|--------|--------|
| O K     | 37.13    | 50.90    | 66.35    | 10.50   | 0.3706  | 1.1029 | 0.9050 | 1.0000 |
| SiK     | 62.87    | 49.10    | 21.87    | 20.37   | 0.5873  | 0.9375 | 0.9960 | 1.0004 |

Intricate porous structure of diatom frustules can be seen in FESEM images in figure 4.1.3 (A to C). The particle size varied from 1200-1800 nm, consistent to the values obtained from dynamic light scattering analysis data in figure 4.1.1. Upon ball-milling, the porous structures were destroyed as can be seen from D to J above. Presence of only silicon and oxygen peaks in the EDAX spectrum (L) is indicative of absence of impurities in the sample. The results were also in alignment with that of XRD analysis which ruled out the presence of other components in the sample.

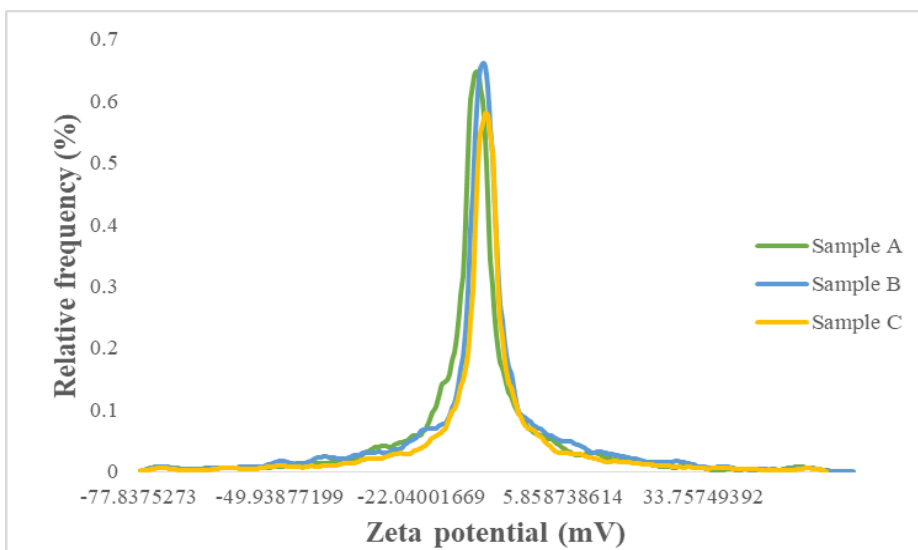
**Figure 4.1.4.** CHNS analysis result of ball-milled diatomaceous earth-derived silica particles



CHNS analysis indicated absence of constituents containing nitrogen, carbon or sulfur. Hydrogen was present at the level of 0.13 %. It is also an indicator of the purity of sample tested.

#### *Effect of ball-milling on zeta potential of silica particles*

**Figure 4.1.5.** Variation of zeta potential values in ball-milled (A and B) and unmilled samples (C)





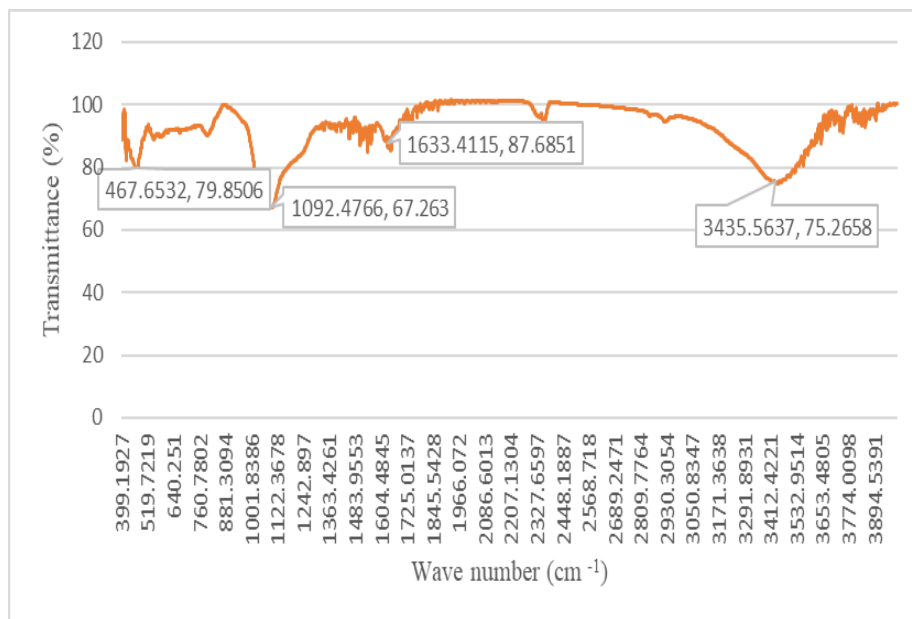
| Sample                                | Zeta potential (mV) (Mean $\pm$ SD) |
|---------------------------------------|-------------------------------------|
| <b>Ball-milled sample A</b> (6h, 4:1) | -10.282 $\pm$ 1.012                 |
| <b>Ball-milled sample B</b> (6h, 8:1) | -10.895 $\pm$ 1.079                 |
| <b>Unmilled sample C</b>              | -4.328 $\pm$ 0.211                  |

Ball-milling involves impact and attrition forces resulting in the reduction of particle size. Reduction in particle size results in increase in surface area with more particles at the surface becoming exposed. This is indicated from and increase in the negative values of zeta potential in the figure above. When the ball-to-powder ratio was increased from 4:1 to 8:1, the reduction in particle size resulted in more negative zeta potential values from the exposure of more negatively charged groups silanol ( $\text{SiO}^-$ ) on the surface.

**Table 4.1.2.** Nitrogen sorption analysis of surface area and pore parameters of silica particles from diatomaceous earth

| Sample                    | Surface area (BET, $\text{m}^2/\text{g}$ ) | Pore-size (BET, nm) | Pore-volume (BJH, $\text{cm}^3/\text{g}$ ) |
|---------------------------|--|---------------------|--|
| <b>Unmilled sample</b>    | 5.6484 $\pm$ 1.59                          | 11.29119 $\pm$ 1.28 | 0.025095 $\pm$ 0.011                       |
| <b>Ball-milled sample</b> | 8.2229 $\pm$ 2.13                          | 16.4373 $\pm$ 2.92  | 0.039542 $\pm$ 0.341                       |

Ball-milling led to reduction of particle size, resulting in an increase in the surface area from 5.6484  $\text{m}^2/\text{g}$  to 8.22  $\text{m}^2/\text{g}$ , with a proportional increase in particle pore-size and pore-volume as can be seen from the figure above.

**Figure 4.1.6.** FTIR spectrum of silica particles from diatomaceous earth**Table 4.1.3.** Chemical interaction as seen from FTIR spectrum of diatomaceous earth derived silica sample

| Wave number (cm <sup>-1</sup> ) | Suggestive chemical interaction |
|---------------------------------|---------------------------------|
| 3700-3100                       | O-H stretching functional group |
| 1250-1000                       | Si-O-Si interaction             |
| ~465                            | Si-OH stretching vibration      |

Presence of chemical interactions between only Si-O-Si, Si-OH and O-H in the FTIR spectrum above is also an indicator of the purity of sample

**Table 4.1.4.** XRF analysis of silica particles derived from diatomaceous earth

| Elemental composition (%) | SiO <sub>2</sub> | Al <sub>2</sub> O <sub>3</sub> | Fe <sub>2</sub> O <sub>3</sub> | P <sub>2</sub> O <sub>5</sub> | MgO  | K <sub>2</sub> O | SO <sub>3</sub> | CaO   | Ti   |
|---------------------------|------------------|--------------------------------|--------------------------------|-------------------------------|------|------------------|-----------------|-------|------|
| SD                        | 85.94            | 0.62                           | 0.34                           | 0.05                          | 0.20 | 0.09             | 0.05            | 12.47 | 0.04 |
|                           | 6.07             | 0.15                           | 0.12                           | 0.01                          | 0.07 | 0.02             | 0.01            | 5.2   | 0.01 |

XRF analysis helps in the elemental analysis of the sample and from the XRF analysis data in table 4.1.4, it can be seen that the silica ( $\text{SiO}_2$ ) levels of the sample were 85.94 %. Traces of oxides of other elements like aluminium, iron, phosphorus, magnesium, potassium, sulfur, calcium were also seen along with 0.04 % titanium. XRF being a more sensitive technique could identify the presence of trace levels of extraneous compounds that was missed in CHNS and XRD analyses.

## 4.2. Production of silica nanoparticles from agricultural biomass

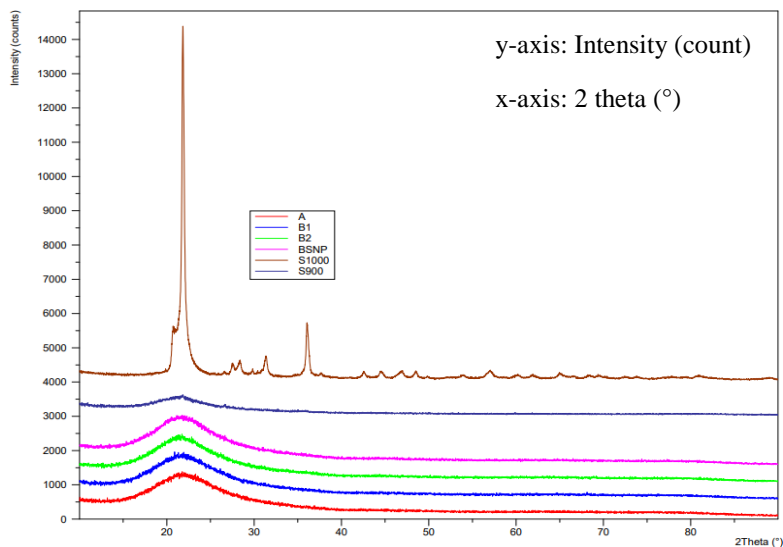
### 4.2.1. Optimization of biogenic silica nanoparticle synthesis in terms of acid pretreatment, incineration temperature, and time of combustion

**Table 4.2.1.** Yield of silica particles from different raw materials used

| <b>Sample</b>             | <b>% Silica ash obtained</b> |
|---------------------------|------------------------------|
| <b>Rice husk</b>          | 14                           |
| <b>Corn husk</b>          | 2.1068                       |
| <b>Indian goose grass</b> | 1.448                        |
| <b>Coffee husk</b>        | 1.032                        |
| <b>Sugarcane bagasse</b>  | 0.896                        |

From table 4.2.1 above, it can be seen that the silica yield from rice husk was found to be highest (14 %), followed by corn husk (2.1 %), grass (1.44 %), coffee husk (1.03 %) and sugarcane bagasse (0.9 %). Factors like silica absorption of plants, variation in soil composition of silica, drought conditions and other seasonal fluctuations may cause variation in the levels of silica in samples.

**Figure 4.2.1.** XRD spectrum of samples heated at different temperatures at constant time of combustion

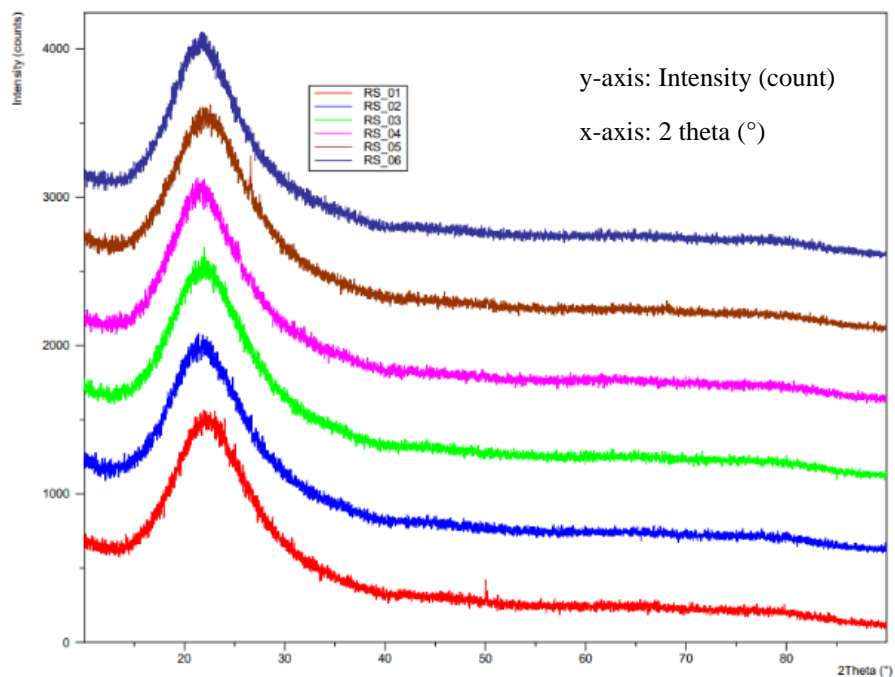


*Note:*

- A- Rice husk sample pretreated with 1N HCl, incinerated at 800 °C for 60 min
- B1- Rice husk sample pretreated with 1N HCl, incinerated at 500 °C for 60 min
- B2- Rice husk sample pretreated with 1N HCl, incinerated at 700 °C for 60 min
- BSNP- Rice husk sample pretreated with 1N HCl, incinerated at 600 °C for 60 min
- S1000- Rice husk sample pretreated with 1N HCl, incinerated at 1000 °C for 60 min
- S900- Rice husk sample pretreated with 1N HCl, incinerated at 900 °C for 60 min

Samples A, B1, b2, BSNP, S900 which were subjected to temperature below 1000 °C during its production resulted in amorphous form of silica as is indicated by the broader peaks at  $2\theta$  of  $\sim 22^\circ$  from the XRD spectrum above. However, an increase in temperature above 1000 °C would have resulted in the molecular rearrangement and re-ordering resulting in crystalline form of silica which is indicated by sharp curve.

**Figure 4.2.2.** XRD spectrum of rice husk-derived silica samples subjected to different incineration periods at constant temperatures of incineration

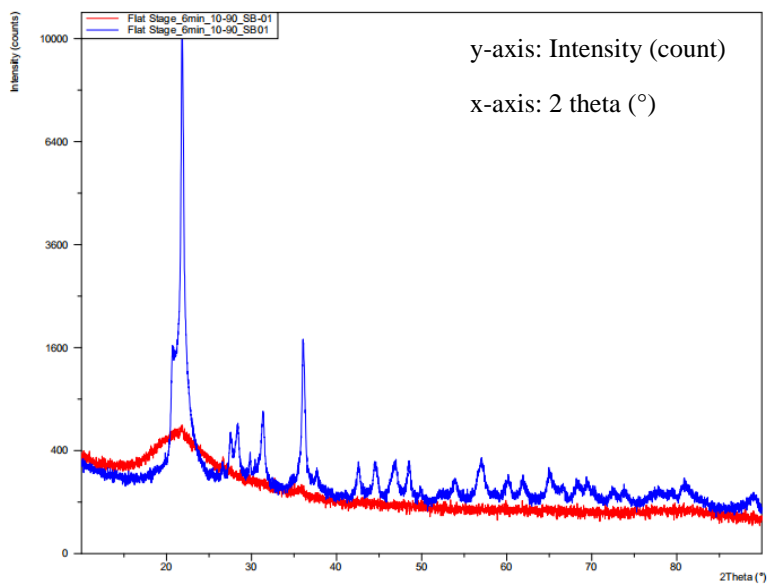


*Note:*

- RS01- Rice husk sample pretreated with 1N HCl, incinerated at 500 °C for 30 min
- RS02- Rice husk sample pretreated with 1N HCl, incinerated at 500 °C for 60 min
- RS03- Rice husk sample pretreated with 1N HCl, incinerated at 500 °C for 80 min
- RS04- Rice husk sample pretreated with 1N HCl, incinerated at 500 °C for 90 min
- RS05- Rice husk sample pretreated with 1N HCl, incinerated at 500 °C for 100 min
- RS06- Rice husk sample pretreated with 1N HCl, incinerated at 500 °C for 240 min

The samples subjected to different incineration periods at constant temperatures of incineration showed similar pattern in the XRD spectrum above, indicating presence of amorphous silica formation in all the synthesis process.

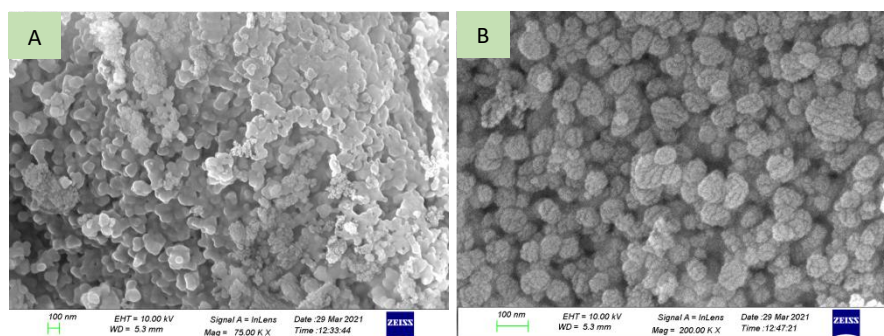
**Figure 4.2.3.** XRD diffractogram of the sample showing transition from amorphous to crystalline phase with an increase in incineration temperature



The spectrum above indicates the influence of temperature on determining the phase of silica formed during the process. Working temperatures above 1000 °C resulted in crystalline form (blue curve in the figure above) of silica, while those below resulted in formation of amorphous form of silica which is indicated as broad peak (red pattern in the XRD spectrum above).

#### 4.2.2. Physicochemical analysis of biogenic silica particles from agricultural biomass

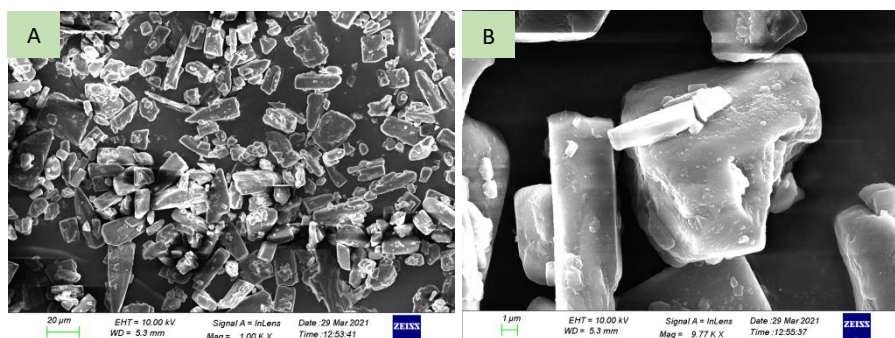
**Figure 4.2.4.** FESEM images of silica particles from Indian goose grass (A) at magnification of 75K X and (B) 200K X



*Note:* Magnification of images respectively are: (A) 75K X and (B) 200K X.

The FESEM images show presence of almost spherical particle of less than 100 nm, with porous structures. The particles are also seen to present as clumps.

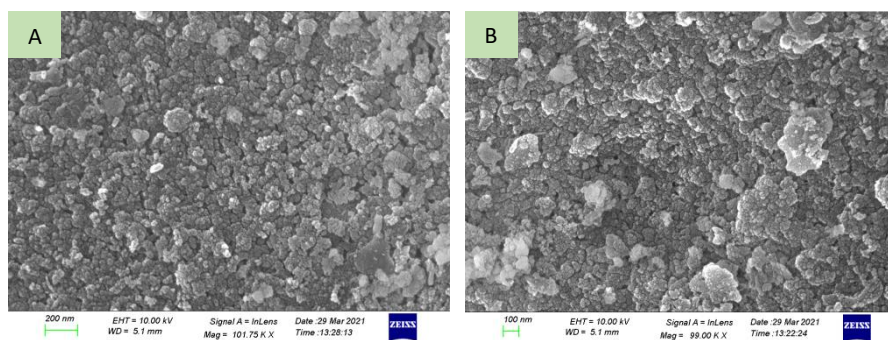
**Figure 4.2.5.** FESEM images of silica particles from coffee husk



*Note:* Magnification of images respectively are: (A) 1K X and (B) 9.77K X.

The FESEM images from figure 4.2.5 show the particles to possess irregular shape. Presence of angular and rhomboid particles in the micrometer size range were seen.

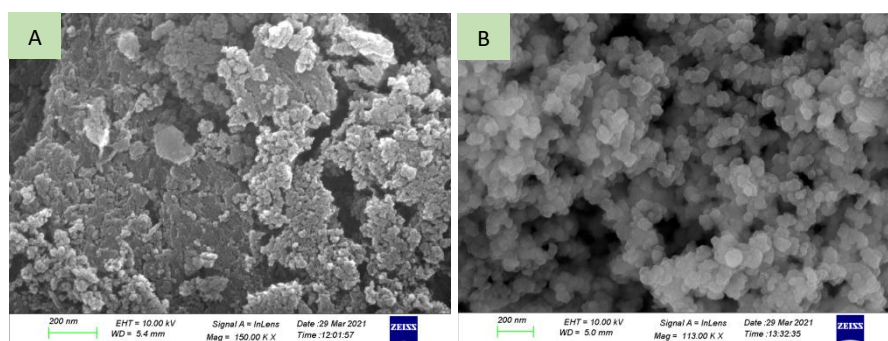
**Figure 4.2.6.** FESEM images of silica particles from corn husk



*Note:* Magnification of images respectively are: (A) 101.75 X and (B) 99K X.

Particles from corn husk could be seen as closely packed and clustered entities with spherical morphology in the figure above.

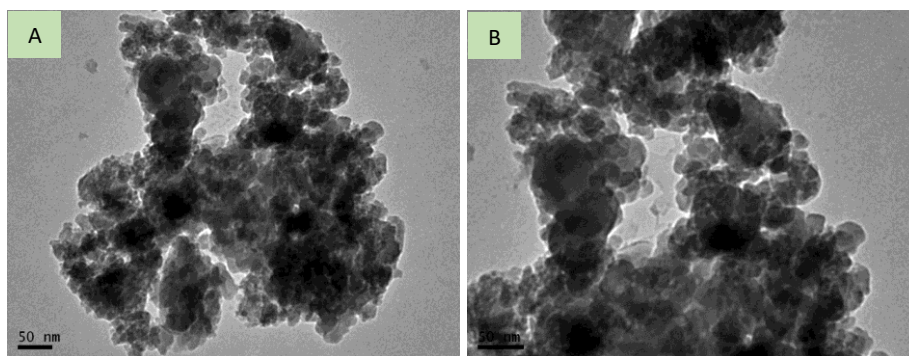
**Figure 4.2.7.** FESEM images of silica particles from rice husk



*Note:* Magnification of images respectively are: (A) 150K X and (B) 113K X.

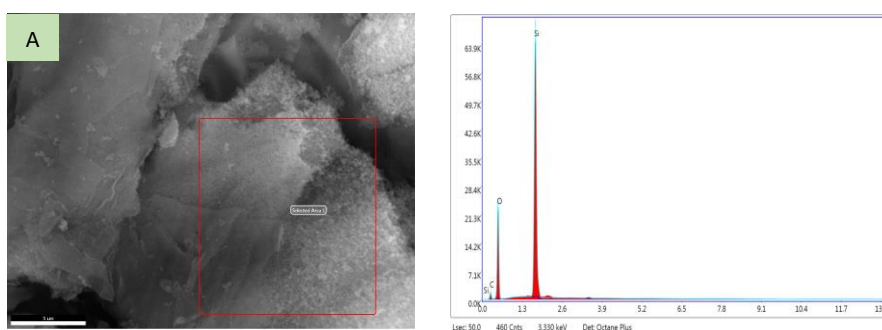
Clumped spherical silica particles are seen in the figure above.



**Figure 4.2.8.** TEM analysis images of rice husk derived silica particles

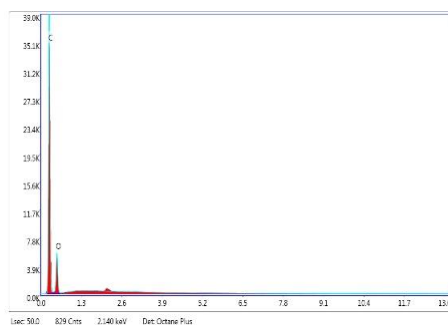
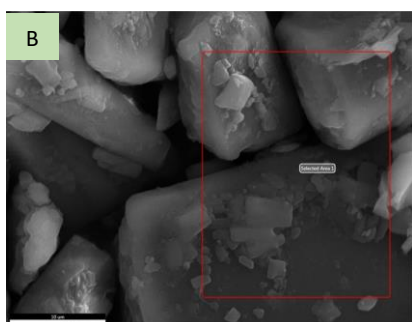
*Note:* Magnification of images respectively are: (A) 102K X and (B) 178K X.

Particles derived from rice husk possessed spherical shape and were seen as clusters as seen from the TEM micrograph above. The particles were of sizes less than 100 nm. The results were in agreement with that from FESEM analysis.

**Figure 4.2.9.** EDAX analysis result of samples from (A) rice husk, (B) Indian goose grass, (C) sugarcane bagasse, (D) corn husk and (E) coffee husk respectively

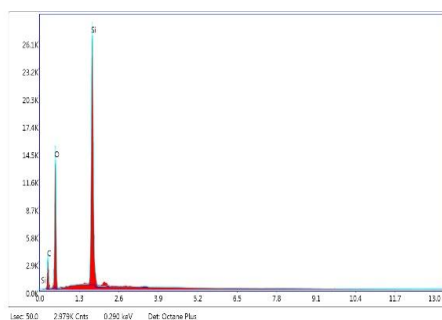
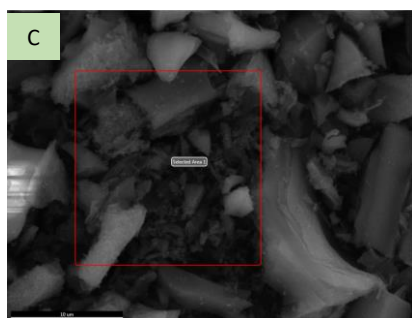
### eZAF Smart Quant Results

| Element | Weight %   | Atomic %   | Net Int.      |
|---------|------------|------------|---------------|
| C K     | 13.43±0.9  | 20.49±0.68 | 215.24±0.42   |
| O K     | 46.75±1.02 | 53.54±0.79 | 3058.63±1.27  |
| SiK     | 39.82±0.15 | 25.97±0.21 | 11621.74±0.37 |



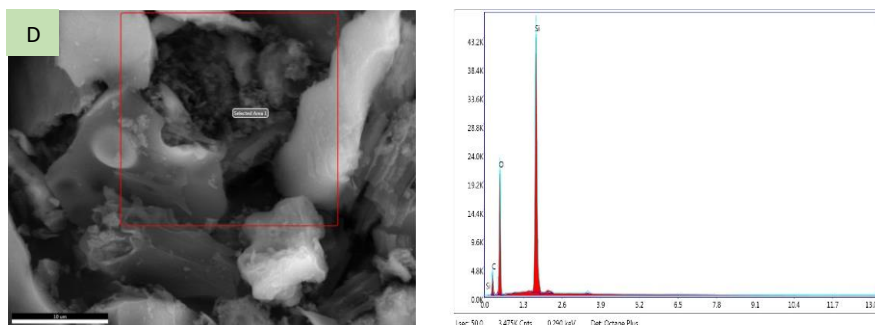
**eZAF Smart Quant Results**

| Element | Weight %  | Atomic %  | Net Int.     |
|---------|-----------|-----------|--------------|
| C K     | 73.42±1.3 | 78.63±1.2 | 4903.32±0.78 |
| O K     | 26.58±1.8 | 21.37±0.9 | 648.37±1.45  |
| SiK     | 65.27±0.9 | 69.83±0.5 | 4578.91±0.87 |



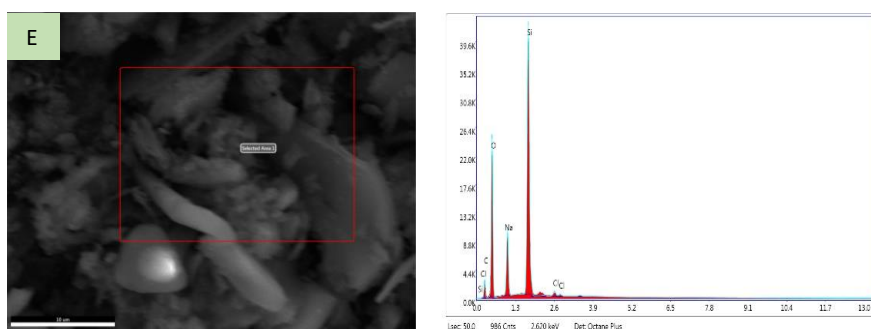
**eZAF Smart Quant Results**

| Element | Weight %   | Atomic %   | Net Int.     |
|---------|------------|------------|--------------|
| C K     | 26.98±0.67 | 36.54±0.89 | 405.99±0.56  |
| O K     | 48.4±1.1   | 49.21±1.02 | 1843.83±0.82 |
| SiK     | 24.62±0.51 | 14.26±0.78 | 4662.97±0.38 |



### eZAF Smart Quant Results

| Element | Weight %   | Atomic %   | Net Int.     |
|---------|------------|------------|--------------|
| C K     | 23.65±1.03 | 32.86±0.62 | 490.64±0.83  |
| O K     | 48.49±0.84 | 50.59±0.75 | 2883.03±0.57 |
| SiK     | 27.86±1.12 | 16.55±0.81 | 7965.86±0.94 |



### eZAF Smart Quant Results

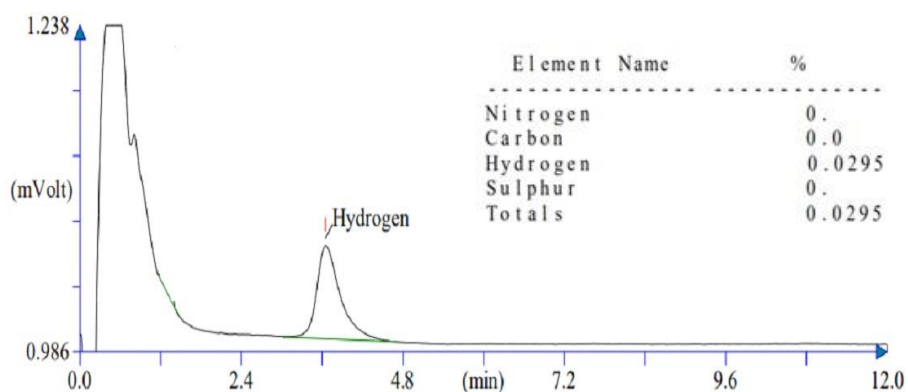
| Element | Weight %   | Atomic %   | Net Int.     |
|---------|------------|------------|--------------|
| C K     | 15.9±2.7   | 23.6±1.27  | 302.05±0.78  |
| O K     | 44.57±0.84 | 49.68±0.68 | 3090.76±0.27 |
| SiK     | 26.72±0.21 | 16.97±0.47 | 7096.2±0.38  |

*NB:* The values are expressed as mean values ± SD from  $n = 6$  for samples (A) to (E)

EDAX analysis was coupled with FESEM analysis. The presence of carbon in the samples could be from the particle fixing and preparation

carried prior to the analysis using carbon tape. Absence of any other elements in the spectra is indicative of the purity of the samples analyzed. In all the samples above, presence of peaks of silicon and oxygen were seen.

**Figure 4.2.10.** CHNS analysis result of rice husk-derived silica particles



CHNS analysis result above, revealed absence of entities containing carbon, nitrogen or sulfur. Traces of hydrogen seen is likely from the presence of water due to the innate hygroscopic nature of silica sample.

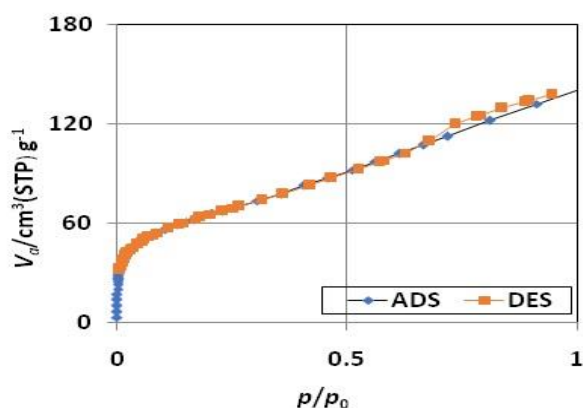
*Surface area and pore properties*

**Table 4.2.2.** Nitrogen sorption evaluation of silica particles derived from different agricultural biomass

| Sample             | BET area (m <sup>2</sup> /g) | Total pore volume (cm <sup>3</sup> /g) | Average pore size (nm) |
|--------------------|------------------------------|--|------------------------|
| Coffee husk        | 1.4327                       | 0.015087                               | 2.121                  |
| Sugarcane bagasse  | 2.3274                       | 0.0016648                              | 2.8612                 |
| Corn husk          | 151.96                       | 0.1027                                 | 2.7028                 |
| Indian goose grass | 211.78                       | 0.1903                                 | 3.5948                 |
| Rice husk          | 232.20                       | 0.2155                                 | 3.7117                 |

BET area of silica samples derived from rice husk was found to possess highest value as compared to other samples. The pore-volume and pore-size of rice-husk derived silica particles were also found to be the highest from the rest of the samples.

**Figure 4.2.11.** Adsorption-desorption isotherm of silica nano particles from rice husk showing type IV pattern characteristic of mesoporous particles



The isotherm in figure 4.2.11 from nitrogen sorption study showed a type IV pattern of adsorption-desorption which is characteristic of mesoporous particles.

**Table 4.2.3.** Nitrogen sorption evaluation of rice husk-derived silica particles as a function of acid pretreatment

| Sample  | BET area (m <sup>2</sup> /g) | Total pore volume (cm <sup>3</sup> /g) | Average pore size (nm) |
|---|------------------------------|--|------------------------|
| HCl treated sample                            | 232.20                       | 0.2155                                 | 3.7117                 |
| H <sub>2</sub> SO <sub>4</sub> treated sample | 207                          | 0.1988                                 | 3.2354                 |

BET surface area and pore properties like pore volume and pore size were found to be higher in samples subjected to pretreatment using hydrochloric acid as compared to those that were treated with sulfuric acid as can be seen in the table above.

#### *Particle size analysis*

**Table 4.2.4.** Variation of particle size of rice husk-derived silica particles as a function of incineration temperature and incineration time

| Temperature (°C) /Time (min) | 60    | 80    | 90    | 100   | 240   |
|------------------------------|-------|-------|-------|-------|-------|
| 500                          | 72.04 | 65.67 | 62.05 | 59.01 | 50.23 |
| 600                          | 74.28 | 62.07 | 57.29 | 52.41 | 46.79 |
| 700                          | 68.29 | 58.34 | 54.26 | 50.72 | 42.30 |
| 800                          | 59    | 56.85 | 52.42 | 41.07 | 39.12 |
| 900                          | 52.25 | 45.4  | 43.16 | 37.4  | 33.54 |
| 1000                         | 40.72 | 38.58 | 35    | 32    | 30.02 |

The figures from the table 4.2.4 showed that there was a decrease in the size of the particles with an increase in incineration time and temperature.

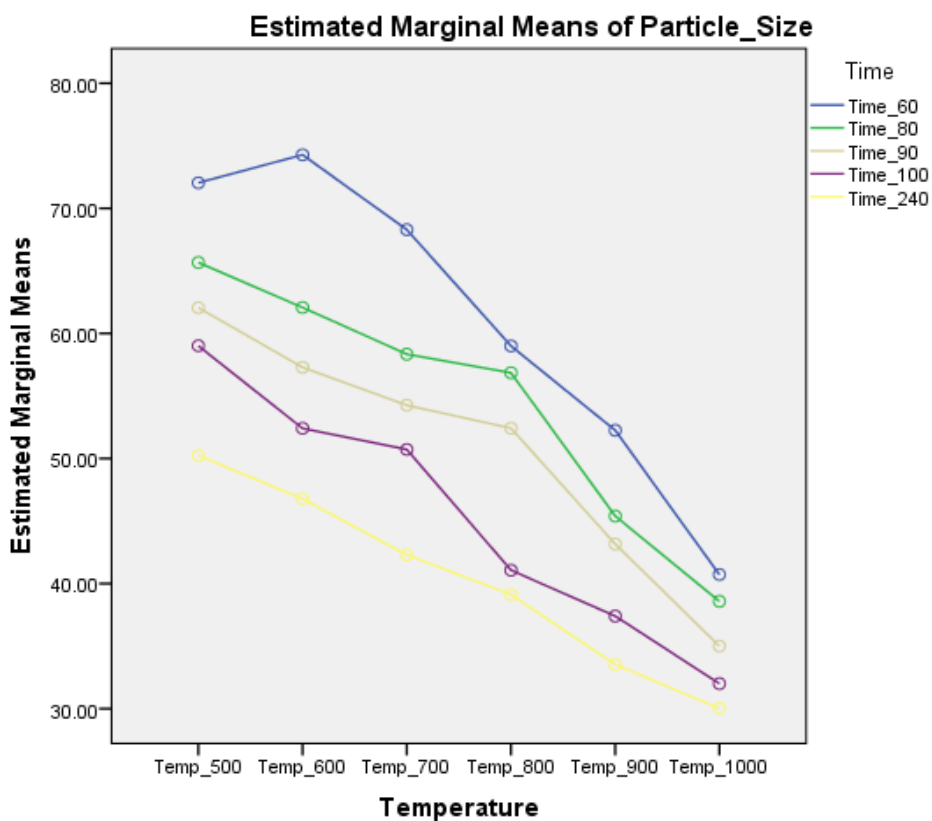
**Table 4.2.5.** Variation of particle size of rice husk-derived silica particles as a function of incineration temperature and acid pretreatment

| Sample/Temperature (°C)                       | 500   | 600   | 700   | 800   | 900   | 1000  |
|---|-------|-------|-------|-------|-------|-------|
| HCl treated sample                            | 50.23 | 46.79 | 42.30 | 39.12 | 33.54 | 30.02 |
| H <sub>2</sub> SO <sub>4</sub> treated sample | 55.40 | 52.23 | 45.83 | 43.71 | 43.29 | 42.08 |

*Note:* The particle size values in the tables are expressed in nm

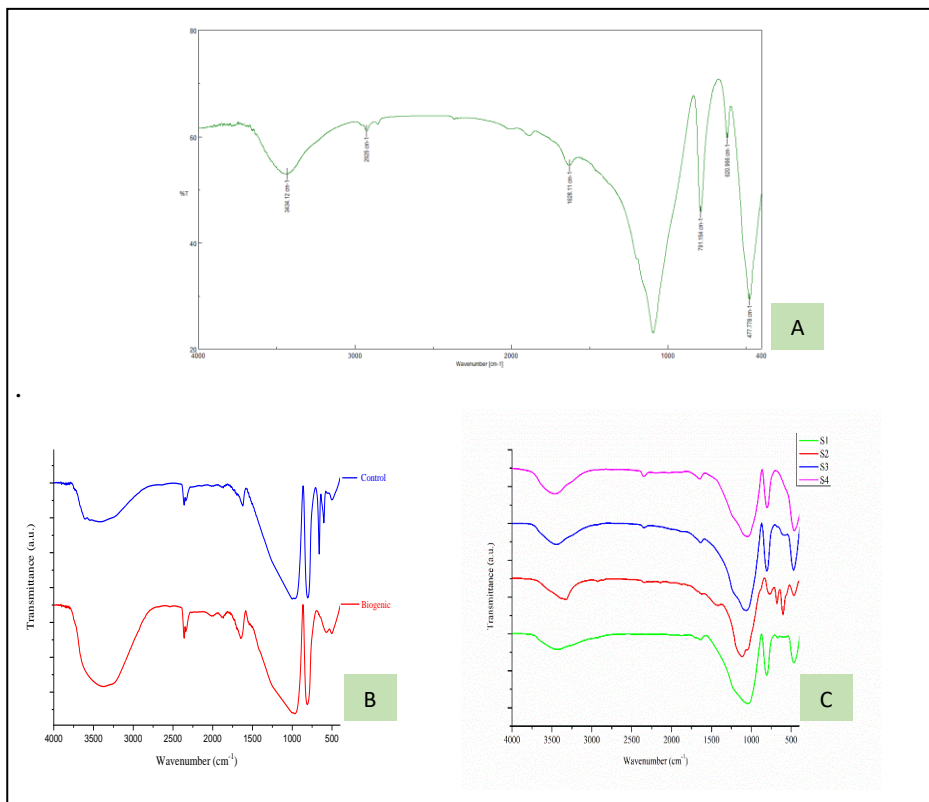
HCl treated sample smallest size at an incineration temperature of 1000 °C while sulfuric acid treated samples resulted in larger sized particles as indicated in table above.

**Figure 4.2.12.** Showing correlation between particle size of end-product with incineration temperature and time



From the above figure, a correlation between particle size and incineration time and temperature can be seen. With an increase in incineration time and temperature a reduction in the size of the particles were observed.

**Figure 4.2.13.** FTIR spectrum of (A) rice husk-derived silica particles (B) chemically synthesized and biogenic silica particles and (C) silica particles derived from Indian goose grass, sugarcane bagasse, corn husk and coffee husk respectively



*Note:*

In figure (C) above,

- S1 - silica particles derived from Indian goose grass
- S2 - silica particles derived sugarcane bagasse
- S3 - silica particles derived from corn husk and
- S4 - silica particles derived from coffee husk

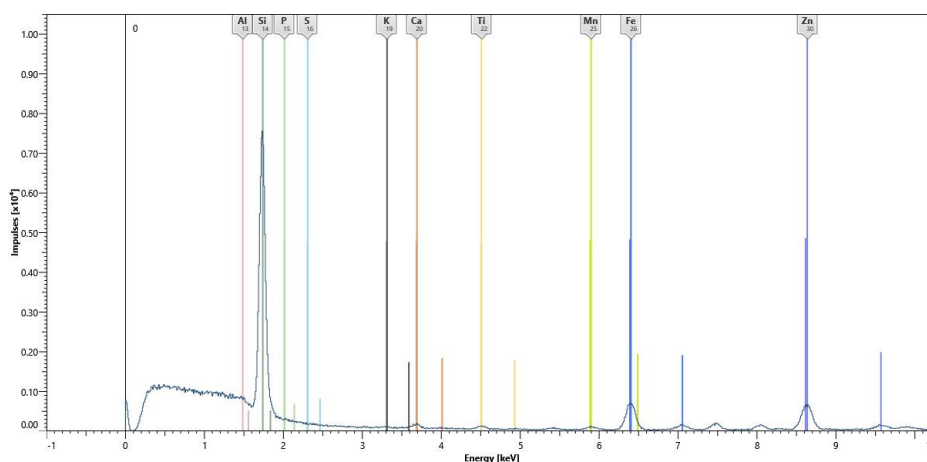
Presence of O-H and Si-O interactions in the figure is indicated in table 4.2.6, suggestive of absence of extraneous contaminants in the sample analyzed.



**Table 4.2.6.** Chemical interaction as seen from FTIR spectrum of rice husk derived silica sample

| Wave number (cm <sup>-1</sup> ) | Suggestive chemical interaction            |
|---------------------------------|--|
| 3700-3000                       | O-H stretching band of water               |
| ~3438                           | Bound water associated with polymer matrix |
| 1700-1550                       | O-H bending band region of water           |
| 800-810                         | Si-O group bending vibration mode          |
| 790-800                         | Si-O bending vibration mode                |
| ~500                            | Rocking mode of Si-O group                 |

**Figure 4.2.14.** XRF spectrum of rice husk derived silica nanoparticles



y-axis: Impulses (x10<sup>4</sup>)

x-axis: Energy (keV)

The spectrum above shows the presence of silicon along with aluminium, phosphorus, sulfur, potassium, calcium, titanium, manganese, iron and zinc as is indicated separately in tables 4.2.7 and 4.2.8.

**Table 4.2.7.** XRF analysis of silica particles derived from rice husk

| Elemental composition (%) | SiO <sub>2</sub> | Al <sub>2</sub> O <sub>3</sub> | Fe <sub>2</sub> O <sub>3</sub> | P <sub>2</sub> O <sub>5</sub> | MgO         | K <sub>2</sub> O | SO <sub>3</sub> | CaO         | Ti           |
|---------------------------|------------------|--------------------------------|--------------------------------|-------------------------------|-------------|------------------|-----------------|-------------|--------------|
|                           | 99.96            | 0.00002141                     | 0.000003152                    | 0.000005135                   | 0.000001113 | 0.000001108      | 0.000001599     | 0.000001532 | 0.0000004907 |
| <b>SD</b>                 | 2.01             | 0.03                           | 0.02                           | 0.01                          | 0.01        | 0.02             | 0.01            | 0.23        | 0.16         |


**Table 4.2.8.** XRF analysis of silica particles derived from agricultural biomass

| Elemental composition (%) | SiO <sub>2</sub> | Al <sub>2</sub> O <sub>3</sub> | Fe <sub>2</sub> O <sub>3</sub> | P <sub>2</sub> O <sub>5</sub> | MgO     | K <sub>2</sub> O | SO <sub>3</sub> | CaO    | Ti       |
|---------------------------|------------------|--------------------------------|--------------------------------|-------------------------------|---------|------------------|-----------------|--------|----------|
| <b>Indian goose grass</b> | 96.14            | 0.272                          | 0.6277                         | 0.3995                        | 0.345   | 0.2859           | 0.2775          | 0.2693 | 0.1703   |
| <b>Sugarcane bagasse</b>  | 92.06            | 2.099                          | 0.3825                         | 0.04803                       | 0.01007 | 1.02823          | 1.1866          | 2.1163 | 0.007336 |
| <b>Corn husk</b>          | 68.55            | 1.561                          | 0.294                          | 5.672                         | 0.552   | 1.411            | 0.137           | 3.661  | 0.01407  |
| <b>Coffee husk</b>        | 48.19            | 14.58                          | 2.265                          | 5.789                         | 1.923   | 2.356            | 13.16           | 9.16   | 0.366    |


**Table 4.2.9.** Zeta potential values of silica samples from different raw materials used in the study

| Sample                    | Mean zeta potential value (mV) | Standard deviation (n=5) |
|---------------------------|--------------------------------|--------------------------|
| <b>Rice husk</b>          | -30.11                         | 2.75                     |
| <b>Indian goose grass</b> | -22.20                         | 1.37                     |
| <b>Corn husk</b>          | -19.40                         | 2.13                     |
| <b>Sugarcane bagasse</b>  | -18.71                         | 2.06                     |
| <b>Coffee husk</b>        | -15.78                         | 2.46                     |


**Figure 4.2.15.** Zeta potential analysis report of (A) rice husk, (B) Indian goose grass, (C) corn husk, (D) sugarcane bagasse and (E) coffee husk respectively

 Summary Statistics Report A


| Type | Start Date/Time     | Sample ID     | Zeta Potential (mV) | Mobility ( $\mu\text{s}/(\text{V}/\text{cm})$ ) | RMS Residual |            |
|------|---------------------|---------------|---------------------|---|--------------|------------|
| PALS | 05-04-2021 15:43:40 | AR0142Y21 - 1 | -33.51              | -1.75   | 1.9634e-02   |            |
| PALS | 05-04-2021 15:45:18 | AR0142Y21 - 2 | -28.84              | -1.50   | 2.3242e-02   |            |
| PALS | 05-04-2021 15:46:55 | AR0142Y21 - 3 | -31.03              | -1.62   | 1.7960e-02   |            |
| PALS | 05-04-2021 15:48:33 | AR0142Y21 - 4 | -26.18              | -1.36   | 2.1518e-02   |            |
| PALS | 05-04-2021 15:50:11 | AR0142Y21 - 5 | -30.98              | -1.61   | 2.2516e-02   |            |
|      |                     |               | Mean:               | -30.11  | -1.57        | 2.0978e-02 |
|      |                     |               | Std Err:            | 1.23  | 0.06         | 9.6376e-04 |
|      |                     |               | Std Dev:            | 2.75  | 0.14         | 2.1550e-03 |

 Summary Statistics Report B


| Type | Start Date/Time     | Sample ID     | Zeta Potential (mV) | Mobility ( $\mu\text{s}/(\text{V}/\text{cm})$ ) | RMS Residual |            |
|------|---------------------|---------------|---------------------|---|--------------|------------|
| PALS | 05-04-2021 14:56:43 | AR0142Y21 - 1 | -24.36              | -1.27   | 6.3474e-02   |            |
| PALS | 05-04-2021 14:58:20 | AR0142Y21 - 2 | -22.76              | -1.19   | 2.8005e-02   |            |
| PALS | 05-04-2021 14:59:58 | AR0142Y21 - 3 | -21.31              | -1.11   | 3.4671e-02   |            |
| PALS | 05-04-2021 15:01:35 | AR0142Y21 - 4 | -21.19              | -1.10   | 1.0128e-02   |            |
| PALS | 05-04-2021 15:03:13 | AR0142Y21 - 5 | -21.36              | -1.11   | 1.2414e-02   |            |
|      |                     |               | Mean:               | -22.20  | -1.16        | 2.9738e-02 |
|      |                     |               | Std Err:            | 0.61  | 0.03         | 9.6181e-03 |
|      |                     |               | Std Dev:            | 1.37  | 0.07         | 2.1507e-02 |

 Summary Statistics Report C

| Type | Start Date/Time     | Sample ID     | Zeta Potential (mV) | Mobility ( $\mu\text{s}/(\text{V}/\text{cm})$ ) | RMS Residual |            |
|------|---------------------|---------------|---------------------|---|--------------|------------|
| PALS | 05-04-2021 15:07:51 | AR0142Y21 - 1 | -23.02              | -1.20   | 2.7520e-02   |            |
| PALS | 05-04-2021 15:09:28 | AR0142Y21 - 2 | -19.35              | -1.01   | 1.0187e-02   |            |
| PALS | 05-04-2021 15:11:06 | AR0142Y21 - 3 | -18.60              | -0.97   | 1.3748e-02   |            |
| PALS | 05-04-2021 15:12:43 | AR0142Y21 - 4 | -18.54              | -0.97   | 1.1386e-02   |            |
| PALS | 05-04-2021 15:14:21 | AR0142Y21 - 5 | -17.47              | -0.91   | 1.1815e-02   |            |
|      |                     |               | Mean:               | -19.40  | -1.01        | 1.4931e-02 |
|      |                     |               | Std Err:            | 0.95  | 0.05         | 3.1990e-03 |
|      |                     |               | Std Dev:            | 2.13  | 0.11         | 7.1531e-03 |

 Summary Statistics Report D

| Type | Start Date/Time     | Sample ID     | Zeta Potential (mV) | Mobility ( $\mu\text{s}/(\text{V}/\text{cm})$ ) | RMS Residual |            |
|------|---------------------|---------------|---------------------|---|--------------|------------|
| PALS | 05-04-2021 15:21:06 | AR0142Y21 - 1 | -17.36              | -0.90   | 2.2853e-02   |            |
| PALS | 05-04-2021 15:22:44 | AR0142Y21 - 2 | -22.32              | -1.16   | 1.4364e-02   |            |
| PALS | 05-04-2021 15:24:22 | AR0142Y21 - 3 | -17.86              | -0.93   | 1.1009e-02   |            |
| PALS | 05-04-2021 15:25:59 | AR0142Y21 - 4 | -18.46              | -0.96   | 1.1200e-02   |            |
| PALS | 05-04-2021 15:27:37 | AR0142Y21 - 5 | -17.58              | -0.92   | 1.2662e-02   |            |
|      |                     |               | Mean:               | -18.71  | -0.97        | 1.4418e-02 |
|      |                     |               | Std Err:            | 0.92  | 0.05         | 2.1933e-03 |
|      |                     |               | Std Dev:            | 2.06  | 0.11         | 4.9044e-03 |

 Summary Statistics Report E

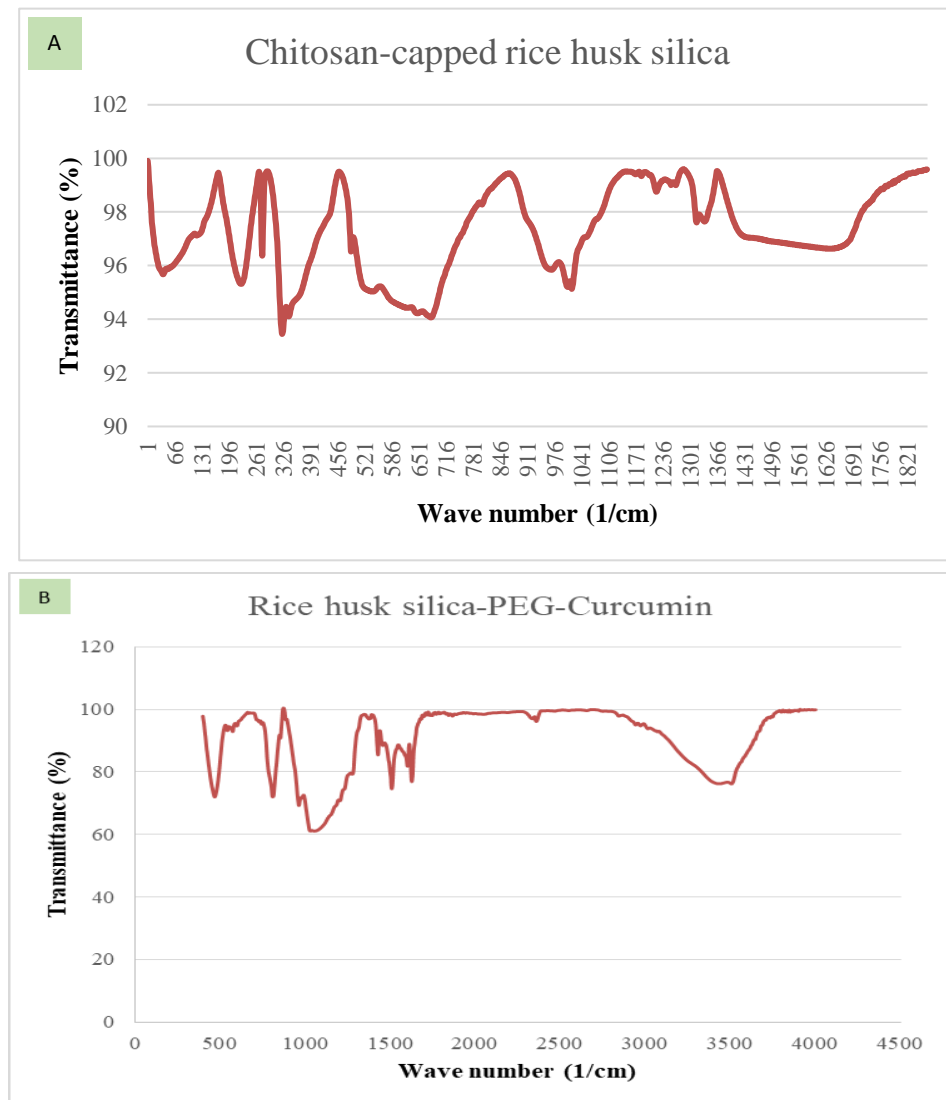
| Type | Start Date/Time     | Sample ID     | Zeta Potential (mV) | Mobility ( $\mu\text{s}/(\text{V}/\text{cm})$ ) | RMS Residual |            |
|------|---------------------|---------------|---------------------|---|--------------|------------|
| PALS | 05-04-2021 15:32:46 | AR0142Y21 - 1 | -19.59              | -1.02   | 1.8636e-02   |            |
| PALS | 05-04-2021 15:34:24 | AR0142Y21 - 2 | -16.84              | -0.88   | 1.8430e-02   |            |
| PALS | 05-04-2021 15:36:01 | AR0142Y21 - 3 | -14.08              | -0.73   | 1.1882e-02   |            |
| PALS | 05-04-2021 15:37:39 | AR0142Y21 - 4 | -13.65              | -0.71   | 1.3700e-02   |            |
| PALS | 05-04-2021 15:39:17 | AR0142Y21 - 5 | -14.73              | -0.77   | 1.2169e-02   |            |
|      |                     |               | Mean:               | -15.78  | -0.82        | 1.4664e-02 |
|      |                     |               | Std Err:            | 1.10  | 0.06         | 1.4900e-03 |
|      |                     |               | Std Dev:            | 2.46  | 0.13         | 3.3318e-03 |

The zeta potential values indicated in table 4.2.9 and figure 4.2.15 shows silica from rice husk to possess high negative values. High negative zeta potential values (greater than  $\pm 30$  mV) are indicative of stability of samples in suspension due the interplay of intermolecular electrostatic repulsive forces.

### 4.3. Surface modification and drug loading studies using biogenic silica nanoparticles

#### 4.3.1 Drug loading onto biogenic silica nanoparticles

**Figure 4.3.1.** FTIR spectrum of surface modified (A) and drug loaded silica nanoparticles (B) and (C)



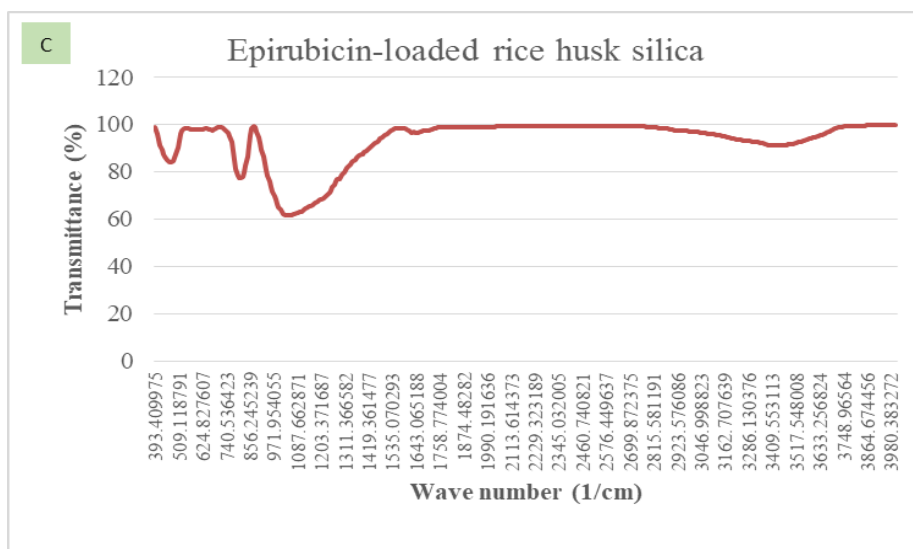


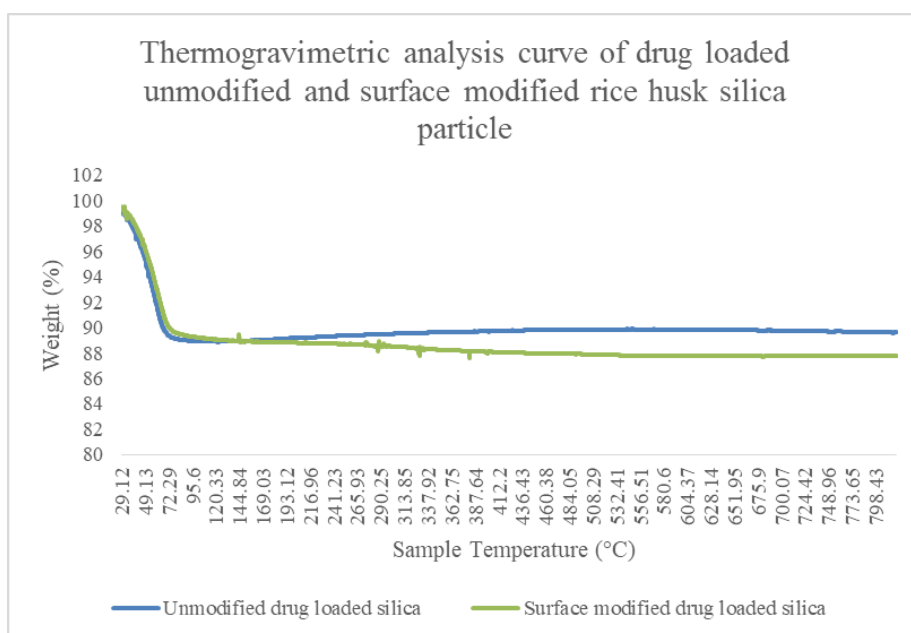
**Table 4.3.1.** Showing different interactions as observed in the FTIR spectra above

| Group                      | Wave number (cm <sup>-1</sup> ) | Suggestive chemical interaction  |
|----------------------------|---------------------------------|--|
| <b>Curcumin</b>            | 3500-3000                       | O-H group stretching vibration   |
|                            | 1512                            | C=O stretching vibration, bending vibration of aliphatic CC-C, CC=O and CC-H groups of keto-enol configuration |
|                            | 1628                            | Overlapping stretching vibrations of alkene C=C and carbonyl C=O groups  |
|                            | 1427                            | Aromatic C=C group stretching vibration  |
|                            | 1277                            | Bending vibration of C-O phenolic band   |
| <b>Polyethylene glycol</b> | 1460                            | CH <sub>2</sub> scissoring mode  |
|                            | 1340                            | CH <sub>2</sub> wagging mode   |

|                   |            |   |
|-------------------|------------|---|
|                   | 1241, 1278 | CH <sub>2</sub> twisting mode....                           |
| ....              | 1145       | CH <sub>2</sub> rocking, C-O stretching modes               |
|                   | 1097       | C-O, C-C stretching mode                                    |
|                   | 1058       | C-O, C-C stretching, CH <sub>2</sub> rocking                |
|                   | 960        | CH <sub>2</sub> rocking, CH <sub>2</sub> twisting modes     |
|                   | 840        | C-O, C-C stretching, CH <sub>2</sub> rocking modes          |
| <b>Epirubicin</b> | 3435       | O-H stretching vibration of water                           |
|                   | 2920, 2850 | CH <sub>2</sub> stretching vibration                        |
|                   | 1632       | C=O, C=C stretching mode                                    |
|                   | 1385       | CH <sub>2</sub> bending vibration                           |
|                   | 1276, 1210 | C-O enol functional group interaction                       |
| <b>Chitosan</b>   | 3291       | N-H stretching vibration                                    |
|                   | 2921, 2877 | Symmetrical and asymmetrical stretching of C-H respectively |
|                   | 1645       | C=O stretching of amide group                               |
|                   | 1325       | C-N stretching of amide group                               |
|                   | 1589       | N-H bending of primary amine                                |
|                   | 1423       | CH <sub>2</sub> bending                                     |
|                   | 1153       | Asymmetric stretching of C-O-C bridge                       |
|                   | 1066, 1028 | C-O stretching mode   |

Figure 4.3.1 A is indicative of successful surface modification with polyethylene glycol and chitosan as is indicated from the corresponding interactions of respective functional groups in table 4.3.1. B and C shows FTIR spectra of silica samples loaded curcumin and epirubicin respectively. Presence of chemical interactions between specific C=C and C=O groups and phenolic groups in respective spectra can be used as a confirmatory result indicative of the successful drug loading onto silica particles.

**Figure 4.3.2.** Thermogravimetric analysis curve to assess drug loading into rice husk-derived silica nanoparticles



Calculation of drug-loading:

$$\text{Drug-loading (\% w/w)} = [(\% \text{ Mass loss} * 100) / \text{Average total mass loss (\% of drug)}] - \text{Mass loss (\% of drug)}^{259}.$$



Mass loss from the isotherm above is used as a confirmatory test to ascertain the drug loading result from spectrophotometric analysis and results were found to be in synchrony as indicated from tables 4.3.2 and 4.3.3.

**Table 4.3.2.** Evaluation of curcumin loading using TGA

| Sample                                     | Average weight-loss (%) | Drug loading (%) |
|--|-------------------------|------------------|
| <b>Curcumin</b>                            | 95.9563                 | -                |
| <b>Silica</b>                              | 2.2664                  | -                |
| <b>Unmodified drug loaded silica</b>       | 10.4915                 | 8.66722          |
| <b>Surface modified drug loaded silica</b> | 10.1165                 | 8.27642          |

**Table 4.3.3.** Results of spectrophotometric analysis of drug loading

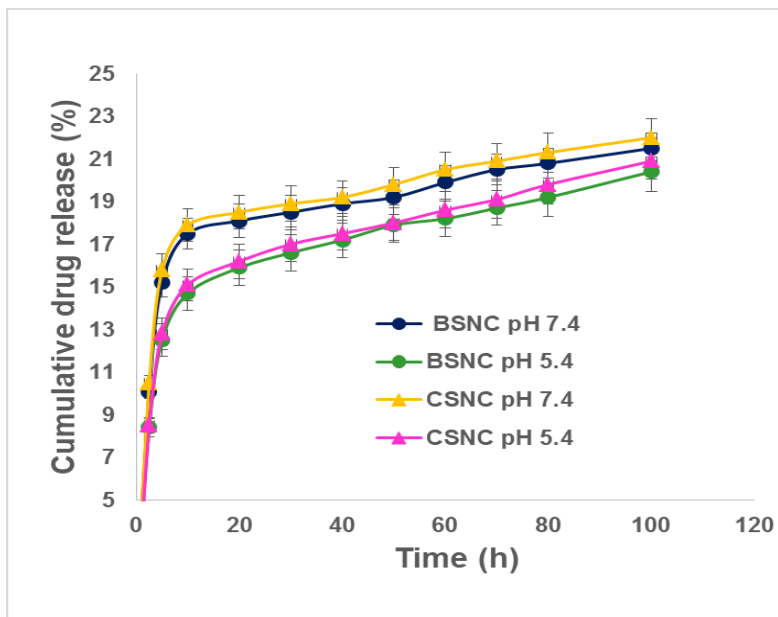
| Drug used         | Type of biogenic silica used | Loading capacity ( $\mu\text{g}/\text{mg}$ ) | Loading efficiency (%) |
|-------------------|------------------------------|--|------------------------|
| <b>Curcumin</b>   | Unmodified                   | 1.765  | 5                      |
|                   | Surface modified             | 0.846  | 4.6                    |
| <b>Epirubicin</b> | Unmodified                   | 3.281  | 9.586                  |
|                   | Surface modified             | 1.487  | 7.24                   |

Unmodified silica samples showed higher loading of both curcumin and epirubicin as seen in tables above.

#### 4.4. Studies on drug release from different nano-formulations

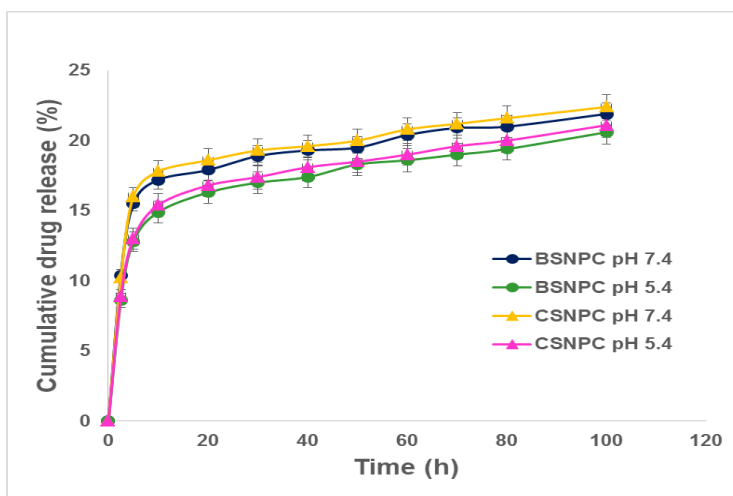
##### 4.4.1. Curcumin release from different nano-formulations

**Figure 4.4.1.** Showing release of curcumin from unmodified silica nanoparticles and control at pH 5.4 and 7.4



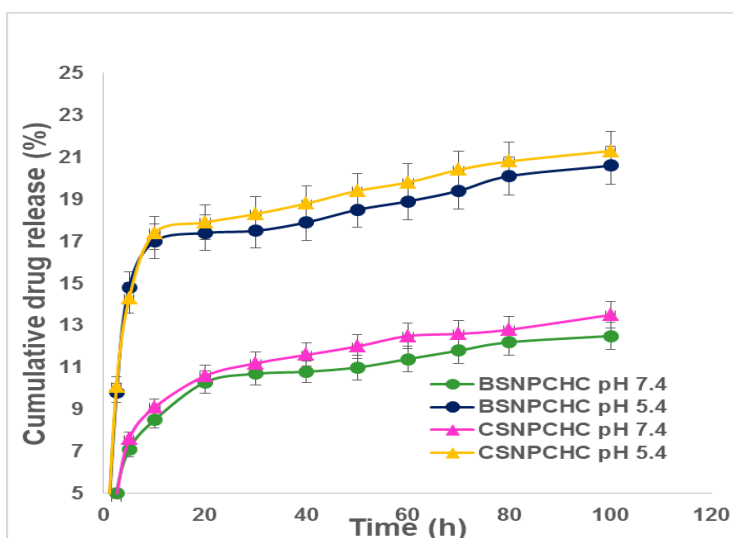
The release of curcumin from unmodified silica samples were higher at alkaline pH as compared to studies replicated in acidic pH. The release of curcumin from CSNC was higher and more uniform as compared to its biogenic counterpart possibly due to more ordered and regular arrangement of molecules from chemical synthesis.

**Figure 4.4.2.** Showing release of curcumin from polyethylene glycolated silica nanoparticles and control at pH 5.4 and 7.4



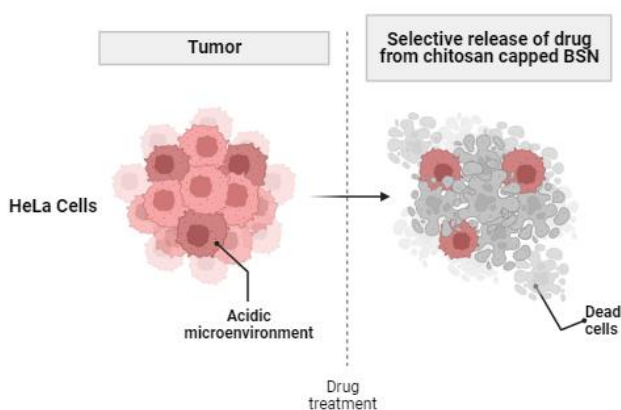
Polyethylene glycolated samples also showed similar pattern as from figure 4.4.1, with higher release of curcumin at alkaline pH.

**Figure 4.4.3.** Showing release of curcumin from polyethylene glycolated, chitosan capped silica nanoparticles and control at pH 5.4 and 7.4



Chitosan capped silica particles loaded with curcumin showed enhanced release at acidic pH. This could likely be due to protonation of amino groups in chitosan at acidic pH, facilitating structural disintegration and increment in the release of curcumin.

**Figure 4.4.4.** Showing mechanism of pH-responsive drug release from chitosan capped nano-formulation



*Note:* Illustration created with [BioRender.com](https://www.biorender.com).

From the drug release studies, it was seen that the curcumin release was higher in chitosan capped samples in acidic pH due to possible disintegration of the chitosan structure. An acidic microenvironment is characteristic of tumour cells, which makes chitosan capping an efficient tool for pH-mediated release of drug only at the tumour sites which prevent the premature release of drug en route to the target site, the mechanism of which is indicated in the figure above.

#### 4.4.2. Epirubicin release from different nano-formulations

**Figure 4.4.5.** Showing release of epirubicin from unmodified silica nanoparticles and control at pH 5.4 and 7.4

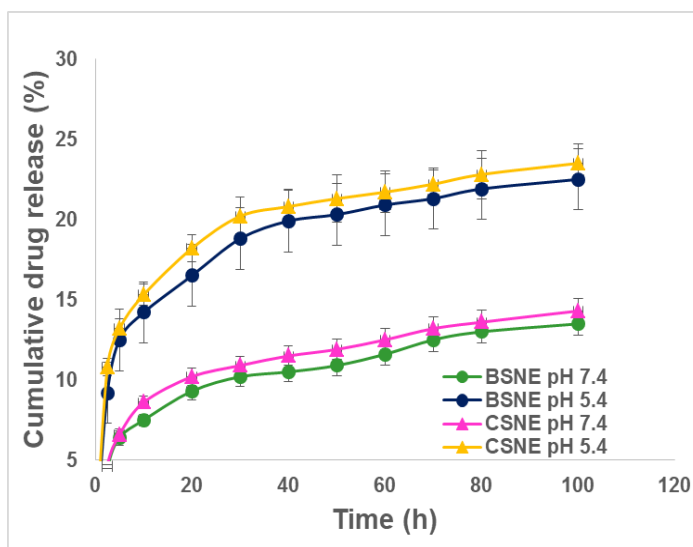


**Figure 4.4.6.** Showing release of epirubicin from polyethylene glycolated silica nanoparticles and control at pH 5.4 and 7.4

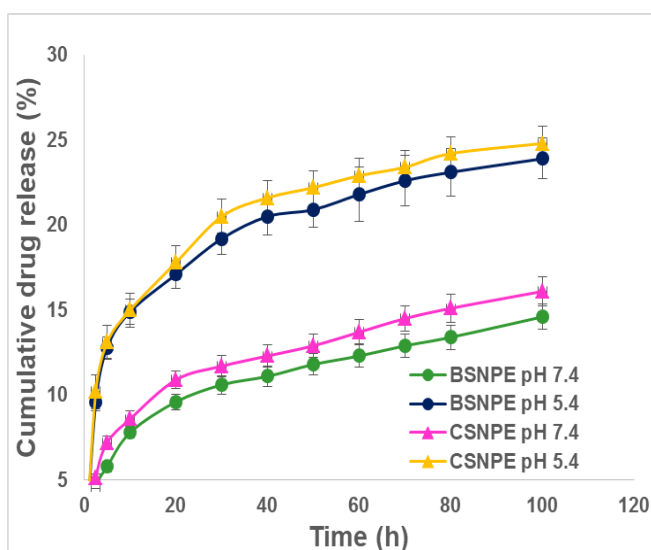
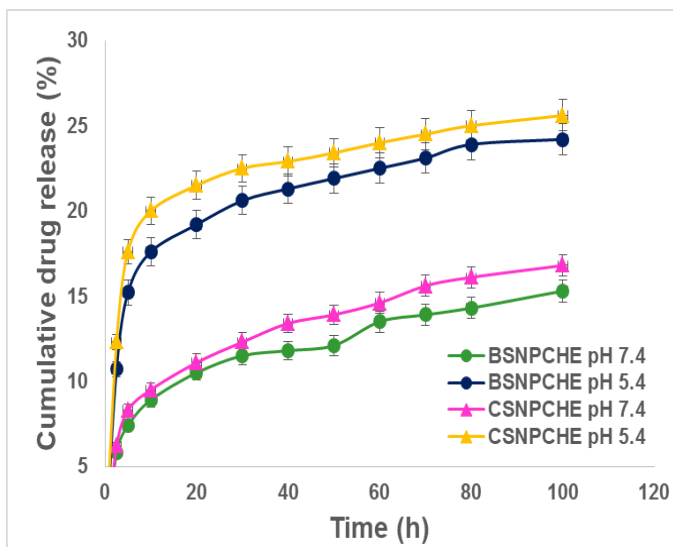


**Figure 4.4.7.** Showing release of epirubicin from polyethylene glycolated, chitosan capped silica nanoparticles and control at pH 5.4 and 7.4

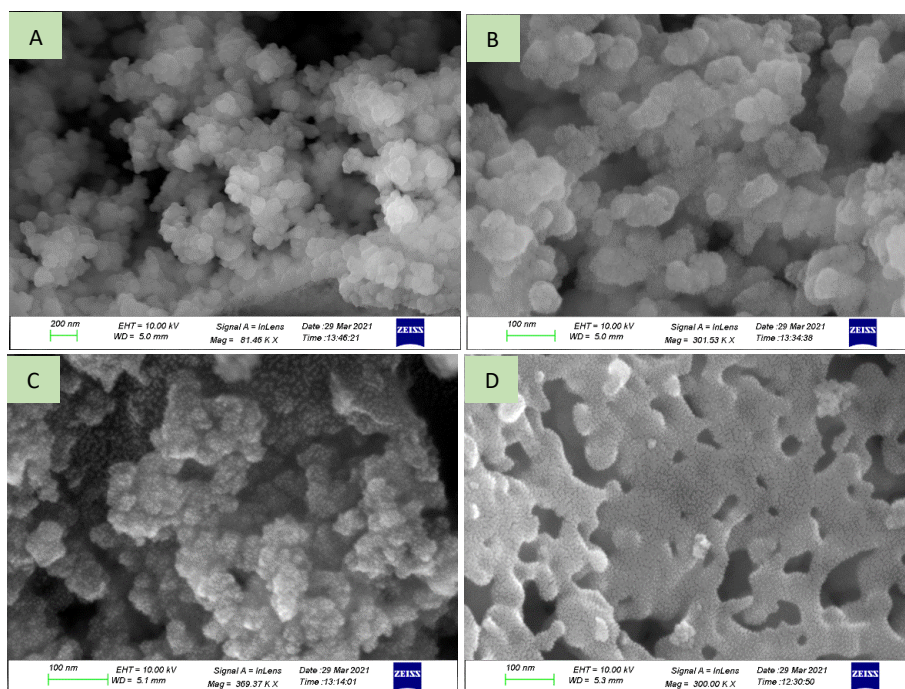


The release of epirubicin was higher and more uniform from chemically synthesized silica. The release was higher in acidic pH from unmodified, polyethylene glycolated and chitosan capped samples as indicated in figures 4.4.5 to 4.4.7.

#### 4.5. Assessment of nanoparticle toxicity and cytocompatibility using cell-lines

##### 4.5.1. *In vitro* degradation behaviour of biogenic silica nanoparticles

**Figure 4.5.1.** Images (A), (B), (C) and (D) showing degradation behaviour of biogenic silica as observed employing FESEM technique



*Note:*

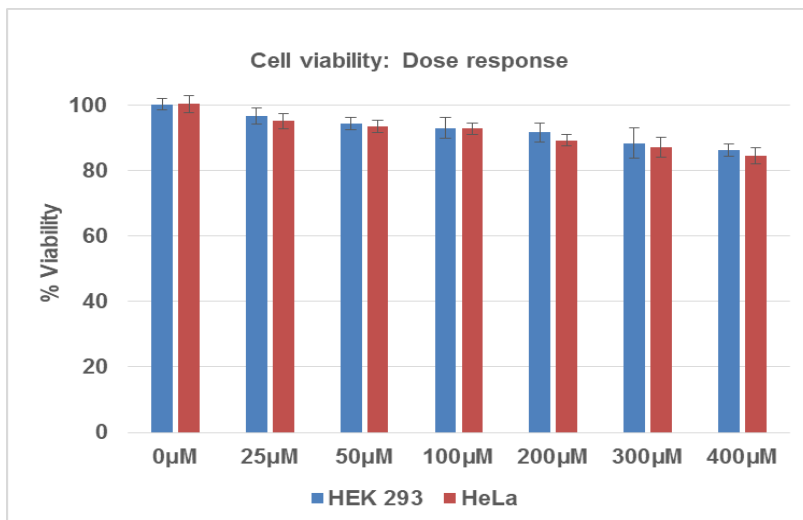
Magnification of images respectively are:

(A) 81.46K X, (B) 301.53K X, (C) 369.37K X and (D) 300K X.

From the above figure progressive disintegration of silica structure from day 01 to day 14 can be observed. This indicates that the particles do not remain long enough in the biological milieu so as to accumulate and impart toxic effects but are capable of remaining in circulation so as to facilitate effective transport and release of the payload.

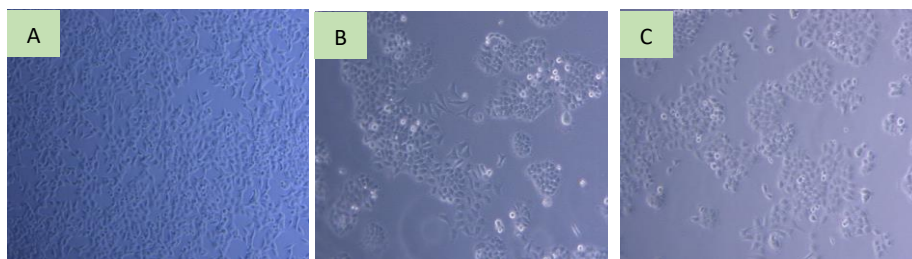
#### 4.5.2. Assessment on cell viability

**Figure 4.5.2.** Showing the viability of HEK 293 and HeLa cells treated with different doses of biogenic silica nano particles from rice husk



There was no significant reduction in the viability of cells treated with BSN upto a concentration of 400 μM as seen in the figure above.

**Figure 4.5.3.** Images (A), (B) and (C) showing HeLa cells after 24, 48 and 72 h of incubation in PEG-modified chitosan capped drug bound biogenic silica nano-formulation respectively



The viability of HeLa cells were reduced to 40.33 % in samples treated with BSNPCHC upon 72 h of incubation.



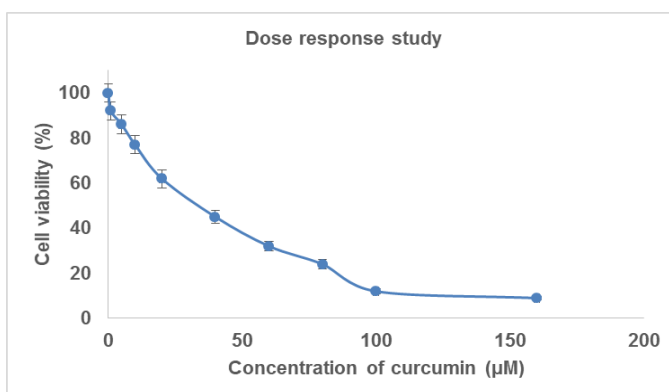
**Figure 4.5.4.** Images (A), (B) and (C) showing HEK293 cells after 24, 48 and 72 h of incubation in PEG-modified chitosan capped drug bound biogenic silica nano-formulation respectively

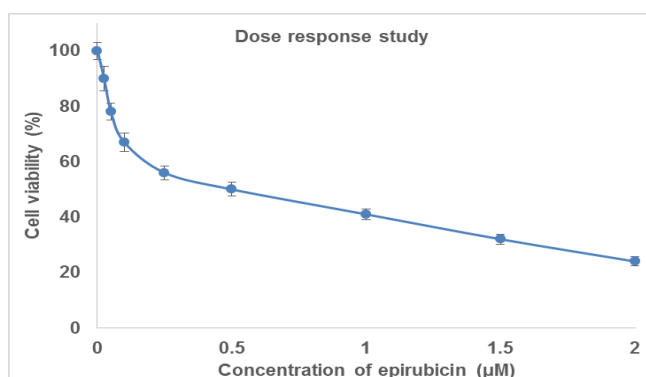


The viability of HEK 293 cells were maintained at level of 96.7 % in samples treated with BSNPCHC UPON 72 h of incubation.

#### 4.5.3. Dose response study

**Figure 4.5.5.** Dose response study of curcumin



**Figure 4.5.6.** Dose response study of epirubicin**Table 4.5.1.** Variation in  $IC_{50}$  values of curcumin and epirubicin as a function of silica encapsulation for HeLa cells under incubation in test samples for a period of 48 h

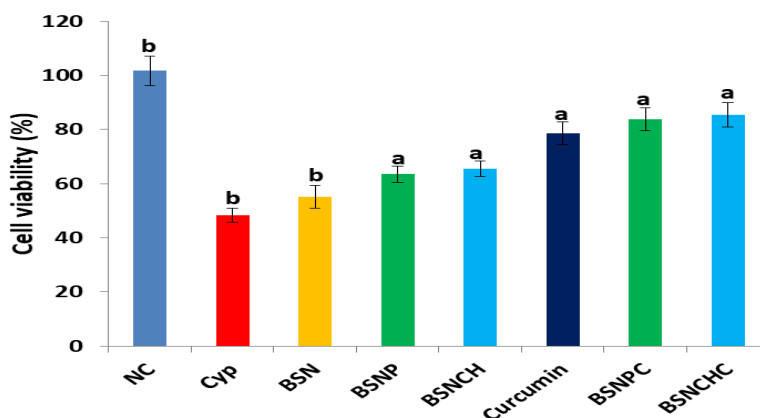
| Sample         | Free curcumin   | Silica-bound Curcumin | Free epirubicin | Silica-bound epirubicin |
|----------------|-----------------|-----------------------|-----------------|-------------------------|
| $IC_{50}$ (µM) | $57.43 \pm 2.5$ | $54.1827 \pm 1.8$     | $1.02 \pm 0.86$ | $0.91350 \pm 2$         |

*Note:* The  $IC_{50}$  values are expressed as mean values  $\pm$  SD from  $n = 6$

From figures 4.5.5, 4.5.6 and from table 4.5.1, it can be seen that there was a reduction in the  $IC_{50}$  of curcumin and epirubicin conjugated with silica nanoparticle, indicating its efficiency to improve the drug activity.

#### 4.5.4. Cytoprotection against toxicity induced by cypermethrin

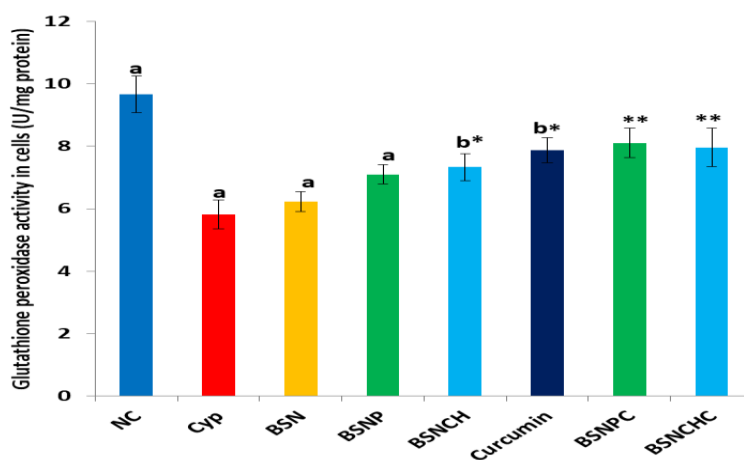
**Figure 4.5.7.** Assessment of cytoprotection against cypermethrin induced toxicity



Note: n=6, values are average of n ( $\pm$ SEM). a:  $p < 0.01$ , b:  $p < 0.05$ .

It can be seen from the above figure that maximum cytoprotective effect of BSNCHC was highest (85.5%) against cypermethrin induced cellular toxicity.

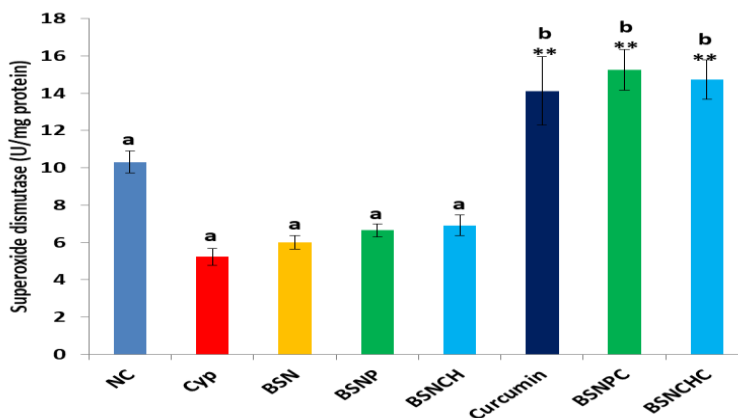
**Figure 4.5.8.** Assessment of glutathione peroxidase activity



Note: n=6, values are average of n ( $\pm$ SEM). a and \*\*:  $p < 0.01$ , b and \*:  $p < 0.05$ .

Maximum cytoprotective activity was observed in cells treated with BSNPC (8.11 U/mg protein) as can be seen from the above figure.

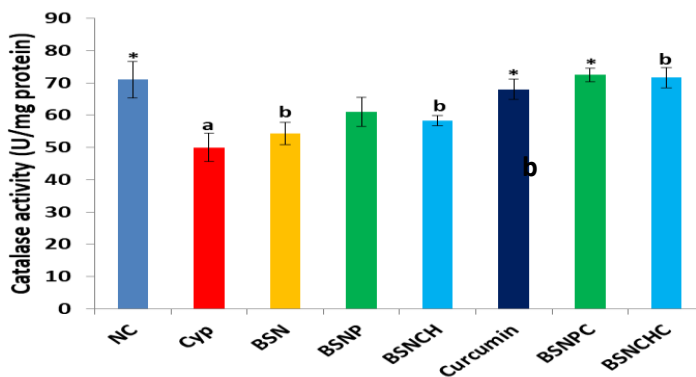
**Figure 4.5.9.** Assessment of superoxide dismutase activity



Note: n=6, values are average of n ( $\pm$ SEM). a and \*\*: p<0.01, b and \*: p<0.05.

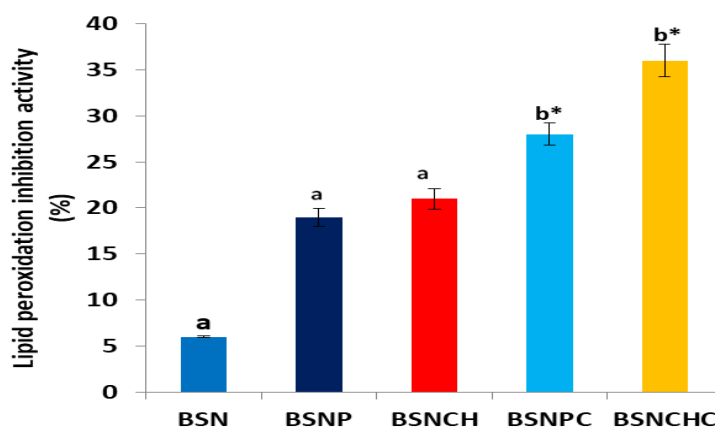
Maximum cytoprotective activity was observed in cells treated with BSNCHC (14.73 U/mg protein) as can be seen from figure 4.5.9.

**Figure 4.5.10.** Assessment of catalase activity



Note: n=6, values are average of n ( $\pm$ SEM). a and \*\*: p<0.01, b and \*: p<0.05.

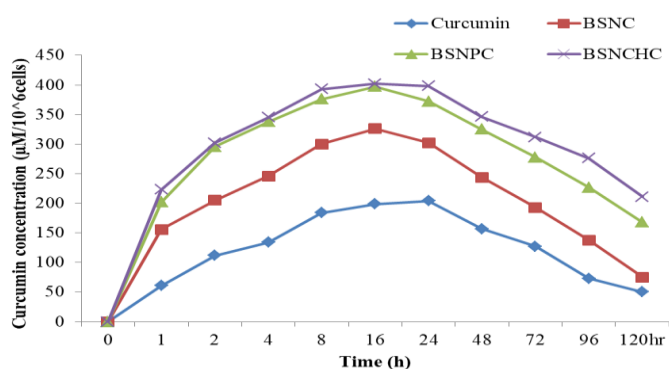
Maximum cytoprotective activity was observed in cells treated with BSNPC (72.5 U/mg protein) as can be seen from the figure above.

**Figure 4.5.11.** Assessment of lipid peroxidation inhibition activity

Note: n=6, values are average of n ( $\pm$ SEM). a and \*\*: p<0.01, b and \*: p<0.05.

Maximum inhibition of lipid peroxidation was seen in samples treated with BSNCH (36 %) as indicated in the above figure.

#### 4.5.5. Cellular uptake of curcumin

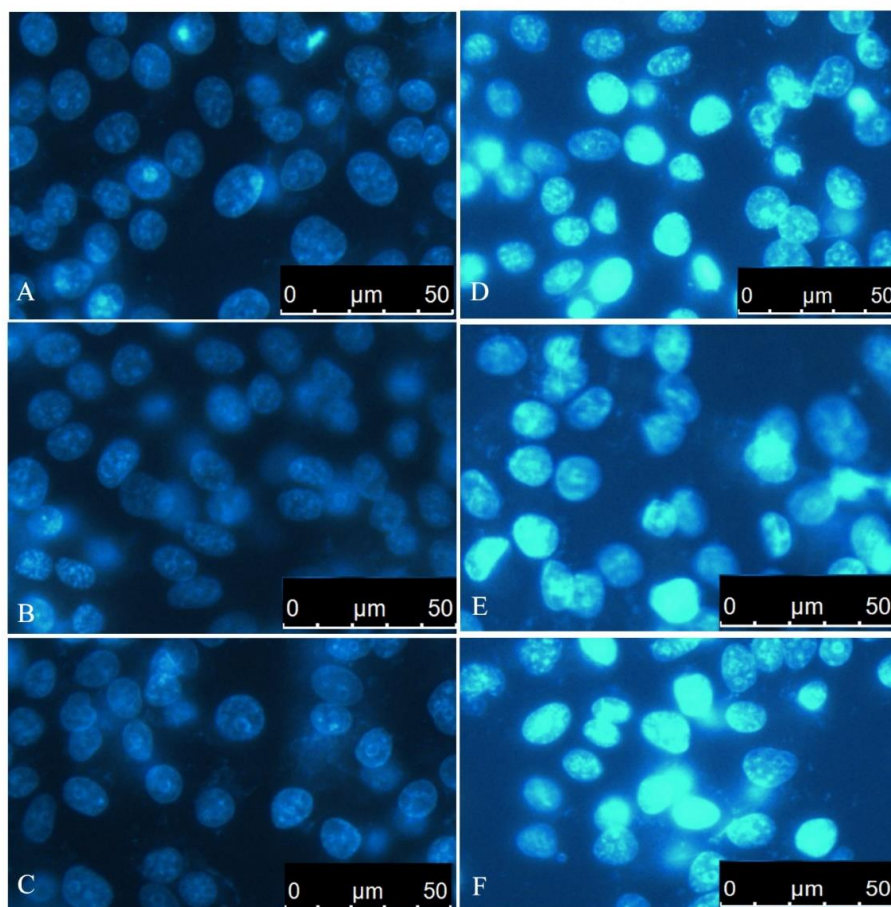
**Figure 4.5.12.** Assessment of curcumin uptake by cells

The cellular uptake of curcumin from BSNCHC was the highest (422  $\mu$ M/10<sup>6</sup> cells) with an absorption maxima at 16h. An increase in cellular uptake from surface modified silica nanoparticles is an

indication of its ability to improve the bioavailability of the loaded drug, as seen in figure 4.5.12.

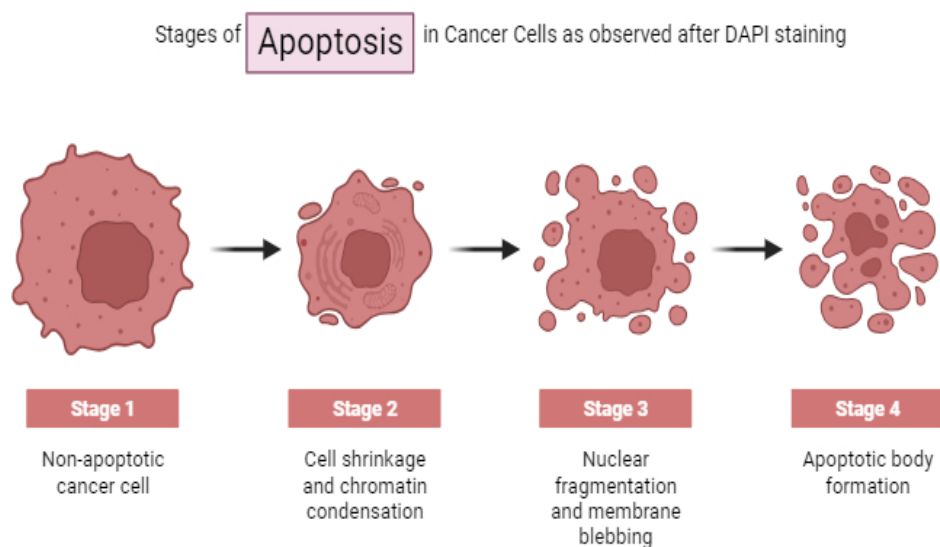
#### 4.5.6. Effect of nano-formulation on the nuclear morphology

**Figure 4.5.13.** Showing HeLa cells stained with DAPI which were subjected to treatment to observe for any alterations in its nuclear morphology (A-Normal control, B-biogenic silica exposed at 200  $\mu\text{g}/\text{mL}$  concentration, C-treated with 200  $\mu\text{g}/\text{mL}$  PEG coated, chitosan capped biogenic silica, D- Biogenic silica bound with drug, E- PEG modified biogenic silica bound with drug and F- PEG modified chitosan capped drug bound biogenic silica)



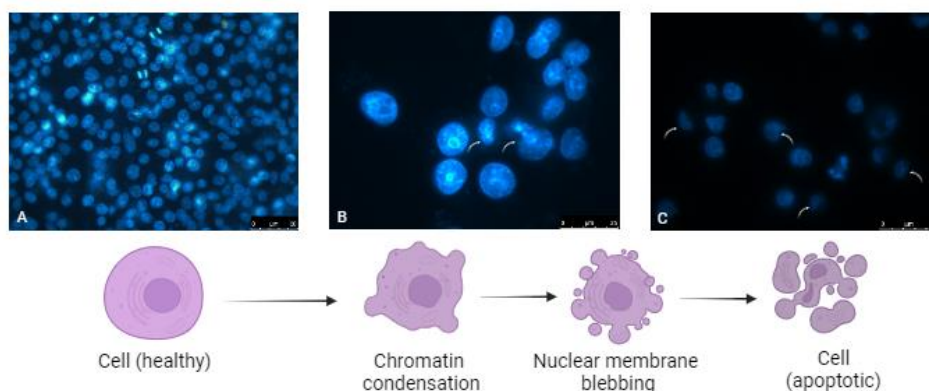
DAPI dye specifically binds to the adenine and thymine rich regions of the DNA. The dye uptake is minimum in normal cells. But in cells with compromised membrane health as in cells in apoptotic phase, the dye uptake increases. The increase in dye uptake can be understood by an increase in the fluorescence of the dye. Though staining of the cells with excessive dye could result in increase in the intensity of fluorescence, normally apoptotic cells fluoresce brighter than normal cells. From the figure above, cells treated with drug loaded nanoformulations fluoresce brighter than normal cells, suggestive of induction of apoptosis in cells.

**Figure 4.5.14.** Showing stages of apoptosis



*Note:* Illustration created with [BioRender.com](https://www.biorender.com).

**Figure 4.5.15.** Showing stages of apoptosis where (A) shows normal cell, white arrows in (B) showing visible signs of chromatin condensation and nuclear membrane blebs while the white arrows in (C) showing signs of final stage apoptosis



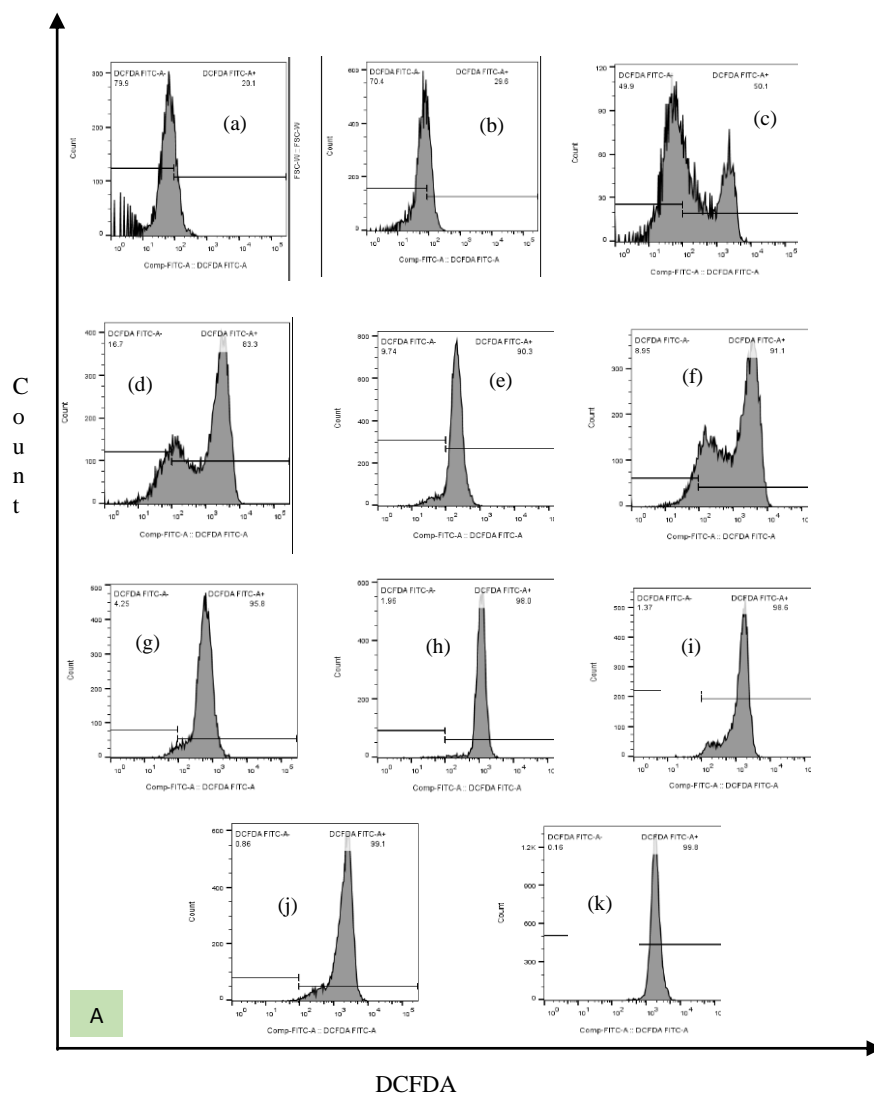
*Note:* Illustration created with [BioRender.com](https://www.biorender.com).

Cells treated with drug conjugated nano-formulation showed visible chromatin condensation and formation of nuclear blebs as indicated in the above figures.



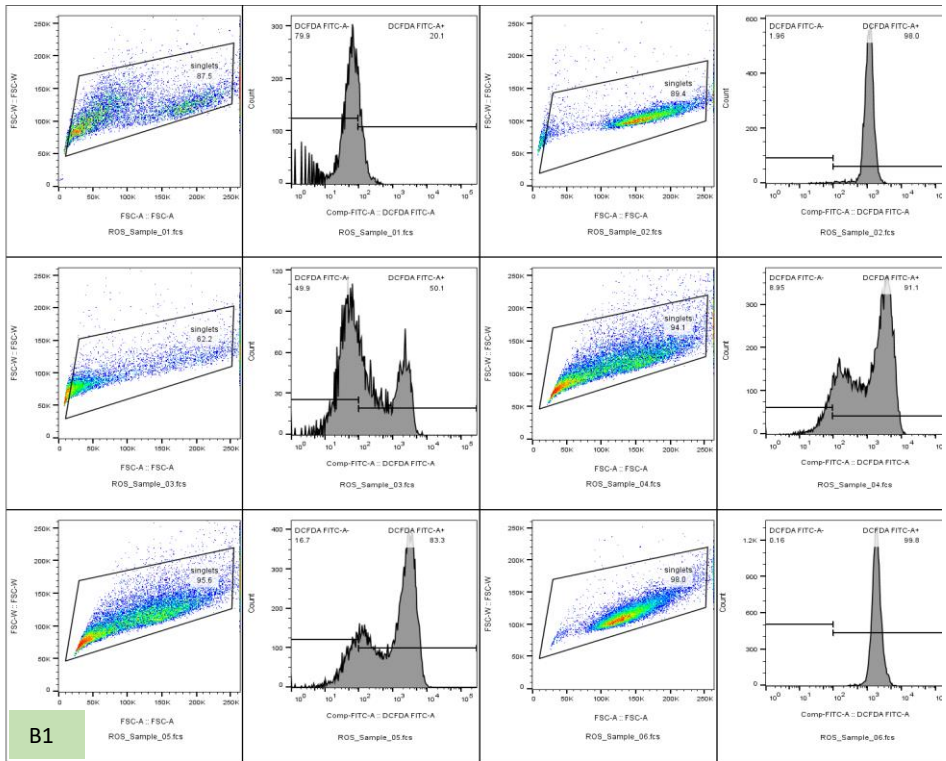
#### 4.5.7. Estimation of intracellular ROS (DCFDA)

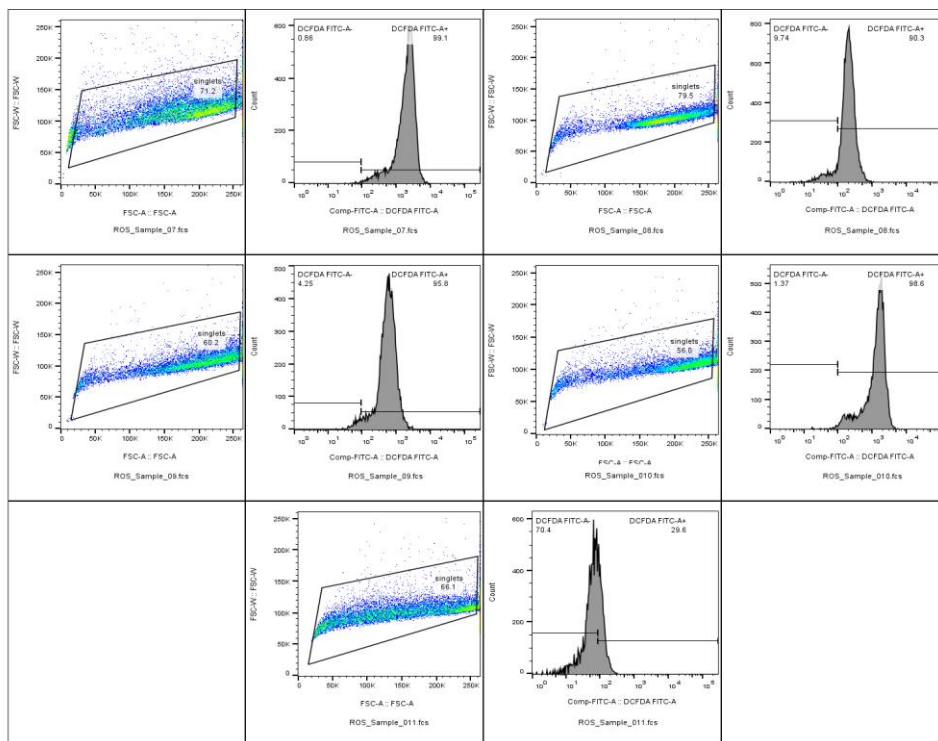
**Figure 4.5.16.** Evaluation of ROS generation using flow cytometry analysis. (A) Showing ROS production in HeLa cells subjected to treatment with different nano-formulations, (B1 and B2) Showing dot-plot and population distribution of samples treated with different nano-formulations



*Note:* Samples and corresponding ROS+ population (%) are- (a) negative control (20.1), (b) BSN (29.6), (c) CSN (50.1), (d) Curcumin treated cells (83.3), (e) BSNC (90.3), (f) CSNC (91.1), (g) BSNPC (95.8), (h) CSNPC (98), (i) BSNPCHC (98.6), (j) CSNPCHC (99.1) and (k) Positive control, 50  $\mu$ M  $H_2O_2$  (99.8).

# Results



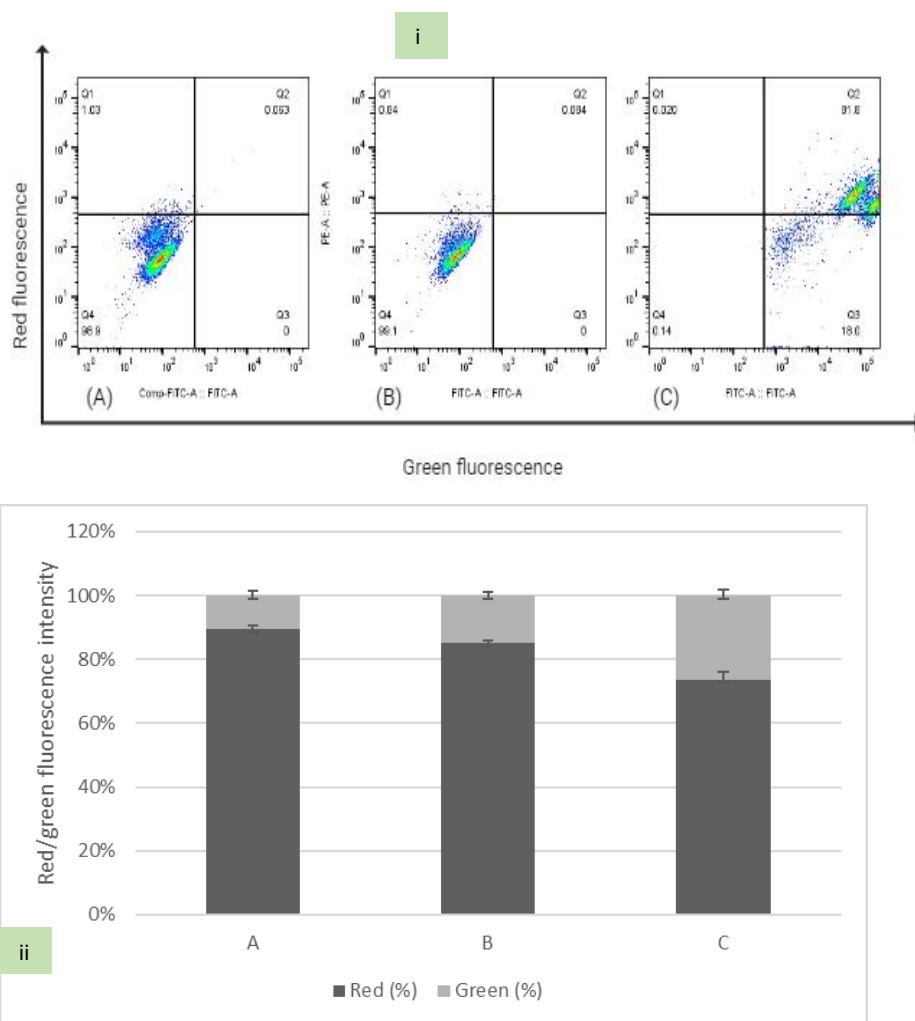


B2

Cells treated with drug loaded nano-formulations resulted in the generation of ROS as indicated from the plots using flow cytometric analyses above. The ROS production in positive sample treated with 50  $\mu\text{M}$   $\text{H}_2\text{O}_2$  was 99.8 %. The maximum ROS production was observed in the samples treated with CSNPCHC (99.1%), followed by samples treated with BSNPCHC (98.6 %).

#### 4.5.8. Mitochondrial membrane potential analysis

**Figure 4.5.17.** Analysis of mitochondrial membrane potential. (i) Fluorescence pattern obtained using flow cytometry analysis of HeLa cells subjected to treatment with different nano-formulations (ii) Red/green intensity ratio of samples A, B and C

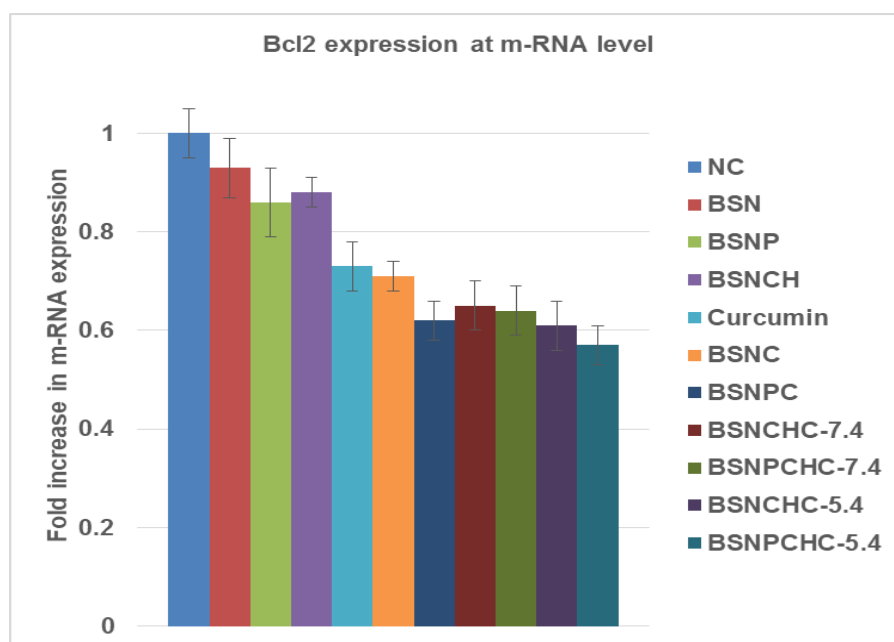


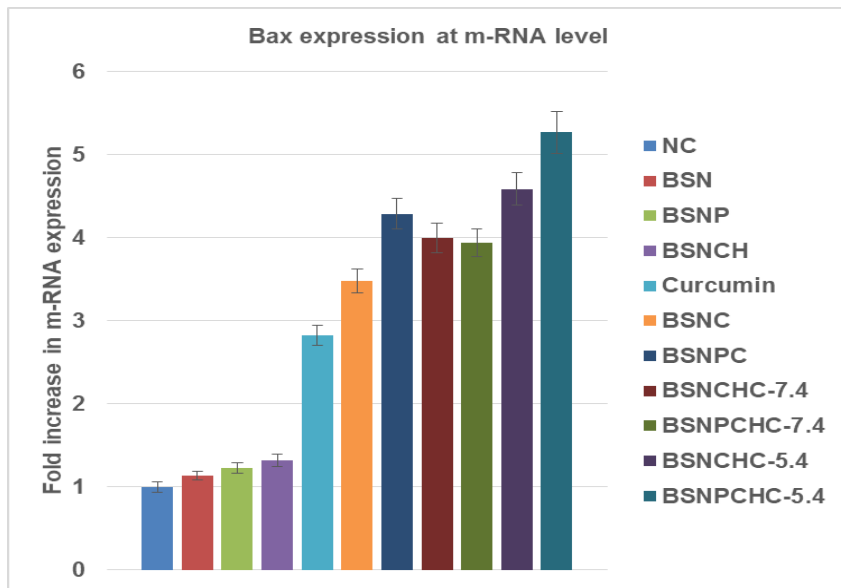
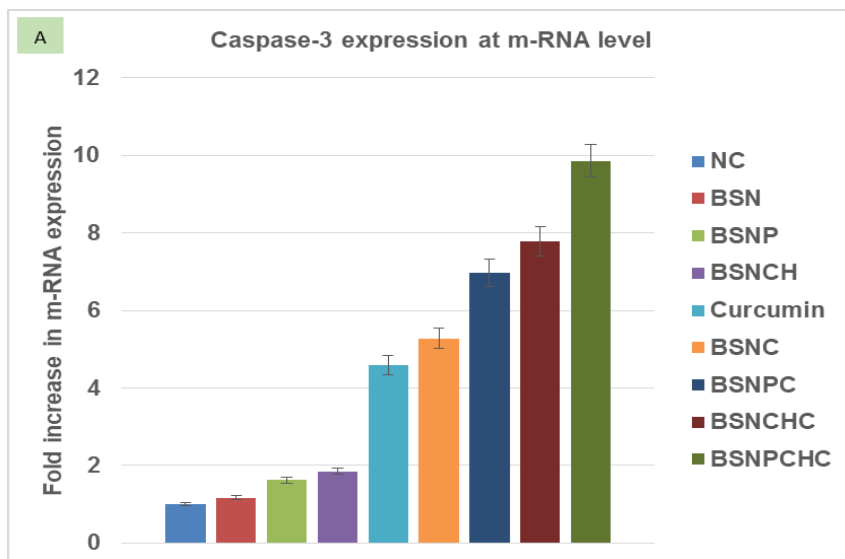
*Note:* The intensity ratios of (A) and (B) cell population distribution is indicative of normal mitochondrial function whereas sample (C) suggests disrupted membrane functioning of mitochondria; data represented as mean $\pm$ SD,  $p < 0.01$ . Samples labelled (A)- BSN, (B)- BSNPCH and (C)-BSNPCHC respectively.

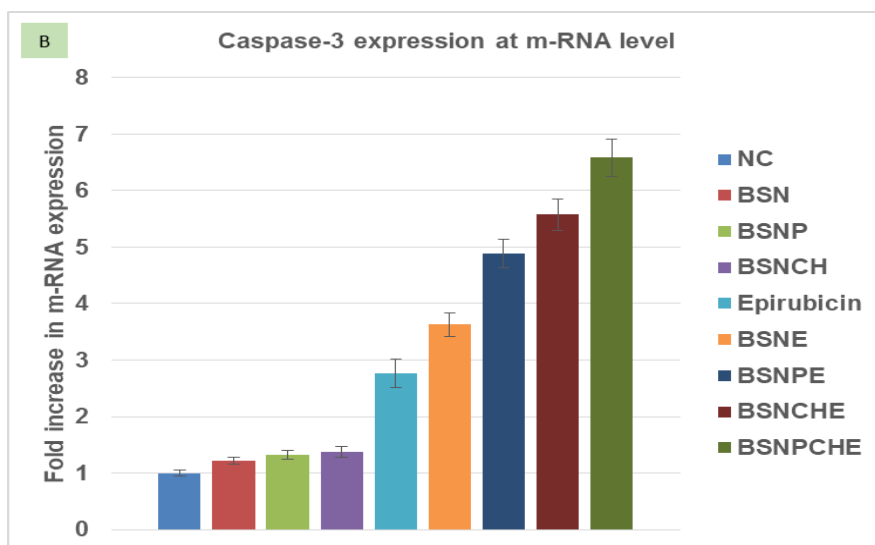
In normal cells, the JC-10 dye concentrates in the mitochondria forming red aggregates. The mitochondrial membrane potential is developed due the electrons of the electron transport chain. In apoptotic cells, the dye retention of the dye in mitochondria decreases as the mitochondrial membrane potential decreases and dye converts into monomeric form which fluoresces green. The collapse of the MMP triggers the release of cytochrome c into the cytosol which triggers a series of events leading to apoptosis of cells.

#### 4.5.9. Gene expression studies

**Figure 4.5.18.** Expression of Bcl2 gene



**Figure 4.5.19.** Expression of Bax gene**Figure 4.5.20.** Caspase 3 expression in cells (A) in set of studies using curcumin, (B) in set of studies using epirubicin drugs

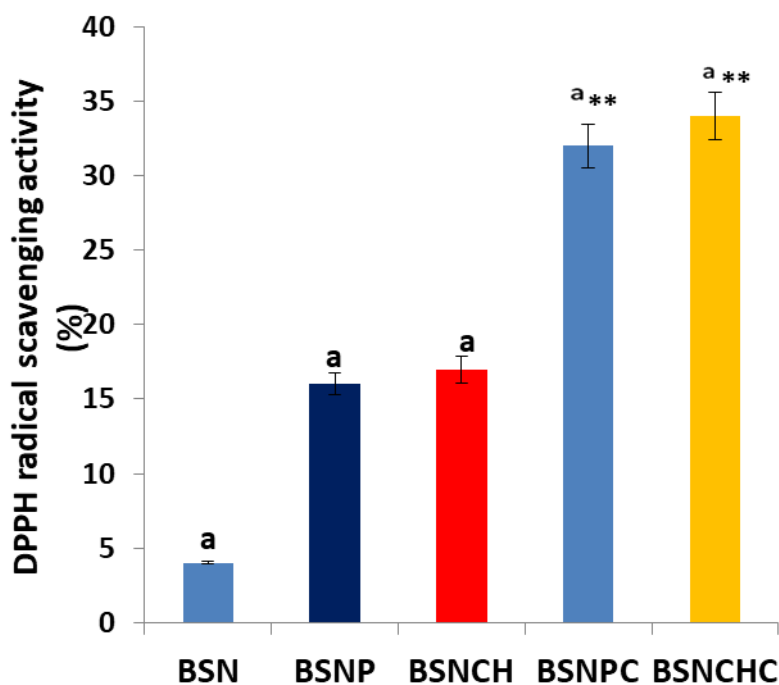


There was upregulation of pro-apoptotic genes in the cells treated with drug conjugated nano-formulation. The activity of the drug was also evident from the downregulation of anti-apoptotic gene in the cell treated with drug loaded nano-formulations as indicated in figures 4.5.20-4.5.20.

#### 4.6. Study on anti-oxidant property of curcumin-loaded biogenic silica particle

##### 4.6.1. 2,2-Diphenyl-1-Picryl Hydrazine (DPPH) Scavenging activity

**Figure 4.6.1.** 2,2-Diphenyl-1-Picryl Hydrazine (DPPH) Scavenging activity



Note: n=6, values are average of n ( $\pm$ SEM). a and \*\*: p<0.01.

DPPH scavenging activity was observed in tests done with BSNCHC sample (34 %). The DPPH scavenging activity of the nano-formulation is due to the curcumin loaded onto it, suggesting sustenance of its activity even after nanoparticle conjugation.



### **5.1. Optimization of synthesis of biogenic silica and physicochemical characterization**

Breakthrough in inventions resulted in the development of precision analysis tools like scanning tunneling microscope and atomic force microscopy, which helped in translation to experimental advancement and defining newer dimensions for nanotechnology. Development of fullerenes and carbon nanotubes were such advancements that opened newer era in revolutionizing nanotechnology for advanced applications. Nanoparticles have been classified based on differences in physical and chemical properties. The synthesis of materials possessing predictable properties demand the production parameters to be strictly controlled, which pose as a challenge to researchers in the field. Scalability is another issue that demands immediate attention. Generally, top-down and bottom-up approaches are employed in the synthesis of nanoparticles. Each production technique requires different parameters to be addressed to obtain end-product of desired characteristics. Top-down approach which utilizes physical methods of production of nanoparticles includes methods like mechanical milling techniques involving plastic and elastic deformation and fracture, to several advanced procedures like laser ablation, electrospinning, magnetron sputtering and other techniques involving explosion of wires made of metals (electro explosion). On the other hand, bottom-up approach is based on

chemical methods like sol-gel processes involving hydrolysis and polymerization reactions, followed by gelation and condensation of polymers with subsequent evaporation of solvents, to others like hydrothermal method and templating methods based on hydrogen bonds, van der Waal's forces, electrostatic attractive and repulsive forces. Reverse micelle method of synthesis method is of particular interest due to its applicability for controlling the size and shape of the nanoparticles generated. In chemical vapour deposition method, suitable chemical precursor in vapour phase is used, which is later subjected to high temperatures in the presence of a suitable catalyst. This method is widely used for production of thin film of carbon-based materials.

Considering the chemical synthesis of silica, the step that play crucial role in controlling the desired physicochemical properties of silica nanoparticles as in sol-gel process, is chiefly particle nucleation. In this method, the type of catalyst used plays a major role in determining the rates of hydrolysis and condensation reactions, as well as the mechanism followed. In reactions were acid-based catalysts are employed, the hydrolysis reaction will occur at a faster rate than condensation process, resulting in the generation of smaller-sized particles of silica based on electrophilic interactions. In contrast, a base catalyst promotes condensation reaction than hydrolysis, leading to the formation of silica nanoparticles of larger sizes based on nucleophilic attacks. The rates of these reactions are also dependent on other parameters like the pH of the medium, the type of solvent used and water-to-alkoxide ratio. Considering reverse microemulsions, the

reverse micelles dispersed in oil determines the shape, size and particle size distribution. In other production techniques using microwaves and ultrasound frequencies, the particle characteristics can be tuned by adjusting the intensity of incident energy and the type of solvents present. In several cases, it is possible to control the pore diameter by altering the length of template molecule. Time, temperature, humidity, rate of addition and speed of stirring of reaction mixture are other factors that influence particle properties like dispersibility and stability. Mesoporous silica nanoparticles to be employed for drug delivery applications are required to have favorable pharmacokinetic properties, biodistribution and should facilitate surface functionalization for the particles to be used for the intended purpose <sup>260</sup>. Factors like biodegradability, compatibility and distribution are largely dependent on particle properties like surface area, shape, size, other morphological aspects and susceptibility to aggregation, pressing on the importance to fine-tuning these parameters to ensure safety for biomedical applications. Several studies have proposed that reducing the number of negatively charged silanol by surface modifying with compounds like polyethylene glycol could improve the hemocompatibility, circulation time, degradation kinetics and reduce tissue accumulation of the particles.

There had been an increased demand for mesoporous silica particles in the field of medicine for application as drug delivery vector owing to its unique physical and chemical attributes. This resulted in intensification of studies for development of facile synthesis methods which yielded high output with desire properties. The production

methods depended on using organic as well as inorganic sources of silica as precursors for the chemical synthesis. Compounds like tetraalkoxysilanes and sodium silicates constituted a major class of synthetic silica precursors, though other inorganic sources like silicon tetrachloride and olivine (magnesium iron silicate with the chemical formula  $[(\text{MgFe})_2\text{SiO}_4]$ ) were also employed for the manufacture <sup>261</sup>. However, commercial production of silica precursors like sodium silicate involves fusion and melting of starting materials like sodium carbonate and quartz at higher temperature (1300-1600 °C) <sup>262,263</sup> which is very much energy demanding and could result in release of combustion products like CO<sub>2</sub> in higher levels, which can have detrimental effect on the environment <sup>264</sup>. Variations in the production parameters can result in variations in the properties of the resultant silica particles and this may require the involvement of technical expert in the field for process optimization <sup>261</sup>. These hurdles made researchers to look for more sustainable sources for production and identified that highly pure silica could be generated from biological sources like diatoms, agricultural products and by-products like wheat husk <sup>265</sup>, rice husk <sup>266</sup>, sugarcane bagasse <sup>238</sup>, coffee husk, barley grass <sup>267</sup> and palm oil effluent <sup>268</sup>. BSN could also be obtained from other natural resources like quartz sand, but their procurement requires tedious processes like mining. Whereas, silica from agricultural biomass serves as an efficient alternative for being economical where the raw materials are also easily accessible <sup>261</sup>. Generation of silica nanoparticles can help in better management of agricultural waste which are otherwise burnt or discarded unscientifically could cause

environmental hazards. It can as well aid in value-addition of the biomass.

### **5.1.1. Diatoms as source of silica nano particles**

The cell-wall of unicellular eukaryotic microalgae, namely diatoms are a treasure house of natural source of opaline silica. The exquisite architectural motifs of siliceous patterns are formed as result of strictly-controlled intracellular biological processes. The silicic acid  $[\text{Si}(\text{OH})_4]$  present in ocean water around a pH of 8.0 enters the cell after passing through the plasmalemma. Silica deposit vesicles present in the diatom cells are found to be responsible for the biomineralization. Once the micro- and macro- morphogenesis is completed within the cell, the silica is transported out of the cells and affixed to the cell wall. Certain polycationic peptides called silaffins are known to catalyze extracellular polymerization of silica in certain benthic diatoms like *Cylindrotheca fusiformis*. With variations in the bioprocess of silicification, a variety of type and forms of frustule structures are seen across different type of diatoms. The chemistry of the cell walls is such that it facilitates functionalization with other chemical groups or metallic ions. The ability to control the silica frustule formation process makes it available for different applications in catalysis, bone tissue engineering and manufacture of biomaterials like bioactive glass and bio ceramics. Diatom-based silica can also be used as substitute to therapeutic metals like zinc, magnesium and strontium owing to its flexibility to attach other metal atoms. The unique topography of diatoms consisting of nano- and micro- pores and ridges provide adequate surface roughness for osseointegration.

The roughness enhances the attachment of osteoblasts over the surface that can promote bone repair. The excellent biocompatibility of diatomite silica enables its use for different medical applications. The particle can be attached with suitable free radical scavengers to reduce oxidative damages to the cell and can be used to reduce inflammatory responses. They also find applications in biosensing and other bioregenerative medicine, especially for the treatment of osteoporosis related complications. Silica from diatom frustules can be used as a natural substitute to high energy-demanding, chemically synthesized silica employing harmful chemicals. From table 4.1.1 and figure 4.1.1, it can be seen that ball-milling of the samples could result in particles with size  $>800$  nm. XRD spectrum (figure 4.1.2) shows diffused broad peak at  $2\theta$  angle  $\sim 22^\circ$ , suggestive of amorphous form of silica. Absence of other peaks in the XRD spectrum is indicative of purity of the which is also in alignment with the results from EDAX [figure 4.1.3 (K) and (L)] and CHNS (figure 4.1.4) analyses. FESEM images (figure 4.1.3) show varied exquisite patterns of silica structure of the diatom frustules showing large pores (macro). Figure 4.1.5 shows the effect of ball-milling on zeta potential values of the sample. It can be seen that samples ball-milled for 6 h at a ball-to-powder ratio of 4:1 (sample A) and 8:1 (sample B), which had lowest particle sizes had higher negative zeta potential values (-10.282 and -10.895 mV respectively) as compared to unmilled samples, which could possibly be due to increase in surface area (table 4.1.2) upon ball milling, which would expose more negatively charged surface silanol groups, resulting in higher negative charges. XRF analysis results showed sample purity to be 85.94%, with the presence of trace amounts oxides

of aluminium, iron, phosphorus, magnesium, potassium, sulfur, calcium and titanium (table 4.1.4).

### **5.1.2. Plant materials as source of silica nano particles**

Depending on the innate properties, the assimilation and accumulation of silica may vary across different plants. Plants absorb soluble silica mainly available as silicic acid  $[\text{Si}(\text{OH})_4]$  through their roots and are accumulated in the body in different hydrated forms <sup>261</sup>. Absorption of soluble silica by terrestrial plants in the form of monosilicic acid abundantly present in the soil results in its accumulation in cell walls and phytoliths, rendering them potential sources of biogenic silica <sup>269</sup>. Based on their ability to accumulate silica, plants may be classified as excluders, accumulators and intermediates which accumulate <0.5 %, >1 % and between 0.5-1 % in their dry weight respectively <sup>270,271</sup>. Plants belonging to *Equisetales*, *Cyperales* and *Poales* were seen to be silica accumulators <sup>272</sup>. The silicification process results in the accumulation of hydrated opaline silica in plants <sup>273</sup>. Also, plant by-products like rice husk are as source of amorphous silica which are proved to be less toxic than its crystalline form as seen in quartz rocks <sup>274</sup>. Naturally existing nano silica exhibit advantages of higher surface area-to-volume ratio with unique physical, thermal and electrical properties <sup>275,276</sup>.

Chemical method is the most commonly used method for the production of silica nanoparticles by virtue of its ability to precisely control the physicochemical properties of end-product by varying the process parameters. However, significant release of carbon dioxide

occurs from the process contributes to addition of greenhouse gases release in the atmosphere. Reports from previous literature mention that for the synthesis of 1 ton of silica nanoparticle employing Stöber process it requires 0.53 tons of sodium carbonate and 0.51 tons of sulfuric acid, which results in the release of carbon dioxide at the levels of 0.23 tons, sodium sulfate nearly 0.74 tons and generates 20 tons of effluents, which greatly impacts environment health. Synthesis of silica may be done using chemical methods like precipitation <sup>277</sup>, sol-gel method <sup>278</sup>, wet-chemical method harnessing surfactants like cetyltrimethylammonium bromide (CTAB) for fine-tuning of particle size and other properties followed by functionalization for various applications in nanomedicine and other industries <sup>279,280</sup>.

Different methods are undertaken for the synthesis of silica nanoparticles, which can generally be categorized into top-down methods involving physical strategies and bottom-up methods utilizing chemical reactions as mentioned before. The physical methods employ principles of attrition, impact forces like milling and reshaping of the substrate material to required sizes and shapes. However, in the chemical methods molecular components rearrange themselves into assemblies and units <sup>281</sup>. Repurposing of agricultural waste materials for the synthesis of silica nanoparticle could be an initiative for cost-effective, environment-friendly production <sup>282</sup>. Large quantities of agricultural by-products like rice husk, coffee husk, sugarcane bagasse is generated every year and its improper management and burning could pose a potential hazard to the ecosystem <sup>283</sup>. Synthesis of silica nanoparticles from these cheap and abundantly available raw materials



suggests a way of value addition using sustainable methods. Synthesis of biogenic silica nanoparticles include acidification of raw materials like rice husk, resulting in the removal of mineral content, followed by incineration in muffle furnace to facilitate removal of carbon content from the raw material <sup>284</sup>. Unlike biogenic silica nanoparticles, artificially synthesized silica nanoparticles may involve the use of inorganic precursor molecules involving costly operating procedures imposing heavy tolls on environmental equilibrium and may often result in bioincompatible end-products. Silica particles based on biomass are generated at a higher volume than those from synthetic organic precursors. However limited literature are available on such studies <sup>283</sup>.

In this study, a hybrid approach was preferred and involved physical as well as chemical processing involving less environmental impact. Various parameters were standardized and characterization of the silica nanoparticles were also done and a better candidate was chosen for subsequent studies.

Recent reports suggested different steps in the preparation of silica nanoparticle involving washing the pre-cut waste samples (like rice husk) using distilled water to remove sand, soil, and other visible extraneous particles, drying in the oven for 24 h at 100 °C (or until sufficiently dry) or sun drying, followed by acid treatment using 2 M HCl, again washing in distilled water to remove HCl, followed by controlled heating at 700 °C for around 5 h. Final step was to dissolve in 10 % HNO<sub>3</sub> for ~3 h and to rinse with distilled water. The samples were then filtered and allowed to cool, during which nano-silica was

precipitated. Heating generally helps in removing any organic contents, while acid reflux helps remove metallic impurities from the materials<sup>267,285</sup>.

By controlling the synthetic process, silica nanoparticles having mesoporous nature could be synthesized with or without pores<sup>286</sup>. They are available in various forms from different commercial manufacturers like Sigma Aldrich. Considering the structural property of silica, it exists in two major forms with crystalline and amorphous structures. Crystalline materials consist of a regular order of atoms and molecules, while such a regular array is missing in the case of amorphous forms. Silica present in crystalline form such as in quartz, cristobalite and tridymite consists of repeated and regular tetrahedral geometry of SiO<sub>4</sub> units, while flint and opal are naturally occurring amorphous forms of silica in nature with irregular arrangement of the central functional unit, SiO<sub>4</sub>. Previous reports suggest impact of increment in burial temperature and pressure in the transformation of opaline silica to cristobalite forms<sup>287</sup>. X-ray crystallography discriminates amorphous form from crystalline forms as short-range repeated units of SiO<sub>2</sub> molecules based on the absence or presence of distinct lines in the diffraction pattern of the silica samples with amorphous silica having complete random orientations while crystalline samples showing sharp reflections in the diffraction pattern<sup>288</sup>. It may occur naturally or may be artificially synthesized. It may be hydrated at the surface or may be anhydrous. In the SiO<sub>2</sub> structure, the oxygen atom is linked to silicon atom through covalent interactions resulting in siloxane, -Si-O-Si- or silanol, -Si-O-H- functional groups.

Proximity of surface silanol groups to each other determines the fate of intramolecular hydrogen bonding, finally resulting in the development of ring structures<sup>288</sup>. Amorphous silica can be distinguished based on chemical composition and other physical and chemical properties.

Synthesized particles are distinguished from one another by evaluation of its different physical and chemical properties. Different analytical techniques are available for the analysis which help determine parameters like particle morphology, chemical composition and other properties that can ultimately decide the fate of particles for specific applications<sup>288</sup>. Different facile methods of synthesis of silica nanoparticles are adopted that can greatly reduce the overall cost of production. However, the percentage of silica content in the final product determines the ultimate usability of the end product for different applications. Pretreatment of raw materials can aid in the sequential removal of extraneous components like metal ions and can also induce hydrolysis of any organic components present in the sample, which ultimately improves the level of silica in the end-product<sup>289,290</sup>.

The application of silica nanoparticles for drug delivery applications requires it to satisfy certain conditions essential for efficient drug loading, cellular uptake, for longer residence time in circulation, high biocompatibility and being metabolizable. Physicochemical analysis of the nanoparticles helps in their characterization and in the selection of processes for the optimization of the desired parameters and generation of particles suitable for particular applications. Different instruments and analytical techniques

are available for the evaluation of different physical and chemical properties and these evaluations can act as guiding tools for predicting the molecular and systemic effects when the particles come in contact with the biological milieu <sup>291</sup>. Morphological analyses of the particles are done with the aid of field emission scanning electron microscopy (FESEM), transmission electron microscopy (TEM) and other techniques involving dynamic light scattering (DLS). Morphological properties chiefly include particle size, surface structure and shape. DLS which is used for measuring the hydrodynamic diameter of particles works on the principle of Brownian movement of the particles, wherein larger and heavier particles move slowly as compared to smaller and lighter ones <sup>292</sup>. Laser light beams are focused onto the particles in the suspension and the doppler shift in the incident radiations as a result of the haphazard motion of the particles are recorded by a photon detector in a time-dependent manner and shows the size distribution of the particles <sup>293</sup>. It helps in predicting the behaviour of particles *in vivo* in terms of susceptibility to aggregation, response to variations in temperature, time and pH and hence determine the stability of suspensions <sup>293</sup>.

Electron microscopes are other tools helpful in the analysis of morphological traits of nanoparticles. Electron microscopes harness high energy electron beams similar to that of a light microscope which works on visible light. However, electron microscopes provide better magnification and resolution of samples. The electron beams emitted from the surface of the sample (backscattering) is captured by an

electron detector which are subsequently converted to digital images corresponding to the brightness levels<sup>294</sup>.

### **5.1.3. Source identification of biogenic silica**

Particle size reduction can be accomplished by two major techniques: precipitation, where the particles are suspended in particular solvents and mechanical processes like milling. The choice of the type of size reduction technique depends on the properties of the individual samples. Some of the most important properties considered include particle hardness, cohesiveness, ductility, elasticity, explosive nature, sensitivity to different chemicals, temperature etc. This study followed a top-down approach for the synthesis of silica nanoparticles from natural sources like diatoms. For diatomaceous earth sample, ball-milling technique which works on the principle of attrition and impact forces was the method undertaken for reduction of particle size. Since the particles were shown to exhibit clumping once in aqueous medium, homogenization was done before analysis of physical and chemical properties for techniques involving the particles to be suspended in aqueous medium. The scalability of the method was also high. The high impact from the rotational and vibrational forces arising from the collision of pulverizing balls with the raw material result in newer atomic surfaces possessing elevated surface energies being exposed. The particles constantly put to pressure during the milling process led the fragmented particles to form interconnections between each other through interatomic binding forces, forming secondary particles. The particles which undergo a welding process, are transformed, fractured and re-welded, resulting in the formation of new

microstructures. The adhesive force between the particles may more clearly be studied using techniques like atomic force microscopy and particle image velocimetry. After ball-milling process, the silica from diatomaceous earth remained in the micrometer-range.

Another set of studies were conducted using biomass generated from agricultural by-products containing silica for isolation of biogenic silica nanoparticles. Facile synthesis of high purity silica was accomplished from these raw materials with minimum processing steps. Maximum yield was obtained from rice husk sample (14 %) followed by corn husk (2.11 %), Indian goose grass (1.45 %), coffee husk (1.03 %) and sugarcane bagasse (0.004 %) (table 4.2.1). Silica purity >99 % were obtained from rice husk samples subjected to acid pretreatment with 1N HCl and incinerated to temperature above 500 °C over an hour (table 4.2.7). Silica samples obtained from rice husk with better yield and purity were chosen for further analyses.

#### **5.1.4. Effect of raw material pretreatment on physical and chemical properties of end-product**

##### ***Dynamic Light Scattering***

Insight into the size of particles for drug delivery applications is essential to predict its properties and safety upon administration to biological system. Dynamic light scattering (DLS) evaluates the particle size distribution in solution. Particles are considered to be spherical single entities that move in random haphazard motion in the solution. The fluctuations arising from this Brownian movement is considered to be proportional to the hydrodynamic diameter of the

particle. A beam of laser light is focused onto the particles in the solution. The intensity of doppler shift of the incident beam is detected and this intensity is time-dependent on the fluctuations. The particle size is calculated using Stokes–Einstein equation which draws relation between timescale of particle diffusion to the corresponding spherical hydrodynamic diameter of particle which is also dependent on the temperature at which the scattered light is collected, as well as on the viscosity of the solution. DLS also helps determine the stability and dispersity of particles in suspension in terms of variations in time and temperature <sup>292</sup>. In addition to evaluation of particle size distribution, light scattering can also be used for determining zeta potential values of samples <sup>293</sup>.

The hydrodynamic diameter values of the samples were seen to be higher than that observed in electron microscopy. Since DLS measurements were carried out in solutions, chances are that the silica particles formed aggregates resulting in the higher readings. The zeta potential values ranged between -4.33 to -30.11 mV (figures 4.1.5, 4.2.15). Silica samples from coffee husk showed highest hydrodynamic diameter value of 1902 nm while the lowest observed one was that of rice husk silica reading 846 nm (from DLS analyses). Derjaguin-Landau-Verwey-Overbeak (DLVO) theory based colloid science principle suggests the interplay of attractive van der Waal's and repulsive forces owing to electrostatic that determines the propensity of nanoparticles to form aggregates <sup>295</sup>, with nanoparticle morphology and surface chemistry being other factors. It also predicts the likelihood of smaller-sized particles to get conglomerated relatively

easier due to increment in relative surface energy and reduction in energy barrier as it tends to lower the free energy of the system<sup>295</sup>. The susceptibility of the particles to form aggregates can be reduced by providing surface coatings of polymers, electrolytes or surfactants that can increase the electrostatic and/or electro steric forces between the particles. The particle aggregation can determine to a great extent the mobility and the ultimate fate of the particles in the biological system as well as in external environment.

DLS also estimates the Poly dispersity index (PDI) of the particles in a suspension. PDI is considered as the ratio of average molecular weight to average molecular weight by mass, which measures the particle dispersity in a suspension. An ideal uniform sample would have a PDI of 0. Here, the PDI values obtained through DLS measurements shows values greater than 0.4, indicating presence of broadly polydisperse particles in the samples. Particle aggregation is also influenced by other factors like pH, type of electrolyte, ionic strength etc.

From figure 4.1.1, it can be seen that the particle size ranged from around 700 nm to around 2  $\mu\text{m}$ . The broader peaks in the particle size distribution shows a wider range of particle sizes suggesting highly polydisperse suspension. Narrower size distribution suggests a greater number of particles in almost similar range of sizes and increased chances of the suspension being monodispersed. Smaller sized particles were obtained when the ball-to-powder ratio was increased to 8:1 and rotational speed to 1000 rpm (table 4.1.1). However, further increase in ball-to-powder ratio or milling speed did



not influence the size of particles. The optimal milling time was 6 h which yielded smaller-sized particles. Hence, it can be assumed that the size-reduction using ball-milling is dependent of parameters like ball-to-powder ratio, milling time as well as milling speed and that it needs to be optimized according to the type of material used.

Correlation between particle size with temperature of incineration and time of incineration in silica samples derived from agricultural biomass is depicted in figure 4.2.12. From table 4.2.4, it can be seen that particle-size were reduced upon increment in incineration temperature. Conversely, smaller particles were observed with longer incineration time (table 4.2.4). Pre-treatment with HCl was favored for production of silica particles with lesser particle size (table 4.2.5). Different acid pre-treatment also showed similar pattern of decrement in particle sizes with increment in incineration temperature.

### ***X-ray diffraction***

The raw materials used in the study are commonly available agricultural by-products, the structural aspects of which were studied using x-ray diffraction, wherein the samples are exposed to collimated beam of x-rays. The instrument is equipped with detectors for the type and intensity of rays scattered at different angles which is used for the subsequent evaluation of the crystalline arrangement of the particles using Bragg's law,  $2d \sin\theta = n\lambda$ , where  $n$  denotes integer value,  $\lambda$  is the wavelength,  $\theta$  is the angle of scattering, and  $d$  is the interplanar distance. In addition to evaluation of crystalline phase of the samples x-ray diffraction studies can also be used for the determination of size of the crystallites applying Debye–Scherrer relation:  $D = \kappa\lambda/\beta \cos\theta$ ,

where  $D$  is the size of the crystallite, constant  $\kappa$  is the shape factor,  $\lambda$  is the wavelength of the x-ray,  $\beta$  is the full-width at-half-maximum of a characteristic diffraction peak, and  $\theta$  is the diffraction angle <sup>296</sup>. Additional peaks other than the characteristic curves of the sample material can also be used as an indicator for the presence of contaminants in the sample.

XRD analysis was used to detect any phase transformation likely to occur as a result of variations in synthesis parameters like type of acid used for leaching of raw material, time of pressurization during acid leaching, intermediate distilled water washing, volume of crucible used during incineration, incineration temperature and time. Broad peaks at  $2\theta$  angle of  $\sim 22^\circ$  seen in figures 4.1.2, 4.2.1 and 4.2.2 are indicative of amorphous form of the sample <sup>238,297,298</sup>. Absence of any other peaks indicate the purity of the sample. From the XRD peaks in figure 4.2.1, no significant variations were observed on altering the above-mentioned parameters, with the exception of incineration temperatures, where a progressive sharpening of peaks were observed with increment in temperatures. The x-ray diffraction patterns (figure 4.2.1) indicated presence of particles with short-range order seen as broadened peaks, for all the other samples (except for sample labelled S1000), suggesting the presence of particles in the amorphous form with the  $2\theta$  equal to  $22^\circ$  characteristic of silica <sup>238,299</sup>. It suggests the influence of incineration temperature on the crystallinity of samples <sup>238,300</sup>. At a temperature of  $1000^\circ\text{C}$ , a sharper peak (figure 4.2.1) was observed which could possibly be due to the transformation of silica from its amorphous opaline forms to cristobalite forms to

keatite forms finally to crystalline quartz forms, owing to the reordering of molecules arising from variations in temperature and pressure of the environment during incineration to which the particles were subjected. In certain cases where the particles are exposed to higher pressures, direct transitions from amorphous to crystalline form may occur without going through the intermediary steps. XRD diffractogram indicated that at higher temperatures, the particles undergo transition from short range orders with random molecular arrangement to long range orders.

***Field Emission Scanning Electron Microscopy (FESEM) & Energy Dispersive X-ray Spectroscopy (EDAX)***

Unlike optical (light) microscope where beams of visible light are used for obtaining magnified images of object, FESEM uses accelerated electrons in a column maintained at high vacuum ( $\sim 10^{-9}$  Torr). FESEM analysis was carried out to analyze morphological traits of the synthesized silica particles. The properties of the samples are such that the primary electrons are deflected at varied angles at varying velocities. These electrons, called secondary electrons are received by a detector where electrical signals are produced, which are then transformed into images to be viewed on an output device like monitor. Unlike in scanning electron microscopy (SEM), where thermionic emission occurs, FESEM uses thermal emission for generating electrons which results in minimum contamination of sample surfaces. The samples are often pre-coated with a conducting substance (sputter coating) to reduce the charge effects as well as for better image quality. FESEM has better resolution and can be used for characterization of physical structures and can even detect contamination through visual

observation of the ultra-fine structures as well as through EDAX commonly attached with the FESEM set up. Elemental composition of samples is analyzed from the emission spectra of electrons generated from the sample which are unique for each atomic structure. The excited x-rays bombard the samples resulting in ejection of electron from inner shells, creating electron holes, which are filled by electrons from outer shells. The differences in different energy levels are released as x-rays, which are measured by a spectrometer. The resultant emission spectrum wherein the electrons return to the ground state to the K-alpha, K-beta or L-shells will be unique for specific atomic structures which will help in identifying the nature of composition of the sample.

Diatoms are unicellular microalgae which contributes to a significant amount of oxygen production and biomass on earth. It consists of intricately arranged pattern of cell wall chiefly comprised of silica in the opaline form. The name of the organism is derived from the unique arrangement of its cell which comprises of two halves (theca) in the form of flat plates which are mostly overlapping to one another and connected together by a gridle band. Diatoms exhibit unique optical properties making them 'living opals'. The shapes of these organism may vary from being circular to elliptical, cuboidal to triangular forms. These organisms after death pile up as fossils resulting in diatomaceous earth, which finds application in filtration, as pest repellent, adsorbent material, filler material, polishing aids, heat insulator etc. The purity of the diatomaceous earth may vary according to the presence of other minerals and clays in the blend. The FESEM pattern of the sample (figure 4.1.3) showed elaborate pattern of porous structure on the surface of the frustules with round centric shapes.

After ball-milling, the structures were seen to be frail and size reduced from around 2.5  $\mu\text{m}$  to 500 nm. Macro porous structures were predominant in the samples, some of which were fractioned as a result of ball-milling, with a broader particle-size distribution even after screening of the particles. The EDAX spectrum [figure 4.1.3 (L)] ruled out the presence of any extraneous matter or contaminants and showed the peaks for silicon and oxygen only, thus verifying the purity of the sample. Since the particle were larger for the intended applications, efforts were redirected to synthesise amorphous silica nanoparticles from other biogenic sources.

The FESEM micrographs (4.2.4 to 4.2.7) showed near spherical structures of the silica particles derived from agricultural biomass. While silica particles derived from coffee husk ranged between 4-20  $\mu\text{m}$ , that from sugarcane bagasse lied between 350-700 nm. Particle diameters were found to be smaller in other samples. Silica derived from rice husk showed particle sizes between 50-80 nm. The porous spherical particles were seen to exist in compactly agglomerated form. TEM images of rice husk silica (figure 4.2.8) were also in agreement with that seen in FESEM measurements.

### ***Transmission Electron Microscopy (TEM)***

Similar to scanning electron microscopy (SEM), TEM uses an electron source, emitting controlled beam of electrons across a vacuum chamber to finally capture the images of samples. Unlike SEM, the samples to be observed through TEM requires them to be thinner (<100 nm). Unlike in SEM, the sample chamber is located in the middle of the whole body of the microscope, while the samples are placed towards the bottom of the electron column. The electron beams

are transmitted through the sample and its interaction with the specimen results in formation of high-resolution images, which are then focused onto photographic screen or scintillator attached to a detector. The primitive model of TEM was developed combinedly by Ernst Ruska and Max Knoll in the year 1931. While SEM is used for analyzing surface morphology, TEM is helpful to assess even the inner structures of the sample.

TEM imaging (figure 4.2.8) showed spherical shaped particles adhered together to form larger clumps. The observations were in alignment with that observed through FESEM. Porous structure of the particles however was not vivid.

### ***CHNS analysis***

CHNS analyzer is an elemental analysis tool that makes use of combustion process at elevated temperatures in the presence of ~99.9% oxygen and inert gases like helium, based on Pregl-Dumas method. The formed oxides are directed through channels leading to elemental analyzers specific for hydrogen, nitrogen, sulfur and carbon for its qualitative and quantitative analysis using methods like mass spectrometry or x-ray fluorescence.

CHNS analysis of silica samples derived from biogenic sources (figures 4.1.4 and 4.2.10) showed that no organic elements or extraneous matter with sulfur and nitrogen content were present in the samples tested. Presence of hydrogen were noted in both samples which can be attributed to the innate hygroscopic property of silica. Absence of even trace amount of carbon indicates successful acid

leaching pretreatment and incineration steps during the synthesis of silica nanoparticles from agricultural sources.

### ***Zeta ( $\zeta$ ) potential analysis***

Nanoparticles in suspensions and colloidal formulations are constantly under the electrostatic attractive and/or repulsive forces operating between the particles as well as the liquid. The electrochemical equilibrium at the interface of the particle and liquid is expressed in terms of a parameter known as zeta potential. It helps predict the stability of the particles in the colloidal system. In theory, zeta potential measures the difference in electrical potential between the colloidal suspension and the rigid phase of the fluid in contact with the layer of the particle. Polish physicist Marian Smoluchowski is credited for the originally developing method for zeta potential calculation. In a zeta potential analyzer, the particles dispersed in solutions venture to electrodes of opposite polarity upon the application of a voltage across the system and the zeta potential is calculated based on factors like solution viscosity, dielectric constant, electrophoretic mobility, velocity of particle, voltage applied and the distance of the electrode according to the computer program of the system. An increase in the repulsive forces between particles prevents its chances of aggregation. Zeta potential analysis involves recording variations in particle velocity under the influence of an electric field and expressed as the difference in electric potential between the shear surface of the particle and that of the solution, which is indicative of the susceptibility of agglomeration of particles in the formulation. Formulations possessing zeta potential values higher than +30 mV and

lower than -30 mV are generally considered to form stable suspensions, while that within the range of -30 to +30 mV are expected to aggregate and flocculate <sup>292</sup>. Studies have shown that particles possessing lower zeta potentials (values less than 5mV) can result in increase in Van der Waal's attractive forces between particles, resulting in a net increase in particle agglomeration reducing its stability in suspensions <sup>301</sup>. Zeta potential estimates the repulsive force acting between particles and hence higher the values ( $\pm$ ), higher the repulsive forces between particles and hence the stability <sup>302</sup>. Accordingly, studies have shown that a better stability of the system is achieved with zeta potential of  $>+30$  mV or  $<-30$  mV <sup>303</sup> resulting in longer circulation time in the physiological system and can be used as an indicator to assess storage stability.

From figure 4.1.5 it is evident that un-milled sample had lowest negative zeta potential compared to ball-milled ones. Variations were observed in the zeta potential values of ball-milled samples with different processing parameters. It can be seen that samples subjected to balling at 400 rpm for 4 h at 1:1 ball-to-powder ratio had more negative zeta potential than unmilled samples, and the values became most negative for the samples subjected to ball-milling for 6 h at 8:1 ball-to-powder ratio and 1000 rpm rotational speed. With more particles getting fractured, the more the surface area and higher the surface charge observed. Table 4.2.9 and reports in figure 4.2.15 indicate the zeta potential values of samples derived from different agricultural biomass. Silica particles derived from rice husk had zeta potential value of -30.11 mV indicating better colloidal stability of the



particles owing to higher repulsive forces in action. Particle size of rice husk derived silica particles were the smallest. Hence, similar trend as observed with the diatomite sample holds good for silica particles derived from agricultural biomass. The higher the surface area, the higher the surface charge and higher the zeta potential.

### ***Nitrogen sorption studies***

Pore properties of the generated silica samples were studied using nitrogen sorption isotherm. While the surface area of unmilled diatomite samples only 5.65 m<sup>2</sup>/g, ball-milled samples showed an improvement in surface area to 8.22 m<sup>2</sup>/g. There was also an improvement in pore-size from 11.29 nm to 16.44 nm and pore-volume from 0.025 cm<sup>3</sup>/g to 0.04 cm<sup>3</sup>/g upon ball-milling (table 4.1.2). The silica particles sourced from various agricultural biomass represented a type IV pattern as per IUPAC classification (figure 4.2.11). This pattern is characteristic of mesoporous material<sup>304</sup>. Table 4.2.2 shows rice husk silica obtained on incineration at 500 °C for 4 h to possess highest specific surface area ( $a_{s,BET}$ ) corresponding to 232 m<sup>2</sup>g<sup>-1</sup>, mean pore diameter of 3.71 nm and total pore volume of 0.22 cm<sup>3</sup>g<sup>-1</sup>. It can be seen from table 4.2.3 that samples pre-treated with HCl had better surface area, pore volume and pore sizes than those subjected to leaching using H<sub>2</sub>SO<sub>4</sub>.

Optimization of pore size, surface area and volume are essential for generating efficient drug carriers. Porosimetry is based on the assessment of mass of inert substances like nitrogen adsorbed onto the pores of the particles under given conditions of temperature and

pressure. Isotherms constructed using equations like Brunauer, Emmett and Teller (BET) can be used to classify particles according to the size of pores. Accordingly, particles with pore sizes  $\leq 2$  nm are considered to have micropores, that between 5-50 nm as mesopores and  $>50$  nm as macroporous and occupy a position between type I-VI in the adsorption isotherm curves<sup>305</sup>.

### ***Fourier Transform Infrared Radiation***

The FTIR spectrum showed peaks in the range of 3700-300  $\text{cm}^{-1}$  corresponding to O-H stretching band of water (figures 4.1.6, 4.2.13 and tables 4.1.3, 4.2.6) indicating presence of bound water associated with polymer matrix as well as O-H bending band region of water. Wavenumbers in the range of 1250-1000, 500-810  $\text{cm}^{-1}$  is indicative of Si-O group bending vibration mode, Si-O bending vibration mode and rocking mode of Si-O group.

In this study, post-synthesis loading of drugs is done to facilitate its conjugation on the surface as well as to the mesoporous structures of the biogenic nanoparticles. The surface modification and drug loading were confirmed by FTIR technique which shows the interactions between functional groups and chemical entities, which established successful loading of curcumin and epirubicin as seen from figure 4.3.1 and associated table 4.3.1. Presence of polyethylene glycol and chitosan in rice husk was confirmed by the presence of characteristic peaks in the IR spectrum. Major interactions of groups in polyethylene glycol structure were C-O and C-C stretching vibrations,  $\text{CH}_2$  twisting, rocking, wagging and scissoring vibrations. These

interactions are evident from figure 4.3.1 (B) with peaks around 840  $\text{cm}^{-1}$  indicating C-O, C-C, C-H<sub>2</sub> rocking interaction. Peak at 960  $\text{cm}^{-1}$  marks the interplay of CH<sub>2</sub> rocking and twisting vibrations. Peaks at 1340 and 1460  $\text{cm}^{-1}$  suggests CH<sub>2</sub> wagging and scissoring vibrations respectively. Presence of strong bands sweeping from 3300- 300  $\text{cm}^{-1}$  confirms N-H and O-H stretching interaction of chitosan structure, while symmetric and asymmetric stretching interactions of C-H group can be seen from peaks around 2900 and 2880  $\text{cm}^{-1}$  in figure 4.3.1 (A). Presence of strong peak at 1645  $\text{cm}^{-1}$  shows the presence of C=O stretching from N-Acetyl groups while that at 1325  $\text{cm}^{-1}$  indicates presence of C-N stretching of amide group in figure 4.3.1 (A). Bending vibration of C-O at 1277  $\text{cm}^{-1}$  in figure 4.3.1 (B) is from the phenolic group of curcumin. Peak at 1512  $\text{cm}^{-1}$  arise from the stretching and bending vibrations of ketone group, CC-C, CC=O and CC-H groups from keto-enol configuration. Peaks around 3400  $\text{cm}^{-1}$  and 3300  $\text{cm}^{-1}$  in figure 4.3.1(C) are those of -OH and -NH stretching vibrations and that around 1600  $\text{cm}^{-1}$  that of ketone (C=O) group lying between two aromatic rings in epirubicin structure. Peak around 1200  $\text{cm}^{-1}$  is that of C-O-C asymmetric stretching interactions<sup>266</sup>.

### ***X-ray fluorescence***

Quality control is of paramount importance to maintain the purity of the end-product. Presence of extraneous elements whether in major, minor or trace levels were analyzed using another non-destructive analysis technique employing x-ray fluorescence spectrometer. Similar to XRD analysis, the atoms in the sample are excited by incoming beam of x-rays which are emitted from the

samples. The fluorescent x-rays emitted from the sample are detected, digital output generated and processed to obtain analytical data. It aids in multi element analysis with detection limits to the level of parts per million (ppm).

The pretreated diatomaceous sample procured was found to contain 85.94 % silicon as silicon dioxide as analyzed using XRF technique. Trace amounts of oxides of aluminium, iron, phosphorus, magnesium, potassium, sulfur, calcium and titanium were also reported to be present (table 4.1.4). In another set of studies biogenic silica particles were successfully synthesized from various sources like coffee husk, corn husk, sugarcane bagasse, Indian goose grass and rice husk with yield per cent from the respective raw materials as 2.256, 2.1068, 0.004432, 1.448 and 14.52 in the order. Greater than 95 % silica was detected from rice husk samples (table 4.2.7), similar to that observed from previous works of Phonphuak *et al* <sup>306</sup>. Presence of other mineral components in negligible quantities indicated successful acid leaching using 1N HCl under pressurized conditions for 1h. Hence, the samples heated at 500 °C for 4 h resulted in superior quality silica.

## **5.2. Surface modification and drug loading studies**

Oral administration is one of the most common routes of drug delivery due to multiple factors like ease of ingestion, better patient compliance, non-invasiveness and flexibility in dosage forms. However, poor bioavailability is a major limiting factor that hampers the effectiveness of such formulations. Bioavailability, the proportion

of drug that enters the systemic circulation that is available to render its effect in the body in turn is determined by other factors like solubility of the drug in aqueous solvents, its permeability, rate of dissolution, metabolism inside the biological milieu and susceptibility to efflux mechanisms<sup>307</sup>. A significant proportion (>40%) of new chemical entities developed in the pharmaceutical sector encounters the problem of poor aqueous solubility<sup>307</sup>. Availability of the active pharmaceutical ingredient in the form of a solution determines its ability to be absorbed to the systemic circulation to exert the pharmaceutical effect. Solubility is an important parameter which determines drug levels in the biological system over a period of time that determines its ability to accomplish a desired pharmacological response<sup>307</sup>. Hydrophobicity is found to be an important reason for the low solubility of several potent drugs which immensely limit its bioavailability, leading to low therapeutic efficiency<sup>308</sup>. This impedes the pharmaceutical development of the drug and such active ingredients require special formulation to improve these features. Several modification strategies involving chemical and physical modifications, size reduction of particles, salt formation, prodrug design, supercritical fluid technology, crystal engineering, incorporation of surfactants, and complexation of the pharmaceutical ingredient may be undertaken to improve upon the solubility. The strategy depends upon drug properties like the expected site of absorption, expected features of the drug formulation, pharmacokinetic properties and so forth<sup>307</sup>. The physical size reduction through comminution, milling and grinding or spray drying could impart mechanical and thermal stress that may result in disintegration of the active pharmaceutical. Another strategy involves

incorporation of drug to hydrophilic matrices like polyethylene glycol (PEG), surfactants like tween-80, resulting in solid dispersions. These procedures however come with the price of high cost of production, possible adverse effects of the solvent on the stability of drug, difficulty in reproducibility of crystal structures and removal of the organic solvents and requirement of technical expertise in the field of computational analysis<sup>309</sup>. While the polar groups in the formulation determines the solubility of the drug, its permeability across membranes is determined by the presence of lipophilic moieties and partition coefficient (Log P), requiring the drug formulation to have optimal hydrophilic and lipophilic properties<sup>310,311</sup>. Proper knowledge and consideration of advantages and disadvantages of individual techniques or combination, physical and chemical properties of the drug can aid in the development of an efficient formulation.

Incorporation of drugs to different drug carriers is another novel strategy that was reported to enhance the drug bioavailability and improved the ability to cross different biological barriers<sup>312</sup>. In addition to improvement in bioavailability, drug carriers also act as a protective barrier against degradation of the active pharmaceutical ingredient and can also be tuned to control the pharmacokinetic and release pattern of the drug<sup>313</sup>. Nanoparticle-drug formulations are designed to improve residence time of the active pharmaceutical ingredient in systemic circulation, targeting affected tissues and retention, controlling pharmacokinetic properties of the drug to facilitate controlled release which are accomplished by manipulation of the nano formulation with different ligands resulting in a net

modification of the intrinsic characteristic of the nano formulation, target selectivity, as well as its interaction within the biological system

314

### **5.2.1. Modification with polyethylene glycol**

Systemic administration of nano formulation enables them to reach and confine to vascularized tissues, with the chances of reaching the target sites higher with prolonged residence time. The body defense system comprising opsonins and mononuclear phagocyte system (MPS) is responsible for identifying, processing and clearing such extraneous particles from the system. As soon as the nanoparticle enter the bloodstream, serum proteins called opsonins identify and form a layer around the nanoparticles, the process of which is referred to as opsonization. Opsonization increases the chances of the nanoparticle identification by the mononuclear phagocyte system <sup>168</sup>. This rapid clearance of nano formulations results in rendering the pharmaceutical inactive. Protein corona formation also weakens the targeting ability of the nano formulation. Incorporation of chemical groups like polyethylene glycol and its derivatives form a covering over the nanoparticle, preventing them from aggregating. The process of coating polyethylene glycol generally referred to as ‘PEGylation’ reduces particle opsonization and phagocytosis. The overall reduction in immunogenicity enhances the circulation time of the particles in biological system <sup>168</sup>. Absorption of opsonins to the nanoparticle occur chiefly through hydrophobic interaction in addition to electrostatic and hydrogen bonding. Grafting nanoparticles with hydrophilic polyethylene glycol chains result in the formation of a hydrated cloud

around the nanoparticles that sterically hinders interparticle interaction as well as opsonin binding, thereby reducing particle agglomeration and recognition by opsonin binding receptors present on the cells in MPS. Particle agglomeration can otherwise result in blocking of capillaries, which can again trigger mechanisms for its removal. The ability of PEGylation to exhibit these effects depends to a large extent upon the density of PEG graft, molecular weight of PEG and physicochemical properties of the nanoparticle in itself. Previous studies have reported better shielding property of PEG graft with molecular weight of 2 kDa or above<sup>315</sup>.

### **5.2.2. Chitosan capping and pH responsive release of drug**

Use of drug loaded on to mesoporous silica nanoparticles (MSNs) cannot fully solve the problems like side effects in non-target tissues, low retention time etc. due to certain inherent handicaps of mesoporous silica nanoparticles. Even small areas on the surface of the nanoparticles as little as 6 % of the total surface area will get exposed to the external environment and the silane groups on the surface of the MSNs interact with biological molecules, such as membrane lipids and proteins of cells leading to the destruction of the structure of MSNs, thus making them invalid. Surface modification of the MSNs could greatly improve their biocompatibility. Another advantage that could be achieved by using MSNs as drug carrier is drug targeting. Most pharmaceutical drugs, especially anti-tumor or anti-cancer drugs are toxic to normal cells also. Targeted- controlled release of these toxic drugs to the tissue to be destroyed is a long-cherished ambition of biomedical scientists and the probability of MSNs emerging as a tool is



of high probability. Use of a cap or gate for the mesopores of MSNs, that respond to tissue specific stimuli can efficiently solve this problem. Dendrimers, antibodies, different metal compounds such as  $\text{Fe}_3\text{O}_4$ , CdS and ZnO etc. are widely used as gatekeepers on the surface of the MSNs. These caps or gates are controlled through different stimuli such as change in pH, enzyme activity etc., and among these, pH-responsive systems have received particular attention, especially for cancer therapies due to acidic microenvironment (pH 5.0–6.8) inside solid tumors. Design and development of pH sensitive nanocarriers for the controlled and targeted release of drugs that prevent premature release of the loaded cytotoxic anti-tumor drugs has gained priority in nano medicine. Such successful pH-triggered systems could greatly lower the side effects of cytotoxic drugs and could help to enhance their therapeutic efficacy. Various kinds of pH-sensitive gatekeepers are being explored, but their low success rate and the difficult multi-step or complex processes involved in their synthesis and application along with limited awareness about their biocompatibility hinder the application of targeted drug delivery leaving them still in its primary stage of development and hinder their further use in therapeutic applications. pH sensitive gate keepers for the pores in MSNs with good biocompatibility, produced using facile synthetic processes are highly desired.

Chitosan is a natural cationic polysaccharide composed of glucosamine units, together with some N-acetyl-d-glucosamine units. Being a compound, which is biodegradable, non-toxic, and antibacterial, chitosan holds great potential in a diverse range of

biomedical applications <sup>9</sup>. The possibility to protonate the amino groups in chitosan within a certain pH range reveals the possibility of using chitosan as smart molecular devices responsive to an external pH-stimuli.

Recently, a pH-responsive chitosan-based hydrogel film has been successfully fabricated and used as a pH responsive nano valve to control the release of the drug insulin. Chitosan is relatively cheap and readily available from nature which stands as an advantage compared with supramolecules, polymers, and polyelectrolytes. These qualities of chitosan are very important for meeting the future clinical demands and its effective utilization would satisfy the increasing demands in both fundamental research and biomedical applications.

Chitosan, a long chain polymer formed by the deacetylation of chitin consists of variable units of N-Acetyl glucosamine monomers <sup>316</sup>. The  $pK_a$  values of the deacetylated C-2 amino groups is  $\sim 6.5$  suggesting the possibility of these groups getting protonated at pH values less than 6.5 imparting the chitosan molecule a net cationic charge. One of the implications of this phenomenon is enhancement in the interaction between positively charged chitosan groups with the negatively charged surfaces of mucosal cells and cell membranes , which enables better absorption of pharmaceutical or antimicrobial agents incorporated with it <sup>317</sup>. This property of chitosan imparts protection of the active pharmaceutical agent against degradation under severe gastrointestinal condition as well as from microbial attack <sup>316,317</sup>. Chitosan also have metal chelating property suggesting its inhibition of metalloprotein activity <sup>318</sup>. Chitosan also aids in faster

wound healing by inhibiting the release of inflammatory cytokines, inducing fibroblasts and improving collagen III deposition<sup>319</sup>.

Release of the active pharmaceutical ingredient in response to variation in pH results in stabilizing the form under normal physiological conditions, while triggering its release when pH drops, as in the case of tumour microenvironment which is more acidic than normal cells owing to generation of acidic by-products as a result of elevated anaerobic glucose metabolism. This increases intracellular drug accumulation in tumour cells while selectively reducing non-specific interaction of drug with normal cells.<sup>320</sup> Here, chitosan in addition to protecting the drug against premature release and its controlled release, is also used as a stabilizer by virtue of its non-toxicity, biodegradability and biocompatibility, better residence time in blood circulation with minimal tissue accumulation<sup>320,321</sup>.

Under high acidic conditions, the amino group protonation occurring in the structure of chitosan results in an increase in osmotic pressure as a result of swelling of the polysaccharide, leading to disintegration of its form, enabling selective release of drug at lower pH<sup>321</sup>. The electrostatic interaction between chitosan possessing positive zeta potential with negatively charged domains of the cell membrane promotes efficient cellular uptake chiefly by adsorptive endocytosis<sup>322</sup>.

The amount of drug loading was analyzed by spectrophotometric analysis and was confirmed again using thermogravimetric analysis. Except for some minor marginal

variations, results from both techniques were well aligned. While the drug loading of curcumin in pristine and surface modified biogenic silica as analyzed by TGA showed 8.67 and 8.28 % respectively, that from spectrophotometric analysis yielded 5 and 4.6 % respectively (tables 4.3.2 and 4.3.3). The loading of epirubicin on unmodified and modified biogenic silica nanoparticles were 9.59 and 7.24 % respectively (table 4.3.3). A general pattern of a reduction in the level of drug loading in surface modified silica nanoparticle as compared to pristine ones could possibly be due to the preoccupation of available surface area of the nanoparticle owing to attachment of ligand groups, making it unavailable for conjugation with the drug molecules. Attachment of ligands resulted in the improvement of hydrophilicity of the nanoparticle. The rate of conjugation of hydrophilic drug was found to be slightly higher than that of hydrophobic one. While spectrophotometric analysis is an indirect method used for the analysis of drug loading efficiency of nanocarrier by assessing the intensity of light, thermogravimetric analysis is a direct method which is based on the thermal stability of individual components in the sample as observed by the weight loss reported with the passage of time (figure 4.3.2).

### **5.3. Release pattern of drug from different nano-formulations**

Like the different textural properties of the nanoparticles play a role in determining the loading efficiency of drug into it, the drug release from these nano-formulations is also determine its different structural and chemical properties. This includes the particle pore properties like pore size and pore volume, drug-carrier interaction,

hydrophilicity of the formulation and the quantity of drug loading<sup>323,324</sup>. Drug release behaviour also alters with variations in the interaction between different nano-formulations and the release medium. Of all the mentioned factors, the magnitude and type of interaction between the drug and the nanoparticles plays a predominant role in deciding the pattern of drug release<sup>325</sup>. The surface of silica molecules consists of isolated, vicinal and geminal silanol groups, which can serve as hydrogen bond donors and acceptors, making hydrogen bond the most common type of bonding noticed for interaction with external molecules<sup>326,327</sup>. When the pH of the solution falls below the isoelectric point (pH 2.0) of silica, the molecules exhibits a net positive charge and a negative charge when the pH is above 2.0, depending on the protonation and deprotonation of silanol groups<sup>328</sup> leading to electrostatic interaction of silica with drug molecules, which in turn is determined by the chemical set up of the drug<sup>329</sup>. The strength of silica-drug binding results in higher or lower drug loading. Stronger binding results in sustained release of drug, while a weaker binding often results in its burst release<sup>330,331</sup>. Ease of functionalization of silica nanoparticles aids in modulating the interaction with drug molecules, hence can be used as a strategy to control the release pattern of drug and site specific release in response to microenvironment stimuli like pH<sup>108,332,333</sup>. With differences in the chemistry of different drug molecules the variation in ionization behaviour in response to fluctuations in pH of the surrounding medium determines the type of interaction between the drug and the nanoparticles. If the pH of the medium favors the solubility of the drug, rapid release from matrix occurs and following alterations in pH,

if the ionization of drug molecule results in acquisition of opposite polarity to that of nanocarrier, mutual electrostatic repulsive force comes into play resulting in higher drug dissolution<sup>334</sup>. A sustained release pattern of drugs was observed in different nano-formulations over a period of 100 h (figures 4.4.1 to 4.4.3 and from figure 4.4.5 to 4.4.7). The release patterns from biogenic silica and control samples were almost similar, but a slightly better release pattern was observed with the control samples, which could be due to more uniform morphological characteristics like particle size distribution, pore size and pore volumes. Unmodified and polyethylene glycolated curcumin loaded samples showed rapid release at pH 7.4 than at pH 5.4, whereas chitosan-capped samples showed enhanced release at pH 5.4 than at pH 7.4, possibly due to the release of drug owing to the disintegration of chitosan structures at such pH. Similar pattern of release from chitosan capped nano-formulations was observed with those loaded with epirubicin drug. The isoelectric point of chitosan is less than pH 6.3 and at this pH, the protonation of amino group in its structure can occur, leading to erosion of the chitosan structure followed by the release of the drug from the matrix. At alkaline pH, however the chitosan forms a gel-like structure which inhibits the release of drug. These results indicate that the nano-formulations are suitable for applications of drug release at specific sites with lower pH conditions as in stomach and tumor microenvironment. The curcumin loaded samples without chitosan capping had higher release at alkaline environment, while epirubicin release enhanced at acidic pH possibly due to enhancement in aqueous solubility of drugs at respective pH conditions.

#### **5.4. Assessment of nanoparticle toxicity and cytocompatibility using cell lines**

The biocompatibility of nanoparticles intended for biomedical applications are to be evaluated to ensure its safety under biological conditions as well as to the environment. Previous literature has established a linear connection between the innate physicochemical properties of the nanoparticles in determining its biocompatibility<sup>335</sup>. Administration of nanoparticles into a living system result in host response which should be acceptable and capable of facilitating the nano-formulation to exert its intended function under the given conditions. The response of the host to the nanoparticles may vary according the host anatomy suggesting that the mode of administration can also result in variations in host immune responses. Residence half-life is yet another parameter that affects particle biocompatibility with longer half-life, the higher the chances of biological interactions<sup>336</sup>. Surface properties of nanoparticles determine its interaction with blood components, stability, degradation together with its accumulation and tissue clearance. However, extrinsic factors like dosage form, route of administration and mode of action can result in triggering immune response which may result in its stimulation or suppression<sup>336</sup>. Biodegradability is yet another property that decides the biocompatibility of the particles. Selection of the carrier particles is also based on considerations of the desired size of the particles for specific application, expected interaction with the active pharmaceutical ingredient, susceptibility to aggregation, hydrophobicity, size, shape, the cargo release pattern as well as

stability of the particles under physiological conditions <sup>335,337,338</sup>. Nanoparticles once administered come in contact with blood components, extracellular fluid, cytoplasm and other cellular components during transit

Limited data on immunological responses to different nanoparticles and its formulations together with the concept of personalized choice on deciding between the gains and demerits of the nanoparticle has delimited an explicit understanding of the biocompatibility. All these points towards the significance of analysis of nanoparticle biocompatibility in a case-by-case basis for different applications over different anatomical locations to ensure its safety and efficiency.

This study aims at the evaluation of different parameters that influence the nanoparticle biocompatibility to predict its behaviour under physiological conditions.

#### **5.4.1. Degradation behaviour of biogenic silica particles**

The biogenic silica has shown excellent biocompatibility as seen from the results reported in other sections. However, in addition to exhibiting high biocompatibility, the nanoparticle also shows acceptable levels of degradation behaviour to prevent chances of toxicity associated with particle accumulation in the body. Depending on its physicochemical properties, the exudation of silica particle occurs through urine or fecal matter. Elimination of these particle are also to a great extend influenced by the charge carried by these particles. Larger sized cationic ones and those with higher surface area



are preferentially taken up by the gastrointestinal tract and excreted by the biliary system and spleen, while those falling in sizes less than 6 nm find its way out through the renal system<sup>339</sup>.

It can be seen from the FESEM micrographs (Figure 4.5.1) that, the beginning of the experiment was marked by the intact porous structures of the silica particles. However, with the passage of time, the porous structures seem to fuse with one another as a result of accelerated degradation in the simulated body fluid. The particle however was not fully broken down by 14 days period which also implies that the particles have the capability to remain in the circulation to facilitate the delivery of drug payload. The results also suggest the narrowing of the chances of the particles getting accumulated in the system to cause any toxicity. However, a concern that may arise in instances where longer residence periods of the particles are demanded is regarding the leakage of the drug due to loss of structure integrity and further studies are needed to verify the phenomenon. The alteration and collapse of the internal structures could be attributed to hydrolytic as well as biodegradative activities. However, a stronger correlation between particle degradation rate and the complexity of its internal structures can only be established upon detailed studies on the influence of different important parameters like surface modification, size, surface charge, media pH, temperature and composition.

Evaluation of degradation behaviour of biogenic silica is essential to predict its degradability under biological milieu. It throws light on its likely pattern of accumulation in different organs and the residence time in blood circulation. Since the degradation pattern of silica are reported to be different with different type of silica, it is

essential to analyze it for individual sample rather than generalizing with the available literature as the particle properties may vary. Silica, chemically silicon dioxide ( $\text{SiO}_2$ ) is found to be less stable in aqueous solutions and are converted to its hydrated silicic acid  $[\text{Si}(\text{OH})_4]$  form which is the absorbable form of silica possessing higher bioavailability<sup>340</sup>. Studies surrounding silica metabolism in animal and human models have established that the end products of certain class of silica are generally regarded as safe and has been approved for use as different food additives and in different pharmaceutical formulations<sup>341</sup>. Silica is mainly excreted through urine<sup>342</sup>. The degradability patterns of different types silica help to utilize it for appropriate applications. While the non-biodegrading property of certain type of silica be utilized for the manufacture of superhydrophobic coatings for waterproofing over a range of weather conditions<sup>343</sup>, its biodegradable forms which gets metabolized over an acceptable period of time, reduces accumulation in human body and reduces impact on environment<sup>340</sup>. Considering the spatial set up, silica molecules are formed by siloxane linkages ( $\equiv\text{Si}-\text{O}-\text{Si}\equiv$ ) between  $\text{SiO}_4$  units resulting in a tetrahedral geometry. Within this structure different type of silanol ( $\equiv\text{Si}-\text{OH}$ ) groups exist, namely, isolated ( $\equiv\text{Si}-\text{OH}$ ), geminal [ $\equiv\text{Si}(\text{OH})_2$ ] and vicinal [ $\equiv\text{Si}(\text{OH})-\text{O}-(\text{OH})\text{Si}\equiv$ ] ones. The vicinal silanol group is responsible for forming hydrogen bond with water molecules. Silica samples subjected to higher calcination temperature can result in excessive degradation of these silanol groups and formation of siloxane ( $\equiv\text{Si}-\text{O}-\text{Si}\equiv$ ) units which can result in drastic reduction of dispersibility of silica in water as oxygen atom in siloxane does not form any hydrogen bond with adjacent protons present within silanol or water moieties thereby increasing the silica hydrophobicity<sup>344</sup>. Previous studies have reported the presence of hydrophilic and

hydrophobic areas on surface of silica to rely on the density of siloxane moieties in them <sup>345</sup>. Amorphous silica on an average contains of silanol groups at a density of 4.8 OH per nm<sup>2</sup> and can vary across different types of silica <sup>340</sup>.

The expected mechanism of dissolution of the silica sample be based on the degradation of the tetrahedral arrangement owing to the derangement of SiO<sub>4</sub> groups controlled by either diffusion process or other surface reactions <sup>346</sup>

The type of interaction of silica with different biological entities may vary based on surface properties and may involve hydrogen bonds, electrostatic attractive and repulsive forces and hydrophobic interactions <sup>345</sup>. An insight into the complexity, magnitude and type of these interactions help to predict behaviour in living system.

Once inside the biological systems, the nanoparticles are likely to be besieged by circulating biomolecules. Of particular interest are serum associated proteins that forms a corona around the nanoparticles. This phenomenon has the potential to affect the ability of the nanocarrier to remain in the biological circulation, which could impede its applicability to be used for purposes involving targeted delivery of therapeutics. The complexity of the processes and lack of strong literature on the correlation between structure and functionality of nanoparticles calls for detailed research over the subject <sup>347</sup>. The physical as well as chemical properties of the nanoparticles greatly determines its interaction with different biological entities. However not much light has been shed on the predictability of such interactions. Dynamic light scattering (DLS), Transmission electron microscopy

(TEM), Field flow fractionation (FFF), Inductively coupled plasma mass spectrometry (ICP-MS), Isothermal microcalorimetry (IMC) are some of the few techniques used for the study of protein corona formation. Properties of nanoparticles like size, surface chemistry, affinity to certain biopolymers and other morphological characteristics like porosity play major roles in deciding the fate of nanoparticles in circulation. These properties and interactions ultimately act as guiding tools to determine the toxicity and applicability of the particles. In certain cases, some unsolicited biological interactions are prevented by subjecting the nanoparticles to surface modification. Some of commonly employed polymers utilized to improve the circulation particle circulation half-life include polyethylene glycol, dextran and polyvinyl pyrrolidone. These polymers are capable of creating a hydrophilic microenvironment around the particles such that it enables the particles to escape recognition and interaction from immune cells as well as certain other surface reactive biomolecules. This aids in improving the circulation time of the particles. However, such modification strategies do not help in completely masking interactions of the particles, as such a synergy is inevitable. Studies have shown that certain specific serum albumin protein adsorption onto titanium oxide nanoparticles were directly proportional to incubation temperature. Whereas, it showed reciprocal interaction with pH values<sup>348</sup>. Further studies have also established the adsorption of bovine hemoglobin onto hydrophobic silica to be higher than on hydrophilic ones and the reaction to follow pseudo zero order kinetics. The interaction involved chemisorption of protein molecules onto silica. Adsorption of multiple layers of proteins were possible according to the affinity of interactions between the two.

#### **5.4.2. Cell viability assay**

MTT or 3-(4,5-dimethylthiazol-2-yl)-2,5-dephenyl tetrazolium bromide is a yellow-colored photosensitive salt which is reduced by NADPH-dependent oxidoreductase (also mitochondrial succinate dehydrogenase) enzyme present in viable cells into water insoluble purple colored formazan crystals which are solubilized using DMSO solvent. Figure 4.5.2 indicates the dose-response of HEK 293 and HeLa cells to treatment of rice husk derived silica nanoparticles in varying concentrations from 0-400  $\mu\text{M}$  over a period of 48 h. Moderate reduction in cellular viability was observed in samples treated with biogenic silica at 200  $\mu\text{M}$  concentration, where HEK 293 cells showed 91.58 % viability while HeLa cell showed 89.17 %. The viability of HEK 293 was reduced only to 86 % and that of HeLa to 84.5 % following incubation at 400  $\mu\text{M}$  concentration of biogenic silica, indicating high cytocompatibility. Figures 4.5.3 and 4.5.4 show HEK 293 and HeLa cells subjected to incubation with surface modified drug loaded biogenic silica samples. The viability of HEK 293 cells varied from 99.82% by 24 h to 98.85 % by 48 h to 96.7 % by 72 h of incubation, while that of HeLa cells varied from 61.17 % to 44.65 % to 40.33 % respectively up on 24, 48 and 72 h of incubation following treatment. The specific decline in viability of HeLa cells could likely be due to the anti-cancer properties of the internalized curcumin, loaded into the silica nanoparticles, promoting apoptosis through mitochondrial dysfunction, induction of oxidative stress or stress on endoplasmic reticulum of cells which are the commonly reported effects of the active ingredient. Figures 4.5.5 and 4.5.6 indicate the dose response curves of curcumin and epirubicin respectively. The  $\text{IC}_{50}$  values (table 4.5.1) of pristine curcumin was  $57.43 \pm 2.5 \mu\text{M}$  while that

of curcumin bound to biogenic silica nanoparticles was  $54.18 \pm 1.8 \mu\text{M}$  indicating an improvement in the drug activity against cancer cells. Similar trend was observed in silica-bound epirubicin samples compared to bare drug samples where the values varied from  $1.02 \pm 0.86 \mu\text{M}$  for free epirubicin to  $0.91350 \pm 2 \mu\text{M}$  for drug bound nano-formulation (table 4.5.1). The cytoprotective effect of drug bound nano-formulations against cypermethrin induced toxicity were studied and it could be seen that the chitosan capped curcumin loaded nano-formulation showed highest cytoprotective activity, followed by poly ethylene glycolated samples, while the samples treated with pristine biogenic samples showed least cytoprotective activity where the cell viability was reduced to 55 % (figure 4.5.7). The chitosan capped drug loaded sample maintained cell viability at 85.5 % as compared to positive control, with reduced cell viability to 48.3 %. From the results, it can be seen that the curcumin incorporated into the nano-formulations is responsible for the cytoprotective effect and that its activity was maintained even after nanoparticle conjugation. The pH of the culture media also determined the rate of release of the conjugated drug and accordingly the effect. The respective release trends of different nano-formulations were reported in figures 4.4.1 to 4.4.3 and 4.4.5 to 4.4.7.

#### **5.4.3. Assay of Glutathione Peroxidase (EC 1.11.1.9)**

Formation of singlet oxygen species and hydrogen peroxide is inevitable during different aerobic processes occurring in the living system. But if the levels are not controlled beyond a certain safety limit, it has the potential to initiate different chain reactions resulting in the formation of lipid peroxides and other organic peroxides. Glutathione peroxidase is responsible for reduction of hydrogen

peroxide, converting it into least harmful end-products like water, thereby preventing membrane lipid deterioration and protecting the membrane functionalities. Figure 4.5.8 shows polyethylene glycolated curcumin loaded sample to show highest activity for the enzyme followed by chitosan capped drug loaded nano-formulation and pristine curcumin samples. The results indicate the cytoprotective role of curcumin in the loaded nano-formulations, indicating the preservation of its activity even after loading into the drug carriers.

#### **5.4.4. Assay of Superoxide Dismutase (SOD, EC 1.15.1.1)**

Superoxide dismutase enzymes are capable of converting superoxide radicals formed in the cells to hydrogen peroxide and diatomic oxygen molecules, which are subsequently acted upon by catalase for conversion into water and more diatomic oxygen molecules. Exposure of cypermethrin significantly reduced the SOD activity (Figure 4.5.9). The curcumin present in different nano-formulations could ameliorate the effect of cypermethrin. The enzyme activity was significantly improved upon surface modification with polyethylene glycol and chitosan, with the highest activity exhibited by polyethylene glycolated sample followed by chitosan modified sample. The results were in agreement with the trend observed in cellular uptake and drug release patterns.

#### **5.4.5. Assay of Catalase (EC 1.11.1.6)**

Reactive oxygen species (ROS) produced as a result of several aerobic metabolic reactions in cells exert beneficial as well as detrimental roles in the system. In several cases ROS are involved in intracellular signaling and regulation of cognitive functions. They are

also known to play beneficial roles in maintaining blood pressure and immune responses. These species are involved in the regulation of several redox-based reactions essential to maintain cellular homeostasis. However, if not controlled, excessive generation of these species can impose oxidative stress on the cells which may ultimately result in damage to cellular structures and development of ailments. Superoxide radicals, hydroxyl radicals and hydrogen peroxide are the chief products of aerobic respiration. These reactive species together with free radicals generated from molecular oxygen constitutes ROS. To counter the deleterious effects of ROS, the living system have evolved defense mechanism to maintain an equilibrium between the production and elimination of ROS. When such an equilibrium is lost, the cell falls into a state of oxidative stress. Considering the chemistry of di-atomic molecules, the spin of electrons exhibits antiparallel pattern permitting sharing of single orbital electrons resulting in covalent bonds between the atoms thereby minimizing the energy levels. In contrast, the energy is not diminished in the case of oxygen, as the electrons spin occurs on rotation parallel to each other resulting in the unpaired electrons to remain in triplet state, which has energy levels higher than in singlet state. This imparts higher reactivity to the ROS. The bi-radical unpaired oxygen predominates in normal cellular conditions which are more stable compared to oxygen in singlet state. However, in some cases, one of the antiparallel electrons may conjugate with an electron donated by an adjacent molecule generating superoxide radical which can effectively be converted to hydrogen peroxide by superoxide dismutase enzyme.

The catalase activity was highest for chitosan capped curcumin bound silica nanoparticles and least for cypermethrin treated samples.



Catalase activity of pristine biogenic silica samples was 54 %, 61 % for polyethylene glycolated samples, 58 % for chitosan capped biogenic silica particle sample and 68 % for samples treated with pristine curcumin sample (figure 4.5.10).

#### **5.4.6. Lipid peroxidation inhibition activity**

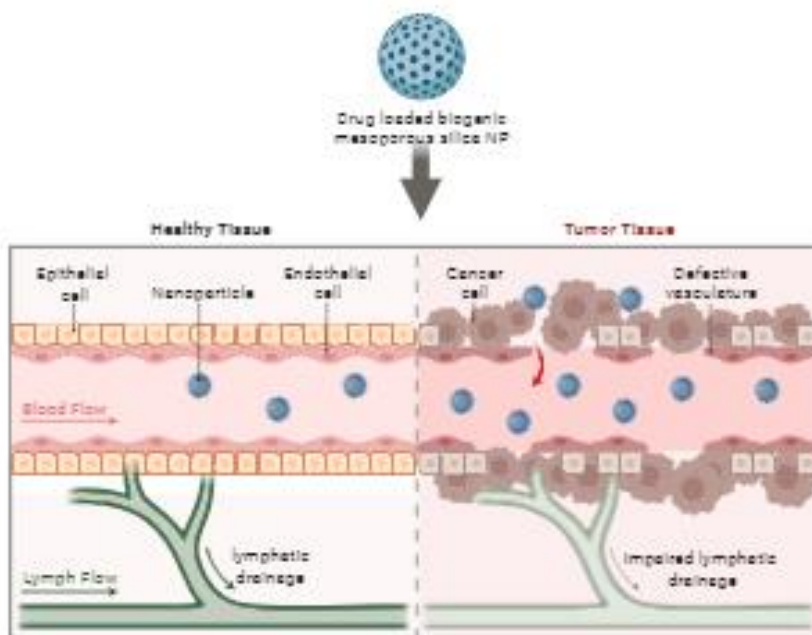
Imbalance in production of free radicals and corresponding anti-oxidant defense mechanism can result in surplus levels of lipid peroxy radicals and hydroperoxides. These radicals attack lipid moiety and can lead to ferroptosis and other oxidative damages. Lipid peroxidation occurs when unsaturated bonds in polyunsaturated fatty acids are attacked by free radicals or reactive oxygen species resulting in oxidation products like lipid hydroperoxides, hydroxyalkenals (HAE) and malondialdehyde (MDA) capable of causing cell membrane damage. HAE and MDA are used as major indicators of lipid peroxidation and oxidative stress of cells. It may result in many vital life processes being affected negatively, leading to pathological conditions and complications causing cardiovascular diseases, cataract, diabetes etc. Figure 4.5.11 indicates chitosan capped curcumin loaded to show highest lipid peroxidation inhibition activity followed by polyethylene glycolated sample, unmodified drug loaded sample, modified biogenic silica while biogenic silica sample showed least activity among others.

#### **5.4.7. Cellular uptake of curcumin**

The cellular uptake of curcumin was determined through spectrophotometric analysis (figure 4.5.12) as a function of intensity of fluorescence of the supernatant of the cell lysate obtained after the

incubation period. Over the assessment period of 0 to 120 h, it could be seen that the uptake was highest at 16 h and the surface modified drug loaded nano-formulation (BSNCHC) exhibited highest uptake of curcumin intracellularly ( $422 \mu\text{M}/10^6\text{cells}$ ) as is evident from the fluorescence intensities, indicating the improvement of bioavailability of the drug upon nanoparticle conjugation on comparison with pristine drugs. Also, the uptake of nano-formulated curcumin is expected to be highest in HeLa cells as compared to HEK 293 cells because of enhanced permeation retention effect, a typical characteristic of cells with compromised membrane structure integrity and vascular drainage.

**Figure 5.4.1.** Showing mechanism of Enhanced Permeation and Retention (EPR) effect for passive targeting of active pharmaceuticals in solid tumour cells



Note: Illustration created with [BioRender.com](https://www.biorender.com).

Previous studies have assessed the intracellular uptake of mesoporous silica nanoparticle to occur majorly through clathrin and/or caveolin mediated endocytosis and through phagocytosis. The particles later escape from endosomal compartments resulting in *in vivo* distribution through blood stream to enter body organs like liver, spleen and to a minor extent in kidneys and lungs, which are finally excreted via feces and urine<sup>349</sup>.

#### **5.4.8. Effect of nano-formulation on the nuclear morphology**

The induction of cell apoptosis is indicated by differences in morphologies of cell organelles and are particularly evident in nuclear membrane and associated structures. The cell exhibits morphological changes towards advanced and late stages of apoptosis showing cell shrinkage, membrane blebbing, fragmentation of nucleic acid (DNA) along with the formation of apoptotic bodies. Shrinkage of cells occur as a result of rearrangement of serine/threonine kinase in cytoskeleton. In the study, DAPI is the dye used to visualize changes in nuclear morphology to assess apoptosis. The dye selectively binds to the adenine-thymine regions in the minor groove of DNA. It absorbs light falling in the ultraviolet range (359 nm) and fluoresces blue (461 nm). The intensity of fluorescence of bound DAPI is almost 20-times than that of unbound form. The greater the amount of DNA present greater will be the fluorescence intensity. The cell membrane integrity of an apoptotic cell will be severely compromised resulting in high influx of DAPI to the cell, staining it in stronger blue colour (figure 4.5.13). Chromosome condensation and fragmentation can be visually examined in apoptotic cells stained with DAPI dye. It also helps in

differentiating apoptotic and necrotic cell by the presence or absence of nuclear blebbing respectively. Necrotic cells do not show nuclear blebbing.

Tension in chromatic structure and subsequent alterations in its organization is apparent in samples exposed to drug-loaded nano formulation over longer period. Irregularity in nuclear morphology, shrinkage and membrane blebs were also observed (indicated by white arrows in the figure 4.5.15) in the cells treated with drug-loaded nano-formulation. Absence of any morphological aberrations in samples treated with pristine biogenic nanoparticles irrespective of its origin showed its biocompatibility to be used for *in vivo* applications like drug-delivery vectors, bioimaging and theragnostic tools.

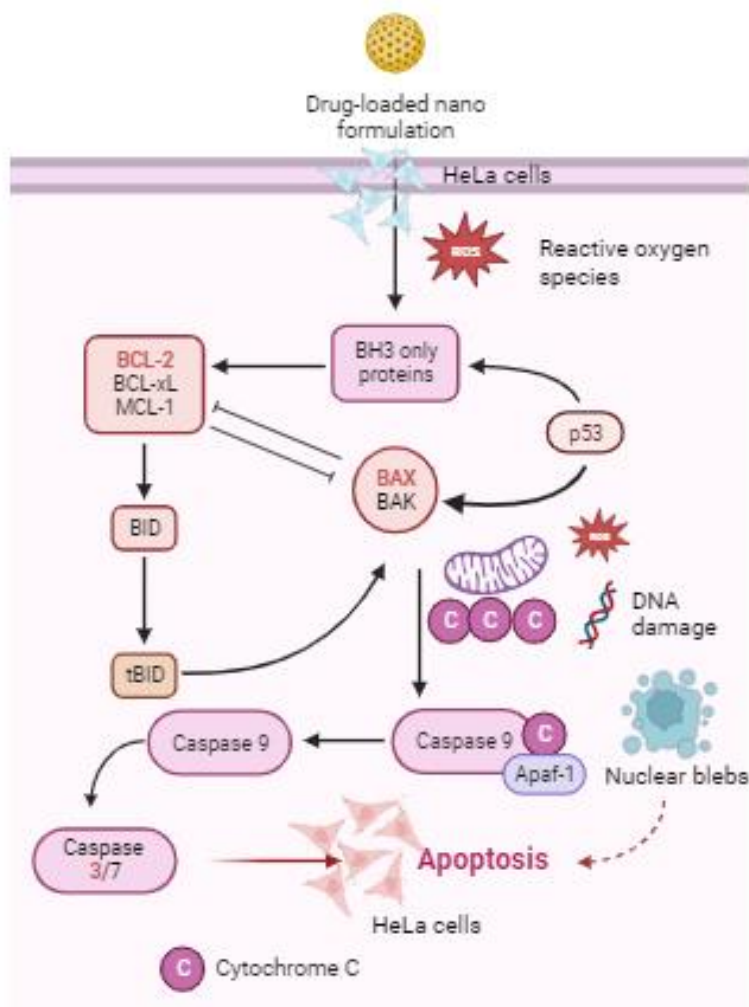
#### **5.4.9. Estimation of intracellular ROS (DCFDA) and mitochondrial membrane potential (MMP)**

Previous studies have established a correlation between production of reactive oxygen species in the inner mitochondrial membrane as a reason for loss of mitochondrial membrane potential<sup>350</sup>. It has also been established from the results that the apoptosis of cells induced by the drug-loaded nano formulation is coincided with the generation of ROS. Figure 4.5.16 shows the ROS levels in cell culture treated with different nano-formulations. ROS production was highest in samples treated with positive control (99.8 % ROS+ population). Chitosan capped curcumin loaded chemically synthesized control silica sample (CSNPCHC) resulted in 99.1 % ROS+ population, followed by chitosan capped curcumin loaded biogenic silica (BSNPCHC) samples leading to 98.6 % ROS+ population. Cells

treated with pristine biogenic silica sample (BSN) formed least percentage of ROS+ population (29.6) next only to negative control (20.1 % ROS+ population) while chemically synthesized silica (CSN) resulted in 50.1 % ROS+ population. Curcumin treated samples showed 83.3 % ROS+ population while surface modified biogenic silica nanoparticle loaded with curcumin (BSNPC) showed 95.8 % ROS+ population, while its chemically synthesized counterpart (CSNPC) showed 98 % ROS+ population, showing improvement in enhancement in anti-cancer activity as compared to pristine curcumin. Unmodified curcumin loaded biogenic silica (BSNC) led to 90.3% ROS+ population while corresponding controls sample (CSNC) produced 91.1% ROS+ population. From figure 4.5.17, it can be seen that samples treated with unmodified biogenic silica nanoparticles (A) and PEGylated chitosan capped biogenic silica nanoparticles (B) maintained normal mitochondrial potential. The red-to-green fluorescence ratio were found to be 8.5 for sample A, 5.77 for sample B and 2.8 for sample C. A reduction in intensity ratio of red-to-green fluorescence in sample C, which was treated with surface modified biogenic silica nanoparticles loaded with curcumin is indicative of aberrations in mitochondrial membrane potential, depolarization and likely induction of abnormalities in mitochondrial structure of the treated cell population. The disrupted membrane activity suggests likely activation of intrinsic pathway of apoptosis in the cells studied.

#### 5.4.10. Gene expression study

**Figure 5.4.2.** Showing predicted mechanism of induction of apoptosis in the cells treated with different nano-formulations



Note: Illustration created with [BioRender.com](https://www.biorender.com).

Induction of extrinsic pathway of apoptosis is marked by the binding of ligands to the Fas receptor (“death receptor”). The mid-phase shows activation of the effector caspases (caspase-3 and caspase-

7). The onset of early stage of intrinsic pathway of apoptosis can be analyzed by the expression levels of B cell lymphoma-2 (Bcl-2) gene of the cell under study. Over expression of Bcl-2 is observed in several cancer as in chronic lymphocytic leukemia. Mid-phase of apoptosis is embarked by the depolarization of mitochondrial membrane, formation of apoptosome and activation of cysteine-aspartic protease-9 (caspase-9). The nano-formulation plays a major role in suppressing cancer cell (HeLa) proliferation with increased generation of ROS along with the induction of caspase activity and disruption of mitochondrial membrane potential. Downregulation of anti-apoptotic Bcl-2 gene expression was observed in all drug loaded nano formulations (figure 4.5.18). However, maximum Bcl-2 expression was observed in normal control, biogenic silica particle treated samples and samples treated with surface modified nano-formulations. This suggests an improvement in the level of apoptosis induction in cells treated with samples containing curcumin which is yet another indication of preservation and enhancement of curcumin against cancer cells. Considering expression levels of pro-apoptotic gene Bax (figure 4.5.19), it can be seen that the levels of expression were least in normal control, followed by pristine and surface modified biogenic silica samples. Maximum expression was observed in cells treated with surface modified drug loaded samples, maintained in medium at pH of 5.4 which facilitated in maximum release of drug and hence cellular internalization. Caspase-3 expression patterns of curcumin and epirubicin loaded nano formulations followed similar pattern (figure 4.5.20). There was maximum expression in chitosan capped PEGylated

samples in both the cases. Biogenic silica particles showed least levels of expression.

## **5.5. Anti-oxidant property evaluation of nano formulations**

### **5.5.1. 2,2-Diphenyl-1-picryl Hydrazine (DPPH) Scavenging activity**

The antioxidant potential of the nano-formulation is dependent on the reduction of the odd electron of the nitrogen atom in DPPH upon receipt of hydrogen atom from the antioxidant, resulting in the production of corresponding hydrazine. The reduction is determined spectrophotometrically at 515 nm by variation in the intensity of purple colour of the solution and the results were compared with a standard solution. It could be seen that the free-radical scavenging activity of the bare curcumin samples showed highest effect while biogenic silica samples was the lowest, indicating that the antioxidant activity of the samples were contributed by the innate activity of the loaded curcumin. The values varied from 16-34 %, with the surface modified curcumin loaded nano-formulations showing intermediate readings of the values (figure 4.6.1).



## SUMMARY AND CONCLUSIONS

---

Efforts were made to synthesize amorphous mesoporous silica nanoparticles from biogenic sources like diatomaceous earth, coffee husk, rice husk, corn husk and grass. The yield of silica particles from rice husk was higher (14%) and the particle size was around 50 nm with surface area of 232.20 m<sup>2</sup>/g, total pore volume of 0.22 cm<sup>3</sup>/g and average pore size of 3.71 nm. These particles were subjected to surface manipulation using polyethylene glycol and chitosan to instill additional functionalities like improvement in hydrophilicity and stimuli-responsive payload release, which could be useful for drug loading applications. The loading capacities of unmodified and modified particles using curcumin were 1.77 µg/mg and 0.85 µg/mg while that for epirubicin were 3.28 µg/mg and 1.49 µg/mg respectively. A moderately strong binding between silica particles and drug molecules are evident from a sustained drug release pattern monitored over 100 h, with rapid release of drug from chitosan capped nano-formulations at acidic pH (5.4), due to possible structural disintegration of chitosan owing to protonation of amino groups at lower pH conditions (isoelectric point pH~6.3). Biodegradation study using simulated physiological conditions showed sustenance of intact silica structure for almost 14 days, making it available in circulation for sustained drug delivery applications, while the structure started disintegrating following prolonged periods in the simulated fluid, indicating that the particles could be eluted from the system without causing accumulation. Viability assay revealed biocompatibility of

particles to both normal cells and cancer cells up to 400  $\mu\text{M}$ .  $\text{IC}_{50}$  values and anti-oxidant assays suggest improvement of drug activity upon particle conjugation. Cellular uptake studies revealed highest uptake peak around 16 h and higher levels in cancer cells compared to normal cells possibly due to enhanced uptake and retention effect of cells owing to disrupted membrane and vasculature. Drug conjugated nano-formulations could result in aberrations in nuclear morphology of cancer cells with the simultaneous production of ROS. The mitochondrial membrane potential deviations were also observed from flow cytometry analysis of the samples, which together with gene expression studies point to the involvement of intrinsic pathway of apoptosis with caspase-3 expression.

Finally, the following conclusions were drawn:

- ◆ Surface modification of the synthesized amorphous, mesoporous biogenic silica particles was found to be very effective for enhancing stimuli-responsive drug release. Chitosan-capping of drug loaded nano-formulations resulted in release of drug at pH 5.4, useful for cancer chemotherapy.
- ◆ Sustained release of drug from nano-formulations were observed from passive release studies.
- ◆ After a series of experimentation, it was found that the biogenic silica nanoparticles showed considerable degradation pattern at 37 °C in simulated body fluid over 14 days, which makes it a useful choice for *in vivo*/medical applications, making it

available in circulation over a reasonable period of time without accumulating.

- ◆ From a range of experiments conducted, biogenic silica particles at concentration up to 400  $\mu\text{M}$  was found to be non-toxic and capable of preserving the viability of HEK 293 and HeLa cells for over 72 h of incubation.
- ◆ The synthesized biogenic silica when used as a drug carrier showed improvement in bioavailability, and hence activity of the loaded drugs.
- ◆ There was upregulation of pro-apoptotic factors in cells treated with different drug loaded nano-formulations, suggesting the preservation of activity of the active pharmaceutical agent even after conjugation into the nanocarriers.
- ◆ Techno-economic analysis of this unique, facile production method proved that it is comparatively a much cheaper alternative to conventional industrial methods of manufacture of mesoporous silica nanoparticles.



## RECOMMENDATIONS

---

This is a preliminary work done to investigate the application of silica nanoparticles derived from biogenic sources as drug delivery agents and to assess the drug release pattern from different nano-formulations with the aim to check its use in cancer chemotherapy. The cost-economic analysis of the process was assessed and it was seen that the production process was almost 100 %\* more economical as compared to chemical methods of synthesis. The process is highly scalable and different properties of the particles could be altered by varying the production conditions. The method employed usage of minimal levels of reagents and pretreatment techniques and is an environmental-friendly alternative to conventional bottom-up approaches. Though mechanical methods like ball-milling helps in reducing particle size, it was not helpful in generating uniform-sized primary particles.

The particles were easily available for surface modification and showed high biocompatibility. The particles remained in simulated body condition for acceptable periods of time so as to facilitate delivery of drug, but not long enough to cause toxicity associated with particle accumulation. The conjugation of hydrophilic as well as hydrophobic, synthetic as well as natural drugs were compared for its efficiency of loading and activity. The conjugation of curcumin could help improve its bioavailability as was evident from increment in the levels of curcumin internalization into the cells under study. Different

---

\* This does not include the expenditure incurred due to fixed capital like machinery, factory, transportation and other utilities.

nano-formulations loaded with curcumin had cytoprotective effect against cypermethrin induced toxicity and maintained its anti-oxidant properties. The drug from chitosan-capped nano-formulations showed higher release rates at lower pH. Tumour microenvironment is normally acidic, suggesting the possibility of success of these nano-formulation for cancer chemotherapy.

The drug loaded nano-formulations induced generation of ROS in cancer cells coupled with the upregulation of pro-apoptotic gene. It was also seen to affect the mitochondrial membrane potential of these cells. The apoptotic cells showed visible signs of chromatin condensation together with the formation of nuclear blebs as wells as apoptotic bodies as were evident from microscopic images taken after nuclear staining (DAPI).

The ultimate intention of nanoparticle-mediated drug delivery system is to reduce the risk imposed by the drug on the patients by increasing its bioavailability and reduction in dosage levels. The ability of nanoparticles to transverse across several biological membrane barriers along with the surfacing of recent studies reporting toxic effects of various carrier systems press on the importance of meticulous and in-depth studies on the interaction and fate of the carrier system with chemical and biological constituents in the body. This is particularly serious in cases were the method of carrier synthesis is based on harmful chemicals<sup>351</sup>. These also reminds us to redirect studies to develop methods for generation of nanoparticles using environment-friendly, economical, energy efficient, sustainable techniques giving priority to value-addition otherwise discarded, least

exploited agricultural biomass, which are also a good source of many economically viable raw materials like silica, cellulose, lignin as well as other carbon sources.

Studies on the application of nanoparticles derived from natural sources for different biomedical purposes involving tissue engineering, dental implants and fillers, biofilm control agents, gene delivery etc. are limited, opening newer research possibilities in the field. Since silica naturally plays a role in maintaining normal bone health, its application as biological scaffolds could permit easier absorption, regeneration and could facilitate release of bioactive agents for improving structural integrity and mechanical strength of bones. Fine-tuning of synthesis parameters helps in the generation of least toxic version of silica nanoparticles which can enhance its usability for biomedical applications. On occasions where the antimicrobial activity of different drugs is delimited by the efflux pumps, multiple drug resistance and low intracellular collocation, silica nanoparticles in addition to acting as carrier for targeted delivery, could also provide physical protection of the active pharmaceutical agent against degradation before reaching the location, thereby improving its therapeutic efficacy. This property could be harnessed for developing medical band-aids and self-healing gels for wound recuperation. By virtue of its physical and chemical properties, silica nanoparticles also find applications in several other fields of life. It can also be used for reinforcement of rubber, for synthesis of wear resistant tyres with high wet grip, anticaking agents enabling free flow of wet powders, fuel cells, ceramics, polymer filaments and garments with high flame

retardancy and thermal stability, immobilizing heavy metals in water supplies, fire extinguishing powders, in nano clays for improved mechanical strength and thermal resistance.

Reduction in particle size of nanoparticle results in substantial increase in surface area, resulting in larger number of atoms of the nanoparticle available for interaction with the adjacent microenvironment. Several carbon ( $^{13}\text{C}$ ) nanoparticles possessing smaller particle size (less than 35 nm) were recovered in the olfactory bulb area of the brain upon exposure route via inhalation, if it is otherwise not specifically directed can result in inflammation, thrombosis and associated complications. Considering toxicity of particles on mass-dose basis, the chances of nanoparticle toxicity is higher compared to that of larger particles of the same material considering similar solubility nature of the materials. This demands precise studies on multiple aspects of toxicity of these sub-micron sized particles considering the dosage to be decided by the surface area rather than based on mass. Many a times, the propensity of the surface chemical moieties on a nanoparticle to interact with other chemical entities would be higher than the desired payload, which may affect the net reactivity of the particle. Conversely, the same principle is employed to potentiate desirable properties of the nanocarrier, which can also help in reducing particle toxicity. In addition to induction of inflammation, another mechanism of possible toxicity induced by nanoparticles include induction of oxidative stress and DNA damage to cells, mainly monocytes, macrophages and keratinocytes. This signals for the higher levels of production of antioxidant enzymes. The counter



mechanism of over production of antioxidant enzymes chiefly by macrophages may fail to nullify the deleterious effects of lipid peroxidation and higher levels of hydrogen peroxide, leaving the cells under severe oxidative stress and the damages follow. The toxicity study of particles should be able to find answers for the interactions of these particles with the biological entities considering its peculiar physical and chemical characteristics, nature of distribution in the system and the effects exerted on the tissue and cellular systems <sup>351</sup>. Effects studied on animal and cellular models may not fully be able to replicate the conditions prevalent in the intended population due to variations. Even though patient-to-patient differences are not simple restricted to medical history, it may vary from health conditions to tolerance limits on a case-to-case basis. Since more studies are concentrated on the toxicological effect in terms of human lives, often the ecotoxicological effects of these particles are neglected. It is an equally important responsibility to check for toxic effect on the ecological system likely to be exposed to these particles. If not deleterious to human beings, the tolerance limit to these particles may be limited in other life forms and it may potentially harm their very existence and hence the relevance of such studies envisaging different strata of environment and life forms. If a nanocarrier system proves to be safe for use under a particular mode administration, it may exhibit different reactions in a different method of administration. In cellular targeting the nano-formulation requires to fall within a size range, which in most of cases may be hard to upkeep due multiple surface modification and combined sizes of drug molecules, adding on to net size of the nano formulation which requires development of more

efficient yet biocompatible nanocarriers for drug loading and targeted delivery.

Several unmodified nanoparticles find way to the liver and other vital organs in the body upon recognition by the mononuclear phagocytic system, which in effect can induce toxicity in the organ in which the accumulation may occur. Surface modification with ligands like polyethylene glycol helps the particles to evade recognition by the mononuclear phagocytic system which improves residence time under circulation and hence ameliorate toxicity due to accumulation in tissues and organs. It is essential to study that the level of nano-formulation tallies the levels of bio transformed or excreted material. This however require intensive studies to help in ruling out the possibility of any tissue accumulation of the nano-formulation and unwarranted interactions. Studies have established differences in the cellular uptake of nanoparticles based on the state of aggregation. It was found that highly dispersed nanoparticles underwent cellular internalization by invoking endocytosis pathway mediated by caveolae. But increased levels of aggregation of particles resulted in particles chiefly being internalized by macropinocytosis.

In certain cases, the conjugation of the active pharmaceutical ingredient may result in the loss of its activity. This may be prevented by customizing the type of formulation to be compatible, considering the type of therapeutic, the drug carrier as well as the intended site of delivery. Often the mode of administration also determines the fate of pharmaceutical conjugated with the nanoparticle and must be designed as per the intended application and tolerability of the cells at the

targeted site towards the nano-formulation. Often, the synthesis process of nanoparticles fails to remove traces of reagent which could have toxic effect on cells. So, setting standards regarding the purity of the nanocarrier helps in identifying the individual effect of such particles on the living system rather than the combined effect of the extraneous components. Van der Waal's attractive forces and electrical repulsive forces are constantly in play between nanoparticles which determine its stability in different systems. Since the surface area of nanoparticles are higher, so are the surface energies and its susceptibility to aggregate. While some applications require the nanoparticles to aggregate, the same may cause detrimental effects in others. Accordingly, the different strategies employing mechanical forces and alterations in surface chemistry may be employed for manipulating the nature of aggregation of these particles. Aggregation of nanoparticles have shown to improve thermal conductivity in comparison to its individually isolated counterpart. Surface coating of nanoparticles with polymers and electrolytes help in controlling particle aggregation while manipulation of hydrophobic and hydrophilic groups on its surface determines its stability in polar and non-polar solvents. Another important area that demands arduous research is the interactions between the particle, drug as well as the molecules used for surface functionalization, as these can influence the pattern of drug interaction, release and toxicity of the nano-formulation.



## REFERENCES

---

1. Farokhzad, O. C. & Langer, R. Impact of Nanotechnology on Drug Delivery. *ACS Nano* **3**, 16–20 (2009).
2. Moorthi, C., Manavalan, R. & Kathiresan, K. Nanotherapeutics to overcome conventional cancer chemotherapy limitations. *J. Pharm. Pharm. Sci.* **14**, 67–77 (2011).
3. DeVane, C. L., Liston, H. L. & Markowitz, J. S. Clinical Pharmacokinetics of Sertraline. *Clin. Pharmacokinet.* **41**, 1247–1266 (2002).
4. Forrest, J. A. H., Clements, J. A. & Prescott, L. F. Clinical Pharmacokinetics of Paracetamol. *Clin. Pharmacokinet.* **7**, 93–107 (1982).
5. Le, J. Drug Bioavailability. *Skaggs Sch. Pharm. Pharm. Sci. Univ. Calif. San Diego* (2020).
6. Powell, J. W. & Presnell, S. E. Loperamide as a Potential Drug of Abuse and Misuse: Fatal Overdoses at the Medical University of South Carolina. *J. Forensic Sci.* **64**, 1726–1730 (2019).
7. Bharti, C., Gulati, N., Nagaich, U. & Pal, A. Mesoporous silica nanoparticles in target drug delivery system: A review. *Int. J. Pharm. Investig.* **5**, 124 (2015).
8. Gelperina, S., Kisich, K., Iseman, M. D. & Heifets, L. The potential advantages of nanoparticle drug delivery systems in chemotherapy of tuberculosis. *Am. J. Respir. Crit. Care Med.* **172**, 1487–1490 (2005).
9. Zhao, G. *et al.* Curcumin inhibits suppressive capacity of naturally occurring CD4<sup>+</sup>CD25<sup>+</sup> regulatory T cells in mice in vitro. *Int. Immunopharmacol.* **14**, 99–106 (2012).
10. Singh, A. K. & Vinayak, M. Curcumin Attenuates CFA Induced Thermal Hyperalgesia by Modulation of Antioxidant Enzymes and Down Regulation of TNF- $\alpha$ , IL-1 $\beta$  and IL-6. *Neurochem. Res.* **40**, 463–472 (2015).
11. Heger, M., van Golen, R. F., Broekgaarden, M. & Michel, M. C. The Molecular Basis for the Pharmacokinetics and Pharmacodynamics of Curcumin and Its Metabolites in Relation to Cancer. *Pharmacol. Rev.* **66**, 222–307 (2014).
12. Puerari, R. C. *et al.* Investigation of toxicological effects of amorphous silica nanostructures with amine-functionalized surfaces on Vero cells. *Chemosphere* **214**, 679–687 (2019).

13. Simone, E. A., Dziubla, T. D. & Muzykantov, V. R. Polymeric carriers: role of geometry in drug delivery. *Expert Opin. Drug Deliv.* **5**, 1283–1300 (2008).
14. Bermudez, H., Brannan, A. K., Hammer, D. A., Bates, F. S. & Discher, D. E. Molecular Weight Dependence of Polymersome Membrane Structure, Elasticity, and Stability. *Macromolecules* **35**, 8203–8208 (2002).
15. Photos, P. J., Bacakova, L., Discher, B., Bates, F. S. & Discher, D. E. Polymer vesicles in vivo: correlations with PEG molecular weight. *J. Control. Release* **90**, 323–334 (2003).
16. Dalhaimer, P., Bates, F. S. & Discher, D. E. Single Molecule Visualization of Stable, Stiffness-Tunable, Flow-Conforming Worm Micelles. *Macromolecules* **36**, 6873–6877 (2003).
17. Ehrlich, H., Demadis, K. D., Pokrovsky, O. S. & Koutsoukos, P. G. Modern Views on Desilicification: Biosilica and Abiotic Silica Dissolution in Natural and Artificial Environments. *Chem. Rev.* **110**, 4656–4689 (2010).
18. Roveri, N., Palazzo, B. & Iafisco, M. The role of biomimetism in developing nanostructured inorganic matrices for drug delivery. *Expert Opin. Drug Deliv.* **5**, 861–877 (2008).
19. Wang, X., Schröder, H., Feng, Q., Draenert, F. & Müller, W. The Deep-Sea Natural Products, Biogenic Polyphosphate (Bio-PolyP) and Biogenic Silica (Bio-Silica), as Biomimetic Scaffolds for Bone Tissue Engineering: Fabrication of a Morphogenetically-Active Polymer. *Mar. Drugs* **11**, 718–746 (2013).
20. Chen, L. *et al.* The toxicity of silica nanoparticles to the immune system. *Nanomedicine* **13**, 1939–1962 (2018).
21. Piela, A. *et al.* Biogenic synthesis of silica nanoparticles from corn cobs husks. Dependence of the productivity on the method of raw material processing. *Bioorg. Chem.* **99**, 103773 (2020).
22. Ariaeenejad, S. *et al.* An efficient nano-biocatalyst for lignocellulosic biomass hydrolysis: Xylanase immobilization on organically modified biogenic mesoporous silica nanoparticles. *Int. J. Biol. Macromol.* **164**, 3462–3473 (2020).
23. Heurtault, B. Physico-chemical stability of colloidal lipid particles. *Biomaterials* **24**, 4283–4300 (2003).
24. Yang, M., Li, H., Javadi, A. & Gong, S. Multifunctional mesoporous silica nanoparticles as labels for the preparation of ultrasensitive electrochemical immunosensors. *Biomaterials* **31**, 3281–3286 (2010).
25. Gan, Q. *et al.* A magnetic, reversible pH-responsive nanogated ensemble

- 
- based on Fe<sub>3</sub>O<sub>4</sub> nanoparticles-capped mesoporous silica. *Biomaterials* **32**, 1932–1942 (2011).
26. He, Q. *et al.* An anti-ROS/hepatic fibrosis drug delivery system based on salvianolic acid B loaded mesoporous silica nanoparticles. *Biomaterials* **31**, 7785–7796 (2010).
27. Zhu, M. *et al.* A mesoporous silica nanoparticulate/ $\beta$ -TCP/BG composite drug delivery system for osteoarticular tuberculosis therapy. *Biomaterials* **32**, 1986–1995 (2011).
28. Hulvat, M. C. Cancer Incidence and Trends. *Surg. Clin. North Am.* **100**, 469–481 (2020).
29. Bray, F. *et al.* Global cancer statistics 2018: GLOBOCAN estimates of incidence and mortality worldwide for 36 cancers in 185 countries. *CA. Cancer J. Clin.* **68**, 394–424 (2018).
30. Schwappach, D. L. B. & Wernli, M. Chemotherapy patients' perceptions of drug administration safety. *J. Clin. Oncol.* **28**, 2896–2901 (2010).
31. Jain, K. K. An Overview of Drug Delivery Systems. in 1–54 (2020). doi:10.1007/978-1-4939-9798-5\_1.
32. Mitchell, M. J. *et al.* Engineering precision nanoparticles for drug delivery. *Nat. Rev. Drug Discov.* **20**, 101–124 (2021).
33. Kohane, D. S. Microparticles and nanoparticles for drug delivery. *Biotechnol. Bioeng.* **96**, 203–209 (2007).
34. Tabata, Y. & Ikada, Y. Macrophage phagocytosis of biodegradable microspheres composed of L-lactic acid/glycolic acid homo- and copolymers. *J. Biomed. Mater. Res.* **22**, 837–858 (1988).
35. Hillaireau, H. & Couvreur, P. Nanocarriers' entry into the cell: relevance to drug delivery. *Cell. Mol. Life Sci.* **66**, 2873–2896 (2009).
36. Mehrizi, T. Z. An Overview of the Latest Applications of Platelet-Derived Microparticles and Nanoparticles in Medical Technology 2010-2020. *Curr. Mol. Med.* **22**, 524–539 (2022).
37. WONG, H., BENDAYAN, R., RAUTH, A., LI, Y. & WU, X. Chemotherapy with anticancer drugs encapsulated in solid lipid nanoparticles☆. *Adv. Drug Deliv. Rev.* **59**, 491–504 (2007).
38. Prasad, P., Cheng, J., Shuhendler, A., Rauth, A. M. & Wu, X. Y. A novel nanoparticle formulation overcomes multiple types of membrane efflux pumps in human breast cancer cells. *Drug Deliv. Transl. Res.* **2**, 95–105 (2012).
-

- 
39. Lohcharoenkal, W., Wang, L., Chen, Y. C. & Rojanasakul, Y. Protein Nanoparticles as Drug Delivery Carriers for Cancer Therapy. *Biomed Res. Int.* **2014**, 1–12 (2014).
  40. Mishra, D., Hubenak, J. R. & Mathur, A. B. Nanoparticle systems as tools to improve drug delivery and therapeutic efficacy. *J. Biomed. Mater. Res. Part A* **101**, 3646–3660 (2013).
  41. Bisker, G., Yeheskely-Hayon, D., Minai, L. & Yelin, D. Controlled release of Rituximab from gold nanoparticles for phototherapy of malignant cells. *J. Control. Release* **162**, 303–309 (2012).
  42. Yu, A., Wang, Y., Barlow, E. & Caruso, F. Mesoporous Silica Particles as Templates for Preparing Enzyme-Loaded Biocompatible Microcapsules. *Adv. Mater.* **17**, 1737–1741 (2005).
  43. Slowing, I. I., Trewyn, B. G., Giri, S. & Lin, V. S.-Y. Mesoporous Silica Nanoparticles for Drug Delivery and Biosensing Applications. *Adv. Funct. Mater.* **17**, 1225–1236 (2007).
  44. Torney, F., Trewyn, B. G., Lin, V. S.-Y. & Wang, K. Mesoporous silica nanoparticles deliver DNA and chemicals into plants. *Nat. Nanotechnol.* **2**, 295–300 (2007).
  45. Muñoz, B., Rámila, A., Pérez-Pariente, J., Díaz, I. & Vallet-Regí, M. MCM-41 Organic Modification as Drug Delivery Rate Regulator. *Chem. Mater.* **15**, 500–503 (2003).
  46. Lin, Y.-S. *et al.* Well-Ordered Mesoporous Silica Nanoparticles as Cell Markers. *Chem. Mater.* **17**, 4570–4573 (2005).
  47. Lai, C.-Y. *et al.* A Mesoporous Silica Nanosphere-Based Carrier System with Chemically Removable CdS Nanoparticle Caps for Stimuli-Responsive Controlled Release of Neurotransmitters and Drug Molecules. *J. Am. Chem. Soc.* **125**, 4451–4459 (2003).
  48. Kim, J. *et al.* Magnetic Fluorescent Delivery Vehicle Using Uniform Mesoporous Silica Spheres Embedded with Monodisperse Magnetic and Semiconductor Nanocrystals. *J. Am. Chem. Soc.* **128**, 688–689 (2006).
  49. SLOWING, I., VIVEROESCOTO, J., WU, C. & LIN, V. Mesoporous silica nanoparticles as controlled release drug delivery and gene transfection carriers☆. *Adv. Drug Deliv. Rev.* **60**, 1278–1288 (2008).
  50. Saravanakumar, G., Jo, D.-G. & H. Park, J. Polysaccharide-Based Nanoparticles: A Versatile Platform for Drug Delivery and Biomedical Imaging. *Curr. Med. Chem.* **19**, 3212–3229 (2012).
  51. Sekhon, B. S. & Kamboj, S. R. Inorganic nanomedicine—Part 2.
-



- 
- Nanomedicine Nanotechnology, Biol. Med.* **6**, 612–618 (2010).
52. Lei Yang and Brian W. Sheldon and Thomas Jay. Nanophase Ceramics for Improved Drug Delivery: Current Opportunities and Challenges. *Am. Ceram. Soc. Bull.* **89**, 24–32 (2010).
53. Radin, S., Falaize, S., Lee, M. H. & Ducheyne, P. In vitro bioactivity and degradation behavior of silica xerogels intended as controlled release materials. *Biomaterials* **23**, 3113–3122 (2002).
54. Akça, B., Can, M., Değirmenci, V., Yilmaz, A. & Üner, D. Single Step Synthesis of Mesoporous Co-Pb/SBA-15 Catalysts. in 317–320 (2007). doi:10.1016/B978-0-444-53202-2.50068-3.
55. Savino, R., Casadonte, F. & Terracciano, R. In Mesopore Protein Digestion: A New Forthcoming Strategy in Proteomics. *Molecules* **16**, 5938–5962 (2011).
56. Jin, L., Kuo, C. & Suib, S. L. Heterogeneous Catalysts for Biomass Conversion. in *New and Future Developments in Catalysis* 253–270 (Elsevier, 2013). doi:10.1016/B978-0-444-53878-9.00012-6.
57. Oumi, Y., Azuma, K., Sasaki, S., Sano, T. & Ikeda, T. The modeling of wall structure of siliceous MCM-41 based on the formation process. in 69–76 (2002). doi:10.1016/S0167-2991(02)80526-2.
58. Zhang, Y., Zhang, J., Jiang, T. & Wang, S. Inclusion of the poorly water-soluble drug simvastatin in mesocellular foam nanoparticles: Drug loading and release properties. *Int. J. Pharm.* **410**, 118–124 (2011).
59. Carriazo, D., del Arco, M., Martín, C., Ramos, C. & Rives, V. Influence of the inorganic matrix nature on the sustained release of naproxen. *Microporous Mesoporous Mater.* **130**, 229–238 (2010).
60. Balas, F., Manzano, M., Horcajada, P. & Vallet-Regí, M. Confinement and Controlled Release of Bisphosphonates on Ordered Mesoporous Silica-Based Materials. *J. Am. Chem. Soc.* **128**, 8116–8117 (2006).
61. Xu, Y. *et al.* Construction of a novel pH-sensitive drug release system from mesoporous silica tablets coated with Eudragit. *Solid State Sci.* **13**, 641–646 (2011).
62. Zhu, Y., Kaskel, S., Ikoma, T. & Hanagata, N. Magnetic SBA-15/poly(N-isopropylacrylamide) composite: Preparation, characterization and temperature-responsive drug release property. *Microporous Mesoporous Mater.* **123**, 107–112 (2009).
63. Yang, S. *et al.* Visible-light degradable polymer coated hollow mesoporous silica nanoparticles for controlled drug release and cell imaging. *J. Mater.*
-

- 
- Chem. B* **1**, 4628 (2013).
64. Coll, C. *et al.* Enzyme-Mediated Controlled Release Systems by Anchoring Peptide Sequences on Mesoporous Silica Supports. *Angew. Chemie Int. Ed.* **50**, 2138–2140 (2011).
65. Chen, X. *et al.* Stimuli-responsive functionalized mesoporous silica nanoparticles for drug release in response to various biological stimuli. *Biomater. Sci.* **2**, 121–130 (2014).
66. Moritz, M. & Geszke-Moritz, M. Mesoporous materials as multifunctional tools in biosciences: Principles and applications. *Mater. Sci. Eng. C* **49**, 114–151 (2015).
67. Liu, Z. *et al.* Hybrid mesoporous gadolinium oxide nanorods: a platform for multimodal imaging and enhanced insoluble anticancer drug delivery with low systemic toxicity. *J. Mater. Chem.* **22**, 14982 (2012).
68. Di, W. *et al.* Single-phased luminescent mesoporous nanoparticles for simultaneous cell imaging and anticancer drug delivery. *Biomaterials* **32**, 7226–7233 (2011).
69. Lu, J., Li, Z., Zink, J. I. & Tamanoi, F. In vivo tumor suppression efficacy of mesoporous silica nanoparticles-based drug-delivery system: enhanced efficacy by folate modification. *Nanomedicine Nanotechnology, Biol. Med.* **8**, 212–220 (2012).
70. Zhang, W. & Zhao, M. Fluidisation behaviour of silica nanoparticles under horizontal vibration. *J. Exp. Nanosci.* **5**, 69–82 (2010).
71. Zhang, J. *et al.* In Situ Loading of Basic Fibroblast Growth Factor Within Porous Silica Nanoparticles for a Prolonged Release. *Nanoscale Res. Lett.* **4**, 1297 (2009).
72. Manivannan, R. & Ramanathan, S. The effect of hydrogen peroxide on polishing removal rate in CMP with various abrasives. *Appl. Surf. Sci.* **255**, 3764–3768 (2009).
73. Li, Z., Zhang, J., Du, J., Han, B. & Wang, J. Preparation of silica microrods with nano-sized pores in ionic liquid microemulsions. *Colloids Surfaces A Physicochem. Eng. Asp.* **286**, 117–120 (2006).
74. Wang, Z. L., Gao, R. P., Gole, J. L. & Stout, J. D. Silica Nanotubes and Nanofiber Arrays. *Adv. Mater.* **12**, 1938–1940 (2000).
75. Hasany, M. *et al.* Silica nanoparticle surface chemistry: An important trait affecting cellular biocompatibility in two and three dimensional culture systems. *Colloids Surfaces B Biointerfaces* **182**, 110353 (2019).
76. Chen, J., Wang, W., Xu, Y. & Zhang, X. Slow-Release Formulation of a
-

- 
- New Biological Pesticide, Pyoluteorin, with Mesoporous Silica. *J. Agric. Food Chem.* **59**, 307–311 (2011).
77. Liu, M. L., Yang, D. A. & Qu, Y. F. Effect of different chemical additives and heat-treatment on ambient pressure dried silica aerogels. *J. Exp. Nanosci.* **5**, 83–91 (2010).
78. Yuvakkumar, R., Elango, V., Rajendran, V. & Kannan, N. High-purity nano silica powder from rice husk using a simple chemical method. *J. Exp. Nanosci.* **9**, 272–281 (2014).
79. Mishra, P., Chakraverty, A. & Banerjee, H. D. Production and purification of silicon by calcium reduction of rice-husk white ash. *J. Mater. Sci.* **20**, 4387–4391 (1985).
80. Banerjee, H. D., Sen, S. & Acharya, H. N. Investigations on the production of silicon from rice husks by the magnesium method. *Mater. Sci. Eng.* **52**, 173–179 (1982).
81. Singh, R. & Dhindaw, B. K. PRODUCTION OF HIGH PURITY SILICON FROM RICE HUSK FOR USE IN SOUR CELLS. in *Sun: Mankind's Future Source of Energy* 776–781 (Elsevier, 1978). doi:10.1016/B978-1-4832-8407-1.50151-3.
82. Mishra, D., Kang, H. C. & Bae, Y. H. Reconstitutable charged polymeric (PLGA)<sub>2</sub>-b-PEI micelles for gene therapeutics delivery. *Biomaterials* **32**, 3845–3854 (2011).
83. Xu, Z. P., Zeng, Q. H., Lu, G. Q. & Yu, A. B. Inorganic nanoparticles as carriers for efficient cellular delivery. *Chem. Eng. Sci.* **61**, 1027–1040 (2006).
84. Bessa, P. C. *et al.* Thermoresponsive self-assembled elastin-based nanoparticles for delivery of BMPs. *J. Control. Release* **142**, 312–8 (2010).
85. Liu, Z., Jiao, Y., Wang, Y., Zhou, C. & Zhang, Z. Polysaccharides-based nanoparticles as drug delivery systems. *Adv. Drug Deliv. Rev.* **60**, 1650–1662 (2008).
86. Christian, D. A. *et al.* Polymersome carriers: From self-assembly to siRNA and protein therapeutics. *Eur. J. Pharm. Biopharm.* **71**, 463–474 (2009).
87. Geethalakshmi, R. & Sarada. Gold and silver nanoparticles from *Trianthema decandra*: synthesis, characterization, and antimicrobial properties. *Int. J. Nanomedicine* 5375 (2012) doi:10.2147/IJN.S36516.
88. Rajendran, N., Natrajan, R., Kumar, R. & Selvaraj, S. Acyclovir-loaded chitosan nanoparticles for ocular delivery. *Asian J. Pharm.* **4**, 220 (2010).
89. Khalil, N. M. *et al.* Pharmacokinetics of curcumin-loaded PLGA and PLGA–PEG blend nanoparticles after oral administration in rats. *Colloids Surfaces B*
-

- 
- Biointerfaces* **101**, 353–360 (2013).
90. Phyto, P. *et al.* Understanding molecular mechanisms of biologics drug delivery and stability from NMR spectroscopy. *Adv. Drug Deliv. Rev.* **174**, 1–29 (2021).
91. Canal, F., Sanchis, J. & Vicent, M. J. Polymer–drug conjugates as nano-sized medicines. *Curr. Opin. Biotechnol.* **22**, 894–900 (2011).
92. Moghimi, S. M., Hunter, A. C. & Andresen, T. L. Factors Controlling Nanoparticle Pharmacokinetics: An Integrated Analysis and Perspective. *Annu. Rev. Pharmacol. Toxicol.* **52**, 481–503 (2012).
93. Beg, S. *et al.* Advancement in carbon nanotubes: basics, biomedical applications and toxicity. *J. Pharm. Pharmacol.* **63**, 141–163 (2011).
94. Jain, A. K. & Thareja, S. In vitro and in vivo characterization of pharmaceutical nanocarriers used for drug delivery. *Artif. Cells, Nanomedicine, Biotechnol.* **47**, 524–539 (2019).
95. Saupe, A., Gordon, K. C. & Rades, T. Structural investigations on nanoemulsions, solid lipid nanoparticles and nanostructured lipid carriers by cryo-field emission scanning electron microscopy and Raman spectroscopy. *Int. J. Pharm.* **314**, 56–62 (2006).
96. Murphy, C. J. *et al.* Gold nanoparticles in biology: beyond toxicity to cellular imaging. *Acc. Chem. Res.* **41**, 1721–30 (2008).
97. Wilhelm, S. *et al.* Analysis of nanoparticle delivery to tumours. *Nat. Rev. Mater.* **1**, 16014 (2016).
98. Hillyer, J. F. & Albrecht, R. M. Gastrointestinal persorption and tissue distribution of differently sized colloidal gold nanoparticles. *J. Pharm. Sci.* **90**, 1927–1936 (2001).
99. Jensen, B. C. & McLeod, H. L. Pharmacogenomics as a risk mitigation strategy for chemotherapeutic cardiotoxicity. *Pharmacogenomics* **14**, 205–213 (2013).
100. Longmire, M., Choyke, P. L. & Kobayashi, H. Clearance properties of nano-sized particles and molecules as imaging agents: considerations and caveats. *Nanomedicine* **3**, 703–717 (2008).
101. Sahay, G., Batrakova, E. V. & Kabanov, A. V. Different Internalization Pathways of Polymeric Micelles and Unimers and Their Effects on Vesicular Transport. *Bioconjug. Chem.* **19**, 2023–2029 (2008).
102. Wang, R. *et al.* Potential adverse effects of nanoparticles on the reproductive system. *Int. J. Nanomedicine* **Volume 13**, 8487–8506 (2018).
-

- 
103. Li, S.-D. & Huang, L. Pharmacokinetics and Biodistribution of Nanoparticles. *Mol. Pharm.* **5**, 496–504 (2008).
  104. Ray, K. Clearance of nanomaterials in the liver. *Nat. Rev. Gastroenterol. Hepatol.* **13**, 560–560 (2016).
  105. Domingo-Espín, J. *et al.* Engineered Biological Entities for Drug Delivery and Gene Therapy. in 247–298 (2011). doi:10.1016/B978-0-12-416020-0.00006-1.
  106. Moghimi, S. M., Hunter, A. C. & Murray, J. C. Long-circulating and target-specific nanoparticles: theory to practice. *Pharmacol. Rev.* **53**, 283–318 (2001).
  107. Pillai, O., Dhanikula, A. B. & Panchagnula, R. Drug delivery: an odyssey of 100 years. *Curr. Opin. Chem. Biol.* **5**, 439–446 (2001).
  108. Vallet-Regí, M., Balas, F. & Arcos, D. Mesoporous Materials for Drug Delivery. *Angew. Chemie Int. Ed.* **46**, 7548–7558 (2007).
  109. Dadwal, A., Baldi, A. & Kumar Narang, R. Nanoparticles as carriers for drug delivery in cancer. *Artif. Cells, Nanomedicine, Biotechnol.* **46**, 295–305 (2018).
  110. Stirland, D. L., Nichols, J. W., Miura, S. & Bae, Y. H. Mind the gap: A survey of how cancer drug carriers are susceptible to the gap between research and practice. *J. Control. Release* **172**, 1045–1064 (2013).
  111. Qamar, Z. *et al.* Nano-Based Drug Delivery System: Recent Strategies for the Treatment of Ocular Disease and Future Perspective. *Recent Pat. Drug Deliv. Formul.* **13**, 246–254 (2020).
  112. Duan, X. & Li, Y. Physicochemical Characteristics of Nanoparticles Affect Circulation, Biodistribution, Cellular Internalization, and Trafficking. *Small* **9**, 1521–1532 (2013).
  113. Moghimi, S. M. Exploiting bone marrow microvascular structure for drug delivery and future therapies. *Adv. Drug Deliv. Rev.* **17**, 61–73 (1995).
  114. Li, S., Ji, Z., Zou, M. Preparation, Characterization, Pharmacokinetics and Tissue Distribution of Solid Lipid Nanoparticles Loaded with Tetrandrine. *AAPS PharmSciTech* **12**, 1011 (2011).
  115. Jindal, A. B. The effect of particle shape on cellular interaction and drug delivery applications of micro- and nanoparticles. *Int. J. Pharm.* **532**, 450–465 (2017).
  116. Mathaes, R., Winter, G., Besheer, A. & Engert, J. Influence of particle geometry and PEGylation on phagocytosis of particulate carriers. *Int. J. Pharm.* **465**, 159–164 (2014).
-

- 
117. Agarwal, R. *et al.* Effect of Shape, Size, and Aspect Ratio on Nanoparticle Penetration and Distribution inside Solid Tissues Using 3D Spheroid Models. *Adv. Healthc. Mater.* **4**, 2269–2280 (2015).
  118. Oh, W.-K., Kim, S., Yoon, H. & Jang, J. Shape-Dependent Cytotoxicity and Proinflammatory Response of Poly(3,4-ethylenedioxythiophene) Nanomaterials. *Small* **6**, 872–879 (2010).
  119. Li, Y., Kröger, M. & Liu, W. K. Shape effect in cellular uptake of PEGylated nanoparticles: comparison between sphere, rod, cube and disk. *Nanoscale* **7**, 16631–16646 (2015).
  120. Doshi, N. & Mitragotri, S. Needle-shaped polymeric particles induce transient disruption of cell membranes. *J. R. Soc. Interface* **7**, (2010).
  121. Zhao, X. *et al.* Cytotoxicity of hydroxyapatite nanoparticles is shape and cell dependent. *Arch. Toxicol.* **87**, 1037–1052 (2013).
  122. Bahrami, A. H., Lipowsky, R. & Weikl, T. R. The role of membrane curvature for the wrapping of nanoparticles. *Soft Matter* **12**, 581–587 (2016).
  123. Decuzzi, P. *et al.* Size and shape effects in the biodistribution of intravascularly injected particles. *J. Control. Release* **141**, 320–327 (2010).
  124. Sun, Y.-N., Wang, C.-D., Zhang, X.-M., Ren, L. & Tian, X.-H. Shape Dependence of Gold Nanoparticles on In Vivo Acute Toxicological Effects and Biodistribution. *J. Nanosci. Nanotechnol.* **11**, 1210–1216 (2011).
  125. Li, L. *et al.* Biodistribution, excretion, and toxicity of mesoporous silica nanoparticles after oral administration depend on their shape. *Nanomedicine Nanotechnology, Biol. Med.* **11**, 1915–1924 (2015).
  126. Huang, X. *et al.* The Shape Effect of Mesoporous Silica Nanoparticles on Biodistribution, Clearance, and Biocompatibility in Vivo. *ACS Nano* **5**, 5390–5399 (2011).
  127. Hao, N. *et al.* In Vitro Degradation Behavior of Silica Nanoparticles Under Physiological Conditions. *J. Nanosci. Nanotechnol.* **12**, 6346–6354 (2012).
  128. Kumar, S., Anselmo, A. C., Banerjee, A., Zakrewsky, M. & Mitragotri, S. Shape and size-dependent immune response to antigen-carrying nanoparticles. *J. Control. Release* **220**, 141–148 (2015).
  129. Kim, W. *et al.* A reliable approach for assessing size-dependent effects of silica nanoparticles on cellular internalization behavior and cytotoxic mechanisms. *Int. J. Nanomedicine* **Volume 14**, 7375–7387 (2019).
  130. Saikia, J., Yazdimamaghani, M., Hadipour Moghaddam, S. P. & Ghandehari, H. Differential Protein Adsorption and Cellular Uptake of Silica Nanoparticles Based on Size and Porosity. *ACS Appl. Mater. Interfaces* **8**,

- 34820–34832 (2016).
131. Schwartz, S. Unmet needs in developing nanoparticles for precision medicine. *Nanomedicine* **12**, 271–274 (2017).
  132. Blanco, E., Shen, H. & Ferrari, M. Principles of nanoparticle design for overcoming biological barriers to drug delivery. *Nat. Biotechnol.* **33**, 941–951 (2015).
  133. Yang, N. J. & Hinner, M. J. Getting Across the Cell Membrane: An Overview for Small Molecules, Peptides, and Proteins. in 29–53 (2015). doi:10.1007/978-1-4939-2272-7\_3.
  134. José Alonso, M. Nanomedicines for overcoming biological barriers. *Biomed. Pharmacother.* **58**, 168–172 (2004).
  135. Pillay, V. *et al.* Parameters and characteristics governing cellular internalization and trans-barrier trafficking of&nbsp;nanostructures. *Int. J. Nanomedicine* 2191 (2015) doi:10.2147/IJN.S75615.
  136. Foroozandeh, P. & Aziz, A. A. Insight into Cellular Uptake and Intracellular Trafficking of Nanoparticles. *Nanoscale Res. Lett.* **13**, 339 (2018).
  137. Stroeve, P. & Mahmoudi, M. *Drug Delivery Systems*. vol. 01 (World Scientific, 2018).
  138. Behzadi, S. *et al.* Cellular uptake of nanoparticles: journey inside the cell. *Chem. Soc. Rev.* **46**, 4218–4244 (2017).
  139. Yue, J., Feliciano, T. J., Li, W., Lee, A. & Odom, T. W. Gold Nanoparticle Size and Shape Effects on Cellular Uptake and Intracellular Distribution of siRNA Nanoconstructs. *Bioconjug. Chem.* **28**, 1791–1800 (2017).
  140. Chen, L. Q. *et al.* Nanotoxicity of Silver Nanoparticles to Red Blood Cells: Size Dependent Adsorption, Uptake, and Hemolytic Activity. *Chem. Res. Toxicol.* **28**, 501–509 (2015).
  141. Shahin, M., Safaei-Nikouei, N. & Lavasanifar, A. Polymeric micelles for pH-responsive delivery of cisplatin. *J. Drug Target.* **22**, 629–637 (2014).
  142. Hocking, K. M. *et al.* Nanotechnology Enabled Modulation of Signaling Pathways Affects Physiologic Responses in Intact Vascular Tissue. *Tissue Eng. Part A* **25**, 416–426 (2019).
  143. Hoshyar, N., Gray, S., Han, H. & Bao, G. The effect of nanoparticle size on in vivo pharmacokinetics and cellular interaction. *Nanomedicine* **11**, 673–692 (2016).
  144. Iлина, P. *et al.* Genetic blockage of endocytic pathways reveals differences in the intracellular processing of non-viral gene delivery systems. *J. Control.*

- 
- Release* **163**, 385–395 (2012).
145. Nan, A., Bai, X., Son, S. J., Lee, S. B. & Ghandehari, H. Cellular Uptake and Cytotoxicity of Silica Nanotubes. *Nano Lett.* **8**, 2150–2154 (2008).
146. Harush-Frenkel, O., Rozentur, E., Benita, S. & Altschuler, Y. Surface Charge of Nanoparticles Determines Their Endocytic and Transcytotic Pathway in Polarized MDCK Cells. *Biomacromolecules* **9**, 435–443 (2008).
147. des Rieux, A., Fievez, V., Garinot, M., Schneider, Y.-J. & Pr at, V. Nanoparticles as potential oral delivery systems of proteins and vaccines: A mechanistic approach. *J. Control. Release* **116**, 1–27 (2006).
148. Layek, B. & Singh, J. Editorial of Special Issue “Surface-Functionalized Nanoparticles as Drug Carriers”. *Int. J. Mol. Sci.* **20**, 6352 (2019).
149. Arruebo, M., Valladares, M. & Gonz alez-Fern andez,  . Antibody-Conjugated Nanoparticles for Biomedical Applications. *J. Nanomater.* **2009**, 1–24 (2009).
150. Rafiee, E. & Eavani, S. pH-responsive controlled release of epirubicin from Fe@Si-PW hybrid nanoparticles. *Mater. Sci. Eng. C* **39**, 340–343 (2014).
151. Mohanraj, V. J. & Chen, Y. Nanoparticles - A review. *Trop. J. Pharm. Res.* **5**, (2007).
152. Guan, S. *et al.* Self-assembled peptide–poloxamine nanoparticles enable in vitro and in vivo genome restoration for cystic fibrosis. *Nat. Nanotechnol.* **14**, 287–297 (2019).
153. Witten, J. & Ribbeck, K. The particle in the spider’s web: transport through biological hydrogels. *Nanoscale* **9**, 8080–8095 (2017).
154. Tian, H. *et al.* Uniform Core-Shell Nanoparticles with Thiolated Hyaluronic Acid Coating to Enhance Oral Delivery of Insulin. *Adv. Healthc. Mater.* **7**, 1800285 (2018).
155. Zhang, S. *et al.* BSA Nanoparticles Modified with N -Acetylcysteine for Improving the Stability and Mucoadhesion of Curcumin in the Gastrointestinal Tract. *J. Agric. Food Chem.* **67**, 9371–9381 (2019).
156. Alcantar, N. A., Aydil, E. S. & Israelachvili, J. N. Polyethylene glycol-coated biocompatible surfaces. *J. Biomed. Mater. Res.* **51**, 343–351 (2000).
157. Lu, J., Liong, M., Zink, J. I. & Tamanoi, F. Mesoporous Silica Nanoparticles as a Delivery System for Hydrophobic Anticancer Drugs. *Small* **3**, 1341–1346 (2007).
158. Meng, H. *et al.* Use of Size and a Copolymer Design Feature To Improve the Biodistribution and the Enhanced Permeability and Retention Effect of
-



- 
- Doxorubicin-Loaded Mesoporous Silica Nanoparticles in a Murine Xenograft Tumor Model. *ACS Nano* **5**, 4131–4144 (2011).
159. He, Q., Zhang, Z., Gao, F., Li, Y. & Shi, J. In vivo Biodistribution and Urinary Excretion of Mesoporous Silica Nanoparticles: Effects of Particle Size and PEGylation. *Small* **7**, 271–280 (2011).
160. Nichols, J. W. & Bae, Y. H. EPR: Evidence and fallacy. *J. Control. Release* **190**, 451–464 (2014).
161. Molineux, G. Pegylation: engineering improved pharmaceuticals for enhanced therapy. *Cancer Treat. Rev.* **28**, 13–16 (2002).
162. Tenzer, S. *et al.* Rapid formation of plasma protein corona critically affects nanoparticle pathophysiology. *Nat. Nanotechnol.* **8**, 772–781 (2013).
163. OWENSIII, D. & PEPPAS, N. Opsonization, biodistribution, and pharmacokinetics of polymeric nanoparticles. *Int. J. Pharm.* **307**, 93–102 (2006).
164. Yang, Q. *et al.* Evading Immune Cell Uptake and Clearance Requires PEG Grafting at Densities Substantially Exceeding the Minimum for Brush Conformation. *Mol. Pharm.* **11**, 1250–1258 (2014).
165. Walkey, C. D., Olsen, J. B., Guo, H., Emili, A. & Chan, W. C. W. Nanoparticle Size and Surface Chemistry Determine Serum Protein Adsorption and Macrophage Uptake. *J. Am. Chem. Soc.* **134**, 2139–2147 (2012).
166. Unsworth, L. D., Sheardown, H. & Brash, J. L. Protein-Resistant Poly(ethylene oxide)-Grafted Surfaces: Chain Density-Dependent Multiple Mechanisms of Action. *Langmuir* **24**, 1924–1929 (2008).
167. Dobrovolskaia, M. A., Aggarwal, P., Hall, J. B. & McNeil, S. E. Preclinical Studies To Understand Nanoparticle Interaction with the Immune System and Its Potential Effects on Nanoparticle Biodistribution. *Mol. Pharm.* **5**, 487–495 (2008).
168. Suk, J. S., Xu, Q., Kim, N., Hanes, J. & Ensign, L. M. PEGylation as a strategy for improving nanoparticle-based drug and gene delivery. *Adv. Drug Deliv. Rev.* **99**, 28–51 (2016).
169. Black, K. C. L. *et al.* Radioactive <sup>198</sup>Au-Doped Nanostructures with Different Shapes for In Vivo Analyses of Their Biodistribution, Tumor Uptake, and Intratumoral Distribution. *ACS Nano* **8**, 4385–4394 (2014).
170. Gooneh-Farahani, S., Naimi-Jamal, M. R. & Naghib, S. M. Stimuli-responsive graphene-incorporated multifunctional chitosan for drug delivery applications: a review. *Expert Opin. Drug Deliv.* **16**, 79–99 (2019).
-

- 
171. Yadav, A., Lomash, V., Samim, M. & Flora, S. J. S. Curcumin encapsulated in chitosan nanoparticles: A novel strategy for the treatment of arsenic toxicity. *Chem. Biol. Interact.* **199**, 49–61 (2012).
172. Smith, J., Wood, E. & Dornish, M. Effect of Chitosan on Epithelial Cell Tight Junctions. *Pharm. Res.* **21**, 43–49 (2004).
173. Stie, M. B. *et al.* Swelling of mucoadhesive electrospun chitosan/polyethylene oxide nanofibers facilitates adhesion to the sublingual mucosa. *Carbohydr. Polym.* **242**, 116428 (2020).
174. Foster, L. J. R., Ho, S., Hook, J., Basuki, M. & Marçal, H. Chitosan as a Biomaterial: Influence of Degree of Deacetylation on Its Physiochemical, Material and Biological Properties. *PLoS One* **10**, e0135153 (2015).
175. Li, Y., Gao, G. H. & Lee, D. S. Stimulus-Sensitive Polymeric Nanoparticles and Their Applications as Drug and Gene Carriers. *Adv. Healthc. Mater.* **2**, 388–417 (2013).
176. Elgadir, M. A. *et al.* Impact of chitosan composites and chitosan nanoparticle composites on various drug delivery systems: A review. *J. Food Drug Anal.* **23**, 619–629 (2015).
177. Prabakaran, M. Review Paper: Chitosan Derivatives as Promising Materials for Controlled Drug Delivery. *J. Biomater. Appl.* **23**, 5–36 (2008).
178. Kashyap, M., Archana, D., Semwal, A., Dutta, J. & Dutta, P. K. Chitosan: A Promising Substrate for Regenerative Medicine in Drug Formulation. in 261–277 (2016). doi:10.1007/978-81-322-2511-9\_10.
179. Suarato, G., Li, W. & Meng, Y. Role of pH-responsiveness in the design of chitosan-based cancer nanotherapeutics: A review. *Biointerphases* **11**, 04B201 (2016).
180. Yi, H. *et al.* Biofabrication with Chitosan. *Biomacromolecules* **6**, 2881–2894 (2005).
181. Heister, E. *et al.* Drug loading, dispersion stability, and therapeutic efficacy in targeted drug delivery with carbon nanotubes. *Carbon N. Y.* **50**, 622–632 (2012).
182. Maurer-Spurej, E., Wong, K. F., Maurer, N., Fenske, D. B. & Cullis, P. R. Factors influencing uptake and retention of amino-containing drugs in large unilamellar vesicles exhibiting transmembrane pH gradients. *Biochim. Biophys. Acta - Biomembr.* **1416**, 1–10 (1999).
183. Ulbrich, K. Polymeric anticancer drugs with pH-controlled activation. *Adv. Drug Deliv. Rev.* **56**, 1023–1050 (2004).
184. Mrkvan, T. *et al.* Chemotherapy based on HPMA copolymer conjugates with
-

- 
- pH-controlled release of doxorubicin triggers anti-tumor immunity. *J. Control. Release* **110**, 119–129 (2005).
185. Etrych, T., Jelínková, M., Říhová, B. & Ulbrich, K. New HPMA copolymers containing doxorubicin bound via pH-sensitive linkage: synthesis and preliminary in vitro and in vivo biological properties. *J. Control. Release* **73**, 89–102 (2001).
186. Etrych, T. *et al.* N-(2-hydroxypropyl)methacrylamide-based polymer conjugates with pH-controlled activation of doxorubicin. I. New synthesis, physicochemical characterization and preliminary biological evaluation. *J. Appl. Polym. Sci.* **109**, 3050–3061 (2008).
187. Mekaru, H., Lu, J. & Tamanoi, F. Development of mesoporous silica-based nanoparticles with controlled release capability for cancer therapy. *Adv. Drug Deliv. Rev.* **95**, 40–49 (2015).
188. Svenson, S. Clinical translation of nanomedicines. *Curr. Opin. Solid State Mater. Sci.* **16**, 287–294 (2012).
189. Çağdaş, M., Sezer, A. D. & Bucak, S. Liposomes as Potential Drug Carrier Systems for Drug Delivery. in *Application of Nanotechnology in Drug Delivery* (InTech, 2014). doi:10.5772/58459.
190. Allen, T. M., Hansen, C. B. & de Menezes, D. E. L. Pharmacokinetics of long-circulating liposomes. *Adv. Drug Deliv. Rev.* **16**, 267–284 (1995).
191. Ricciardi, A. S. *et al.* In utero nanoparticle delivery for site-specific genome editing. *Nat. Commun.* **9**, 2481 (2018).
192. Wu, Z. *et al.* Nanoparticles functionalized with supramolecular host–guest systems for nanomedicine and healthcare. *Nanomedicine* **10**, 1493–1514 (2015).
193. Hong, E. J., Choi, D. G. & Shim, M. S. Targeted and effective photodynamic therapy for cancer using functionalized nanomaterials. *Acta Pharm. Sin. B* **6**, 297–307 (2016).
194. McInnes, S. J. P. *et al.* Surface engineering of porous silicon to optimise therapeutic antibody loading and release. *J. Mater. Chem. B* **3**, 4123–4133 (2015).
195. Krausz, A. E. *et al.* Curcumin-encapsulated nanoparticles as innovative antimicrobial and wound healing agent. *Nanomedicine Nanotechnology, Biol. Med.* **11**, 195–206 (2015).
196. Maeda, H. The enhanced permeability and retention (EPR) effect in tumor vasculature: the key role of tumor-selective macromolecular drug targeting. *Adv. Enzyme Regul.* **41**, 189–207 (2001).
-

- 
197. Amjad MT, Chidharla A, K. A. Cancer Chemotherapy. *StatPearls Publ.* **2022 Jan**, (2022).
198. Petros, R. A. & DeSimone, J. M. Strategies in the design of nanoparticles for therapeutic applications. *Nat. Rev. Drug Discov.* **9**, 615–627 (2010).
199. Greish, K., Nehoff, H., Parayath, N., Domanovitch, L. & Taurin, S. Nanomedicine for drug targeting: strategies beyond the enhanced permeability and retention effect. *Int. J. Nanomedicine* 2539 (2014) doi:10.2147/IJN.S47129.
200. Baetke, S. C., Lammers, T. & Kiessling, F. Applications of nanoparticles for diagnosis and therapy of cancer. *Br. J. Radiol.* **88**, 20150207 (2015).
201. Sreejayan, N. & Rao, M. N. Free radical scavenging activity of curcuminoids. *Arzneimittelforschung.* **46**, 169–71 (1996).
202. Priyadarsini, K. I. *et al.* Role of phenolic O-H and methylene hydrogen on the free radical reactions and antioxidant activity of curcumin. *Free Radic. Biol. Med.* **35**, 475–484 (2003).
203. Sudheer, A. R., Chandran, K., Marimuthu, S. & Menon, V. P. Ferulic Acid Modulates Altered Lipid Profiles and Prooxidant/Antioxidant Status in Circulation During Nicotine-Induced Toxicity: A Dose-Dependent Study. *Toxicol. Mech. Methods* **15**, 375–381 (2005).
204. Radhakrishna, Pillai, G., Srivastava, A. S., Hassanein, T. I., Chauhan, D. P. & Carrier, E. Induction of apoptosis in human lung cancer cells by curcumin. *Cancer Lett.* **208**, 163–170 (2004).
205. Mou, S., Zhou, Z., He, Y., Liu, F. & Gong, L. Curcumin inhibits cell proliferation and promotes apoptosis of laryngeal cancer cells through Bcl-2 and PI3K/Akt, and by upregulating miR-15a. *Oncol. Lett.* **14**, 4937–4942 (2017).
206. Kunati, S. R., Yang, S., William, B. M. & Xu, Y. An LC–MS/MS method for simultaneous determination of curcumin, curcumin glucuronide and curcumin sulfate in a phase II clinical trial. *J. Pharm. Biomed. Anal.* **156**, 189–198 (2018).
207. Zhao, S., Pi, C., Ye, Y., Zhao, L. & Wei, Y. Recent advances of analogues of curcumin for treatment of cancer. *Eur. J. Med. Chem.* **180**, 524–535 (2019).
208. Liu, C. *et al.* Elaboration of curcumin-loaded rice bran albumin nanoparticles formulation with increased in vitro bioactivity and in vivo bioavailability. *Food Hydrocoll.* **77**, 834–842 (2018).
209. Bolger, G. T. *et al.* Pharmacokinetics of liposomal curcumin (Lipocure™) infusion: effect of co-medication in cancer patients and comparison with

- 
- healthy individuals. *Cancer Chemother. Pharmacol.* **83**, 265–275 (2019).
210. Ranjan, A. P., Mukerjee, A., Helson, L., Gupta, R. & Vishwanatha, J. K. Efficacy of liposomal curcumin in a human pancreatic tumor xenograft model: inhibition of tumor growth and angiogenesis. *Anticancer Res.* **33**, 3603–9 (2013).
211. Golombick, T., Diamond, T. H., Manoharan, A. & Ramakrishna, R. The Effect of Curcumin (as Meriva) on Absolute Lymphocyte Count (ALC), NK Cells and T Cell Populations in Patients with Stage 0/1 Chronic Lymphocytic Leukemia. *J. Cancer Ther.* **06**, 566–571 (2015).
212. Greene, J. & Hennessy, B. The role of anthracyclines in the treatment of early breast cancer. *J. Oncol. Pharm. Pract.* **21**, 201–212 (2015).
213. Minotti, G., Menna, P., Salvatorelli, E., Cairo, G. & Gianni, L. Anthracyclines: Molecular Advances and Pharmacologic Developments in Antitumor Activity and Cardiotoxicity. *Pharmacol. Rev.* **56**, 185–229 (2004).
214. Ning, S.-T. *et al.* Targeting Colorectal Cancer Stem-Like Cells with Anti-CD133 Antibody-Conjugated SN-38 Nanoparticles. *ACS Appl. Mater. Interfaces* **8**, 17793–17804 (2016).
215. Yi, Y. *et al.* Glucose-linked sub-50-nm unimer polyion complex-assembled gold nanoparticles for targeted siRNA delivery to glucose transporter 1-overexpressing breast cancer stem-like cells. *J. Control. Release* **295**, 268–277 (2019).
216. Khasraw, M., Bell, R. & Dang, C. Epirubicin: Is it like doxorubicin in breast cancer? A clinical review. *The Breast* **21**, 142–149 (2012).
217. Guo, Q. *et al.* Spectroscopic and cytotoxicity studies on the combined interaction of (–)-epigallocatechin-3-gallate and anthracycline drugs with human serum albumin. *Spectrochim. Acta Part A Mol. Biomol. Spectrosc.* **222**, 117213 (2019).
218. Drummond, D. C., Meyer, O., Hong, K., Kirpotin, D. B. & Papahadjopoulos, D. Optimizing liposomes for delivery of chemotherapeutic agents to solid tumors. *Pharmacol. Rev.* **51**, 691–743 (1999).
219. Birtle, A. J. Anthracyclines and Cardiotoxicity. *Clin. Oncol.* **12**, 146–152 (2000).
220. Raje, S., Pandav, K. & Barthwal, R. Dual mode of binding of anti cancer drug epirubicin to G-quadruplex [d-(TTAGGGT)]<sub>4</sub> containing human telomeric DNA sequence induces thermal stabilization. *Bioorg. Med. Chem.* **27**, 115131 (2019).
221. Buhl, A. S. K. *et al.* Predicting efficacy of epirubicin by a multigene assay in
-

- 
- advanced breast cancer within a Danish Breast Cancer Cooperative Group (DBCG) cohort: a retrospective-prospective blinded study. *Breast Cancer Res. Treat.* **172**, 391–400 (2018).
222. Weenen, H., Van Maanen, J. M. S., De Planque, M. M., McVie, J. G. & Pinedo, H. M. Metabolism of 4'-modified analogs of doxorubicin. Unique glucuronidation pathway for 4'-epidoxorubicin. *Eur. J. Cancer Clin. Oncol.* **20**, 919–926 (1984).
223. Bonadonna, G. *et al.* Drugs ten years later: Epirubicin. *Ann. Oncol.* **4**, 359–369 (1993).
224. Cersosimo, R. J. & Hong, W. K. Epirubicin: a review of the pharmacology, clinical activity, and adverse effects of an adriamycin analogue. *J. Clin. Oncol.* **4**, 425–439 (1986).
225. Germain, E. Anthracycline-induced cardiac toxicity is not increased by dietary omega-3 fatty acids. *Pharmacol. Res.* **47**, 111–117 (2003).
226. Le Bot, M. A. *et al.* Different cytotoxicity and metabolism of doxorubicin, daunorubicin, epirubicin, esorubicin and idarubicin in cultured human and rat hepatocytes. *Biochem. Pharmacol.* **37**, 3877–3887 (1988).
227. Robert, J. Clinical Pharmacokinetics of Epirubicin. *Clin. Pharmacokinet.* **26**, 428–438 (1994).
228. Sercombe, L. *et al.* Advances and Challenges of Liposome Assisted Drug Delivery. *Front. Pharmacol.* **6**, (2015).
229. Elsharkasy, O. M. *et al.* Extracellular vesicles as drug delivery systems: Why and how? *Adv. Drug Deliv. Rev.* **159**, 332–343 (2020).
230. McSweeney, M. D. *et al.* A minimal physiologically based pharmacokinetic model that predicts anti-PEG IgG-mediated clearance of PEGylated drugs in human and mouse. *J. Control. Release* **284**, 171–178 (2018).
231. Risma, K. A. *et al.* Potential mechanisms of anaphylaxis to COVID-19 mRNA vaccines. *J. Allergy Clin. Immunol.* **147**, 2075-2082.e2 (2021).
232. Jarvis, M. *et al.* Detachment of ligands from nanoparticle surface under flow and endothelial cell contact: Assessment using microfluidic devices. *Bioeng. Transl. Med.* **3**, 148–155 (2018).
233. Cox, A. *et al.* Evolution of Nanoparticle Protein Corona across the Blood–Brain Barrier. *ACS Nano* **12**, 7292–7300 (2018).
234. von Roemeling, C., Jiang, W., Chan, C. K., Weissman, I. L. & Kim, B. Y. S. Breaking Down the Barriers to Precision Cancer Nanomedicine. *Trends Biotechnol.* **35**, 159–171 (2017).
-

- 
235. Butcher, K. S. A. *et al.* A luminescence study of porous diatoms. *Mater. Sci. Eng. C* **25**, 658–663 (2005).
236. Zhu, D., Pan, J., Lu, L. & Holmes, R. J. Iron ore pelletization. in *Iron Ore* 435–473 (Elsevier, 2015). doi:10.1016/B978-1-78242-156-6.00015-0.
237. Goyal, A., Demmenie, M., Huang, C.-C., Schall, P. & Dohnalova, K. Photophysical properties of ball milled silicon nanostructures. *Faraday Discuss.* **222**, 96–107 (2020).
238. Athinarayanan, J., Periasamy, V. S., Alhazmi, M. & Alshatwi, A. A. Synthesis and biocompatibility assessment of sugarcane bagasse-derived biogenic silica nanoparticles for biomedical applications. *J. Biomed. Mater. Res. - Part B Appl. Biomater.* **105**, 340–349 (2017).
239. Sigalingging, R., Susanto, E. & Panggabean, S. The effect of rice husk mass on temperature and characteristics of its ash using a pyrolysis equipment organic-inorganic waste. *IOP Conf. Ser. Earth Environ. Sci.* **454**, 012043 (2020).
240. Ghazaeian, M., Khorsandi, K., Hosseinzadeh, R., Naderi, A. & Abrahamse, H. Curcumin–silica nanocomplex preparation, hemoglobin and DNA interaction and photocytotoxicity against melanoma cancer cells. *J. Biomol. Struct. Dyn.* **39**, 6606–6616 (2021).
241. Buchman, J. T. *et al.* Chitosan-Coated Mesoporous Silica Nanoparticle Treatment of *Citrullus lanatus* (Watermelon): Enhanced Fungal Disease Suppression and Modulated Expression of Stress-Related Genes. *ACS Sustain. Chem. Eng.* **7**, 19649–19659 (2019).
242. Hanafi-Bojd, M. Y. *et al.* Surface functionalized mesoporous silica nanoparticles as an effective carrier for epirubicin delivery to cancer cells. *Eur. J. Pharm. Biopharm.* **89**, 248–258 (2015).
243. Yan, T., He, J., Liu, R., Liu, Z. & Cheng, J. Chitosan capped pH-responsive hollow mesoporous silica nanoparticles for targeted chemo-photo combination therapy. *Carbohydr. Polym.* **231**, 115706 (2020).
244. Huang, P. *et al.* Molecularly organic/inorganic hybrid hollow mesoporous organosilica nanocapsules with tumor-specific biodegradability and enhanced chemotherapeutic functionality. *Biomaterials* **125**, 23–37 (2017).
245. Pillai, R. G. *Advances in Cell and Molecular Biology*. (Department of Life Sciences, University of Calicut, 2018).
246. Li, J. & Bi, H. The effect and mechanism of cypermethrin-induced hippocampal neurotoxicity as determined by network pharmacology analysis and experimental validation. *Bioengineered* **12**, 9279–9289 (2021).

- 
247. Agergaard, N. & Jensen, P. T. Procedure for blood glutathione peroxidase determination in cattle and swine. *Acta Vet. Scand.* **23**, 515–527 (1982).
248. Kakkar, P., Das, B. & Viswanathan, P. N. A Modified Spectrophotometric Assay of Superoxide Dismutase. (1984).
249. Maehley AC, and C. B. *The assay of catalases and peroxidases.* (1954).
250. Xiao, F., Xu, T., Lu, B. & Liu, R. Guidelines for antioxidant assays for food components. *Food Front.* **1**, 60–69 (2020).
251. Sari, T. P. *et al.* Preparation and characterization of nanoemulsion encapsulating curcumin. *Food Hydrocoll.* **43**, 540–546 (2015).
252. Shipman, C. M., Rogers, M. J., Apperley, J. F., Russell, R. G. G. & Croucher, P. I. Bisphosphonates induce apoptosis in human myeloma cell lines: a novel anti- tumour activity. *Br. J. Haematol.* **98**, 665–672 (1997).
253. Chazotte, B. Labeling Nuclear DNA Using DAPI. *Cold Spring Harb. Protoc.* **2011**, pdb.prot5556 (2011).
254. Eruslanov, E. & Kusmartsev, S. Identification of ROS Using Oxidized DCFDA and Flow-Cytometry. in 57–72 (2010). doi:10.1007/978-1-60761-411-1\_4.
255. Fauzi, A. N., Norazmi, M. N. & Yaacob, N. S. Tualang honey induces apoptosis and disrupts the mitochondrial membrane potential of human breast and cervical cancer cell lines. *Food Chem. Toxicol.* **49**, 871–878 (2011).
256. Sigma, M. M. membrane potential analysis kit. No Title. doi:<https://www.sigmaaldrich.com/deepweb/assets/sigmaaldrich/product/documents/128/122/mak159bul.pdf>.
257. Renganathan, S. Comparative evaluation of the effect of bone marrow derived stem cells SE2 and dhanwantaram kashaya in diabetic rats. (2021).
258. BLOIS, M. S. Antioxidant Determinations by the Use of a Stable Free Radical. *Nature* **181**, 1199–1200 (1958).
259. Almaghrabi, M. *et al.* Evaluating thermogravimetric analysis for the measurement of drug loading in mesoporous silica nanoparticles (MSNs). *Thermochim. Acta* **730**, 179616 (2023).
260. Florensa, M., Llenas, M., Medina-Gutiérrez, E., Sandoval, S. & Tobías-Rossell, G. Key Parameters for the Rational Design, Synthesis, and Functionalization of Biocompatible Mesoporous Silica Nanoparticles. *Pharmaceutics* **14**, 2703 (2022).
261. Porrhng, S., Davaran, S., Rahemi, N., Allahyari, S. & Mostafavi, E. How Advancing are Mesoporous Silica Nanoparticles? A Comprehensive Review
-



- 
- of the Literature. *Int. J. Nanomedicine* **Volume 17**, 1803–1827 (2022).
262. Alam, Q. *et al.* Novel low temperature synthesis of sodium silicate and ordered mesoporous silica from incineration bottom ash. *J. Clean. Prod.* **211**, 874–883 (2019).
263. Lazaro, A., Quercia, G., Brouwers, H. J. H. & Geus, J. W. Synthesis of a Green Nano-Silica Material Using Beneficiated Waste Dunites and Its Application in Concrete. *World J. Nano Sci. Eng.* **03**, 41–51 (2013).
264. Tong, K. T., Vinai, R. & Soutsos, M. N. Use of Vietnamese rice husk ash for the production of sodium silicate as the activator for alkali-activated binders. *J. Clean. Prod.* **201**, 272–286 (2018).
265. Naqvi, J., Shah, F.H., & Mansha, M. Extraction of Amorphous Silica from Wheat Husk by Using KMnO<sub>4</sub>. *J. Fac. Eng. Technol.* **18**, 39–46 (2011).
266. Athinarayanan, J., Periasamy, V. S., Alhazmi, M., Alattiah, K. A. & Alshatwi, A. A. Synthesis of biogenic silica nanoparticles from rice husks for biomedical applications. *Ceram. Int.* **41**, 275–281 (2015).
267. Akhayere, E., Kavaz, D. & Vaseashta, A. Synthesizing Nano Silica Nanoparticles from Barley Grain Waste: Effect of Temperature on Mechanical Properties. *Polish J. Environ. Stud.* **28**, 2513–2521 (2019).
268. Awal, A. S. M. A. & Hussin, M. W. The effectiveness of palm oil fuel ash in preventing expansion due to alkali-silica reaction. *Cem. Concr. Compos.* **19**, 367–372 (1997).
269. Mathur, P. & Roy, S. Nanosilica facilitates silica uptake, growth and stress tolerance in plants. *Plant Physiol. Biochem.* **157**, 114–127 (2020).
270. Laane, H.-M. The Effects of Foliar Sprays with Different Silicon Compounds. *Plants* **7**, 45 (2018).
271. Mitani, N. Uptake system of silicon in different plant species. *J. Exp. Bot.* **56**, 1255–1261 (2005).
272. Shi, Y. *et al.* Silicon improves seed germination and alleviates oxidative stress of bud seedlings in tomato under water deficit stress. *Plant Physiol. Biochem.* **78**, 27–36 (2014).
273. Guerriero, G., Stokes, I., Valle, N., Hausman, J.-F. & Exley, C. Visualising Silicon in Plants: Histochemistry, Silica Sculptures and Elemental Imaging. *Cells* **9**, 1066 (2020).
274. Rabovsky, J. Biogenic amorphous silica. *Scand. J. Work. Environ. Health* **21 Suppl 2**, 108–10 (1995).
275. Jeelani, P. G., Mulay, P., Venkat, R. & Ramalingam, C. Multifaceted
-

- 
- Application of Silica Nanoparticles. A Review. *Silicon* **12**, 1337–1354 (2020).
276. Imai, S. *et al.* Size and surface modification of amorphous silica particles determine their effects on the activity of human CYP3A4 in vitro. *Nanoscale Res. Lett.* **9**, 651 (2014).
277. Dabbaghian, M. A., Babalou, A. A., Hadi, P., & Jannatdoust, E. (2010). A Parametric Study of the Synthesis of Silica Nanoparticles via Sol-Gel Precipitation Method. *Int. J. Nanosci. Nanotechnol.* **6**, 104–113 (2010).
278. Stöber, W., Fink, A. & Bohn, E. Controlled growth of monodisperse silica spheres in the micron size range. *J. Colloid Interface Sci.* **26**, 62–69 (1968).
279. Dubey, R. S., Rajesh, Y. B. R. D. & More, M. A. Synthesis and Characterization of SiO<sub>2</sub> Nanoparticles via Sol-gel Method for Industrial Applications. *Mater. Today Proc.* **2**, 3575–3579 (2015).
280. Liberman, A., Mendez, N., Trogler, W. C. & Kummel, A. C. Synthesis and surface functionalization of silica nanoparticles for nanomedicine. *Surf. Sci. Rep.* **69**, 132–158 (2014).
281. Reverchon, E. & Adami, R. Nanomaterials and supercritical fluids. *J. Supercrit. Fluids* **37**, 1–22 (2006).
282. Imoisili, P. E., Ukoba, K. O. & Jen, T.-C. Synthesis and characterization of amorphous mesoporous silica from palm kernel shell ash. *Boletín la Soc. Española Cerámica y Vidr.* **59**, 159–164 (2020).
283. Prabha, S., Durgalakshmi, D., Rajendran, S. & Lichtfouse, E. Plant-derived silica nanoparticles and composites for biosensors, bioimaging, drug delivery and supercapacitors: a review. *Environ. Chem. Lett.* **19**, 1667–1691 (2021).
284. Hassan, A. F., Abdelghny, A. M., Elhadidy, H. & Youssef, A. M. Synthesis and characterization of high surface area nanosilica from rice husk ash by surfactant-free sol–gel method. *J. Sol-Gel Sci. Technol.* **69**, 465–472 (2014).
285. Mitra, S. *et al.* Microwave synthesis of ZnO@mSiO<sub>2</sub> for detailed antifungal mode of action study: Understanding the insights into oxidative stress. *J. Colloid Interface Sci.* **444**, 97–108 (2015).
286. Narayan, R., Nayak, U., Raichur, A. & Garg, S. Mesoporous Silica Nanoparticles: A Comprehensive Review on Synthesis and Recent Advances. *Pharmaceutics* **10**, 118 (2018).
287. Lichtfouse, E. & Rullkötter, J. Accelerated transformation of organic matter below the silica transition zone in immature sediments from the Japan Sea. *Org. Geochem.* **21**, 517–523 (1994).
288. Waddell, W. H. Silica, Amorphous. in *Kirk-Othmer Encyclopedia of*
-

- 
- Chemical Technology* (John Wiley & Sons, Inc., 2006). doi:10.1002/0471238961.0113151823010404.a01.pub2.
289. Ganesan, K., Rajagopal, K. & Thangavel, K. Evaluation of bagasse ash as supplementary cementitious material. *Cem. Concr. Compos.* **29**, 515–524 (2007).
290. Huabcharoen, P., Wimolmala, E., Markpin, T. & Sombatsompop, N. Purification and Characterization of Silica from Sugarcane Bagasse Ash as a Reinforcing Filler in Natural Rubber Composites. *BioResources* **12**, (2017).
291. Berbel Manaia, E. *et al.* Physicochemical characterization of drug nanocarriers. *Int. J. Nanomedicine* **Volume 12**, 4991–5011 (2017).
292. Lin, P.-C., Lin, S., Wang, P. C. & Sridhar, R. Techniques for physicochemical characterization of nanomaterials. *Biotechnol. Adv.* **32**, 711–726 (2014).
293. Brar, S. K. & Verma, M. Measurement of nanoparticles by light-scattering techniques. *TrAC Trends Anal. Chem.* **30**, 4–17 (2011).
294. Reimer, L. Scanning Electron Microscopy: Physics of Image Formation and Microanalysis, Second Edition. *Meas. Sci. Technol.* **11**, 1826–1826 (2000).
295. Hotze, E. M., Phenrat, T. & Lowry, G. V. Nanoparticle Aggregation: Challenges to Understanding Transport and Reactivity in the Environment. *J. Environ. Qual.* **39**, 1909–1924 (2010).
296. Anthony, W. R. *Solid State Chemistry and its Applications*. Wiley & Sons vol. 1 (1992).
297. Alshatwi, A. A., Athinarayanan, J. & Periasamy, V. S. Biocompatibility assessment of rice husk-derived biogenic silica nanoparticles for biomedical applications. *Mater. Sci. Eng. C* **47**, (2015).
298. Kalapathy, U. A simple method for production of pure silica from rice hull ash. *Bioresour. Technol.* **73**, 257–262 (2000).
299. Such, G. K., Yan, Y., Johnston, A. P. R., Gunawan, S. T. & Caruso, F. Interfacing materials science and biology for drug carrier design. *Advanced Materials* vol. 27 2278–2297 (2015).
300. Khaenamkaew, P., Manop, D., Tanghengjaroen, C. & Palakawong Na Ayuthaya, W. Crystal Structure, Lattice Strain, Morphology, and Electrical Properties of SnO<sub>2</sub>Nanoparticles Induced by Low Calcination Temperature. *Adv. Mater. Sci. Eng.* **2020**, (2020).
301. Gumustas, M., Sengel-Turk, C. T., Gumustas, A., Ozkan, S. A. & Uslu, B. Effect of Polymer-Based Nanoparticles on the Assay of Antimicrobial Drug Delivery Systems. in *Multifunctional Systems for Combined Delivery*,
-

- 
- Biosensing and Diagnostics* 67–108 (Elsevier, 2017). doi:10.1016/B978-0-323-52725-5.00005-8.
302. Banerjee, D. Nanofluids and Applications to Energy Systems. in *Encyclopedia of Sustainable Technologies* 429–439 (Elsevier, 2017). doi:10.1016/B978-0-12-409548-9.10144-7.
303. Fatfat, Z., Karam, M., Maatouk, B., Fahs, D. & Gali-Muhtasib, H. Nanoliposomes as safe and efficient drug delivery nanovesicles. in *Advanced and Modern Approaches for Drug Delivery* 159–197 (Elsevier, 2023). doi:10.1016/B978-0-323-91668-4.00002-2.
304. Ellahioui, Y. *et al.* Mesoporous silica nanoparticles functionalised with a photoactive ruthenium(  $\text{II}$  ) complex: exploring the formulation of a metal-based photodynamic therapy photosensitiser. *Dalt. Trans.* **48**, 5940–5951 (2019).
305. Giesche, H. Mercury Porosimetry: A General (Practical) Overview. *Part. Part. Syst. Charact.* **23**, 9–19 (2006).
306. Phonphuak, N. & Chindaprasirt, P. 6 - *Types of waste, properties, and durability of pore-forming waste-based fired masonry bricks. Eco-efficient Masonry Bricks and Blocks* (Elsevier Ltd, 2015). doi:10.1016/B978-1-78242-305-8.00006-1.
307. Savjani, K. T., Gajjar, A. K. & Savjani, J. K. Drug Solubility: Importance and Enhancement Techniques. *ISRN Pharm.* **2012**, 1–10 (2012).
308. Kumar, M., Bishnoi, R. S., Shukla, A. K. & Jain, C. P. Techniques for Formulation of Nanoemulsion Drug Delivery System: A Review. *Prev. Nutr. Food Sci.* **24**, 225–234 (2019).
309. Kumar, S., Bhargava, D., Thakkar, A. & Arora, S. Drug Carrier Systems for Solubility Enhancement of BCS Class II Drugs: A Critical Review. *Crit. Rev. Ther. Drug Carrier Syst.* **30**, 217–256 (2013).
310. Lipinski, C. A., Lombardo, F., Dominy, B. W. & Feeney, P. J. Experimental and computational approaches to estimate solubility and permeability in drug discovery and development settings 1PII of original article: S0169-409X(96)00423-1. The article was originally published in *Advanced Drug Delivery Reviews* 23 (1997). *Adv. Drug Deliv. Rev.* **46**, 3–26 (2001).
311. Dahan, A., Miller, J. M. & Amidon, G. L. Prediction of Solubility and Permeability Class Membership: Provisional BCS Classification of the World's Top Oral Drugs. *AAPS J.* **11**, 740–746 (2009).
312. Ingle, A. P., Shende, S., Gupta, I. & Rai, M. Recent trends in the development of nano-bioactive compounds and delivery systems. in *Biotechnological Production of Bioactive Compounds* 409–431 (Elsevier,

- 
- 2020). doi:10.1016/B978-0-444-64323-0.00014-X.
313. Singh, R., Mann, B., Sharma, R. & Singh, S. Application of Nanotechnology in Functional Foods. in *Nanoscience for Sustainable Agriculture* 547–579 (Springer International Publishing, 2019). doi:10.1007/978-3-319-97852-9\_21.
314. Shreffler, Pullan, Dailey, Mallik & Brooks. Overcoming Hurdles in Nanoparticle Clinical Translation: The Influence of Experimental Design and Surface Modification. *Int. J. Mol. Sci.* **20**, 6056 (2019).
315. Owens III, D. & Peppas, N. Opsonization, biodistribution, and pharmacokinetics of polymeric nanoparticles. *Int. J. Pharm.* **307**, 93–102 (2006).
316. Pelgrift, R. Y. & Friedman, A. J. Nanotechnology as a therapeutic tool to combat microbial resistance. *Adv. Drug Deliv. Rev.* **65**, 1803–1815 (2013).
317. Wu, X. *et al.* Cationic chitosan- modified silica nanoparticles for oral delivery of protein vaccine. *J. Biomed. Mater. Res. Part A* **109**, 2111–2119 (2021).
318. Huh, A. J. & Kwon, Y. J. “Nanoantibiotics”: A new paradigm for treating infectious diseases using nanomaterials in the antibiotics resistant era. *J. Control. Release* **156**, 128–145 (2011).
319. Friedman, A. J. *et al.* Antimicrobial and Anti-Inflammatory Activity of Chitosan–Alginate Nanoparticles: A Targeted Therapy for Cutaneous Pathogens. *J. Invest. Dermatol.* **133**, 1231–1239 (2013).
320. Luesakul, U., Puthong, S., Neamati, N. & Muangsin, N. pH-responsive selenium nanoparticles stabilized by folate-chitosan delivering doxorubicin for overcoming drug-resistant cancer cells. *Carbohydr. Polym.* **181**, 841–850 (2018).
321. Unsoy, G. *et al.* Chitosan magnetic nanoparticles for pH responsive Bortezomib release in cancer therapy. *Biomed. Pharmacother.* **68**, 641–648 (2014).
322. Huang, M., Ma, Z., Khor, E. & Lim, L.-Y. Uptake of FITC-chitosan nanoparticles by A549 cells. *Pharm. Res.* **19**, 1488–94 (2002).
323. Smirnova, I., Mamic, J. & Arlt, W. Adsorption of Drugs on Silica Aerogels. *Langmuir* **19**, 8521–8525 (2003).
324. Jambhrunkar, S. *et al.* Modulating in vitro release and solubility of griseofulvin using functionalized mesoporous silica nanoparticles. *J. Colloid Interface Sci.* **434**, 218–225 (2014).
325. Hate, S. S., Reutzel-Edens, S. M. & Taylor, L. S. Influence of Drug–Silica
-

- 
- Electrostatic Interactions on Drug Release from Mesoporous Silica-Based Oral Delivery Systems. *Mol. Pharm.* **17**, 3435–3446 (2020).
326. Zhuravlev, L. T. The surface chemistry of amorphous silica. Zhuravlev model. *Colloids Surfaces A Physicochem. Eng. Asp.* **173**, 1–38 (2000).
327. Delle Piane, M., Corno, M. & Ugliengo, P. Ab Initio Modeling of Hydrogen Bond Interaction at Silica Surfaces With Focus on Silica/Drugs Systems. in *Modelling and Simulation in the Science of Micro- and Meso-Porous Materials* 297–328 (Elsevier, 2018). doi:10.1016/B978-0-12-805057-6.00009-0.
328. Colilla, M. *et al.* Synthesis and Characterization of Zwitterionic SBA-15 Nanostructured Materials. *Chem. Mater.* **22**, 6459–6466 (2010).
329. Song, S.-W., Hidajat, K. & Kawi, S. Functionalized SBA-15 Materials as Carriers for Controlled Drug Delivery: Influence of Surface Properties on Matrix–Drug Interactions. *Langmuir* **21**, 9568–9575 (2005).
330. Rosenholm, J. M. & Lindén, M. Towards establishing structure–activity relationships for mesoporous silica in drug delivery applications. *J. Control. Release* **128**, 157–164 (2008).
331. McCarthy, C. A., Ahern, R. J., Dontireddy, R., Ryan, K. B. & Crean, A. M. Mesoporous silica formulation strategies for drug dissolution enhancement: a review. *Expert Opin. Drug Deliv.* **13**, 93–108 (2016).
332. Doadrio, J. C. *et al.* Functionalization of mesoporous materials with long alkyl chains as a strategy for controlling drug delivery pattern. *J. Mater. Chem.* **16**, 462–466 (2006).
333. Muhammad, F. *et al.* pH-Triggered Controlled Drug Release from Mesoporous Silica Nanoparticles via Intracellular Dissolution of ZnO Nanolids. *J. Am. Chem. Soc.* **133**, 8778–8781 (2011).
334. van Speybroeck, M. *et al.* Preventing release in the acidic environment of the stomach via occlusion in ordered mesoporous silica enhances the absorption of poorly soluble weakly acidic drugs. *J. Pharm. Sci.* **100**, 4864–4876 (2011).
335. Dobrovolskaia, M. A. & McNeil, S. E. Immunological properties of engineered nanomaterials. *Nat. Nanotechnol.* **2**, 469–478 (2007).
336. Naahidi, S. *et al.* Biocompatibility of engineered nanoparticles for drug delivery. *J. Control. Release* **166**, 182–194 (2013).
337. Mahapatro, A. & Singh, D. K. Biodegradable nanoparticles are excellent vehicle for site directed in-vivo delivery of drugs and vaccines. *J. Nanobiotechnology* **9**, 55 (2011).
338. Fischer, H. C. & Chan, W. C. Nanotoxicity: the growing need for in vivo
-

- 
- study. *Curr. Opin. Biotechnol.* **18**, 565–571 (2007).
339. Selvarajan, V., Obuobi, S. & Ee, P. L. R. Silica Nanoparticles—A Versatile Tool for the Treatment of Bacterial Infections. *Front. Chem.* **8**, (2020).
340. Croissant, J. G. & Brinker, C. J. Biodegradable Silica-Based Nanoparticles: Dissolution Kinetics and Selective Bond Cleavage. in 181–214 (2018). doi:10.1016/bs.enz.2018.07.008.
341. Croissant, J. G., Fatieiev, Y. & Khashab, N. M. Degradability and Clearance of Silicon, Organosilica, Silsesquioxane, Silica Mixed Oxide, and Mesoporous Silica Nanoparticles. *Adv. Mater.* **29**, 1604634 (2017).
342. Croissant, J. G., Fatieiev, Y., Almalik, A. & Khashab, N. M. Mesoporous Silica and Organosilica Nanoparticles: Physical Chemistry, Biosafety, Delivery Strategies, and Biomedical Applications. *Adv. Healthc. Mater.* **7**, 1700831 (2018).
343. Doshi, D. A. *et al.* Investigating the Interface of Superhydrophobic Surfaces in Contact with Water. *Langmuir* **21**, 7805–7811 (2005).
344. Pfeiffer-Laplaud, M., Costa, D., Tielens, F., Gaigeot, M.-P. & Sulpizi, M. Bimodal Acidity at the Amorphous Silica/Water Interface. *J. Phys. Chem. C* **119**, 27354–27362 (2015).
345. Hassanali, A. A. & Singer, S. J. Model for the Water–Amorphous Silica Interface: The Undissociated Surface. *J. Phys. Chem. B* **111**, 11181–11193 (2007).
346. LIANG, D.-T. & READEY, D. W. Dissolution Kinetics of Crystalline and Amorphous Silica in Hydrofluoric-Hydrochloric Acid Mixtures. *J. Am. Ceram. Soc.* **70**, 570–577 (1987).
347. Kopac, T. Protein corona, understanding the nanoparticle–protein interactions and future perspectives: A critical review. *Int. J. Biol. Macromol.* **169**, 290–301 (2021).
348. Kopac, T., Bozgeyik, K. & Yener, J. Effect of pH and temperature on the adsorption of bovine serum albumin onto titanium dioxide. *Colloids Surfaces A Physicochem. Eng. Asp.* **322**, 19–28 (2008).
349. Farjadian, F., Roointan, A., Mohammadi-Samani, S. & Hosseini, M. Mesoporous silica nanoparticles: Synthesis, pharmaceutical applications, biodistribution, and biosafety assessment. *Chem. Eng. J.* **359**, 684–705 (2019).
350. Abdoul-Azize, S., Buquet, C., Vannier, J.-P. & Dubus, I. Pyr3, a TRPC3 channel blocker, potentiates dexamethasone sensitivity and apoptosis in acute lymphoblastic leukemia cells by disturbing Ca<sup>2+</sup> signaling, mitochondrial

- membrane potential changes and reactive oxygen species production. *Eur. J. Pharmacol.* **784**, 90–98 (2016).
351. de Jong. Drug delivery and nanoparticles: Applications and hazards. *Int. J. Nanomedicine* 133 (2008) doi:10.2147/IJN.S596.



## PRESENTATIONS

---

- **Aparna Menon A and G Radhakrishna Pillai.** Delivered oral presentation on ‘Studies on the synthesis of biogenic silica nanoparticles and its effects as a drug carrier in epirubicin based cancer therapy’ at the 8<sup>th</sup> International Translational Cancer Research Conference on Role of Inflammation & Immune system for Cancer Prevention & Treatment held at the Department of Biochemistry, Institute of Science, Banaras Hindu University, Varanasi, India during February 13-16, 2020.
- **Aparna Menon A and G Radhakrishna Pillai.** Delivered oral presentation on ‘Investigations on mesoporous silica nanoparticles derived from rice husk as drug carrier in cancer therapy’ in the International Conference on *Sustainable Utilization of Bioresources* during January 10-15, 2022 conducted by the Department of Botany, University of Kerala, Thiruvananthapuram, India.



## PUBLICATIONS

---

- Menon, A. A., & Pillai, R. G. (2022). Source optimization, characterization, assessing biocompatibility and drug loading efficiency of biogenic silica particles from agro wastes. *Chemical Biology Letters*, 9(1), 311. Retrieved from <https://pubs.thesciencein.org/journal/index.php/cbl/article/view/311>
- Johnson, J. P., Renganthan, S., Menon, A., & Pillai, R. G. (2021). Beneficial impacts of Astaxanthin on Biomarkers of Antioxidant status and oxidative damage in Rats exposed to Ambient air. *Chemical Biology Letters*, 8(1), 1–9. Retrieved from <https://pubs.thesciencein.org/journal/index.php/cbl/article/view/158>



## APPENDIX

### ◆ Techno-economic analysis

This calculation was done purely based on raw material cost.

#### *Synthesis cost of biogenic silica*

|  |            |
|--|------------|
| <i>Price of 1tonne rice husk (RH) (in INR)</i>             | 5000       |
| <i>Price of 1kg rice husk</i>                              | 5          |
| <i>Price of 50g rice husk</i>                              | 0.25       |
| <i>Price of 1L Industrial gr. HCl 1N</i>                   | 3.5        |
| <i>Price of 600mL Industrial gr. HCl 1N</i>                | 2.1        |
| <i>Yield (%) of silica NP (SiNP) obtained in the study</i> | 14         |
| <i>g of SiNP obtained from 50g RH</i>                      | 7          |
| <i>Total cost incurred for production of 7g SiNP</i>       | 2.35       |
| <i>Total cost incurred for production of 1kg SiNP</i>      | <b>336</b> |

#### *Synthesis cost of control silica*

##### *Considering 1% yield from the sol-gel process*

|  |                |
|--|----------------|
| <i>CTAB (500g)</i>                                       | 2500           |
| <i>NaOH (500g)</i>                                       | 310            |
| <i>TEOS (2.5L)</i>                                       | 22500          |
| <i>Absolute ethanol (1L)</i>                             | 1400           |
| <i>Industrial grade HCl (1L)</i>                         | 3.5            |
| <i>Total cost for the production of 1kg control SiNP</i> | <b>26713.5</b> |

**PEG modification cost**

|  |             |
|--|-------------|
| <i>200mg SiNP requires 10mL 2% w/v peg (2g in 100mL solvent)</i> |             |
| <i>1kg SiNP requires 50L 2% peg (1kg in 50L solvent)</i>         |             |
| <i>Price of 1kg peg</i>  | 100         |
| <i>Price of 1L distilled water (solvent used)</i>                | 70          |
| <i>Price of 50L solvent</i>                                      | 3500        |
| <i>Total cost incurred for peg modification of 1kg SiNP</i>      | <b>3600</b> |

**Chitosan modification cost**

|  |              |
|--|--------------|
| <i>50mg SiNP requires 10mL 1.2% w/v chitosan (1.2g in 100mL solvent)</i> |              |
| <i>1kg SiNP requires 200mL 1.2% w/v chitosan (2.4g in 200mL solvent)</i> |              |
| <i>Price of 100g chitosan</i>  | 150          |
| <i>Price of 2.4g chitosan</i>  | 3.6          |
| <i>Price of 500mL acetic acid (99.9%)</i>                                | 260          |
| <i>Price of 200mL acetic acid</i>  | 104          |
| <i>Total cost incurred for chitosan capping</i>                          | <b>107.6</b> |

**Drug loaded SiNP with curcumin**

|  |                |
|--|----------------|
| <i>Curcumin loading capacity of the silica nanoparticle is 0.846<math>\mu</math>g/mg</i> |                |
| <i><math>\therefore</math> 1kg SiNP can load 846mg curcumin</i>                          |                |
| <i>Cost of 1kg curcumin (95% natural extract)</i>  | 5000           |
| <i>Cost of 846mg curcumin</i>  | 4.23           |
| <i>Total cost of production of 1kg peg modified curcumin loaded chitosan capped SiNP</i> | <b>4047.83</b> |

**Drug loaded SiNP with epirubicin**

|  |                |
|--|----------------|
| <i>Epirubicin loading capacity of the silica nanoparticle is 1.487<math>\mu</math>g/mg</i> |                |
| <i><math>\therefore</math> 1kg SiNP can load 1.487g epirubicin</i>                         |                |
| <i>Cost of epirubicin HCl (100mg)</i>  | 2,000          |
| <i>Cost of 1.487g epirubicin</i>   | 29740          |
| <i>Total cost of production of 1kg peg modified epirubicin loaded chitosan capped SiNP</i> | <b>33783.6</b> |